A novel *in vitro* model for mature *Toxoplasma gondii* tissue cysts allows functional characterization of bradyzoite biology

Dissertation

zur Erlangung des akademischen Grades

doctor rerum naturalium

(Dr. rer. nat.)

im Fach Biologie

eingereicht an der Lebenswissenschaftlichen Fakultät

der Humboldt-Universität zu Berlin

von

Céline Christiansen, MSc.

Präsidentin der Humboldt-Universität zu Berlin

Prof. Dr. Julia von Blumenthal

Dekan der Lebenswissenschaftlichen Fakultät:

Prof. Dr. Dr. Christian Ulrichs

Gutachter: 1. Prof. Dr. Kai Matuschewski

2. Prof. Dr. Frank Seeber

3. Prof. Dr. Carsten Lüder

Tag der mündlichen Prüfung: 14.10.2022

Acknowledgements

This space I want to fill with really thankful words for the people, which supported me during this intense journey. First of all, I want to thank my supervisor Martin Blume who gave me the chance to work in this project, to learn so much and to fall in love with this fascinating parasite. Although, not everything went as we wished or expected (but hey this is science), you were always supportive, and you came along with (a lot of) new ideas. I want to thank Frank Seeber for fruitful discussions, good advice, and an open ear when it was needed.

Many thanks as well to my colleagues, especially Deborah, Ellen, Ben and Jana. To cite a wise man: "Happiness can be found even in the darkest of times, but only to those who remember to turn on the light." You guys always cheered me up with your presence and especially with coffee.

I want to thank my family and my closest friends Marlene and Katrin. You always supported me in what I ever needed and showed a lot of patience. Alexander, without sounding melancholic, you always were and will be my rock. Last, I want to thank Kim Wild, you always keep me hanging on!

All you people helped me to be at the point where I am now, proud, and happy and ready for the next exciting steps! Thank you again so much.

Table of content

List of abbreviations

A	amylopectin granules
ApiATs	Apicomplexan amino acid transporters
ara	arabinosyl
AT	adenosine transporter
BAG	bradyzoite antigen
BCAA	branched chain amino acid
BKI	bumped kinase inhibitor
BMM	bone marrow derived macrophages
BrdU	5-bromo-2'- deoxy uridine
BrdU	bromodeoxyuridine
BSA	bovine serum albumine
CACT	carnitine-acylcarnitine translocase
cAMP	cyclic adenosine monophosphate
CARN	carnitine
CDPK1	calcium-dependent protein kinase 1
CFSE	carboxyfluorescein succinimidyl ester
cGMP	cyclic guanosine monophosphate
CHO	chinese hamster ovaries
CoA	coenzyme A
CPT	carnitine palmitoyl transferase system
CW	cyst wall
D3	deuterated
DBA	*Dolichos biflorus* agglutinin
DBL	*Dolichos biflorus* lectin
DMEM	Dulbecco's Modified Eagle's Medium
DMSO	dimethyl sulfoxide
DP	diphosphate
EdA	7-deaza-7-ethynyl-2-deoxyadenosine
EdU	5-ethynyl-2-deoxyuridine
ELISA	enzyme-linked immunosorbent assay
ENO	enolase
ER	endoplasmic reticulum
EtOH	ethanol

FA	fatty acid
FAE	fatty acid elongation
FAS	fatty acid synthesis
FOR	forodesine
GC / MS	gas chromatography-coupled mass spectrometry
GRA	dense granule protein
HDQ	1-hydroxy-2-dodecyl-4(1H)-quinolone
HFF	human foreskin fibroblast
HSP	heat shock protein
hxgprt	*hypoxanthine-xanthine-guanine phosphoribosyl transferase*
IC_{50}	half inhibitory concentration
IFA	immunofluorescence assay
IFN-γ	interferon gamma
IL-6	interleucin-6
IMC	inner membrane complex 3
LA	linoleic acid
LC / MS	liquid chromatography-coupled mass spectrometry
LD	lipid droplets
LDH	lactate dehydrogenase
LPS	lipopolysaccharide
M1	pro-inflammatory macrophages
mAb	monoclonal antibody
MEL	meldonium
MeOH	methanol
mETC	mitochondrial electron transport chain
MF	myosin heavy chain
MOI	multiplicity of infection
MP	monophosphate
MT	myotubes
NaFAc	sodium fluoroacetate
NO	nitric oxygen
P	protein
PBQC	pooled biological quality control
PBS	phosphate buffered saline
PC	principal component

PFA	paraformaldehyde
PVM	parasitophorous vacuolar membrane
PYR	pyrimethamine
qPCR	real-time polymerase chain reaction
ribo	ribosyl
RPMI	Roswell Park Memorial Institute 1640
RS	resistance score
RT	room temperature
SAG	surface antigen
spp.	species
SULF	sulfadiazine
T. gondii / *Tg*	*Toxoplasma gondii*
TCA	tricarboxylic acid cycle
td	tandem
TMR	5-carboxytetramethylrhodamine-azide
TP	triphosphate
TRI	trimetazidine
TZ	tachyzoites
WB	western blot

Commonly used abbreviations and SI units are not listed. The used abbreviations are introduced for each main chapter.

List of figures

List of tables

Abstract

Toxoplasma gondii forms persistent encysted bradyzoites inside neuronal and muscle tissue of its intermediate host, which resist immune responses and medical treatments. These largely asymptomatic stages present a key source of transmission and can cause recurring disease in immune-weakened individuals that is lethal if untreated. However, experimental access to mature tissue cysts is limited to *ex vivo* models and the biology of bradyzoites remains understudied. In particular aspects like the metabolome or bradyzoite-host-interactions and mechanisms of persistence are difficult to address using current *in vitro* and *in vivo* models. To overcome these restrictions, the aim of this thesis was the establishment and characterization of an *in vitro* model for the generation of matured *T. gondii* tissue cysts. This system then should be used to (1) characterize the metabolome of matured encysted bradyzoites in comparison with tachyzoites, (2) interrogate bradyzoite-host-interactions and (3) establish a cell division marker for bradyzoites that allows studying bradyzoite heterogeneity. Encysted bradyzoites were grown in terminally differentiated human myotubes and showed typical ultrastructural hallmarks and antigen expression. These bradyzoites also contained functional hallmarks like resistance to pepsin, temperature and commonly used antiparasitics that were dependent on the maturation time. The metabolic fingerprint of bradyzoites was compared to tachyzoites using an untargeted HILIC-UHPLC / MS based metabolomics platform. While tachyzoites succumbed to inhibition of their aconitase by sodium fluoroacetate, bradyzoites tolerated prolonged inhibition of this enzyme. Further, bradyzoites interact with their host in a previously unknown fashion. Stable isotope-metabolic labeling and pharmacological modulation of host lipid metabolism indicated a critical role of host carnitine esters for fatty acid import and for the detoxification of the antimicrobial effect of linoleic acid. To develop a single cell-resolved cell division marker, we screened click chemistry-detectable pyrimidine-based and purine-based nucleoside analogues for toxicity on both stages and their respective incorporation profile. Three compounds labelled both bradyzoite and tachyzoite nuclei without toxic effects. In summary, we developed an *in vitro* culture model of functionally matured and chronically infectious encysted bradyzoites of *T. gondii*. As demonstrated in this thesis, this is a door opener for novel targeted and untargeted studies on the chronic form of *T. gondii* with many implications for therapeutic intervention with chronic *T. gondii* infections.

Zusammenfassung

Toxoplasma gondii bildet im Nerven- und Muskelgewebe seines Zwischenwirts persistente enzystierte Bradyzoiten, die Immunreaktionen und medizinischen Behandlungen widerstehen. Diese weitgehend asymptomatischen Stadien stellen eine Hauptübertragungsquelle dar und können bei immungeschwächten Individuen zu wiederkehrenden Erkrankungen führen, die unbehandelt tödlich verlaufen. Der experimentelle Zugang zu reifen Gewebezysten ist jedoch auf *ex vivo* Modelle beschränkt und die Biologie von Bradyzoiten ist unzureichend erforscht. Insbesondere Aspekte wie das Metabolom oder Wirtszell-Bradyzoiten-Interaktionen und Persistenzmechanismen sind mit aktuellen *in vitro* und *in vivo* Modellen schwer zu adressieren. Um diese Einschränkungen zu überwinden, war es das Ziel dieser Arbeit ein *in vitro* Modell zur Generierung reifer *T. gondii* Gewebszysten zu etablieren und zu charakterisieren. Dieses System wurde dann verwendet, um (1) das Metabolom von reifen enzystierten Bradyzoiten im Vergleich zu Tachyzoiten zu charakterisieren, (2) Wirtszell-Bradyzoiten-Interaktionen zu untersuchen und (3) einen Zellteilungsmarker für Bradyzoiten zu etablieren, der die Untersuchung der Heterogenität von Bradyzoiten ermöglicht. Enzystierte Bradyzoiten wurden in terminal differenzierten menschlichen Myotuben generiert und zeigten typische ultrastrukturelle Charakteristika und Antigenexpression. Diese Bradyzoiten zeigten auch funktionelle Merkmale wie Resistenz gegen Pepsin, Temperatur und häufig verwendete Antiparasitika, die von der Reifungszeit abhängig waren. Der metabolische Fingerabdruck von Bradyzoiten wurde mit Tachyzoiten unter Verwendung einer ungezielten HILIC-UHPLC / MS-basierten Metabolomik-Plattform verglichen. Während die Hemmung der Aconitase durch Natriumfluoracetat letal in Tachyzoiten wirkte, tolerierten Bradyzoiten eine längere Hemmung dieses Enzyms. Darüber hinaus interagieren Bradyzoiten mit ihrem Wirt auf bisher unbekannte Weise. Eine stabile isotopenmetabolische Markierung und pharmakologische Modulation des Lipidstoffwechsels des Wirts wiesen auf eine entscheidende Rolle der Carnitinester des Wirts für den Fettsäureimport und die Entgiftung der antimikrobiellen Wirkung von Linolsäure hin. Um einen Zellteilungsmarker auf Einzelzellebene zu entwickeln, haben wir durch Klick-Chemie nachweisbare Pyrimidin- und Purin-basierte Nukleosidanaloga auf Toxizität in beiden Stadien und ihr jeweiliges Inkorporationsprofil untersucht. Drei der Analoga wurden ohne toxische Wirkungen in die DNA von sowohl Bradyzoiten als auch Tachyzoiten eingebaut. Zusammenfassend haben wir ein *in vitro* Kulturmodell funktionell reifer und chronisch infiösér *T. gondii* Gewebezysten entwickelt. Wie in dieser Dissertation gezeigt, ist dies ein Türöffner für neue gezielte und ungezielte Studien zur chronischen Form von *T. gondii* mit vielen Implikationen für therapeutische Interventionen bei chronischen *T. gondii* Infektionen.

Chapter 1: Introduction

1.1 *Toxoplasma gondii*

1.1.1 Life cycle

Toxoplasma gondii (*T. gondii*) is an obligate intracellular protozoan parasite belonging to the phylum Apicomplexa and is the causative agent of toxoplasmosis. The phylum Apicomplexa includes other important pathogens such as *Plasmodium, Eimeria, Cyclospora, Babesia* and *Cryptosporidium* (Weiss and Kim, 2000). The common taxonomic characteristic of the Apicomplexa is the "apical complex", a structure consisting of several cell organelles (conoid, rhoptries and micronemes) and the apicoplast, a four membrane-bound organelle acquired through secondary endosymbiosis (Ferguson, 2014; Köhler et al., 1997). *T. gondii* is generally transmitted via the oral route and its life cycle, displayed in **Figure 1**, alternates between sexual reproduction by gamogony in the intestinal epithelium of the final host (felids) and asexual reproduction by schizogony in the intermediate hosts (warm-blooded vertebrates).
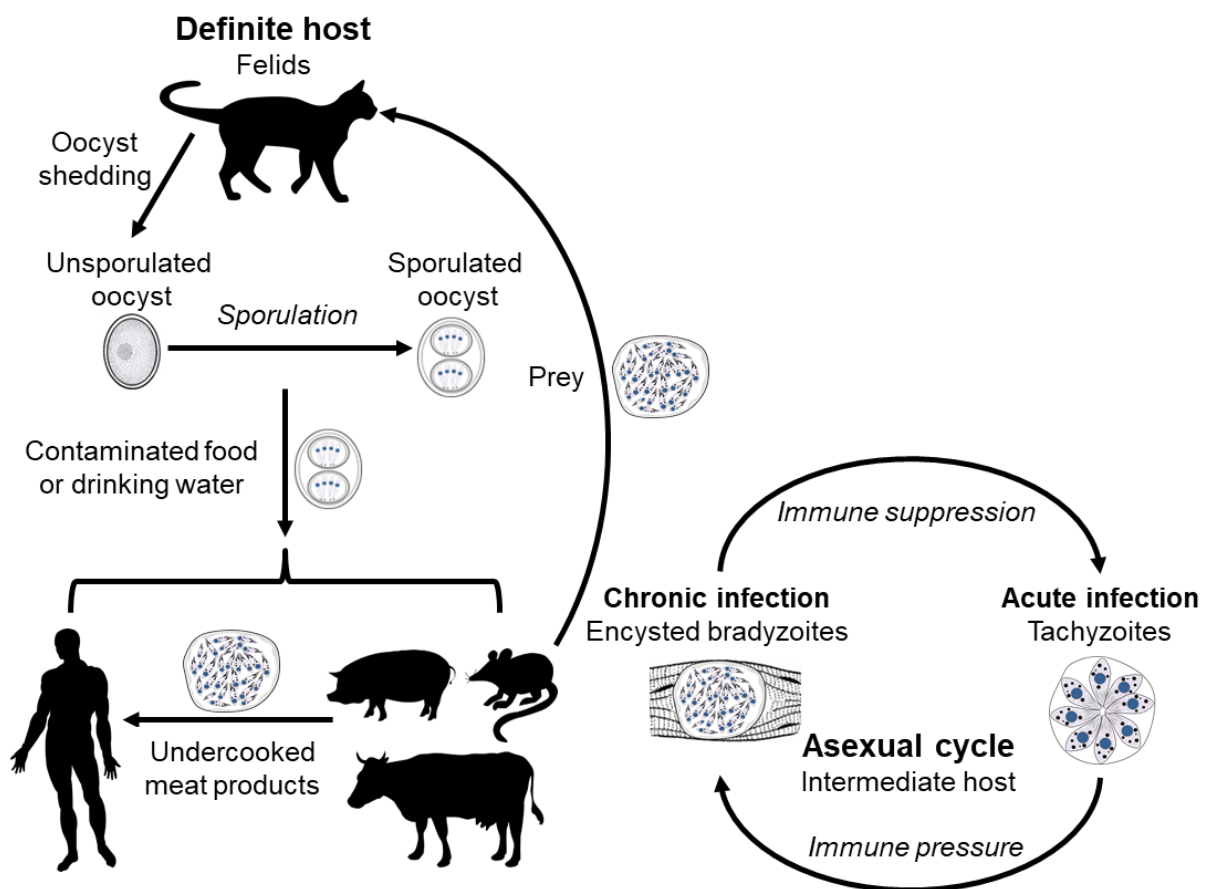
Figure 1: Main transmission routes and the asexual life cycle of *T. gondii*.
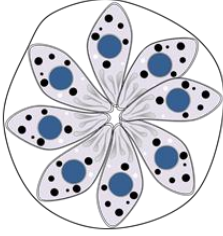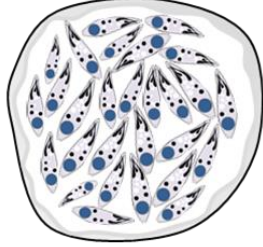
During sexual reproduction oocysts are formed and disseminated in the environment via the feces of felids. After sporulation oocysts are taken up by intermediate hosts and sporozoites

within the oocysts enter the asexual cycle by differentiating into rapidly dividing tachyzoites that disseminate throughout the intermediate host. Upon immune pressure these fast-growing forms differentiate into slowly dividing bradyzoites, preferentially in muscle and neuronal tissue (Dubey et al., 1998). These bradyzoites, surrounded by a glycan-rich cyst wall, evade the host immune system, and establish a life-long chronic infection. In contrast to the acute form of the infection, chronic forms of *T. gondii* cannot be cleared with available treatments. The infections are largely asymptomatic, but can cause recurring disease in immune-weakened individuals that is lethal if untreated (Luft et al., 1983). One key of success of this single-celled eukaryote is its peerless cycle flexibility and the resulting diverse dissemination and transmission pathways. In contrast to its near relatives, *T. gondii* has the unique ability to bypass the sexual life cycle by horizontal infection between different intermediate hosts resulting in an unparalleled range of intermediate hosts including humans. The main transmission route in humans is via tissue cysts in undercooked meat products (Desmonts et al., 1965) and leads to an estimated global seroprevalence in humans of one third (Molan et al., 2019). In Germany, a recent study reported that 50 % of the population is positive for anti-*T. gondii* antibodies, with a 24 % difference in prevalence between the former East and West of the country, likely caused by different dietary habits (Wilking et al., 2016). Therefore *T. gondii* can be acquired via food and toxoplasmosis is considered a zoonotic disease.

1.1.2 The bradyzoite: A key developmental stage for persistence and transmission

Like other infectious protozoa, including the Apicomplexan *Plasmodium vivax* and the kinetoplastidae *Trypanosoma cruzi* and *Leishmania* species *(*spp.), *T. gondii* forms specialized persistent stages that resist immune responses and many medical treatments (Barrett et al., 2019). The ability of *T. gondii* to build these latent tissue cysts is an evolutionary trade-off that in parallel reduces virulence while increasing transmission (Sullivan and Jeffers, 2012). The chronic form of *T. gondii* displays a key role during horizontal transmission between intermediate hosts as well as vertical transmission to the definite host. The conversion of tachyzoites to encysted bradyzoites is accompanied with the development of characteristic features and traits, briefly summarized in **Figure 2**.

	Tachyzoites (acute infection)	**Bradyzoites** (chronic infection)
Outer membrane	PVM	Cyst wall
Metabolic activity	High	Low
Main carbon source	Glucose, glutamine	Glucose, unknown
Replication	Fast, synchronously	Slow, asynchronously
Host cell type	Any nucleated cell	Mostly neuronal and muscle cells
Treatment	Antifolates, spiramycin, atovaquone	none
Oral infectivity	No	Yes

Figure 2: Characteristic traits of *T. gondii* tachyzoites and bradyzoites. Adapted from (Lüder and Rahman, 2017). PVM: parasitophorous vacuolar membrane.

Encysted bradyzoites develop stage specific morphology and antigen expression, described in detail in **Figure 3**. Furthermore, a change of proliferation behavior, energy metabolism and developing resistances against temperature stresses, pepsin and commonly used antiparasitics is accompanied with stage conversion.

1.1.2.1 *Toxoplasma gondii* strains differ in their capability to form tissue cysts

Three predominant linages (type I, type II, type III) of *T. gondii* were identified by genetic analysis of isolates from Europe and North America (Su et al., 2003). These strains distinctly differ in their proliferation rate, virulence, their transmigration ability to cross epithelial layers, and their ability to convert into encysted bradyzoites (Barragan and Sibley, 2003; Howe and Sibley, 1995).

Type I strains generally show a faster proliferation and are more virulent in mice. The most commonly used laboratory strain is the type I RH strain isolated in 1938 (Sabin, 1938). This strain is predominantly used in *in vitro* tachyzoite cultures in human fibroblast (HFF) cells over decades. It is marked by a high replication rate and its amenability to reverse genetic manipulation and hence presents an indispensable tool for tachyzoite studies. However, in current *in vitro* and most mouse-based *in vivo* models, RH parasites show a limited ability to convert into cysts limiting the study of conversion from tachyzoite to bradyzoite. Under stress conditions, RH tachyzoites upregulate bradyzoite specific genes and produce bradyzoite

specific proteins (Bohne and Roos, 1997; Lescault et al., 2010; Soête et al., 1994), however the parasites fail to slow down replication to convert into mature cysts.

Type II and III lineages are marked by a slower replication rate. They readily convert to encysted bradyzoites and are generally less virulent in mice than type I stains. These hallmarks change with prolonged *in vitro* passage in HFFs suggesting differences in conversion capacity between these strains are influenced by adaption *in vitro*.

1.1.2.2 Morphology and antigen expression

Tissue cysts vary in size and shape. Early cysts of mice brain can be as small as 5 µM in diameter with as few as two bradyzoites, while mature cysts can be up to 70 µM in diameter containing 1,000-2,000 bradyzoites (Dubey et al., 1998; Watts et al., 2015). Bradyzoite formation and their maturation is accompanied by the expression of stage specific proteins and the development of specific ultrastructural features (Ferguson, 2004) shown in **Figure 3**. In this section, only markers for tachyzoites and bradyzoites that are important for this work will be introduced.
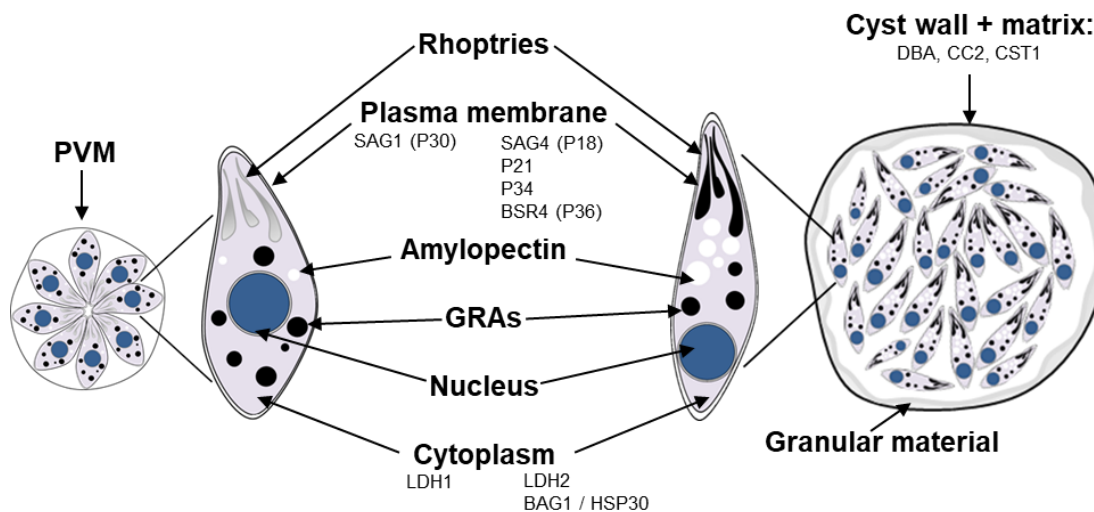
Figure 3: Morphologic hallmarks and commonly used markers for tachyzoite and bradyzoite stages. PVM: parasitophorous vacuolar membrane; SAG: surface antigen; P: protein, GRAs: dense granule proteins; LDH: lactate dehydrogenase; BAG: bradyzoite antigen; DBA: *Dolichos biflorus* agglutinin.

The parasitophorous vacuolar membrane (PVM), which is typical for tachyzoites, develops into a thick glycan rich cyst wall indicated by the apparent deposition of electron-dense vesicular-tubular material (Lemgruber et al., 2011). This cyst wall, expanding to > 0.5 µM thickness, is built from glycoproteins and chitin which is secreted by *T. gondii* (Boothroyd et al., 1997; Zhang et al., 2001). The glycoproteins can interact with lectins like *Dolichos biflorus* agglutin (DBA) (Sethi et al., 1977), a commonly used diagnostic tool for cyst wall staining. The bradyzoites inside their tissue cysts are not arranged in a specific orientation like it is known for tachyzoites

(Ferguson et al., 1991; Ferguson and Hutchison, 1987b). Bradyzoites develop electron dense micronemes and rhoptries establish. The nucleus migrates to a posterior position and amylopectin storages accumulate over time (Dubey et al., 1998), which can be detected via periodic acid shift staining.

Studies with monoclonal antibodies (mAbs) demonstrated the sequential regulation of marker protein (P) expression in tachyzoites and bradyzoites (Ferguson, 2004). The most used marker for the tachyzoite stage is surface antigen (SAG) 1 (P30). Bradyzoite development is accompanied with a maturation-dependent loss of SAG1-expression and its absence in fully matured bradyzoites (Tomavo et al., 1991). The working group of Tomavo discovered several specific bradyzoite specific SAGs (SAG4 (P18); P21; P34; BSR4 (P36)), which were then extensively applied to characterize early events of *in vitro* bradyzoite formation (Tomavo et al., 1991). P18, P34 and P36 were shown to be markers which are expressed early during stage conversion whereas till now P21 is the latest established bradyzoite marker, which appears in a median of five days after bradyzoite induction *in vitro* (Soête et al., 1994). Nowadays, the commonly used markers for bradyzoite formation are cytoplasmic antigens bradyzoite antigen 1 (BAG1) and lactate dehydrogenase 2 (LDH2). A further established marker is CC2 which confers to a cyst wall antigen in bradyzoites (Gross et al., 1995). Taking advantage of these antibodies or fluorescent reporter proteins, the kinetics of *in vitro* cyst formation could be observed via microscopy. Upstream forming fully matured encysted bradyzoites, the conversion occurs as a continuum through transitional intermediate forms which show expression of tachyzoite as well as bradyzoite specific markers.

1.1.2.3 Proliferation

Differentiation from tachyzoites to bradyzoites is accompanied with slowed down replication and a prolonged cell cycle (Jerome et al., 1998). Mature *ex vivo* bradyzoites isolated from mice brain which were infected with oocysts were stated as a growth-arrested stage with parasites standing in G0 with uniform 1N DNA content (Radke et al., 2003). In *in vitro* models using a type II strain, the formation of encysted bradyzoites was observed replicating slow and asynchronously using a combination of endogeny and endopolygeny (Dzierszinski et al., 2004). For a decade, this proliferative behavior was only conferred to *in vitro* bradyzoites and was correlated to a lack of differentiation. Studies led to the conviction that mature *in vivo* bradyzoites are dormant, non-dynamic entities, with all cysts and therefore bradyzoites being equal (Watts et al., 2015). This confined mindset prevailed for decades due to the absence of adequate markers which allowed the discrimination of the potential heterogeneity of physiological states of single bradyzoites inside a tissue cyst. The work of Elisabeth Watts in 2015 led to a paradigm shift. This study revealed that also *in vivo*, different stages of immature

and mature tissue cysts can be found, and even fully matured cysts can contain slow asynchronously dividing parasites. This behavior can lead to a highly heterogenous population inside one single tissue cyst (Watts et al., 2015).

These observations changed the view on bradyzoites from a static population which cannot be targeted with common drugs because of its dormancy to a population, which is highly flexible and able to survive treatments through their high heterogeneity and therefore capability to adapt to fluctuating environments.

1.1.2.4 Energy metabolism

Since the differentiation from tachyzoites to bradyzoites is accompanied with slowed down replication and a prolonged cell cycle (Jerome et al., 1998), that implies significantly altered demand on carbon and energy metabolism. A number of metabolic enzymes are expressed as tachyzoite- and bradyzoite-specific isoforms further suggesting the fine tuning of metabolism between these two stages (Weiss and Kim, 2000). The proposed metabolic shift may also be associated with tolerance against many antiparasitic treatments as the metabolic state of microbes has important implications for the lethality of antimicrobials (Lopatkin et al., 2019). Hence unsurprisingly, multi drug resistant and non-drug resistant bacteria possess a distinct different metabolic fingerprint and this metabolic phenotype might be interrogated to study drug resistance mechanisms (Lin et al., 2019).

Bradyzoites depend on the turnover of the storage polysaccharide amylopectin by glycogen phosphorylase (Murata et al., 2017), the hexose kinase (Shukla et al., 2018) and on a dedicated isoform of LDH, LDH2 (Abdelbaset et al., 2017). In recent studies it was shown that cyst burden of LDH2 knockdown parasites were significantly lower in brains of infected mice compared to wildtype (Al-Anouti et al., 2004). Besides the significantly higher expression of glycolytic key enzyme glucose-6-phosphate isomerase in encysted bradyzoites (Dzierszinski et al., 1999), a stage-specific enolase-1, catalyzing the conversion of 2-phosphoglycerate to phosphoenolpyruvate, was identified (Manger et al., 1998; Yahiaoui et al., 1999). In previous studies glycolytic enzymes (Weiss and Kim, 2000) like LDH2 (Al-Anouti et al., 2004) of bradyzoites were shown to be resistant to acidic pH. This resistance is consistent with bradyzoite energy metabolism building on the catabolism of amylopectin to lactate and suggests bradyzoites to be resistant to acidification resulting from the aggregation of these glycolytic products (Denton et al., 1996). The glycolytic shift in bradyzoites is further supported by biochemical analyses of active enzymes in tachyzoite and bradyzoite lysates (Denton et al., 1996).

Together, data indicate a major shift of the carbohydrate metabolism and an important role of glycolysis in bradyzoites. However, the relevance of mitochondrial and amino acid metabolism remains unclear. Bradyzoite formation is induced by several electron transport inhibitors, including atovaquone, rotenone, oligomycin and antimycin (Boothroyd et al., 1997; Ferreira da Silva Mda et al., 2008; Tomavo and Boothroyd, 1995). Moreover, *T. gondii* cysts survive extended atovaquone exposure *in vivo* (Araujo et al., 1992; Ferguson et al., 1994b), indicating that their mitochondrial electron transport chain (mETC) may not strictly be essential. Similarly, bradyzoites can also be induced by limiting supply of exogenous amino acids (Ferreira da Silva Mda et al., 2008), and their viability depends on proteolysis in their plant-like vacuolar compartment (Di Cristina et al., 2017) and on autophagy (Smith et al., 2021). This indicates a substantial remodeling of metabolic homeostasis in bradyzoites as a strategy to cope with nutrient limitations (Lüder and Rahman, 2017).

1.1.2.5 Developing resistances and tolerances

Encysted bradyzoites develop resistance to digestion by gastric juices (Jacobs et al., 1960), they can escape the host immune system and cannot be eliminated with available therapeutic interventions (Antczak et al., 2016). The underlying persistence mechanisms are largely unknown, and it remains unclear in which weighting the cyst wall or the bradyzoites themselves contribute to persistence.

As expected from their oral infectivity, bradyzoites are inherently resistant to pepsin and acidic pH even after degradation of the cyst wall. In contrast, they are susceptible to osmotic stress and freezing (Jacobs et al., 1960). Resistance to the immunological response of the host is presumed to be ensured by unique antigens and metabolism of encysted bradyzoites (Weiss and Kim, 2000). Additionally, the cyst wall may limit antigen presentation to the host contributing to the persistence of this intracellular parasite (Weiss and Kim, 2000). The determinants underlying drug tolerance of tissue cysts is not well understood and may be multifactorial. On the one hand, there is the cyst wall which may act as a physical and diffusion barrier that excludes pharmacological compounds from the cyst lumen and thus prohibits these to interact with bradyzoites (Acquarone, 2017). Studies using fluorescent tracer molecules indicate that compounds up to 40 kDa can pass the cyst wall (Lemgruber et al., 2011). Hence, the ability to pass the cyst wall appears to be dependent on size besides polarity or the availability of transporters. On the other hand, bradyzoites themselves were long thought to be a difficult target as their metabolically quiescence likely implies vulnerabilities that cannot be extrapolated from pathways that are critical to proliferating tachyzoites. In addition, the pronounced phenotypic heterogeneity of bradyzoites may also underly the drug tolerance. The ability of clonal microbial populations to survive antibiotic treatments is often a consequence

of phenotypic heterogeneity due to various factors. Sources of this heterogeneity include intrinsic noise during gene expression (Elowitz et al., 2002), differential cell age and cell cycle states (Sumner et al., 2003), a diversity of the metabolome (Balaban et al., 2004) and flux states (van Heerden et al., 2014). These phenotypic traits underlie stress resistance mechanisms and have been linked to resistance against copper (Sumner et al., 2003), antibiotics (Balaban et al., 2004) and carbon source utilization (van Heerden et al., 2014), respectively. Phenotypic variation in parasitic protozoans is much less researched. Antigenic variation is an established example and a major determinant of pathogenicity. *Plasmodium*, *Trypanosoma* and potentially *T. gondii* parasites vary their antigens as an immune evasion mechanism based on mutations and transcriptional regulation (Guizetti and Scherf, 2013; Morrison et al., 2009; Xue et al., 2020). In general, heterogeneity has been identified as a microbial bet-hedging strategy that allows the survival under potentially catastrophic environmental changes (Grimbergen et al., 2015)

1.2 Triggers and *in vitro* models for bradyzoite formation and cystogenesis

The "gold standard" to work with mature encysted bradyzoites up to now remains the *in vivo* mouse model. Nevertheless, studies in animal models are limited due to various factors which led to the establishment of manifold *in vitro* models for bradyzoite induction.

It is well documented that conversion to the latent stage is a stress-mediated response, coupled with a slowing of the parasite cell cycle (Jerome et al., 1998). However, the molecular factors that drive differentiation largely remain unknown, but are considered to encompass both parasite and host cell factors. A myb-like transcription factor, named bradyzoite-formation deficient 1, acts as the master regulator of differentiation (Waldman et al., 2020). Bradyzoite formation-deficient 1 appears essential for differentiation in HFF cells and during mouse infections. It is induced under stress conditions and regulates differentiation by binding to promoters of other stage-specific transcription factors such as the Apicomplexan apetala 2 family (Waldman et al., 2020).

1.2.1 Stress-induced tissue cyst formation

Formation of encysted bradyzoites represents a stress response of *T. gondii* and hence various stress factors are used by current protocols for *in vitro* generation of bradyzoites. Established protocols for stress induced *in vitro* formation of bradyzoites are listed in **Table 1**. It is noteworthy these studies report the use of bradyzoite cultures that are generally not older than two or in rare cases three (Di Cristina et al., 2017; Fox et al., 2004) weeks. Furthermore, most of these studies do not state the purity of their bradyzoite culture.

Triggers and *in vitro* models for bradyzoite formation and cystogenesis

Table 1: *In vitro* models for stress-induced tissue cyst formation. Summarized are respective stressors, host cell background, parasite strain, the applied assays, and markers for validation of tachyzoite to bradyzoite conversion, the purity of bradyzoite cultures, cultivation time, grade of maturation and selected reference. *End of assay due to host cell lysis; **additionally alkaline pH was applied. HFF: human fibroblasts IFA: immunofluorescence assay; WB: western blot; qPCR: real-time polymerase chain reaction; SAG: surface antigen, BAG: bradyzoite antigen, ENO: enolase; LDH: lactate dehydrogenase; GRA: dense granule protein; DBA: *Dolichos biflorus* agglutinin; DBL: *Dolichos biflorus* lectin; PM: peritoneal macrophages BMM: bone marrow-derived macrophages; CHO: Chinese hamster ovaries.

Stress	Host	Strain	Assay and marker	Tachyzoites	Cultivation	Stage conversion	Reference
Alkaline pH							
Continious							
pH 8.0	HFF, Vero	RH	IFA: P36, P34, P18, P21, P30	yes	<7 days*	Bradyzoites, cyst-like vacuoles	(Soête et al., 1994)
pH 8.1	HFF	ME49	IFA: P36/P21; transcriptome	No data	8 days	Bradyzoites, cyst-like vacuoles	(Manger et al., 1998)
	Vero	ME49	IFA/ WB: SAG1, BAG1	No data	10 days	Bradyzoites, cyst-like vacuoles	(Lei et al., 2005)
pH 8.2	HFF	GT1, ME49, CTG, MAS, CAST, COUG, GPHT, FOU	IFA: BAG1, CST1, DBL, SAG1; qPCR: BAG1, SAG1, SAG2A, LDH2	No data	Up to 9 days	Bradyzoites, cyst-like vacuoles	(Fux et al., 2007)
pH 8.2	HFF	RH, ME49	qPCR: BAG1, ENO1, LDH2	yes	6 days*	Bradyzoites	(Galizi et al., 2013)
	HFF	ME49	IFA/ WB: BAG-1, SAG1, GRA5	yes	4 days	Bradyzoites, cyst-like vacuoles	(Weiss et al., 1995)
	HFF	VEG	Transcriptome	No data	3 days	Describes as mature in regard to transcriptomics	(Radke et al., 2005)
Preexposure	HFF	PRU	IFA: LDH2-dependent GFP expression	yes	Up to 21 days	Bradyzoites	(Di Cristina et al., 2017)
pH 8.1	HFF	RH	IFA: GRA1, SAG1, BAG1; WB: BAG1	No data	3 days	No induction	(Weiss et al., 1998)
pH 8.1	HFF	ME49	IFA: GRA1, SAG1, BAG1; WB: BAG1	No data	3 days	Bradyzoites, cyst-like vacuoles	(Weiss et al., 1998)
Acidic							
Continious							
pH 6.8	HFF	ME49	IFA / WB: BAG-1, SAG1, GRA5	yes	4 days	Bradyzoites, cyst-like	(Soête et al., 1994)
pH 8.8-7.0	HFF, Vero	RH	IFA: P36, P34, P18, P21, P30	yes	<7 days*	No induction	(Weiss et al., 1995)

Stress	Host	Strain	Assay and marker	Tachyzoites	Cultivation	Stage conversion	Reference
Immunomodulators							
Interferon gamma	Murine PM	NTE	IFA: BAG1 (4F8)	yes	6 days	Bradyzoites	(Bohne et al., 1993)
	Murine BMM Mφ	NTE	IFA: BAG1 (4F8, 7E5)	yes	6 days	Bradyzoites	(Bohne et al., 1994)
	HFF	RH	IFA: P36, P34, P18, P21, P30	yes	2 days	No induction	(Soête et al., 1994)
	HFF	ME49	IFA / WB: BAG-1, SAG1, GRA5	yes	4 days	No induction	(Weiss et al., 1995)
	Rat neurons, astrocytes, microglia	NTE	IFA: DC11	yes	4 days	No induction	(Lüder et al., 1999)
	HFF	VEG	IFA: BAG1, DBA; WB: BAG1; qPCR: BAG1, LDH2	yes	3 days	No induction	(Radke et al., 2006)
Nitric oxygen	Murine Mφ	NTE	IFA: BAG1 (4F8, 7E5)	No data	6 days	Bradyzoites	(Bohne et al., 1994)
	Rat neurons, astrocytes	NTE	IFA: DC11	yes	4 days	No induction	(Lüder et al., 1999)
	Rat neurons, microglia	NTE	IFA: DC11	yes	4 days	Bradyzoites	(Lüder et al., 1999)
	HFF	PLK, ME49	IFA: DBA	yes	3 days	Cyst-like vacuoles	(Kirkman et al., 2001)
IL6	HFF	ME49	IFA / WB: BAG-1, SAG1, GRA5	yes	4 days	Bradyzoites, cyst-like vacuoles (free floating)	(Weiss et al., 1995)
LPS	Murine BMM Mφ	NTE	IFA: BAG1 (4F8, 7E5)	yes	6 days	Bradyzoites	(Bohne et al., 1994)

Stress	Host	Strain	Assay and marker	Tachyzoites	Cultivation	Stage conversion	Reference
Chemicals							
Pyrimethamine	Murine BMM MΦ	NTE	IFA: BAG1 (4F8, 7E5)	yes	6 days	Bradyzoites	(Bohne et al., 1994)
	HFF	PRU	IFA: P36 qPCR: 42.m03416,20.m00351	No data	3 days	Bradyzoites, cyst-like vacuoles	(Maubon et al., 2010)
Myxothiazol, rotenone, antimycin, atovaquone (+/- mtDNA)	Vero, HFF	PLK	WB: SAG1, P18, P36	No data	60 h	Bradyzoites	(Tomavo and Boothroyd, 1995)
Atovaquone	LLLC-MK2	RH	IFA: SAG1, DBA	yes	6 days*	Cyst-like vacuoles	(de Lima et al., 2015)
Oligomycin, antimycin A (+/- mtDNA)	Murine BMM MΦ, HFF	NTE	IFA: BAG1 (4F8, 7E5)	yes	6 days	Bradyzoites	(Bohne et al., 1994)
Indomethacin	HFF	ME49	IFA: GRA1, SAG1, BAG1: WB: BAG1	No data	3 days	Bradyzoites, cyst-like vacuoles	(Weiss et al., 1998)
Quercetin	HFF	ME49	IFA: GRA1, SAG1, BAG1; WB: BAG1	No data	3 days	No induction	(Weiss et al., 1998)
Compound 1	HFF	ME49, VEG	IFA: BAG1, DBA WB: BAG1 qPCR: BAG1, LDH2	yes	3 days	Bradyzoites, cyst-like vacuoles	(Radke et al., 2006)
	HFF	RH, GT1	IFA: BAG1, DBA: WB: BAG1 qPCR: BAG1, LDH2	yes	3 days	No to weak induction	(Radke et al., 2006)
	HFF	RH	IFA: SAG1, P36, DBA	yes	7 days	Bradyzoites, cyst-like vacuoles	(Nare et al., 2002)
	HFF	ME49	Reporter strain: beta-GAL expression under BAG1 promoter	yes	3 days	Bradyzoites, cyst-like vacuoles	(Eaton et al., 2006)
3-Bromopyruvate	LLLC-MK2	RH	IFA: SAG1, DBA	yes	6 days*	Cyst-like vacuoles	(de Lima et al., 2015)
Sodium arsenite	Vero, HFF	RH	IFA: P36, P34, P18, P21, P30	yes	2 days	Bradyzoites, no cyst-like vacuoles	(Soête et al., 1994)
Cadmium	Vero	RH	IFA: P36, P34, P18, P21, P30	yes	2 days	No induction	(Soête et al., 1994)
FR235222	HFF	PRU, RH	IFA: P36; qPCR: 42.m03416, 20.m00351;	yes	3 days	Cyst-like vacuoles	(Bougduor et al., 2009)
Tunicamycin	HFF	PRU	IFA: DBL qPCR: BAG1, LDH2	yes	3 days	Bradyzoites, cyst-like vacuoles	(Narasimhan et al., 2008)

Stress	Host	Strain	Assay and marker	Tachyzoites	Cultivation	Stage conversion	Reference
Cyclic nucleotide signaling modulators							
CPT-cAMP, IBMX, forskolin–IBMX	HFF	PLK, ME49	IFA: DBA	yes	3 days*	No induction	(Kirkman et al., 2001)
CPT-cGMP, forskolin	HFF	PLK, ME49	IFA: DBA	yes	3 days	Cyst-like vacuoles	(Kirkman et al., 2001)
H-89	HFF	PLK, ME49	Reporter strain: beta-GAL expression under BAG1 promotor	yes	3 days	Bradyzoites	(Eaton et al., 2006)
Heat shock							
43°C	Vero	RH	IFA: P36, P34, P18, P21, P30	yes	<7 days*	Bradyzoites, cyst-like vacuoles	(Soête et al., 1994)
Nutrients							
Arginine starvation	HFFs	RH, ME49	IFA: DBA, SAG1	yes	21 days	Bradyzoites, cyst-like vacuoles	(Fox et al., 2004)
Pyrimidine deprivation (Δuprt)	HFFs	RHΔuprt	IFA: BAG1	yes	4 days	Bradyzoites	(Bohne and Roos, 1997)
Pyrimidine deprivation (0.03% CO₂)	HFFs	PRU	IFA: BAG1, DBA, SAG1	yes	14 days	Bradyzoites, cyst-like vacuoles	(Dzierszinski et al., 2004)
Cholesterol deprivation	CHO, HFF	ME49	IFA: BAG1, SAG1	yes	3 days	Bradyzoites	(Ihara and Nishikawa, 2014)
Adenosine **	Astrocytes (CD73-/-)	ME49	IFA: SAG1, BAG1, DBA; qPCR: SAG1, BAG1, ENO1;	yes	8 days	Bradyzoites, cyst-like vacuoles	(Mahamed et al., 2012)

28

1.2.1.1 pH stress

The most robust and therefore most used *in vitro* method for tissue cyst induction, is the cultivation at alkaline pH 8.0-8.2 in Vero or HFF cells. Since continuous exposure to alkaline pH leads to frequently and consistent formation of encysted bradyzoites, this model is widely used as control for other cyst inducing methods. In most studies, cultures are incubated in HEPES-buffered medium and without the use of CO_2 to keep the pH consistent throughout the experiment. This works for cystogenic strains (Di Cristina et al., 2017; Fux et al., 2007; Galizi et al., 2013; Lei et al., 2005; Manger et al., 1998; Radke et al., 2005; Weiss et al., 1995) and to a limited extent also for the laboratory type I strain (Soête et al., 1994). Immunofluorescence assay with a type II strain confirmed that single parasites started to express BAG1 while losing the tachyzoite SAG1 antigen after 3-4 days of cyst induction. Electron microscopy revealed a cyst-like morphology of these parasites (Weiss et al., 1995). However, cultivation time is limited since host cell viability is severely decreased by alkaline pH.

Interestingly, stage conversion of cystogenic type II, but not type I strain, can also be induced by exposing extracellular tachyzoites to alkaline pH for 1 h and subsequent cultivation in host cells under physiological pH (Weiss et al., 1998). This system ensures a favorable environment for the host cell compared to alkaline pH, but stage conversion is less pronounced compared to continuous alkaline conditions (Weiss et al., 1998). This shifts the limiting factor from the host tolerance of alkaline stress to host lysis though extensive tachyzoite proliferation.

Few studies report also testing of acidic pH stress (pH 6.8) on stage conversion. In type I strain this did not lead to cyst formation (Soête et al., 1994), whereas cystogenic type II parasites showed partial conversion and the expression of bradyzoite specific antigens (Weiss et al., 1998).

1.2.1.2 Immunomodulators

A broadly used strategy to induce tachyzoite to bradyzoite conversion, is the application of immunomodulators, in particular proinflammatory cytokines. The idea behind this is to imitate the stress of the immune response the parasites are exposed to in the host in *in vivo* scenario.

Particularly, interferon gamma (IFN-γ) was tested for its effects on cyst induction since it is a major factor in the inflammatory defense against *T. gondii* (Suzuki et al., 1988). IFN-γ distinctly inhibits the proliferation of tachyzoites (Bohne et al., 1993, 1994; Nathan et al., 1983; Weiss et al., 1995), but its effects on encysted bradyzoite formation remains controversial. In summary, cyst induction via IFN-γ involves a number of host cell-dependent mechanisms. Strain independent, IFN-γ leads to cyst induction in murine macrophages, but not in HFFs (Bohne et al., 1993, 1994; Radke et al., 2006; Soête et al., 1994; Weiss et al., 1995) or rat neuronal cells

(Lüder et al., 1999), presumably via triggering releases of nitric oxygen (NO), which itself is a driver of bradyzoite formation (Bohne et al., 1994). This was further underpinned by successful cyst induction of cystogenic type II strains in HFFs, murine macrophages and rat brain cells by continuous NO supplementation (Bohne et al., 1994; Kirkman et al., 2001; Lüder et al., 1999; Weiss et al., 1998).Since NO interacts with enzymes of the respiratory chain via their iron-sulfur center, the conversion of *T. gondii* might be two-fold by modulating both the parasite as well as the host cell respiratory capacities (Bohne et al., 1994; Tomavo and Boothroyd, 1995).

Interleucin-6 (IL-6), a key cytokine in the transition from mechanisms of innate immunity to mechanisms of adaptive immunity within inflammatory processes, was also tested for its impact on *in vitro* encysted bradyzoite formation. In HFFs IL-6 induced tachyzoite to bradyzoite conversion in cystogenic type II strain, but interestingly most of the cyst-like structures were not intracellular but free floating (Weiss et al., 1995). Synergistic effects of IL-6 and IFN-γ could not be shown working in the same system (Weiss et al., 1995), suggesting again the host cell specificity of IFN-γ. Since IL-6 enhances the activation of anti-inflammatory macrophages and as an effect lowers Lipopolysaccharide (LPS) or IFN-γ-dependent NO release (Fernando et al., 2014), it is assumed that there is also no synergistic effect in macrophages.

LPSs, which leads to activation of macrophages to pro-inflammatory macrophages (M1) and triggers respective signaling cascades, enhances bradyzoite formation in murine macrophages. (Bohne et al., 1994). In the same system, synergistic effects between LPS and IFN-γ exist, although the degree of macrophage activation is crucial. If macrophages were activated too far in M1 direction, the anti-inflammatory storm completely suppressed tachyzoite replication and conversion could no longer take place (Bohne et al., 1994).

Summarized, the effect of immunomodulators on bradyzoite formation and cystogenesis of *T. gondii* seems to be highly host cell- and dose-dependent since the actual induction does not only take place directly but rather indirectly via triggered inflammatory signaling cascades in the host. Furthermore, the cell types that have been demonstrated *in vitro* to promote bradyzoite development after being proinflammatory activated are by no means preferred cells in which encysted bradyzoites persist *in vivo* (Lüder and Rahman, 2017).

1.2.1.3 Chemicals

Noticeable for this part is that studies have been performed in different strains and manifold host cell backgrounds, making it difficult to correlate the respective results.

Early studies showed that stage conversion is closely related to parasite replication (Bohne et al., 1994). Broadly used chemotherapies against acute toxoplasmosis are pyrimethamine and

sulfadiazine. These agents restrict parasite replication, but also lead to tachyzoite to bradyzoite formation in cystogenic strains (Bohne et al., 1994; Maubon et al., 2010). However, it is suggested that these conditions do not enhance the switching rate from tachyzoites to bradyzoites, but rather enrich spontaneously forming cysts by preventing tachyzoite overgrowth of the culture (Murata et al., 2017; Weiss et al., 1998).

In contrast, mETC inhibitors, such as atovaquone, enhance bradyzoite antigen expression and the formation of cyst-like structures (Bohne et al., 1994; de Lima et al., 2015; Tomavo and Boothroyd, 1995). Experiments with mETC inhibitors in an HFF cell line with a nonfunctional mETC revealed inhibition of parasite mitochondrial function as a trigger of stage conversion (Bohne et al., 1994; Tomavo and Boothroyd, 1995). In line with this, *in vivo* studies showed that treatment with atovaquone results in a significant reduction of cyst burden in mice brains, but not complete clearance (Araujo et al., 1992). Ultrastructural investigations of an atovaquone-treated type II strain underpinned the suggestion that the mETC is not strictly essential in mature bradyzoites (Ferguson et al., 1994b). In addition to mETC inhibitors, functional modulation of heat shock proteins (HSPs) suing quercetin and indomethacin can repress and induce cystogenesis (Weiss et al., 1998). Inhibition of HSP72 (belonging to HSP70 family) (Weiss et al., 1998) and HSP90 by quercetin decreased the efficiency of bradyzoite formation *in vitro*. Nevertheless, expression data of HSP70 as well as pharmacological inhibition of HSP90 suggests these HSPs also be involved in bradyzoite to tachyzoite development (Echeverria et al., 2005). This data indicates that HSPs do not play a key role in tachyzoite to bradyzoite formation. Since HSP70 and HSP90 function as chaperones (Shonhai et al., 2011; Weiss et al., 1998), it is likely that these HSPs are important for maintaining protein structure and may indirectly have a role by alleviating intracellular stress during the stage conversion of *T. gondii*.

Compound I, a trisubstituted pyrole, displays a potent anti-tachyzoidal effect and also induces cystogenesis and bradyzoite formation in cystogenic, but only inconsistently in non-cystogenic strains (Eaton et al., 2006; Nare et al., 2002; Radke et al., 2006). Interestingly, in this scenario bradyzoite formation is dependent on the expression of cell division autoantigen-1 by the host cells. This demonstrated for the first time that a drug acts and modulates the host cell transcription and that this directly impacts the differentiation behavior of *T. gondii*. Lately 3-bromopyruvate, an antimetabolite that blocks glycolysis in tumor cells (Pedersen, 2012), was shown to partially enhance the formation of cyst-like structures in non-cystogenic type I strain (de Lima et al., 2015). *In vitro* in Vero and HFF cells, highly glycolytic activity of host cells could be correlated with the inhibition of bradyzoite formation under stress conditions (Lüder and Rahman, 2017; Weilhammer et al., 2012). Hence, applying 3-bromopyruvate might act on the

metabolic state of the host cell and therefore create preferential conditions to switch from the tachyzoite to the bradyzoite state. However, these observations *in vitro* are somehow contrary to the findings that tachyzoite to bradyzoite conversion is highly induced in muscle and neuronal tissue which itself offer a highly glycolytic environment (Malinska et al., 2012).

Not only anti-*T. gondii* compounds were studied for their influence on stage conversion, but also different chemical compounds, e.g., sodium arsenite or cadmium. Whereas cadmium showed no induction, sodium arsenite induced expression of bradyzoite genes in non-cystogenic type I strain, but not cyst formation (Soête et al., 1994). This revealed for the first time the independent uncoupled development of cystogenesis and bradyzoite formation, suggesting the formation of matured encysted bradyzoites underlies more than one checkpoint. Another family of inhibitors which underpinned these suggestions are the histone deacetylase inhibitors including FR235222. FR235222 does not inhibit tachyzoite proliferation but sufficiently induces cyst formation in type I and type II strain without the expression of bradyzoite specific genes (Bougdour et al., 2009; Maubon et al., 2010). This pointed towards cystogenesis also being regulated on an epigenetic level.

Treatment with tunicamycin, a mixture of homologous nucleoside antibiotics, and the caused endoplasmic reticulum stress led to induced cystogenesis and expression of bradyzoite specific antigens in type II strain cultured in HFF cells (Narasimhan et al., 2008). This finding revealed translation initiation factor 2-α-phosphorylation to play a role in tachyzoite to bradyzoite formation.

1.2.1.4 Cyclic nucleotides

Cyclic nucleotides are important second messengers and hold manifold functions. In *Plasmodium falciparum* cyclic nucleotides are implicated in gametocyte formation (Read and Mikkelsen, 1991). In *T. gondii* cyclic nucleotides are implicated in the lytic cycle and bradyzoite differentiation (Brown and Sibley, 2018; Eaton et al., 2006; Kirkman et al., 2001; Sugi et al., 2016).

Exogenous host cell cyclic adenosine monophosphate (cAMP) impacts stage conversion as exposure of HFF cells to forskolin increased levels of cAMP were detected and fostered cyst conversion (Kirkman et al., 2001). Transient elevation of cAMP leads to enhanced cyst-like bradyzoites in cystogenic type II strains. In contrast, permanent exposure suppressed this stage conversion (Kirkman et al., 2001; Eaton et al., 2006; Sugi et al., 2016). Additionally, pharmacological modulation of downstream cAMP- and cyclic guanosine monophosphate (cGMP)-dependent protein kinases enhanced tachyzoite to bradyzoite conversion (Kirkman et al., 2001). cAMP-signaling has a bidirectional effect on parasite replication involving different

protein kinases (Sugi et al., 2016). Continuous elevation of cGMP promotes bradyzoite formation (Kirkman et al., 2001). However, the precise role of cGMP in *T. gondii* bradyzoite differentiation still needs to be determined since cGMP controls cAMP levels in parasites suggesting that effects of cGMP are indirect via the modulation of cAMP level (Kirkman et al., 2001).

1.2.1.5 Heat shock

Immune responses to *T. gondii* infection involve fever. Interestingly, exposure to high temperatures lead to stage conversion of *T. gondii* non-cystogenic type I strain (Soête et al., 1994). Converted bradyzoites established a cyst wall and expressed early bradyzoite specific markers (Soête et al., 1994). The mechanism remains unclear, but heat shock- or stress-induced activation of a set of HSPs may be involved (Weiss et al., 1998). Among HSP30 (BAG1), several HSPs are induced during differentiation. However, knock-out studies revealed that BAG1 appears non-essential for the differentiation process *in vitro* and *in vivo* (Bohne et al., 1998). Furthermore, heat shock is not the preferred method to induce stage conversion since it is accompanied with decreased host cell viability, inhibited parasite survival and invasion (Soête et al., 1994).

1.2.1.6 Nutrient stress

Fast replicative tachyzoites and encysted slowly dividing bradyzoites demand distinct amounts of nutrients from their environment. As an obligate intracellular parasite, *T. gondii* lacks many enzymes for the *de novo* synthesis of molecules and is therefore dependent on scavenging required nutrients from the host cell. Limiting the availability of some of these essential nutrients exerts nutrient stress and favors stage conversion.

T. gondii is arginine auxotroph and starvation of this amino acid leads to decreased replication, but stable viability of parasites. Furthermore, consistent conversion of tachyzoites to encysted bradyzoite which lose SAG1 marker over time was achieved up to three weeks in both non-cystogenic type I as well as in cystogenic type II strains (Fox et al., 2004).

T. gondii is capable of *de novo* synthesis and salvage of pyrimidines (Schwartzman and Pfefferkorn, 1981). The pyrimidine salvage pathway involves the uracil phosphoribosyltransferase (*uprt*) gene and CO_2 is required for the synthesis of the pyrimidine ring. Blocking pyrimidine supply pathways by knocking out the uracil phosphoribosyltransferase (Δ*uprt*) and culture at ambient CO_2 concentration (0.03 %) triggers bradyzoite formation in type I and type II parasites (Bohne and Roos, 1997; Dzierszinski et al., 2004). The mechanism likely involves depletion of uridine monophosphate-levels and subsequently limiting proliferation rates of the parasites. Consistently, providing exogenous

uridine, which is a precursor of uridine monophosphate, abrogated cyst formation of CO_2 limited parasites *in vitro* (Weilhammer et al., 2012).

T. gondii salvages low-density lipoprotein-derived cholesterol from its host. Interestingly, the depletion of low-density lipoprotein-bound cholesterol led to the formation of encysted bradyzoites working with cystogenic type II strain (Ihara and Nishikawa, 2014).

T. gondii relies on import of purines from its host and differentiates preferentially in neuronal tissue. In brain tissue of mice, the availability of free adenosine depends on CD73. In CD73$^{-/-}$ mice, type II parasites established a very low cyst burden (Mahamed et al., 2012). Consistently, *in vitro*, adenosine supplementation rescued tissue cyst formation in CD73-deficient astrocytes and enhanced tissue cyst formation in other cell types under CO_2-limiting conditions (Mahamed et al., 2012; Weilhammer et al., 2012).

These findings suggest that the switch from metabolic active tachyzoites to metabolic less active bradyzoites presents a coping mechanism against nutrient stress. In contrast to this stands the adenosine-triggered formation of encysted bradyzoites. However, whether the encysted form of *T. gondii* has an unexpected high demand on adenosine or whether adenosine acts as a messenger molecule remains to be elucidated further.

1.2.2 Spontaneous stage conversion

External stressors facilitate *T. gondii* stage conversion and respective protocols are useful to investigate early events of bradyzoite formation and cystogenesis. Noteworthy, these experimental environments do likely not reflect the conditions that induce stage conversion *in vivo*. However, the diversity of stress factors that induce bradyzoites indicate that stage conversion may represent a general stress response that can be triggered through many pathways. The occurrence of spontaneous stage conversion at low rates in absence of external triggers is frequently observed in diverse primary and cell line-derived myotubes (Ferreira-da-Silva Mda et al., 2009a; Ferreira-da-Silva Mda et al., 2009b; Swierzy and Lüder, 2015) but also to a lesser extend in HFF and Vero cells (Soête and Dubremetz, 1996; Weiss et al., 1995). However, without a permanent exogenous trigger, stage conversion remains either incomplete and *T. gondii* or tissue cysts re-differentiate. Both factors result in replicating tachyzoites that cause extensive host cell lysis.

Interestingly, encysted bradyzoites are mostly found in brain and muscle tissue of infected animals (Remington and Cavanaugh, 1965). These cells appear to offer a microenvironment which is particularly suitable to promote stage conversion (Ferreira-da-Silva Mda et al., 2009a; Ferreira-da-Silva Mda et al., 2009b; Swierzy and Lüder, 2015). In addition, these tissues may

represent immune-privileged niches that allow for long-term persistence of the tissue cysts (Streilein, 1995; Swierzy and Lüder, 2015; Wiendl et al., 2005). Neurons, but not glia cells, are primary hosts for tissue cysts *in vivo* (Cabral et al., 2016; Ferguson and Hutchison, 1987a, b) and interestingly, this is reflected by higher spontaneous differentiation rates *in vitro* in neurons in comparison to microglia or astrocytes (Creuzet et al., 1997; Lüder et al., 1999). Additionally, astrocytes, but not neurons are capable to kill *T. gondii* in an IFN-γ dependent fashion (Halonen et al., 2001; Peterson et al., 1995; Schlüter et al., 2001). Hence a suitable microenvironment for cyst formation and favorable immune responses may contribute to the preferential persistence of *T. gondii* cysts in neurons.

As stated above, muscle tissue is the second type of tissue in which bradyzoites persist in the intermediate host. Like neurons, murine myotubes support spontaneous stage conversion (Ferreira da Silva et al., 2008a; Ferreira da Silva et al., 2008b; Ferreira da Silva et al., 2009; Swierzy et al., 2015). Transcriptomic comparison of C2C12 myotubes with their C2C12 precursor myoblasts, which do not support spontaneous differentiation, indicated that the cell cycle regulator CDA-1/Tspyl2, the cell cycle inhibitor p21$^{Waf1/Cip1}$ and a lack of cyclin B1 may be responsible for a G1 cell cycle arrest in myotubes (Swierzy and Lüder, 2015). This cell cycle withdrawal correlated with the rates of stage conversion of *T. gondii* in myotubes (Swierzy and Lüder, 2015). Consistently, a human CDA-1/Tspyl2 homolog is induced by Compound 1 in HFF cells and found to be required for stage conversion inducing activity of this compound (Radke et al., 2006).

Summarized, both myotubes and neurons are post-mitotic cell types as they cannot reenter the productive cell cycle (Deneris and Hobert, 2014; Frade and Ovejero-Benito, 2015; Walsh and Perlman, 1997). These long-living cell types may provide a perfect environment for long-living *T. gondii* tissue cysts. It remains to be established if and how known inducers of stage conversion such as pH and nutrient stress are associated with elevated stage conversion in particular cell types. In addition, reduced immune responses may further facilitate long-term survival of *T. gondii* in certain types of host cells (Lüder and Rahman, 2017).

1.2.3 Bottlenecks of current protocols

1.2.3.1 *In vivo*

Current methods to experimentally generate mature *T. gondii* tissue cysts are confined to murine infections with cystogenic *T. gondii* strains (Ferguson and Hutchison, 1987a, b; Watts et al., 2015). So far, the murine infection model is the "gold standard" for the generation of matured tissue cysts. However, this method is clearly limited in some respects. For some studies, e.g., metabolomics, large quantities of encysted bradyzoites are needed and it is

difficult to obtain large amount of tissue cysts with not using too many animals. This leads to ethical and financial limitations. Also, the purification procedure via percoll or dextran of brain cysts includes many steps and detergents and is therefore not compatible with metabolic measurements. Furthermore, the animal model also serves a limited ability to control and modulate multiple parameters throughout the experiment. Studies on *ex vivo* cysts are in general endpoint assays, i.e., it remains impossible to investigate driving factors during the infection or host-parasite interaction. Additionally, infection experiments and the impact of drugs is generally conferred to the number of brain cysts. That approach is not suitable for research into drugs that cannot cross the blood-brain barrier, although such drugs are of great importance for a zoonotic pathogen such as *T. gondii*.

1.2.3.2 *In vitro*

Current *in vitro* models for the generation of *T. gondii* tissue cysts are scalable but fail to enable the generation and long-term culture of fully matured tissue cysts. They are suitable to investigate the early stages of the transition from tachyzoite to bradyzoites and to explore potential pathways associated with early bradyzoite development. Medium-length culture is only facilitated in systems using alkaline pH as an artificial stressor, leading to a highly artificial system remotely not comparable to *in vivo* situation. Generally, maturation times of *in vitro*-cysts remain brief, but cysts develop detectable tolerance against short exposure to low doses of pyrimethamine after three days (Murata et al., 2017) and become orally infectious to mice at high doses after five days of culture (Fux et al., 2007). However, establishment of long-term cultures that allow development of pure pan-antimicrobial- and temperature stress-tolerant cysts (Dubey et al., 1990; Dunay et al., 2018) remains a challenge. Incomplete differentiation leads to expansion of proliferating parasite populations and subsequent host cell lysis that limits the scale and duration of current *in vitro* culture systems.

1.3 Fatty acid metabolism in *Toxoplasma gondii* and mammalian cells

Since *T. gondii* is an obligate intracellular parasite, parasite-host interaction is critical for this pathogen. Taking our generated metabolomic data into account, we focused on lipid metabolism. Lipid metabolism including fatty acid (FA) availability possesses critical functions in most organisms and is of crucial importance for pathogens. FA form the main component of membranes and thus represent a fundamental building block of cells. They serve as energy-storing molecules, play an important role in the post-translational modification of numerous proteins and act as pathogenesis factors.

1.3.1 *Toxoplasma gondii*

So far, investigations of the lipid inventory of *T. gondii* revealed that the pathogen evolved different main mechanisms to satisfy its FA needs (Ramakrishnan et al., 2013). FA can be scavenged from the host, they can be synthesized in large amounts by the parasite itself or they are produced *de novo* using mostly scavenged precursors (Martins-Duarte É et al., 2016; Mazumdar et al., 2006; Ramakrishnan et al., 2012). The dynamics of these pathways are suggested to differ dramatically between the different stages of *T. gondii* (Ramakrishnan et al., 2013). The parasite can synthesize FA via three distinct biochemical pathways: cytosolic FA synthetic pathway I (FAS I) (Harwood, 1996), FA synthetic pathway II (FASII) located in the apicoplast (Waller et al., 1998) and FA elongation (FAE) in the endoplasmic reticulum (ER) (Martins-Duarte É et al., 2016) (**Figure 4**).
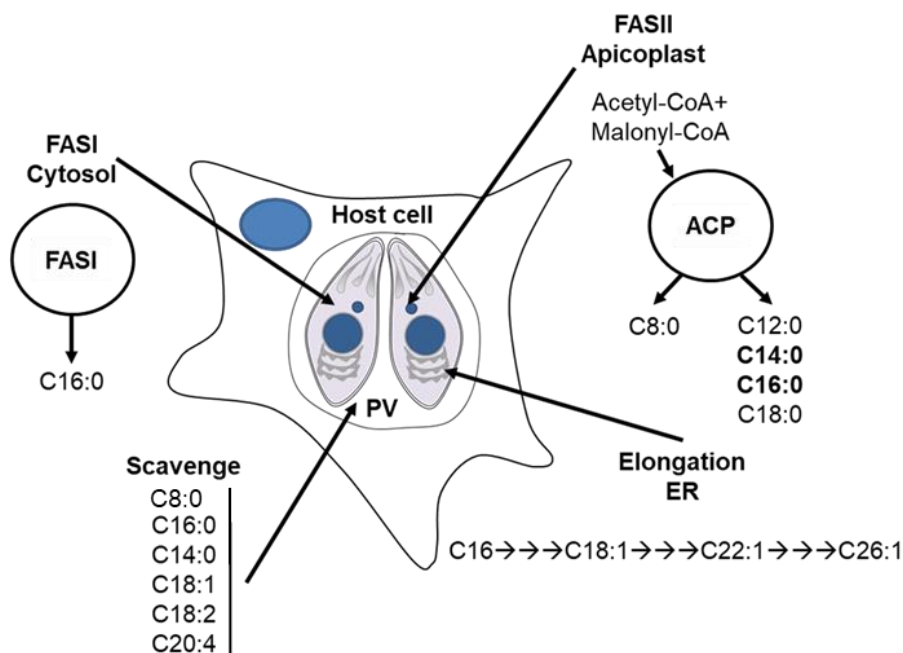
Figure 4: Fatty acid uptake and synthesis in *T. gondii*. FAS: fatty acid synthesis pathway; PV: parasitophorous vacuole; ACP: acyl carrier protein; ER: endoplasmic reticulum (Figure modified from Coppens, 2014).

Introduction
Fatty acid metabolism in *Toxoplasma gondii* and mammalian cells

Cytoplasmic FASI and apicoplast located FASII are responsible for *de novo* synthesis of FAs by a series of decarboxylative reactions from acetyl-CoA and malonyl-CoA bound to the acyl carrier protein (ACP) (Ramakrishnan et al., 2013). FASI consists of a single large polypeptide and can be found in vertebrates and fungi, but also in various protozoan parasites. Besides *de novo* synthesis, the Apicomplexan FASI appears to be mainly involved in long-chain FA elongation (Zhu et al., 2004; Zhu et al., 2010). The bulk product of FASI is palmitic acid (C16:0). During FASII elongation cycles, dodecanoic acid (C12:0) and stearic acid (C18:0), but mainly myristic acid (C14:0) and palmitic acid (C16:0) are generated (Mazumdar et al., 2006; Ramakrishnan et al., 2012). FASII is central for *de novo* synthesis of short-chain lipoic acid (C8:0), which is required as cofactor for manifold dehydrogenase complexes. Since FASII-synthesized lipoic acid cannot reach other organelles e.g. mitochondria, it is also scavenged from the host (Crawford et al., 2006). FASII is suggested to be essential in the tachyzoite stage since it provides the major parts of FAs used for membrane lipid classes (Amiar et al., 2016; Mazumdar et al., 2006; Ramakrishnan et al., 2012; Sidik et al., 2016). Carbon labeling studies revealed that major FAs synthesized in the apicoplast are subsequently shuttled to the ER and further modified (Ramakrishnan et al., 2012). During FAE in the ER, long-chain monounsaturated FAs (18:1, 22:1, 26:1) are formed from saturated FAs like myristic and palmitic acid (Ramakrishnan et al., 2012). The FAs required for this were either scavenged from the host or produced by *de novo* FA synthesis of type I or II.

Besides the existing biosynthetic pathways, *T. gondii* scavenges selected FAs from its host including linoleic acid (C18:2) and arachidonic acid (C20:4) which cannot be synthesized by the parasite (Quittnat et al., 2004; Tomavo et al., 1989). The parasite demands these exogenous FAs to generate membrane phospholipids and to sustain survival (Amiar et al., 2016). Whereas FA import in mammalian cells is orchestrated by protein- and non-protein-mediated mechanisms (Schaffer, 2002), the mechanisms of FA import in *T. gondii* are largely unknown. One described mechanism of non-directional passive transport of small nutrients is a molecular pore in the PVM (Blume and Seeber, 2018). Besides this pore, an intravacuolar membranous tubulovesicular network has been identified to take part in the uptake of host proteins and lipids (Coppens et al., 2006; Dou et al., 2014; Nolan et al., 2017). Furthermore, infection with *T. gondii* leads to a global reorganization of host cell organelles (Laliberté and Carruthers, 2008). Especially the association of host cell mitochondria to the PVM of type I and type III parasites suggests a metabolic network and lipid exchange between host mitochondria and the PV (Pernas et al., 2018). These host-pathogen interactions are suggested to be mostly attributed to the competition between host organelles and pathogens for limited nutrients (Pernas et al., 2018). *T. gondii* can utilize manifold sources of host-derived FAs like FAs exogenously supplemented to the medium, FAs synthesized by the host cell or

FAs which are stored in lipid droplets (LDs) (Hu et al., 2017; Nolan et al., 2017; Nolan et al., 2018). The FAs of host LDs can either be devoured into the PV (Hu et al., 2017; Nolan et al., 2017) or liberated from triacyclglycerols by stimulating lipophagy (Pernas et al., 2018). Following lipid uptake, the parasite stores excess lipids in LDs inside the PVM which is underpinned by *T. gondii* genome encoding several enzymes for storing neutral lipids in cytoplasmic LD (Lige et al., 2013; Nishikawa et al., 2005; Sonda et al., 2001).

However, *T. gondii* cannot utilize FAs as sources of ATP. The pathogen lacks homologues encoding adipose triglyceride synthase which breaks down triacyclglycerols (Nolan et al., 2018). The parasite apparently contains the genes for most steps of lipid oxidation, but it lacks the carnitine / acylcarnitine translocase, thus a mitochondrial pathway is ambiguous (Seeber et al., 2008). In contrast to mammalian cells, *T. gondii* cannot prevent lipotoxicity of FA surplus by channeling FAs to the mitochondrial β-oxidation pathway. This goes in line with studies showing that *T. gondii* cannot control FA influx when provided in large quantities in culture medium displaying the inability of this parasite to balance synthesis, salvage, and usage of FAs. Thus, *T. gondii* is highly vulnerable towards lipid overload and connected cellular dysfunctions (Nolan et al., 2018). FAs leading to an impaired growth of *T. gondii* differ from those which impact mammalian cells. In mammalian cells saturated FAs have a strong cytotoxic effect, whereas unsaturated FAs are either non-toxic or even favorable (Gehrmann et al., 2015; Plötz et al., 2016). In contrast, in *T. gondii* saturated FAs do not impact *T. gondii* growth, whereas supplementation of unsaturated FAs like linoleic acid and especially oleic acid leads to uncontrolled lipid uptake which results in parasite membrane defects, and ultimately death (Coppens et al., 2006; Nolan et al., 2018).

1.3.2 Mammalian cells

In mammalian cells, FA homeostasis represents a balanced metabolism consisting of production processes and utilization processes. Upon lipid excess, FA break down through β-oxidation can be upregulated (Schaffer, 2002). FA β-oxidation is the process by which FAs are catabolized to produce energy and covers the oxidative breakdown of FAs to acyl-Coenzyme A (CoA) mainly in the mitochondrial matrix and in peroxisomes. Short- and medium-chain FAs can freely diffuse through the mitochondrial membrane into the mitochondrial matrix. In contrast, the mobilization of long-chain FAs depends on carnitine (**Figure 5**).
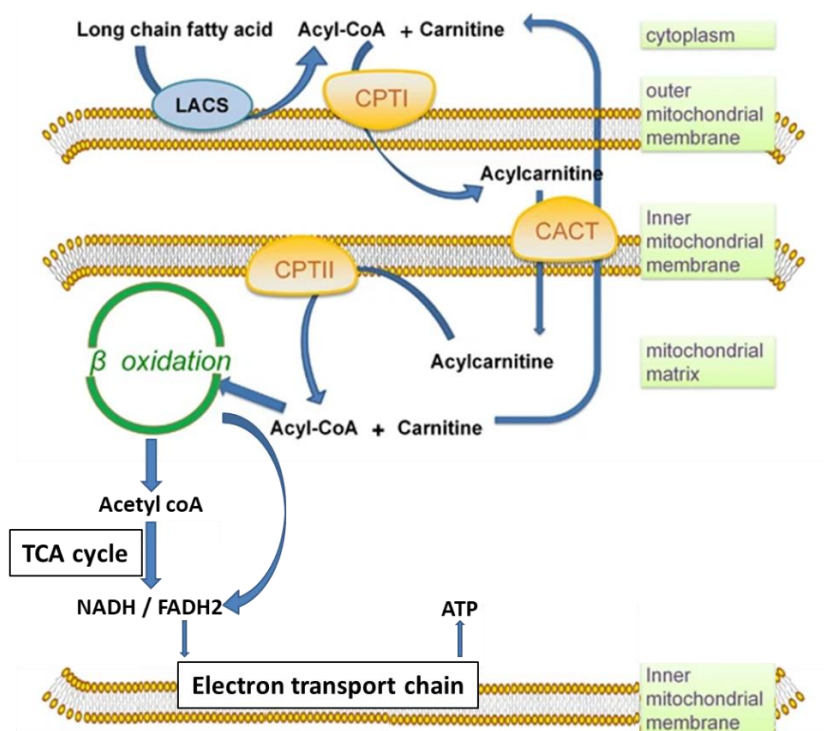
Figure 5: Mitochondrial catabolism of long-chain fatty acids in mammalian cells. LACS: long-chain acyl-Coenzyme A synthetase; CPT: carnitine palmitoyl transferase system; CACT: carnitine-acylcarnitine translocase; CoA: coenzyme A; TCA: tricarboxylic acid.

In the cytosol long-chain FAs are activated via CoA catalyzed by long-chain acyl-CoA synthetase (LACS) resulting in acyl-CoA. Subsequently, the activated FA is transported into the mitochondrial matrix via a carnitine acyltransferase system I (CPTI). The acyl residue of the acyl-CoA is transferred to carnitine via the carnitine transferase which results in acylcarnitine. The acylcarnitine is transported into the mitochondrion via the antiporter carnitine-acylcarnitine translocase (CACT) in exchange with free carnitine. The acyl residue is transferred to free CoA catalyzed by carnitine transferase II (CPTII) resulting in new acyl-CoA which is than funneled into β-oxidation. The resulting acetyl-CoA is than fed into the tricarboxylic acid (TCA) cycle and the electron carriers which are formed during oxidation, are utilized for the ATP synthesis via the respiratory chain.

1.4 Tools to study cell division on a single cell level

In contrast to tachyzoites, bradyzoites were shown to divide asynchronously and thus develop a range of cell division states in one single tissue cyst (Watts et al., 2015). These different cell division states result in highly heterogenous phenotypes and are often connected to drug treatment failure (Barrett et al., 2019). Most studies including omic-technologies still focus on the whole pathogen pool as a readout for drug susceptibility which misses the impact of heterogeneity within pathogen populations. Therefore, it is of great interest to establish a "cell division history" marker which is detectable on a single cell level. This would facilitate to correlate the presence and also the frequency of cell division events of single cells or cell population to drug susceptibility.

1.4.1 Proteins involved in cell division events

Fluorescent probes have become important for the identification and characterization of dormant persisting populations. Constitutively expressed fluorescent reporters such as enhanced green fluorescence protein, ds red variants or tandem (td) Tomato are widely used to identify and track parasites (Barrett et al., 2019). An approach to track cell division on a single cell level is the tagging of proteins implicated in cell division events. In *T. gondii* several inner membrane complexes (IMC1 / 3 / 6 / 10), were identified to be enriched in forming daughter buds during endodyogeny (Lorestani et al., 2012). IMCs are most intensely expressed in newly formed/forming daughter cells and decay in the absence of further division. The application of anti-IMC3 antibody led to the discovery of endodyogeny-based cell division events in mature *in vivo* bradyzoites for the first time (Watts et al., 2015).

However, such markers can provide information on the general presence or absence of proliferative events, but not the frequency within a period of interest. To track and to correlate the occurring division events and subsequent different marker protein expression to drug resistance, live cell imaging approaches would be needed.

1.4.2 Cell tracker

Fluorescently labeled probes offer a tool to differentiate and further characterize replicating and non-replicating cells. These probes diffuse into cells upon pulsed exposure, covalently bind to lysins and other primary amines of cytoplasmic proteins and a reduction in fluorescence intensity should be largely due to cell division (Bronner-Fraser, 1985; Nose and Takeichi, 1986). Carboxyfluorescein succinimidyl ester (CFSE) or other cell trackers are widely used tools. One bottleneck of CFSE labeling is that reductions in fluorescence appearing due to the excretion of effector molecules cannot be distinguished from reductions resulting from actual cell division (Atwal et al., 2016). CFSE has been successfully used in extracellular bacteria to

distinguish non-dividing persistent cells and dividing cells (Gollan et al., 2019; Wong et al., 2020). Furthermore, it was shown to be a powerful tool to monitor early stages of entry and divisions of intracellular pathogens (Atwal et al., 2016). For *Leishmania* parasites cell tracker red was successfully applied to identify non-dividing persisting parasites retaining the dye up to 120 days post infection *in vivo* (Jara et al., 2019).

Nevertheless, the labeling must be done prior infection of host cells to avoid high fluorescent background of host cell cytosol which likely also integrates cell trackers. This limits the study of processes occurring after one or two rounds of cell division using this dye (Atwal et al., 2016). Therefore, this approach is not suitable for studies implying the maturation of pathogens since the dye is not detectable anymore when the desired dormant stage is reached.

1.4.3 Nucleoside analogues

The most reliable and accurate method of assessing cell proliferation is a measurement of DNA-synthesizing cells. Detection of DNA synthesis in proliferating cells relies on the incorporation of labeled DNA precursors into cellular DNA during the S-phase of the cell cycle (Bick and Davidson, 1974; Gratzner, 1982; Waldman et al., 1991). Non-replicating cells do not incorporate new bases into their DNA, but replicating cells do. This simple aspect makes nucleoside analogues a powerful tool to track cell division events during a time of interest and subsequently tear apart proliferative and non-proliferative cells. Pyrimidine deoxy nucleosides are the most used labeled DNA precursors. Besides radioactive [^{3}H] thymidine, the traditional approach for DNA synthesis detection utilizes an antibody to detect the incorporation of 5-bromo-2'- deoxy uridine (BrdU), an analogue of the nucleoside thymidine or deoxy uridine, into the newly synthesized DNA after pulse labeling. To facilitate the access by the antibody to the BrdU incorporated in the chromosomal DNA, the BrdU labeling, and detection method involves harsh treatments such as nuclease digestion or acid treatment, leading to inevitable negative consequences when used in combination with other functional probes. A progression of BrdU assay relies on the incorporation of ethynyl-labeled deoxyuridine (EdU), a thymidine analogue in which a terminal alkyne group replaces the methyl-group in the 5´ position. EdU is incorporated into cellular DNA during DNA replication and the terminal alkyne group is then detected through its reaction with fluorescent azides, in a Cu(I)-catalyzed [3 + 2] cycloaddition (click chemistry) (Rostovtsev et al., 2002; Tornøe et al., 2002). Unlike assays using BrdU staining, these analogues are detectable in fixed and live cells by fluorescent azides and do not require DNA denaturation for detection of the incorporated nucleoside. A variety of these pyrimidine and purine nucleoside analogues bearing alkyne or other functional groups are commercially available. Both, BrdU and EdU incorporation into replicating DNA was shown to be a sufficient tool to monitor cell division in *Leishmania* spp. and *Trypanosoma cruzi* (Barrett

et al., 2019). *T. gondii* and *Plasmodium spp.* do not possess the thymidine kinase, which is the enzyme that converts deoxythymidine to deoxythymidine phosphate and thus is essential for the incorporation of nucleoside analogues into new DNA. Stable transfection of the Herpes simplex-derived thymidine kinase led to successful incorporation of BrdU and EdU in both species (Fox et al., 2001; Merrick, 2015). Another approach to overcome the lack of a thymidine kinase, is the application of already monophosphorylated analogues which can diffuse via membranes shielded by a masking group (**Figure 6**).
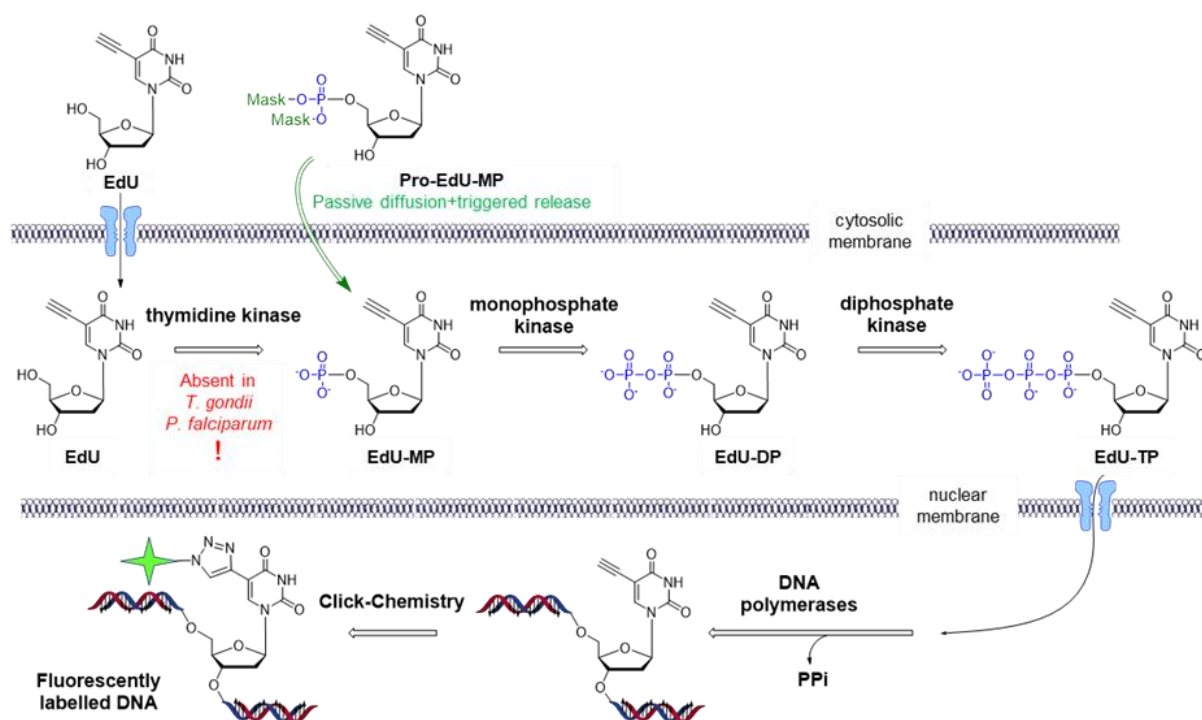
Figure 6: Schematic steps of metabolization, incorporation and detection of EdU and masking group-bearing monophosphate nucleoside analogues. EdU: 5-Ethynyl-2'-deoxyuridine; MP: monophosphate; DP: diphosphate; TP: triphosphate.

Shielded by a masking group, monophosphate-analogues can diffuse into the cell and be further metabolized by monophosphate (MP)- and diphosphate (DP) kinase to EdU-triphosphate (EdU-TP), making thymidine kinase dispensable in this process. Nucleoside analogues can then be incorporated into DNA of dividing cells and detected via click chemistry.

Besides pyrimidine-based nucleoside analogues, purine-based analogue 7-deaza-7-ethynyl-2′-deoxyadenosine (EdA) was shown to be incorporated into DNA of dividing cells (Neef et al., 2012). In a study investigating the adenosine kinase, it was also demonstrated that EdA is sufficiently incorporated in *T. gondii* DNA (Galazka et al., 2006).

Chapter 2: Aim of the project

Encysted bradyzoites are a key source of vertical and horizontal transmission and dissemination of *T. gondii*. They persist life-long and can cause recurring disease in immune-weakened individuals that is lethal if untreated (Luft et al., 1984).However, there is a lack of adequate *in vitro* models which enable the long-term culture of this chronic form of the parasite. The experimental access to mature tissue cysts is limited to *in vivo* models and is widely restricted to transcriptomic and proteomic data. Other important aspects of bradyzoite biology like the metabolome or bradyzoite-host interactions are hardly understudied. As a result, underlying mechanisms of resistance and persistence remain a black box and identification of compounds that target tissue cysts efficiently remains challenging.

To overcome these limitations, *the first aim* of this thesis was the establishment of an *in vitro* system which enables the generation and long-term culture of *T. gondii* tissue cysts which resemble *in vivo* tissue cysts concerning their structural and functional hallmarks.

Since it was reported that the metabolic state of microbes is closely connected to drug susceptibility (Lopatkin et al., 2019) and the metabolome of bradyzoites up to now has only been characterized indirectly (Olson et al., 2020), *the second aim* was to record the metabolic finger print of encysted bradyzoites and tachyzoites to examine stage- and host cell-dependent metabolic traits of the acute and chronic form.

Since *T. gondii* is an obligate intracellular parasite, parasite-host interaction can be considered critical for the persistence of this pathogen. Thus, *the third aim* was to study aspects of bradyzoite-host interaction. Taking our generated metabolomic data into account we focused on lipid metabolism.

Lately it was shown that bradyzoites are asynchronously dividing individuals which form heterogenous populations inside one single tissue cyst, possessing different cell cycle and likely metabolic states (Watts et al., 2015). This phenotypic heterogeneity is connected with treatment failure in other persisters and single cell-resolved markers are a valuable tool to gain more detailed insights in how phenotypic diversity can translate into persisting pathogen populations (Barret et al., 2020). Thus, *the fourth aim* was to establish a single cell-resolved division marker for *T. gondii* that allows monitoring bradyzoite cell division.

Chapter 3: Materials

3.1 Chemicals

Table 2: Chemicals. DMEM: Dulbecco's Modified Eagle's Medium; RPMI: Roswell Park Memorial Institute 1640.

Chemical	Manufacturer
Ascorbic acid	Sigma-Aldrich Chemie GmbH, Schnelldorf, GER
Bovine serum albumin	Carl Roth GmbH & Co. KG, Karlsruhe, GER
Bovine serum albumin, fatty acid free	Thermo Fisher Scientific, Waltham, USA
Calf serum	Thermo Fisher Scientific, Waltham, USA
Chloroform	Carl Roth GmbH & Co. KG, Karlsruhe, GER
Copper sulfate ($CuSO_4$)	Sigma-Aldrich Chemie GmbH, Schnelldorf, GER
D-Glucose	Sigma-Aldrich Chemie GmbH, Schnelldorf, GER
DAPI	Sigma-Aldrich Chemie GmbH, Schnelldorf, GER
DMEM powder, without additives	Thermo Fisher Scientific, Waltham, USA
DMSO	Sigma-Aldrich Chemie GmbH, Schnelldorf, GER
Dynabeads™ MyONE™ Streptavdin T1	Thermo Fisher Scientific, Waltham, USA
Ethanol ≥ 99.5 %, pure or denatured with 1 % methyl ethyl ketone	Carl Roth GmbH & Co. KG, Karlsruhe, GER
Epoxy resin	Sigma-Aldrich Chemie GmbH, Schnelldorf, GER
Fetal calve serum	Capricorn Scientific GmbH, Ebsdorfergrund, GER
Fluoromount™	Sigma-Aldrich Chemie GmbH, Schnelldorf, GER
Glutaraldehyde	Thermo Fisher Scientific, Waltham, USA
HEPES	Carl Roth GmbH & Co. KG, Karlsruhe, GER
Horse serum	Capricorn Scientific GmbH, Ebsdorfergrund, GER
Human holo-transferin	Sigma-Aldrich Chemie GmbH, Schnelldorf, GER
Human recombinant insulin	PAN Biotech, Aidenbach, GER
L-carnitine	Sigma-Aldrich Chemie GmbH, Schnelldorf, GER
L-carnitine:HCL (methyl-D3, 98 %)	Cambridge Isotope Laboratories, Inc., Tewksbury, USA

Lead citrate	Sigma-Aldrich Chemie GmbH, Schnelldorf, GER
Low melting point agarose	Thermo Fisher Scientific, Waltham, USA
Methanol, GER*C Ultra grade*	Carl Roth GmbH & Co. KG, Karlsruhe, GER
Mitotracker Deepred™	Thermo Fisher Scientific, Waltham, USA
N,O-bis(trimethylsilyl)trifluoroacetamide	Thermo Fisher Scientific, Waltham, USA
Paraformaldehyde	Carl Roth GmbH & Co. KG, Karlsruhe, GER
Penicillin/Streptomycin (100 units / 100 µg)	Biochrom AG, Berlin, GER
Pyridine	Thermo Fisher Scientific, Waltham, USA
Resazurin sodium salt	Sigma-Aldrich Chemie GmbH, Schnelldorf, GER
RPMI powder, with phenol red	Thermo Fisher Scientific, Waltham, USA
Scyllo-inositol	Abcam, Cambridge, GERB
Sodium bicarbonate	Biochrom AG, Berlin, GER
Sodium selenite	Thermo Fisher Scientific, Waltham, USA
Triton X-100	Fluka, Seelze, GER
Trypsin/EDTA solution (10 x)	Biochrom AG, Berlin, GER
Ultroser® G	PAN Biotech, Aidenbach, GER
Uranyl acetate	Thermo Fisher Scientific, Waltham, USA
3-(trifluoromethyl)phenyltrimethylammonium	Tokyo Chemical Industry, Tokio, JPN

3.2   Consumables

Table 3: Consumables.

Consumables	Manufacturer
BRAND® 96-well deep well plates	Merck KGaA, Darmstadt, GER
Cannula 23 G / 27 G	VWR International GmbH, Darmstadt, GER
Cap, 9 mm blue screw	Agilent Technologies, Santa Clara, USA
Cap insert for Cryovial® tube, white	Simport Scientific inc., Belœil, USA

Materials

C-Chip *Disposable Hemocytometer*	NanoEnTek Inc., Seoul, KOR
Cell culture dishes T60 / T150	TPP AG, Trasadingen, CH
Cell culture flasks T25 / T75 / T150	TPP AG, Trasadingen, CH
Cell scrapers	TPP AG, Trasadingen, CH
Centrifuge tubes 15 ml / 50 ml	TPP AG, Trasadingen, CH
Combitips, 1-10 µl / 2-20 µl / 20-200 µl / 100-1000 µl	Eppendorf AG, Hamburg, GER
Copper slot grits	Plano GmbH, Wetzlar, GER
Coverslips, 12 mm Ø	VWR International GmbH, Darmstadt, GER
Cryovial® int cap, PK / 100, round bottom, 2 ml	Simport Scientific inc., Belœil, USA
Gloves MICROFLEX® NeoTouch® 25-201	Ansell Ltd., Brussels, BE
Microtiter plates, 6- / 24- / 96-well	TPP AG, Trasadingen, CH
Micro inserts for GCMS vials, 300 µL, 6x30 mm, conical, tip 13 mm	Klaus Trott Chromatographie-Zubehör, Kriftel, GER
Parafilm®	Pechiney Plastic Packaging, Chicago, USA
Petri dishes 94x16 mm	Carl Roth GmbH & Co. KG, Karlsruhe, GER
Polycarbonate filter, 3 µM	Cytiva Europe GmbH, Freiburg, GER
Razor blades	Edgewell Personal Cares, Shelton, USA
Reaction tubes, 1.5 ml / 2 ml	Eppendorf AG, Hamburg, GER
Screw neck GCMS vials 1.5 mL, clear	Klaus Trott Chromatographie-Zubehör, Kriftel, GER
Serological pipettes, 5 ml / 25 ml / 50 ml	TPP AG, Trasadingen, CH
Syringe filters *Minisart*, 0.22 µM	Sartorius AG, Göttingen, GER
Syringes *Omnifix*®, 1 ml / 5 ml / 10 ml / 20 ml	B. Braun Melsungen AG, Melsungen, GER
WHEATON® Liquid Scintillation Vials 22-400 with Polyethylene Cone, 20 ml	DWK Life Sciences GmbH, Mainz, GER

3.3 Medium, buffers and solutions

All solutions were prepared using ultrapure water (resistivity 18.2 MΩ) and analytical grade reagents. If required, the pH was adjusted using sodium hydroxide or hydrochloric acid.

3.3.1 Medium for parasite and cell culture

All medium was supplemented with 4.5 g/l glucose (high glucose) or 1 g/l glucose (low glucose), 4 mM L-glutamine, 1 mM sodium pyruvate, 100 U/ml penicillin, 100 µg/ml streptomycin and 15 mg/l phenol red, otherwise indicated differently. For assays that were dependent on plate reader-based fluorescence measurements, phenol red was omitted from the media.

Table 4: Medium for parasite and cell culture. DMSO: dimethyl sulfoxide; DMEM: Dulbecco's Modified Eagle's Medium; RPMI: Roswell Park Memorial Institute 1640; HOS: horse serum.

Name	Composition
Cryologic cultivation	
Cryologic medium	90 % (v/v) of heat-inactivated fetal calf serum added with 10 % DMSO
Host cell cultivation	
Human fibroblast medium	DMEM (high glucose) supplemented with 10 % heat-inactivated calf serum
Myoblast medium	DMEM (high glucose) supplemented with 20 % heat-inactivated fetal calf serum and 2 % Ultroser® G
Myotube Medium	DMEM (high glucose) supplemented with 2 % heat-inactivated horse serum,10 µg/ml human insulin, 5 µg/ml human holo-transferrin, 1.7 ng/µl sodium selenite
Parasite cultivation	
Bradyzoite medium (pH 7.4 or 8.3)	RPMI (low glucose) supplemented with 1 % heat-inactivated fetal calf serum, 2 % heat-inactivated HOS, 10 µg/ml human insulin, 5 µg/ml human holo-transferrin, 1.7 ng/µl sodium selenite
Tachyzoite medium	DMEM (high glucose) supplemented with 1 % heat-inactivated fetal calf serum

3.3.2 Buffers and solutions

All used buffers and solutions were adjusted to a pH of 7.4, otherwise stated differently. Phosphate buffered saline (PBS) and paraformaldehyde solution were prepared and provided in house.

Table 5: Buffer and solutions. PBS: phosphate buffered saline; BSA: bovine serum albumin.

Name	Composition
General solutions for imaging	
Fixation solution A	4 % (v/v) paraformaldehyde; 250 mM NaCl in PBS
Fixation solution B	2% (v/v) paraformaldehyde; 0.005 % glutaraldehyde; 250 mM NaCl in PBS
Neutralization solution	0.1 M glycin in PBS
PBS	13.7 mM NaCl; 8.0 mM Na_2HPO_4; 2.7 mM KCl; 1.5 mM KH_2PO_4
Cyst isolation	
Coupling solution	2 % (w/v) BSA in PBS
Wash solution A	0.05 % (w/v) BSA in PBS
Wash solution B	0.1 % (w/v) BSA in PBS
Click chemistry (alkyne-azide)	
Permeabilization solution	0.5 % (v/v) Triton X-100 in PBS
Reaction solution	0.5 mM ascorbate, 0.005 mM copper sulfate ($CuSO_4$) in Milli-Q water
Wash solution	2 % (w/v) BSA in PBS
Cytotoxicity	
Resazurin solution (10x)	400 µM resazurin sodium salt in 10x PBS
Electron microscopy	
Fixation solution	1 % paraformaldehyde, 2.5 % glutaraldehyde, 0.05 M HEPES
Wash solution	0.05 M HEPES in PBS
Storing solution	2.5 % glutaraldehyde in 0.05 M HEPES in PBS
Immunofluorescence assay	
Permeabilization solution	0.1 % (v/v) Triton X-100 in PBS
Wash solution	0.1 % (v/v) Triton X-100 in PBS
Blocking solution	2 % (w/v) BSA in PBS

Primary antibody solution	0.1 % (v/v) Triton X-100 in 2 % (w/v) BSA in PBS
Fatty acid labeling	
Fatty acid-coupling solution	20 % fatty acid free BSA (w/v) in Milli-Q water
Pepsin digestion	
Pepsin solution	5.05 g/l pepsin; 0.88 g/l glycine; 0.65 g/l NaCl in Milli-Q- (pH 1.2); supplemented with 5 mM glucose
Neutralization solution	1.2 % (w/v) NaHCO$_3$, 0.016 g/l phenol red in Milli-Q water (pH≈8.3)

3.4 Antibodies and biotinylated conjugates

Following antibodies were used for immunofluorescence. The source and used dilutions are stated. All primary antibodies were diluted in primary antibody solution (**Table 5**), secondary antibodies were diluted in blocking solution (**Table 5**).

Table 6: Antibodies and biotynilated conjugates and the applied working dilutions. SAG: surface antigen; mAb: monoclonal antibody; IMC: inner membrane complex; MF: myosin heavy chain; DBA: *Dolichos biflorus* agglutinin.

Antibody (origin)	Working dilution	Manufacturer / reference, provider
Primary antibodies		
Anti-SAG1 DG52 (mouse mAb)	1/300	(Bülow and Boothroyd, 1991), provided by D. Sibley
Anti-CC2 (rat mAb)	1/1000	(Gross et al., 1995), provided by C. Lueder
Anti-IMC3 (rat mAb)	1/1000	(Anderson-White et al., 2011), provided by M.J. Gubbels
Anti-MF20 (mouse mAb)	1/400	eBioscience™, San Diego, USA
Biotynilated conjugates		
DBA	1/1000	Sigma-Aldrich Chemie GmbH, Schnelldorf, GER
Secondary antibodies		
Goat anti-rat-Alexa546	1/300	Invitrogen, Carlsbad, USA
Goat anti-rat-Alexa375	1/300	Thermo Fisher Scientific, Waltham, USA

Goat anti-rabbit-FITC	1/300	Thermo Fisher Scientific, Waltham, USA
Rabbit anti-mouse-Cy3	1/400	Dianova GmbH, Hamburg, GER
Donkey anti-mouse-Cy5	1/300	Dianova GmbH, Hamburg, GER
Streptavidin-Alexa48	1/2500	Invitrogen, Carlsbad, USA
Streptavidin Cy5	1/2500	Jackson ImmunoResearch Laboratories, Inc., West Grove, USA

3.5 Inhibitors and modulators

All inhibitors and modulators were prepared in the named respective solvent in recommended stock concentrations, aliquoted and stored at -80 °C. Working vials were stored at -20 °C.

Table 7: Inhibitors and modulators and respective solvents. BKI: bumped kinase inhibitor; DMSO: dimethyl sulfoxide; HDQ: 1-hydroxy-2-dodecyl-4(1H)-quinolone.

Inhibitor / modulator	Solvent	Manufacturer / reference, provider
BKI1294	DMSO	(Winzer et al., 2015), provided by W. C. Van Voorhis
BKI1553	DMSO	(Scheele et al., 2018), provided by W. C. Van Voorhis
HDQ	DMSO	(Saleh et al., 2007), provided by W. Bohne
L-carnitine	Milli-Q water	Sigma-Aldrich Chemie GmbH, Schnelldorf, GER
Meldonium	50 % DMSO, 50 % Milli-Q water	Sigma-Aldrich Chemie GmbH, Schnelldorf, GER
Pyrimethamine	DMSO	Sigma-Aldrich Chemie GmbH, Schnelldorf, GER
Sodium fluoroacetate	Milli-Q water	abcr GmbH, Karlsruhe, GER
Sulfonamide	DMSO	Sigma-Aldrich Chemie GmbH, Schnelldorf, GER
Trimetazidine	Milli-Q water	Sigma-Aldrich Chemie GmbH, Schnelldorf, GER

3.6   Nucleoside analogues and azide-bearing compounds

All nucleoside analogues were prepared in DMSO as a 50 mM stock, aliquoted and stored at -80 °C. Working vials were stored at -20 °C. Forodesine was prepared in water as a 10 mM stock. All thymidine-based analogues were provided by Sally-Ann Poulsen, Griffith University Australia.

Table 8: Pyrimidine-based nucleoside analogues, their respective parent nucleoside, and the intracellular cleavage mechanism. EdU: 5-ethynyl-2-deoxyuridine; ribo: ribosyl; ara: arabinosyl.

Name	Parent nucleoside	Cleavage mechanism
EdU	EdU	thymidine kinase
Compound 1	F-ribo-EdU	pH (hydrolytic)
Compound 2	di-fluoro-EdU	pH (hydrolytic)
Compound 3	F-ara-EdU	pH (hydrolytic)
Compound 4	F-ara-EdU	esterase
Compound 5	F-ara-EdU	esterase
Compound 6	F-ara-EdU	esterase
Compound 7	EdU	esterase
Compound 8	EdU	nitroreductase
Compound 9	EdU	esterase
Compound 10	EdU	nitroreductase
Compound 11	EdU	pH (hydrolytic)
Compound 12	EdU	pH (hydrolytic)
Compound 13	di-fluoro-EdU	pH (hydrolytic)

Table 9: Purine-based nucleoside analogues and fluorophore coupled azides. EdA: 7-deaza-7-ethynyl-2-deoxyadenosine.

Name	Manufacturer / provider
Purine-based analogues	
EdA	Jena Bioscience, Jena, GER

Forodesine	Sigma-Aldrich Chemie GmbH, Schnelldorf, GER
Fluorophor-coupled azides	
5-carboxytetramethylrhodamine Azide	Baseclick GmbH, Neuried, GER
Azide-Alexa488	Jena Bioscience, Jena, GER

3.7 Fatty acids

3.7.1 Preparation of fatty acid solutions

Linoleic acid (LA), uniformly labeled $^{(U13)}$C LA and ^{U13}C fatty acid (FA) labeling mix were dissolved in 99.7 % EtOH at a concentration of 1 M. In parallel, a 3 mM FA free bovine serum albumin (BSA) solution was prepared in Milli-Q water. The in EtOH dissolved FAs were added dropwise to the BSA solution at a molar ratio of 1:6, vortexed and sonicated till dissolved completely. Subsequently, the mix was incubated for 1 h at 37 °C to ensure BSA-FA complex formation. The mixture was stored in the dark at 4 °C.

Table 10: Fatty acids and their nomenclature. ^{U13}: uniformly labeled.

Fatty Acid	Nomenclature	Provider
Linoleic acid	18:2	Sigma-Aldrich Chemie GmbH, Schnelldorf, GER
^{U13}C Linoleic acid	18:2	Cambridge Isotope Laboratories, Inc., Tewksbury, USA
^{U13}C Fatty acid mix	-	Cambridge Isotope Laboratories, Inc., Tewksbury, USA

3.8 Animals, eukaryotic cell lines and *Toxoplasma gondii* strains

3.8.1 Animals

Infection experiments were performed together with Mateo Murillo Leon and Tobias Steinfeldt. Groups of five 10-week-old female and male mice (C57BL/6JRj) were obtained from certified breeders (Janvier Labs, Route du Genest, 53940 Le Genest-Saint-Isle, France) and kept under specific-pathogen-free conditions in the local animal facility (Department for Microbiology and Hygiene, Freiburg). All animal experiments were performed in accordance with the guidelines of the German animal protection law and the Federation for Laboratory Animal Science Associations. Experiments were approved by the state of Baden-Württemberg (Regierungspräsidium Freiburg; reference number 35-9185.81/G-19/89). Mice were housed in

groups of 6-8 animals in a cage with ground corncob bedding. Room temperature was maintained at 22 ± 0.5 °C with a relative humidity between 40 % and 60 %. A 12 h / 12 h light and dark cycle was applied. Water was provided *ad libitum* from nipple drinkers.

3.8.2 Eukaryotic cell lines

Table 11: Eukaryotic cell lines

Eukaryotic cell line (catalogue number)	Species, cell type	Reference / provider
BJ-5ta (ATCC® CRL-4001™)	Homo sapiens, foreskin fibroblasts	LGC Standards GmbH, Wesel, GER
KD3	Homo sapiens, myoblasts	(Shiomi et al., 2011), provided by N. Hashimoto

3.8.3 *Toxoplasma gondii* strains

Table 12: *Toxoplasma gondii* strains. *hxgprt*: *hypoxanthine-xanthine-guanine phosphoribosyl transferase*; GFP: green fluorescent protein; td: tandem.

Strain	Reference, provider
Type I	
GT1	(Dubey, 1980), provided by F. Seeber
RH	(Sabin, 1938), provided by G. Schares
RH-Δ*ku80*	(Huynh and Carruthers, 2009), provided by F. Seeber
Type II	
ME49	(Lunde and Jacobs, 1983), provided by F. Seeber
NTE	(Gross et al., 1991), provided by F. Seeber
Pru-Δ*ku80*Δ*hxgprt*-GFP	(Cleary et al., 2002; Singh et al., 2002), provided by F. Seeber
Pru-Δ*hxgprt*-tdTomato	(Chtanova et al., 2008), provided by F. Seeber
Type III	
NED	(Dardé et al., 1992), provided by F. Seeber
VEG	(Sibley et al., 2002), provided by G. Schares

3.9 Software, databases and online tools

3.9.1 Software

Table 13: Software.

Name	Manufacturer / Reference
Compound Discoverer 3.1	Thermo Fisher Scientific, Waltham, USA
Dexsi	(Dagley and McConville, 2018)
Endnote 7X	Clarivate analytics, Philadelphia, USA
Geneious® 11.1.5	Biomatters Ltd., Auckland, NZ
GraphPad Prism 8	GraphPad Software Inc., La Jolla, USA
i-control 1.10	Tecan Group Ltd., Männerdorf, CH
ImageJ 1.51g	Wayne Rasband, National Institutes of Health, Bethesda, USA
MSD Chemstation	Agilent Technologies, Santa Clara, USA
Zen 2012 (blue and black)	Carl Zeiss Microscopy GmbH, Göttingen, GER

3.9.2 Databases and online tools

Table 14: Databases and online tools.

Name	Reference / manufacturer
Blast Local Alignment search tool	National Center for Biotechnology Information, Bethesda, USA
m/z cloud database	Thermo Fisher Scientific, Waltham, USA
Pubmed	National Center for Biotechnology Information, Bethesda, USA
Toxo DB	(Gajria et al., 2008)

Chapter 4: Methods

For all experiments, tachyzoite and bradyzoite samples were generated as described in detail in section 4.1.3. Bradyzoites were generated in bradyzoite medium pH 7.4, if not indicated differently. The respective host cell type, parasite strain, multiplicity of infection (MOI), duration of infection or maturation time and treatment details are stated in the respective figure legends in the results section.

4.1   Cell culture

The cell culture work was performed in S2 laboratory rooms of the Robert Koch-Institute Berlin. The host cell and parasite cultures were kept in incubators at 37 °C in a humidified atmosphere (5 % (v/v) of water) and a constant CO_2 concentration of 10 % (v/v) or 0 % (v/v) in case of bradyzoites, if not indicated differently. All procedures requiring sterility were carried out under a laminar flow sterile hood. Medium and solutions were prepared in sterile bottles, with sterile plastic pipettes and filter sterilized if necessary.

4.1.1   Cultivation of eukaryotic host cell lines

Human foreskin fibroblast (HFF) monolayers were cultured in Dulbecco's Modified Eagle's Medium (DMEM) supplemented with 25 mM glucose, 4 mM L-glutamine, 1 mM sodium pyruvate, 100 U/ml penicillin, 100 µg/ml streptomycin and 10 % heat-inactivated calf serum (human fibroblast medium, **Table 4**). Immortalized human KD3 myoblasts were cultured in DMEM supplemented with 25 mM glucose, 4 mM L-glutamine, 1 mM sodium pyruvate, 100 U/ml penicillin, 100 µg/ml streptomycin, 2 % Ultroser® G and 20 % heat inactivated fetal calf serum (myoblast medium, **Table 4**). HFF and KD3 cells were sub-cultured at a confluency of 100 % and 70 %, respectively. The medium of the cell culture flasks (T75) was aspirated, and cells were washed with 10 ml of prewarmed phosphate buffered saline (PBS). Cells were detached by adding 2 ml of trypsin / EDTA solution (1x), followed by a ~5 min incubation at 37 °C. Subsequently the trypsin was neutralized by adding at least the 5x volume of medium to the cell suspension. Depending on the desired application, the cell suspension was diluted in the respective medium and distributed in T25 / 75 cell culture flasks, T60 or T150 dishes or 6- / 12- / 24- / 48- / 96-well plates. For immunofluorescence assays (IFAs) Ø 12 mm coverslips were seeded within a 24-well plate.

The differentiation of myoblasts into terminally differentiated myotubes was induced at confluency of 70 % by washing the monolayer with prewarmed PBS and changing medium to DMEM supplemented with 25 mM glucose, 4 mM L-glutamine, 1 mM sodium pyruvate, 100 U/ml penicillin, 100 µg/ml streptomycin, 2 % horse serum, 10 µg/ml human insulin, 5 µg/ml

human holo-transferrin, 1.7 µg/ml sodium selenite (myotube medium, **Table 4**) for five to seven days (Shiomi et al., 2011). Medium was changed every second day.

4.1.2 Maintenance of *Toxoplasma gondii* tachyzoites

Type I strain (RH, RH*Δku*80, GT1), type II (ME49, NTE, Pru-*Δku*80*Δhxgprt (*Pru-GFP*)*, Pru-*Δhxgprt*-tdTomato (Pru-tdTomato) and type III (NED, VEG) were maintained *in vitro* in HFF monolayers cultured in DMEM supplemented with 25 mM glucose, 4 mM L-glutamine, 1 mM sodium pyruvate, 100 U/ml penicillin, 100 µg/ml streptomycin and 1 % heat-inactivated fetal calf serum (tachyzoite medium, **Table 4**). Depending on the parasite strain, every second to fifth day ~0.5 ml freshly egressed parasites were transferred into a new 6-well containing confluent HFF cells.

4.1.3 Tachyzoite infection and *in vitro* bradyzoite generation

For infection experiments, the *T. gondii* cell number was determined. For this purpose, infected HFF cells just prior lysis were used. Cells were scraped of a 6-well or T60 / T150 dish, passed through a 27G needle mounted on a syringe two times for intracellular parasite release, then transferred into a 15 ml or 50 ml centrifuge tube, topped off with fresh tachyzoite medium and centrifuged at 100 x g for 5 min at room temperature (RT). The supernatant, containing the parasites, was then transferred to a new centrifuge tube, and again centrifuged at 300 x g for 10 min. The supernatant was aspirated and the pellet, containing the parasites, was resuspended in either 1 ml tachyzoite medium for tachyzoite experiments or 1 ml bradyzoite medium for bradyzoite experiments. Subsequently, the solution was transferred into a 1.5 ml vessel and a 1:10 dilution in the respective medium was prepared. 10 µl of the parasite solution was transferred into a C-chip Neubauer counting chamber and parasites were counted according to the manufacturer's instructions. For infection experiments appropriate number of parasites for the desired MOI (**Table**) were diluted in the respective medium and applied to the respective host cell monolayer. Depending on the desired application, the parasite suspension was used for infection of monolayers cultures in T25 / 75 cell culture flasks, T60 or T150 dishes or 6- / 12- / 24- / 48- / 96-well plates. Medium was changed 2 to 4 h post infection to remove parasites that did not invade host cells.

For bradyzoite experiments, KD3 myotubes were used as host cell line for infection. Differentiation of *T. gondii* tachyzoites into tissue cysts was facilitated either by CO_2 depletion and a basic pH shift to pH 8.3 or CO_2 depletion on its own using medium with pH 7.4. To avoid medium acidification, the medium was changed to low glucose (5 mM), 50 mM HEPES buffered Roswell Park Memorial Institute 1640 (RPMI) medium supplemented with 4 mM L-glutamine, 100 U/ml penicillin, 100 µg/ml streptomycin, 2 % horse serum and insulin-

transferrin-selenium at pH 7.4 or pH 8.3 (bradyzoite medium, **Table 4**). The cells were incubated at 37 °C and ambient CO_2 levels. The day after infection, monolayers were washed with prewarmed PBS to remove not invaded parasites. Medium was changed every second day and washed with PBS once a week.

Table 15: Number of tachyzoites used for infection at multiplicity of infection (MOI) of 1 for respective cell culture formats.

Format	96-well	24-well	6-well	T60	T75	T150
Tachyzoites for MOI 1	2.4×10^4	1.3×10^5	6.4×10^5	4.3×10^6	5.4×10^6	10.8×10^6

4.1.4 Freezing and thawing of eukaryotic cells and *Toxoplasma gondii*

For freezing of eukaryotic cell lines or *T. gondii,* FCS supplemented with 10 % dimethyl sulfoxide (DMSO) (cryogenic medium, **Table 4**) was added to either trypsinized cells or extracellular parasites, which were then aliquoted into cryogenic vials on ice and slowly cooled to -80 °C. After 24 to 72 h later the cryotubes were transferred into the liquid nitrogen tank for long-term storage. The frozen cells were defrosted in a water bath at 37 °C and the 10-fold amount of respective prewarmed medium was added to compensate for toxic effects of DMSO. The cell suspension was centrifuged at 300 x g for 10 min. The supernatant was discarded; the cells were resuspended in their respective medium and plated on the appropriate number of plates or seeded in flasks. In case of *T. gondii*, parasites were resuspended in fresh tachyzoite medium and seeded in a 6-well containing confluent HFF cells. 4 h post infection, infected wells were washed with fresh tachyzoite medium to wash away not invaded parasites. Cell lines and parasites were cultured at least one passage before starting experiments.

4.1.5 Cyst isolation

On the day of harvest, dishes were placed on ice and medium was removed. Infected and uninfected monolayers were washed three times with 10 ml ice-cold PBS. Cells were then harvested by scraping into 10 ml ice-cold 0.05 % bovine serum albumin (BSA) in PBS (wash solution A, **Table 5**) per dish and collected in a 15 ml centrifuge tube. Cysts were released from the monolayer via syringing through a 23G needle 25 times and collected via centrifugation (1,200 x *g*, 10 min, 0 °C). Centrifuge tubes were placed on ice, supernatant was removed, and the resultant pellet was gently resuspended in 2 ml 2 % BSA in PBS (coupling solution, **Table 5**), containing the respective amount of coupled beads (preparation described in section 4.1.5.1). Samples containing cysts and beads were transferred into 2 ml tubes and samples were incubated for 1 h at 4 °C with gentle shaking. Subsequently, the samples were

placed in a magnetic stand on ice, washed five times with 1 ml 0.1 % BSA (wash solution B, **Table 5**) in PBS to wash away cell debris, followed by two washing steps with 1 ml PBS to remove residual BSA. Cysts and beads were then collected via centrifugation (1,200 x g, 10 min, 0 °C), shock frozen in liquid nitrogen and stored at -80 °C until extraction. Depending on application, all samples were either extracted simultaneously in 80 % acetonitrile for liquid chromatography-coupled mass spectrometry (LC / MS) analysis or extracted via chloroform / methanol (MeOH) / water extraction for gas chromatography-coupled mass spectrometry (GC / MS) analysis as described in section 4.4. Uninfected controls and bead-only controls were processed equally.

4.1.5.1 Preparation of beads

Coupling of Dynabeads^{TM} MyONE^{TM} Streptavdin T1 to *Dolichos biflorus* agglutinin (DBA) was done as described in the manufacturer's protocol. Briefly, the beads were resuspended in the vial by vortexing. 40 µl beads / T60 dish were resuspended in 1 ml PBS, washed three times with PBS in a magnetic stand and resuspended in 1 ml PBS containing 10 µg DBA / T60 dish. The tube containing the DBA-magnetic bead mixture was placed on a rotary sample mixer and mixed for 45 min at RT. The unlinked DBA was removed by washing the coated beads three times with PBS. After washing, the DBA-coated beads were resuspended in 1.5 ml 2 % BSA in PBS (coupling solution, **Table 5**) per sample.

4.2 Imaging techniques

4.2.1 Electron microscopy

Bradyzoites were prepared in T60 dishes. At the desired maturation time, the medium was removed, and samples were fixed by covering the monolayer with 1 % paraformaldehyde (PFA) and 2.5 % glutaraldehyde in 0.05 M HEPES buffer (fixation solution, **Table 5**). After incubation at RT for 3 h, the flasks were sealed with parafilm and stored in the fridge until further processing.

Electron microscopy was performed by Tobias Hoffmann. For plastic embedding cells were scraped off with a cell scraper, sedimented by centrifugation (3,000 x *g*, 10 min, 0°C) and washed twice with PBS supplemented with 0.05 M HEPES (wash solution, **Table 5**) to remove the fixative. The washed cell pellets were mixed with 3 % low-melting point agarose (1:1 [v/v]) at 40 °C, centrifuged at 3,000 x *g* for 5 min and cooled on ice. The cell pellets were cut off from the agarose gel block using a sharp razor blade and stored in 2.5 % glutaraldehyde in 0.05 M HEPES buffer (storing solution, **Table 5**). Post-fixation, block contrasting, dehydration and embedding in epoxy resin was performed according to a standard procedure (Laue, 2010). Ultrathin sections with a thickness of ~65 nm were generated with an ultramicrotome using a diamond knife (45 °), collected on copper slot grids and contrasted with 2 % uranyl acetate and 0.1 % lead citrate.

Electron microscopy of ultrathin sections was performed with a transmission electron microscope at 120 kV. Images were recorded with a side-mounted CCD camera and the montage function of the camera software (Multiple Image Alignment) to cover larger field of views with sufficient pixel resolution.

4.2.2 Immunofluorescence assay

For IFAs, uninfected host cells, tachyzoites and bradyzoites were grown in monolayers on glass coverslips (Ø 12 mm). After desired infection period, the medium was aspirated, and the cell layer was washed with 1 ml of PBS. Samples were fixed in 200 µl 4 % PFA in PBS (fixation solution A, **Table 5**) or 4 % PFA in PBS supplemented with 0.005 % glutaraldehyde (fixation solution B, **Table 5**) depending on staining protocol for 20 min at RT, followed by a washing step in 200 µl 0.1 M glycine in PBS (neutralization solution, **Table 5**) and permeabilization in 200 µl 0.1 % Trition X-100 in PBS (permeabilization solution, **Table 5**) for 20 min at RT. The cells were blocked in 200 µl 2 % BSA solution in PBS (blocking solution, **Table 5**) for 1 h at RT or over-night at 4 °C. Then, using curved cannula and forceps, coverslips were transferred upside down onto parafilm on 50 µl of the appropriate first antibody diluted in 2 % BSA solution in 0.1 % Triton X-100 in PBS (first antibody solution, **Table 5**) and incubated for 1 h at RT.

Coverslips were then transferred back to the plate for three washing steps with 1 ml 0.1 % Triton X-100 in PBS (wash solution, **Table 5**), 10 min each. Staining with the secondary antibody diluted in 2 % BSA solution (blocking solution, **Table 5**) in PBS was performed similarly to the primary antibody for 1 h at RT in the dark. Coverslips were transferred back into the wells and after three washing steps with 1 ml PBS, 10 min each, coverslips were mounted on microscopy slides on 10 µl *Fluoromount*™ containing DAPI (1:3,000) and lightly pressed. After hardening, monochromatic images were recorded on a Zeiss Apotome Imager equipped with a Plan-Fluar" 63x/1.45 oil M27 objective or on a Zeiss Axio Observer imager equipped with Plan-NeoFluar" 10x/0.3 or a Plan-Apochromat" 63x/1.4 oil objective and imported into ImageJ (Schneider et al., 2012) for coloring and the generation of overlays. The antibodies used and the respective dilutions used can be found in **Table 6**.

4.2.2.1 Mitochondrial staining

Mitochondrial staining was done prior fixation for 30 min with Mitotracker™ deep red FM at 200 nM in tachyzoite medium at 37 °C in a humidified CO_2 (10 %) incubator. Cultures were chased for 15 min in tachyzoite medium and washed three times with PBS and further processed for IFA as described above.

4.2.2.2 Alkyne-azide-based click chemistry

Tachyzoite samples were cultured in 1 ml medium supplemented with respective nucleoside analogue (**Table 8**, **Table 9**) in indicated concentration for 24 h. For bradyzoite samples, nucleoside labeling was applied in indicated concentrations for 48 h.

At the end of experiment, infected monolayers were washed once with PBS, fixed in 200 µl 4 % PFA containing 0.005 % glutaraldehyde (fixation solution B, **Table 5**) and click chemistry was conducted according to manufacturer's protocol. Briefly, after fixation samples were washed two times with 2 % BSA solution (wash solution, **Table 5**), permeabilized in 200 µl 0.5 % Triton X-100 in PBS (permeabilization solution, **Table 5**) for 20 min at RT. Washed again three times with 2 % BSA solution (wash solution, **Table 5**), following incubation in 250 µl click reaction buffer (reaction solution, **Table 5**) containing 1 µM azide-bearing compound for 30 min in the dark. After click reaction, cells were washed three times with 2 % BSA solution (wash solution, **Table 5**), 10 min each, followed by immunofluorescence staining as indicated. For each click reaction, 5-ethynyl-2'-deoxyuridine (EdU) labeled host nuclei were used as staining control.

4.3 Assays

4.3.1 Pepsin digestion and *in vitro* oral transmission assay

Tachyzoite, bradyzoite and uninfected monolayers were prepared in 6-well plates. Prior to the pepsin digestion of bradyzoite, tachyzoite and uninfected samples, the medium of the cultures was aspirated, and the monolayers were washed with 1 ml prewarmed PBS. The digestion was performed inside the well by adding 1 ml of a modified pepsin solution (Dubey, 1998) (**Table 5**) to the cells for 20, 40 and 60 min at 37 °C. Digestion was terminated by adding 4 ml of neutralization solution (**Table 5**) into the well. Digested infected monolayers and uninfected and untreated controls were collected with a cell scraper, transferred into a 15 ml tube, and harvested via centrifugation (1,200 x g, 10 min) at RT. The supernatant was removed, the pellets were resuspended in 450 µl tachyzoite medium and used to infect HFF cells in a 96-well plate in triplicates, if not indicated differently. Parasite recovery was monitored by measuring tandem (td)Tomato fluorescence intensity (excitation 554 nm / emission 589 nm) in a fluorescence plate reader every second day for up to 21 days. Medium was exchanged after each measurement.

For the oral transmission assay, scraped infected monolayers and respective controls were challenged by the indicated combination of stresses: cold stress (4 °C for 4 and seven days), heat stress (55 °C or 65 °C for 5 min), incubation at RT for two days and pepsin digestion (60 min).

The resistance score (RS) was calculated as the difference of days passed between the detection of mock-treated and treated cultures. This difference was normalized to the number of days of total observation to account for differences in re-growth between experiments:

$$RS = 1 - (\#days_{treatment} - \#days_{vehicle}) / \#days_{observed}$$

Hence, a RS of 0 indicates no recovery from the treatment and a RS of 1 means equal growth to the untreated control, indicating full resistance to the treatment.

4.3.2 *In vivo* oral transmission assay

Tachyzoite and bradyzoite cultures were prepared in T25 cell culture flasks and 6-well plates. The cultures were then prepared for shipping and sent to Freiburg at RT within 24 h. The infected monolayers were washed once with PBS, scraped in 10 ml fresh respective medium and harvested via centrifugation (1,200 x g, 10 min) at RT. The supernatant was removed after centrifugation, the pellet was resuspended in 2 ml PBS and placed on ice. For tachyzoite controls, scraped monolayers were syringed with a 27G needle to release intracellular parasites and counted in a Neubauer chamber. For cyst quantification, 10 µl of the cyst solution

was placed on a glass slide and cysts were counted based on the fluorescence of tdTomato in a fluorescence microscope. For *in vivo* cyst generation, one C57BL/6JRj mouse was infected with 1x10^3 *T. gondii* tachyzoites via intraperitoneal injection. 30 days post infection the mouse was euthanized by cervical dislocation. The brain was harvested in 2 ml PBS and minced using an 18G and 21G needle for cysts inspection via DBA staining as described previously (Matta et al., 2019). Briefly, 50 µL out of 200 µL DBA-stained sample were pipetted in a clear-bottomed 96 well plate and quantified at 20x magnification using DBA positivity as a first criterion and tdTomato positivity to confirm brain cyst.

4.3.2.1 Mouse infection

Groups of five mice were infected by oral gavage with 50 or 500 freshly prepared *in vitro*-generated Pru-tdTomato cysts, 10 freshly prepared *in vivo*-derived Pru-tdTomato cysts and 10,000 myotube- or HFF-derived extracellular tachyzoites in a total volume of 200 µl PBS.

Infected mice were monitored and weighted daily for the duration of the experiment. Relative weight loss was calculated based on the weight at the day of infection. Brains and blood from moribund animals were collected starting from two days post infection. After 30 days post infection blood samples of all surviving mice were collected from the facial vein. Blood was allowed to clot at RT for 30 min before centrifugation at (500 x g, 10 min) at RT. Serum was collected and either immediately analyzed or stored at -20 °C until further analysis. Animals were euthanized by cervical dislocation. Brains were harvested and cysts per brain sample were blindly counted as described previously:

Cysts / brain = cysts in 50 µL x 40

Seroconversion was evaluated via enzyme-linked immunosorbent assay (ELISA) as described previously (Matta et al., 2019). Serum from non-infected (n.i.) mice were included to calculate the cutoff:

Cutoff = mean absorbance$^{450\,nm\text{-}570\,nm}$ (n.i.) + 2 x standard deviation of absorbance$^{450\,nm\text{-}570\,nm}$ (n.i.)

An individual cutoff was calculated per each individual ELISA. To compare the *T. gondii* specific-antibody titters from different independent experiments a reactivity index was calculated per sample:

Reactivity index= mean absorbance$^{450\,nm\text{-}570\,nm}$ / cutoff
Reactivity index values higher than one were considered as positive.

4.3.3 Drug assays

Tachyzoite and bradyzoite samples were prepared in 96-well plates. At indicated time points monolayers were washed with prewarmed PBS and cultures received a compound-pulse for indicated times set in tachyzoite or bradyzoite medium. At the end of treatment, cultures were washed with 150 µl prewarmed PBS to remove drugs. Re-differentiation and regrowth of cultures were initiated by applying 150 µl fresh tachyzoite medium to the wells and incubation under CO_2 replete conditions. Parasite recovery was monitored by measuring tdTomato fluorescence for 28 days and the resistance score was calculated as described in 4.3.1. Medium was exchanged every second to third day throughout the experiment.

4.3.3.1 Half inhibitory concentration

Growth of tachyzoites was monitored throughout the respective compound-pulse. Normalized fluorescence was determined by normalizing treated parasites to solvent-treated parasites. The half inhibitory concentration (IC_{50}) values were determined at day five to seven by fitting the dose response curve by non-linear regression in GraphPad Prism v8.

4.3.3.2 Host cell cytotoxicity assay

Host cells were seeded in 96-well plates and treated for seven days with drug candidates or for 24 h with nucleoside analogues at the indicated concentrations. At the end of the pulse, the medium was aspirated, and monolayers were washed once with 100 µl prewarmed PBS. 100 µl resazurin solution (**Table 5**) was applied per well and cells were incubated for 3 h in a humidified incubator at 37 °C and 10 % CO2. The resorufin formed in the assay was quantified by measuring the fluorescence intensity using a plate reader (excitation 530-570 nm / emission 590-620 nm). Host cell viability was determined relative to solvent-treated controls.

4.4   Metabolome analyses

For GC / MS and LC / MS analyses only chemicals with GC / MS or LC / MS grade were used. All steps using solvents were performed under a fume hood.

4.4.1   Gas chromatography mass spectrometry analysis

4.4.1.1 Sample preparation

Tachyzoite samples and respective host cell and filter controls were prepared in 6-well plates. For fatty acid (FA) labeling experiments, cultures were prepared in low glucose tachyzoite medium. The samples were quenched by placing cultures on ice and covering monolayers in ice-cold PBS. Infected samples were scraped with a cell scraper, syringed through a 27G needle to release intracellular parasites, and passaged through a 3 µM polycarbonate filter to remove host cell debris. Samples were transferred into a 1.5 ml tube or a 15 ml tube, followed by centrifugation (1,200 x g, 10 min, 0 °C). Pellets were washed once with 1 ml ice-cold PBS. Uninfected scraped monolayers were prepared in the same way and served as filter controls to estimate host cell contamination in tachyzoite samples. Uninfected controls were prepared equal to tachyzoite and filter controls, but the unfiltered monolayer was harvested after scraping. Bradyzoites and respective controls were generated in T60 dishes for indicated times. Uninfected and infected samples and bead-only controls were prepared as described in section 4.1.5. Uninfected controls served to estimate host cell contamination in bradyzoite samples. Bead-only controls served to estimate contamination caused by the purification procedure. Samples were shock-frozen in liquid nitrogen and collected as pellets at -80 °C till further analysis.

4.4.1.2 Extraction and analysis of polar and apolar metabolites

For the extraction of metabolites, infected and uninfected pellets were extracted in 100 µl chloroform, scraped against the tube rack to dislodge the pellet and sonicated in a water bath for 10 min. 400 µl of 3:1 MeOH:water (containing 1 µl *scyllo*-inositol / 400 µl as internal standard) were added and the monophasic suspension was centrifuged (10 min, 21,500 x g, 0 °C). The supernatant was collected and added to 200 µl water, vortexed and centrifuged again (3 min, 21,500 x g, 0 °C) to facilitate phase separation. For the analysis of polar metabolites, ˜600 µl of the upper phase were transferred into a new 1.5 ml tube without touching the interphase to avoid contamination with proteins. The 600 µl were dried into 250 µl GC / MS inserts using a speed vac concentrator by adding not more than 120 µl / sample / centrifugation. When the 600 µl were dried, the samples were washed two times with 30 µl MeOH and the inlets were transferred into prepared GC / MS vials. Subsequently the samples were solved in 20 µl pyridine containing 20 mg/ml methoxyamine into the inlet for 1 h at 37 °C, followed derivatization by adding 20 µl N,O-bis(trimethylsilyl)trifluoroacetamide to the samples.

Samples were carefully vortexed and incubated for 1 h at RT. In parallel a metabolite mix (**Appendix II**) was prepared by adding and drying 1 µl of the mix into an inlet. Further preparation was equal as described for polar phases. The metabolite mix was prepared fresh for each run and served for peak identification in DExSI (Dagley and McConville, 2018). For the analysis of apolar metabolites, ~80 µl of the apolar phase was collected, dried into 250 µl GC / MS inserts using a speed vac concentrator and washed two times with 30 µl MeOH. The MeOH-washed lipids were then trans-methylated by adding 40 µl of 3-(trifluoromethyl) phenyltrimethylammonium hydroxide (5 % in MeOH) diluted 1:1 in 2:1 chloroform:MeOH to the inserts for 1 h at RT.

Tachyzoite samples were analyzed on an electron impact GC / MS (Agilent 5977B / 890B) equipped with a HES ion source and a HP5ms-ui column (30 m x 0.25 mm x 2.5 µM) and bradyzoite samples on a DB5-MS column (30 m x 0.25 mm x 2.5 µM) preceded by a 10 m duragard column. Helium was used as a carrier gas at a flow rate of 1 ml/min. The temperature gradients applied in this work were as follows: For polar samples, the injector insert, and GC / MS transfer line temperatures were 270 °C. Oven temperature gradient was programmed as follows: 70 °C (1 min hold); 70 °C to 295 °C at 12.5 °C/min; 295 °C to 325 °C at 30 °C/min; 325 °C (4 min hold). For apolar phases, initial oven temperature was 80 °C. Temperature was ramped from 80 °C to 140 °C with 30 °C/min and increased to 250 °C at 5 °C/min (10 min hold) and ramped further to 320 °C at 15 °C/min. All data were analyzed in MSD ChemStation and DExSI (Dagley and McConville, 2018), corrected for their natural abundance according to procedures in DExSI (Nanchen et al., 2007; van Winden et al., 2002).

4.4.2   Liquid chromatography mass spectrometry analysis

4.4.2.1 Sample preparation

Tachyzoite samples, host cell samples and filter controls were generated in T150 dishes. Bradyzoite samples and host cell controls were prepared in two T150 dishes per sample. Samples and controls were further processed as stated in section 4.4.1.1. For tachyzoite samples, parasites were counted and adjusted to 1×10^8 parasites / sample prior extraction. Bead-supplemented tachyzoite controls were generated equally to cyst samples, replacing washing steps via magnetic stand by centrifugation (1,200 x *g*, 10 min, 0°C).

4.4.2.2 Extraction and analysis of metabolites

The general extraction and analysis of metabolites was done as follows: Metabolites were extracted in 80 % acetonitrile and 20 % water containing an internal standard mix (Phenolphthalein, CAPS, PIPES). Cell pellets were sonicated for 5 min and after centrifugation

(21.500 x g, 5 min, 0 °C), supernatants were transferred to MS vials for LC / MS analysis. 5 µL of each sample was collected to generate a pooled biological quality control (PBQC).

LC / MS analyses and subsequent data analyses was mainly done by Deborah Maus. Chromatographic separation was achieved on a Vanquish Flex fitted with an ACQUITY UPLC BEH amide column. Running a 25 min linear gradient starting with 90 % eluent A (10 mM ammonium carbonate in acetonitrile) / 10 % eluent B (10 mM ammonium carbonate in water) and ending with 40 % eluent A / 60 % eluent B, followed by washing and equilibration steps. Compound Discoverer 3.1 software was used for peak detection, combination of adducts and compound annotation. Metabolite identifications were based on either retention time and accurate mass match to 160 compounds of an inhouse library of 160 authentic standards (**Appendix III)**, or by matching accurate mass and MS2 fragments to m/z cloud database. Depending on the experiment, the general process was adjusted as follows:

Untargeted metabolic analysis of *in vitro*-derived tissue cysts and tachyzoites
Following metabolite extraction as detailed in section 4.4.2.2, 20 µl of the *in vitro* cysts, bead control and host cell background samples, and 5 µl of the tachyzoite samples were injected. The injection order of the samples was randomized, blanks and PBQCs were injected periodically. The samples were analyzed on a Q-Exactive Plus mass spectrometer via 70k MS1 scans, with intermittent 35k data-dependent 35k MS2 scans in positive and negative mode separately.

Peak integration was checked in Compound Discoverer 3.1 software before data export to Excel for grouping, combination of datasets from positive and negative ionization runs and blank subtraction. At this point, compounds with a coverage less than 50 % in at least one sample set were excluded, and all missing values were replaced with either the respective mean of each sample set or the minimum value of the whole dataset (gap filling). After internal standard normalization the fractional abundances for each sample were calculated and adjusted between 1 and -1.

Carnitine-dependent assays
Metabolites were extracted and chromatographically separated as described in section 4.4.2.2. 5 µL of each sample were injected and analyzed a 70k Full-MS 35k Top 3 ddMS2 experiment in positive mode. With Compound Discoverer 3.1 software peaks were detected, adducts combined and compounds annotated.

Detection of free linoleic acid
LC was performed as described in section 4.4.2.2, but mass spectra were acquired at a resolution of 140k in full scan mode without generating fragmentation spectra.

4.5 Statistical analysis

All tests were performed in GraphPad Prism v8 as detailed in the results section. Principal component analyses were computed using ClustVis (Metsalu and Vilo, 2015).

Chapter 5: Results

5.1 Establishment of an *in vitro* protocol for matured *Toxoplasma gondii* tissue cysts

5.1.1 KD3 human myoblasts differentiate into multinucleated myotubes

T. gondii persists in skeletal muscle tissue (Dubey et al., 1998), but robust *in vitro* culture systems supporting long-term maturation of tissue cysts in these natural host cells are lacking. An immortalized human skeletal muscle cell clone (KD3) (Shiomi et al., 2011) was tested for its ability to develop into myotubes and serve as natural host cell for *T. gondii* tissue cysts. Sub-confluent myoblast cultures were differentiated into myotubes through serum starvation for five days (**Figure 7**).
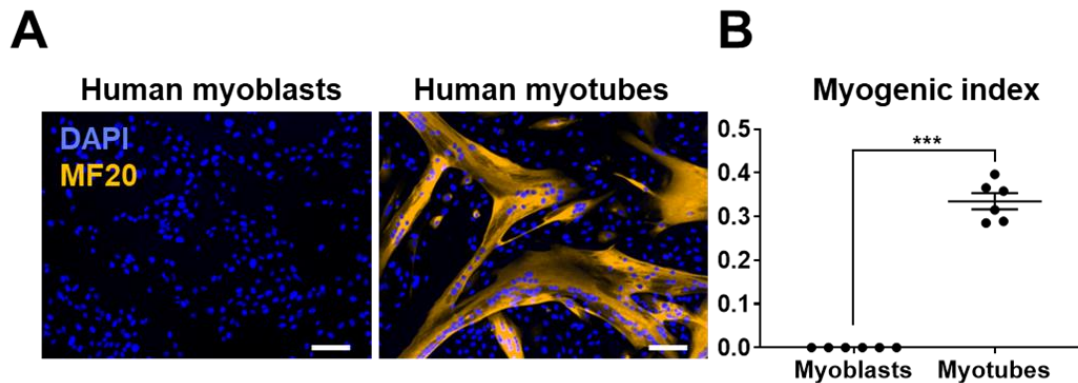
Figure 7: Myogenic index of KD3 human myoblasts and myotubes. (A.) Representative immunofluorescence images of KD3 myoblasts and myotubes after five days of differentiation stained for myosin heavy chain (MF20) and DNA (DAPI). (B.) Quantification of the myogenic index for myoblasts and myotubes. As a morphological parameter of myotube formation, the myogenic index (fraction of nuclei in a multinucleated cell) was measured in at least 10 different randomly selected locations by CCEAN software (Neumann, 2014). Values are expressed as mean ± SEM of two individual experiments performed in triplicates (***$p < 0.001$, Mann-Whitney-U-test). Scale bar indicates 100 μm. Data was mostly generated by Jana Scholz.

As indicated by the DAPI stain, myoblast cells fused into multinucleated tubes that were expressing myosin heavy chain (MF20) (**Figure 7**A) and developed spontaneous contraction activity (data not shown) as described previously (Shiomi et al., 2011). Accordingly, the myogenic index, which reflects the fraction of nuclei in multinucleated cells, rose above 0.3 (**Figure 7**B).

Together, these data indicate that *in vitro* differentiated KD3 myotubes develop hallmarks of mature myotubes which qualifies them to be a valuable model to study *T. gondii* encysted bradyzoites in a natural host cell.

5.1.2 KD3 human myotubes induce spontaneous stage conversion to encysted bradyzoites

Rat and mice primary skeletal muscle cells (Ferreira-da-Silva Mda et al., 2009a; Ferreira-da-Silva Mda et al., 2009b) and C2C12 myotubes (Swierzy and Lüder, 2015) are described to facilitate the spontaneous conversion of tachyzoites to early encysted bradyzoite stages. To test whether this ability is also harbored by human KD3 myotubes, we infected negative control human fibroblast (HFF) cells, KD3 myoblasts and KD3 myotubes under standard CO_2-replete culture conditions with PruΔku80Δhxgprt-GFP parasites. These parasites express GFP under the bradyzoite-specific lactate dehydrogenase 2 (LDH2)-promoter, which was used to monitor spontaneous differentiation. To compare dynamics of cystogenesis, samples were stained with *Dolichos biflorus* agglutinin (DBA) for their cyst wall and the tachyzoite-specific marker surface antigen 1 (SAG1) 48 h, 72 h and 96 h post infection (p.i.) (**Figure 8**, **Figure 9**, **Figure 10**).
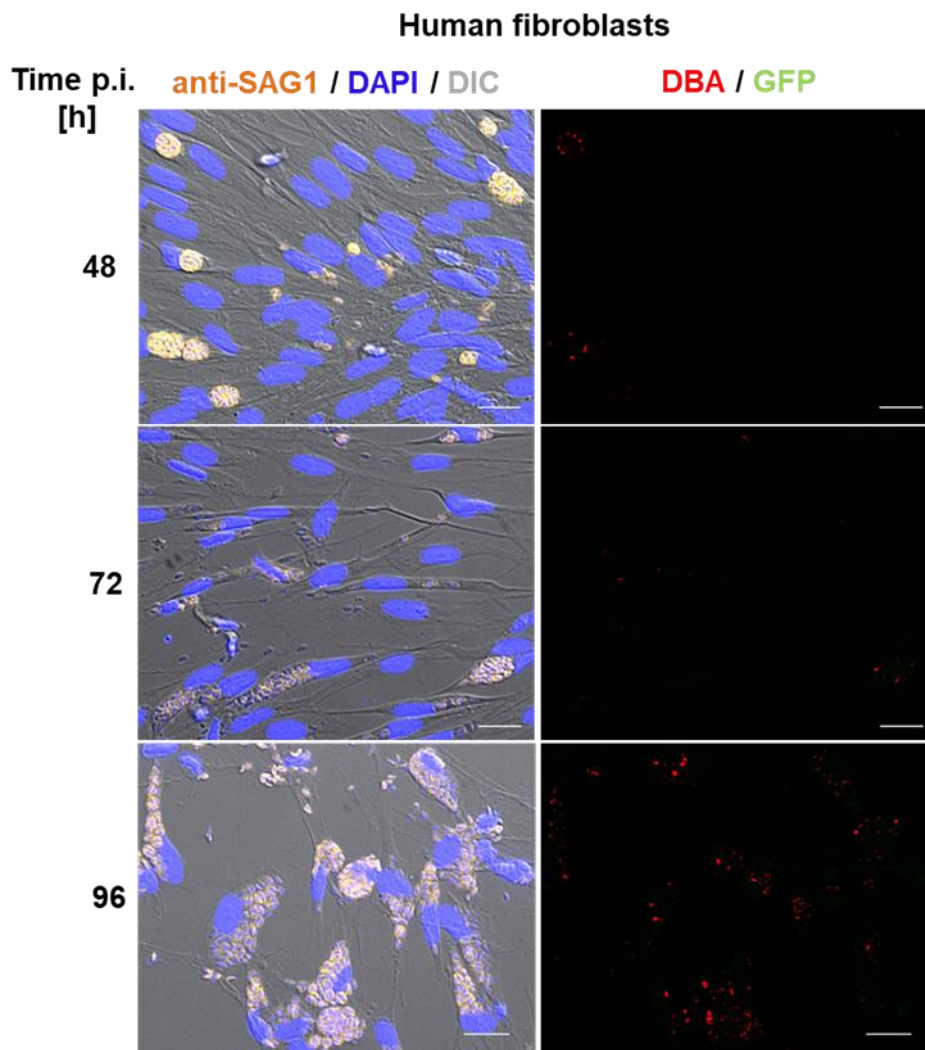
Figure 8: Spontaneous differentiation of *T. gondii* in human fibroblasts. Representative immunofluorescence images of human fibroblasts (HFFs) infected with PruΔku80Δhxgprt-GFP parasites. HFFs were infected with *T. gondii* PruΔku80Δhxgprt-GFP tachyzoites (MOI: 0.5) that express GFP under the bradyzoite-specific lactate dehydrogenase 2 (LDH2)-promotor. Monolayers are stained

for DNA (DAPI), tachyzoite surface antigen 1 (SAG1) and the cyst wall (*Dolichos biflorus* agglutinin (DBA)) 48 h, 72 h and 96 h post infection (p.i.). The GFP signal indicates spontaneous stage conversion of tachyzoites to bradyzoites. Scale bar indicates 20 µm.

In HFFs, 48 h post infection the cells were packed with vacuoles mostly containing 16-32 parasites. A distinct tachyzoites-specific SAG1 signal was detectable in all vacuoles, whereas DBA staining appeared in parts of very few vacuoles. 72 h post infection antigen expression remained consistent, but major part of the host cell layer was already lysed and egressed extracellular tachyzoites were abundant. 96 h post infection the remaining host cells were densely packed with SAG1-expressing tachyzoites. Spotty DBA staining was observed as well and did not indicate the formation of intact cyst walls. LDH2-promoter driven GFP expression appeared absent throughout the time course.
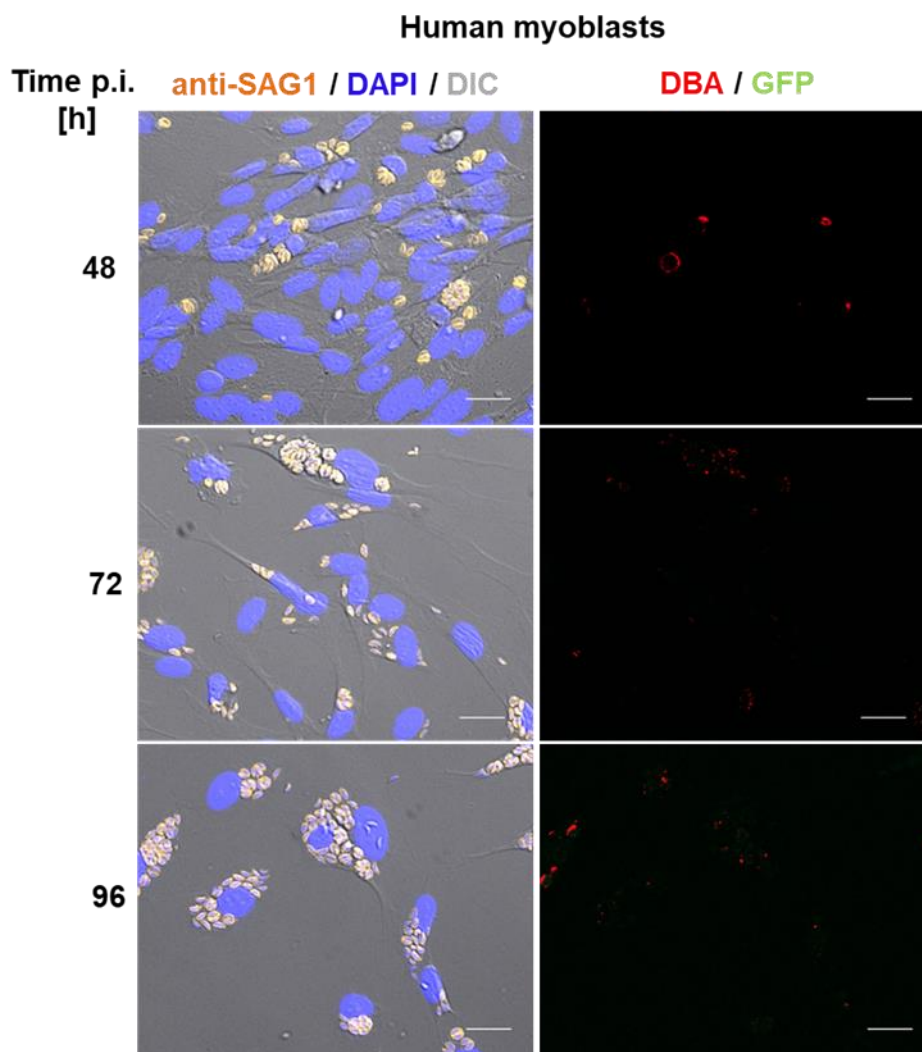
Figure 9: Spontaneous differentiation of *T. gondii* in human myoblasts. Representative immunofluorescence images of KD3 myoblasts infected with Pru*Δku80Δhxgprt*-GFP parasites. Human myoblasts were infected with *T. gondii* Pru*Δku80Δhxgprt*-GFP tachyzoites (MOI: 0.5) that express GFP under the bradyzoite-specific lactate dehydrogenase 2 (LDH2)-promotor. Monolayers are stained for DNA (DAPI), tachyzoite surface antigen 1 (SAG1) and the cyst wall (*Dolichos biflorus* agglutinin (DBA)) 48 h, 72 h and 96 h post infection (p.i.). The GFP signal indicates spontaneous stage conversion of tachyzoites to bradyzoites. Scale bar indicates 20 µm.

Upon infection of myoblasts, vigorous parasite proliferation was visible already after 48 h. Detected vacuoles showed distinct SAG1-expression and very few also showed a faint, but non-punctate DBA staining of the cyst wall. At 72 h post infection parts of the host cell monolayer were lysed and extracellular tachyzoites emerged. The parasites showed a prominent SAG1-expression, but no consistent staining of the cyst wall. 96 h post infection the same pattern was visible, but host cell monolayer was nearly completely lysed and remaining cells were filled with parasites.
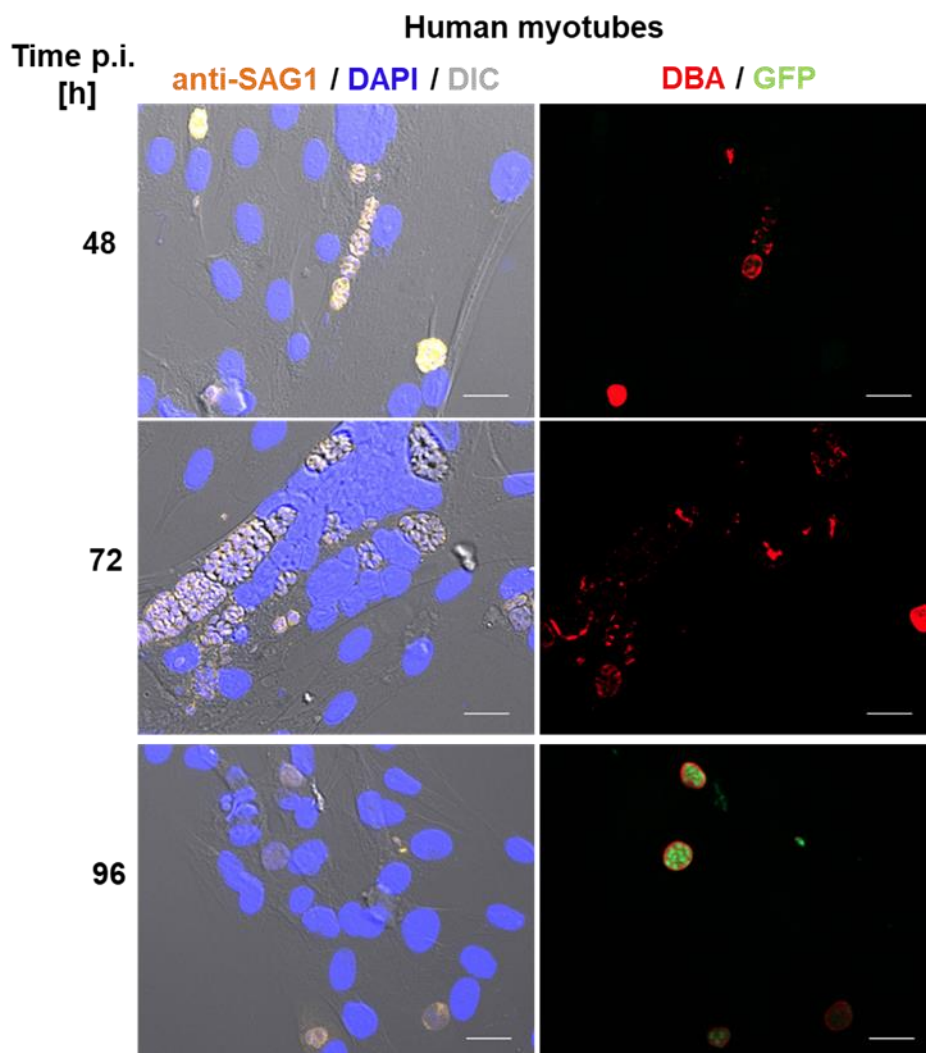
Figure 10: Spontaneous differentiation of *T. gondii* in human myotubes. Representative immunofluorescence images of human myotubes infected with Pru*Δku80Δhxgprt*-GFP parasites.Human myotubes were infected with *T. gondii* Pru*Δku80Δhxgprt*-GFP tachyzoites (MOI: 0.5) that express GFP under the bradyzoite-specific lactate dehydrogenase 2 (LDH2)-promotor. Monolayers are stained for DNA (DAPI), tachyzoite surface antigen 1 (SAG1) and the cyst wall (*Dolichos biflorus* agglutinin (DBA)) 48 h, 72 h and 96 h post infection (p.i.). The GFP signal indicates spontaneous stage conversion of tachyzoites to bradyzoites. Scale bar indicates 20 µm.

In contrast, infection of human myotubes for 48 h resulted in few parasites per vacuole and DBA stain indicated the formation of a cyst wall in a major fraction of the vacuoles. All detected parasites showed a prominent SAG1 signal. 72 h post infection, the host cell monolayer was

still intact, no free parasites were visible while DBA staining was detected in a large proportion of vacuoles. 96 h post infection, myotube monolayer was still intact with no egressed parasites. All vacuoles were positive for DBA and about half of parasites expressed a distinct GFP, while losing SAG1-expression.

In summary, HFFs and myoblasts allowed vigorous proliferation of *T. gondii* tachyzoites and host cell layers were destroyed after a short infection period. Spontaneous stage conversion appeared to occur at a low rate. In contrast, myotubes led to a slowed down proliferation of *T. gondii* and favored spontaneous formation of encysted bradyzoites. Interestingly, cyst wall formation indicated by DBA staining was earlier initiated than the expression of bradyzoite specific gene LDH2. These findings indicate that KD3 myotubes provide a promising host cell background for the study of encysted bradyzoites.

5.1.3 KD3 human myotubes enable cyst formation and long-term culture of virulent and avirulent *Toxoplasma gondii* strains

T. gondii strains differ greatly in their capacity to form tissue cysts *in vitro* and *in vivo* (Sullivan et al., 2009) and their maturation is accompanied by sequential regulation of marker protein expression (Ferguson, 2004). To test the suitability of KD3 myotubes to long-term culture tissue cysts of multiple *T. gondii* strains, the formation of tissue cysts of eight parasite strains of the three major isotypes was monitored under CO_2-deplete conditions at neutral and basic pH for 7, 14 and 21 days. Stage conversion was detected by staining the cyst wall with DBA and antibodies against the CC2 protein (Gross et al., 1995) of bradyzoites and by the absence of the tachyzoite-specific marker SAG1. Myotubes infected with laboratory high passage type I RH*Δku80Δhxgprt* parasites that do not easily form tissue cysts *in vitro* served as a tachyzoite control (**Figure 11**).
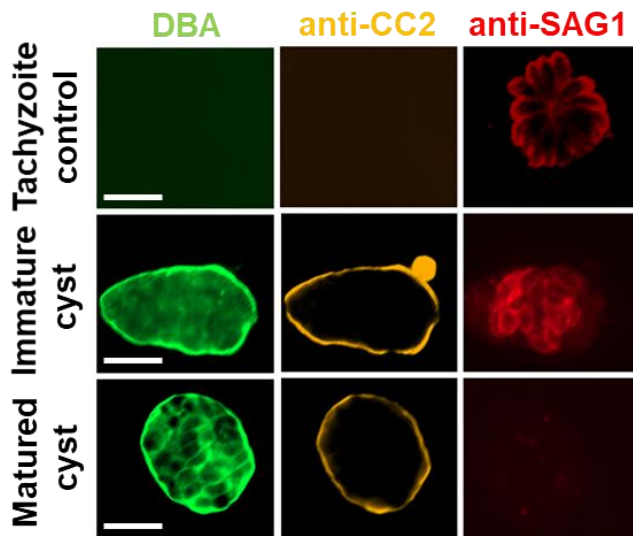
Figure 11: Marker protein expression of tachyzoites, immature and matured cysts in KD3 myotubes. Representative immunofluorescence imaging of KD3 myotubes infected with RH*Δku80Δhxgprt* (MOI: 2) for 24 h in CO_2-replete conditions (tachyzoites, lower panel) and with NED parasites (MOI: 0.1) for 14 days under CO_2-deplete conditions (immature and matured tissue cysts, middle and lower panel). Samples were stained with anti-CC2, anti-surface antigen 1 (SAG1) antibodies, *Dolichos biflorus* agglutinin (DBA) and DAPI. Scale bar indicates 5 µm.

The tachyzoite control remained negative for bradyzoite marker CC2 and cyst wall marker DBA, while SAG1 was readily detected (**Figure 11**, upper panel). Parasites that expressed all three antigenic markers were classified as immature cysts (**Figure 11**, middle panel), whereas cysts that exclusively expressed CC2 bradyzoite-specific marker and were positive for DBA staining were classified as matured cysts (**Figure 11**, lower panel). Strikingly, under both conditions all cultures were DBA-positive and remained stable without being overgrown by tachyzoites for 21 days. The quantification of this time- and pH-dependent maturation process is displayed in **Figure 12**.
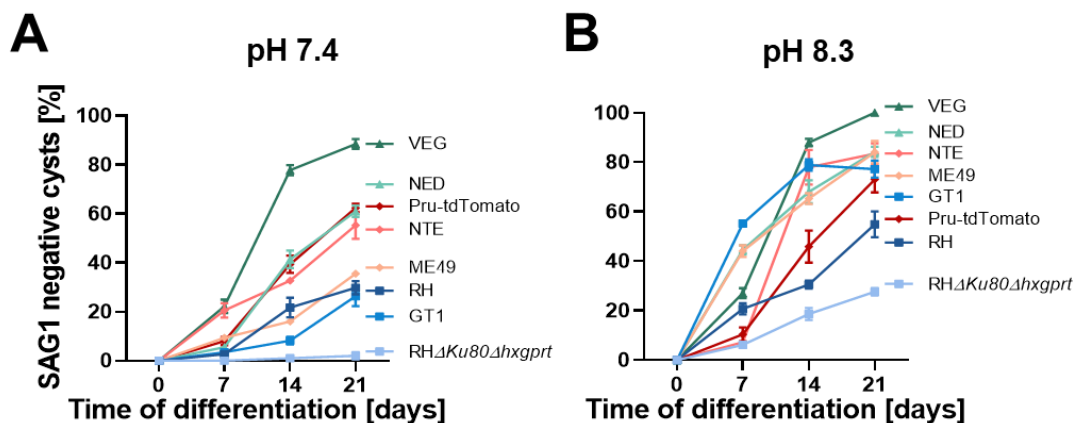
Figure 12: Time- and pH-dependent cyst maturation of type I, II and III *T. gondii* strains in KD3 myotubes. (A.-B.) Relative numbers of SAG1-negative cysts via immunofluorescence assay of KD3 myotubes infected with type I (RH, RH*Δku80Δhxgprt*, GT1), type II (ME49, NTE, Pru-tdTomato) and type III (NED, VEG) parasites (MOI: 0.1). Cyst formation was induced for 7, 14 and 21 days under (A.) neutral or (B.) basic pH. Cultures were stained with anti-CC2, anti-surface antigen 1 (SAG1) antibodies and *Dolichos biflorus* agglutinin (DBA). Relative numbers of SAG1-negative but DBA- and CC2-positive

cysts counted from three independent blinded experiments performed in triplicates. At least 25 DBA positive cysts per strain, time point, and replicate were counted. Values represent means ± SEM.

Significant amounts of matured cysts under all conditions were observed except with the high-passage laboratory adapted RH*Δku80Δhxgprt* strain, which did not differentiate at neutral pH but required basic conditions. We observed almost complete differentiation of type III VEG parasites into DBA- and CC2-positive and SAG1-negative cysts. All type II strains and the type III NED strain showed intermediate maturation (between 35 % and 63 %) that was considerably increased in basic pH to 73 % and 83 %, respectively. Also, wild-type type I strains GT1 and RH exhibited differentiation up to 30 % that increased to 77 % and 55 % at basic pH, respectively. Generally, the fraction of matured cysts increased over time and was highest for all strains after three weeks. Higher pH increased the number of matured cysts presumably since it acts as an additional stressor leading to differentiation. In particular, the type I strains responded to higher pH.

Together, these data show that KD3 myotubes enable the culture of tissue cysts of cystogenic and non-cystogenic parasite strains without contaminating tachyzoite growth at physiological pH over the course of 21 days.

5.1.4 KD3 human myotubes promote the formation of encysted bradyzoites with *in vivo*-like ultrastructure

The stage conversion of *T. gondii* is accompanied by the development of ultrastructural hallmarks (Dubey et al., 1998) that are noticeable by transmission electron microscopy. To confirm the ultrastructural maturation of encysted bradyzoites in KD3 myotubes, we infected myotubes with Pru-tandem (td)Tomato parasites for 7, 14 and 21 days under bradyzoite inducing conditions and samples were analyzed via electron microscopy (**Figure 13**)

Establishment of an *in vitro* protocol for matured *Toxoplasma gondii* cysts
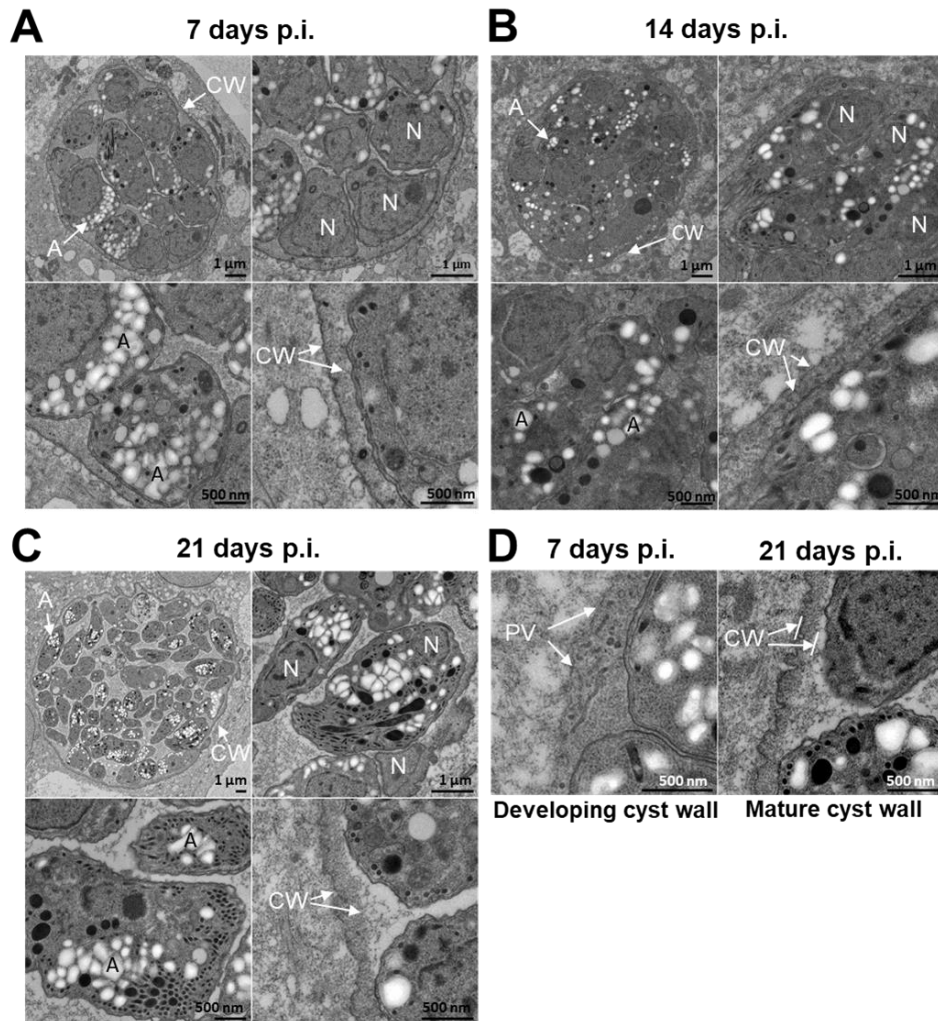
Figure 13: Time-resolved formation of ultrastructural bradyzoite characteristics of *in vitro* encysted bradyzoites in KD3 human myotubes. Representative transmission electron microscopy images of (A.) 7-, (B.) 14- and (C.) 21-day-old Pru-tdTomato tissue cysts matured in KD3 myotubes (MOI: 0.3). Images of a single section plane through entire cysts were taken for each time point. Each overview image (upper left) is grouped with three images showing enlarged areas, such as individual parasites with their nuclei (N), amylopectin granules (A) or the cyst wall (CW). In the example shown here, the cyst wall is already well developed seven days post infection. Other cysts at this time point reveal an immature cyst wall, which is shown in the left image of the additional image panel on the lower right side (D.). At this stage the parasitophorous vacuolar membrane (PVM) is associated with a loose matrix containing vesicles and membrane-bound tubules. In cysts 21 days post infection (shown at the right side of this image panel), the CW is formed by a dense and rather homogenous matrix which is associated with the PVM. post-infection; p.i.. Electron microscopy was performed by Tobias Hoffmann.

Evaluation of the ultrastructure of the encysted parasites by electron microscopy revealed hallmarks of bradyzoites developing already seven days post infection (**Figure 13**A). The "unorganized" bradyzoite-like structure inside the cyst became visible, amylopectin granules (A) accumulated and bradyzoites already showed a posteriorly located nucleus (N). The thickness of the cyst wall (CW) increased throughout the course of infection through the apparent deposition of electron-dense vesicular-tubular material under the parasitophorous vacuolar membrane (PVM) (**Figure 13**A-D).

Establishment of an *in vitro* protocol for matured *Toxoplasma gondii* cysts

Evidently, *in vitro* encysted bradyzoites in KD3 myotubes developed the ultrastructural features of *in vivo* bradyzoites in a time-dependent manner.

5.1.5 KD3 myotube-derived encysted bradyzoites develop resistance to acid-pepsin and temperature stresses

Oral transmission of *T. gondii* tissue cysts in undercooked meat products requires resistance against acid-pepsin digestion and temperature stresses (Dubey et al., 1990). To test whether *in vitro*-derived encysted bradyzoites develop acid-pepsin resistance, Pru-tdTomato parasites were differentiated in myotubes for 14 to 28 days. Intracellular cysts were digested with pepsin for 20, 40 and 60 min, the reaction mix was then neutralized, and cysts were seeded onto HFF cells to allow re-differentiation in tachyzoite medium under CO_2-replete conditions. Untreated tachyzoite and cyst cultures and pepsin-digested tachyzoite cultures served as positive and negative controls, respectively (**Figure 14**).
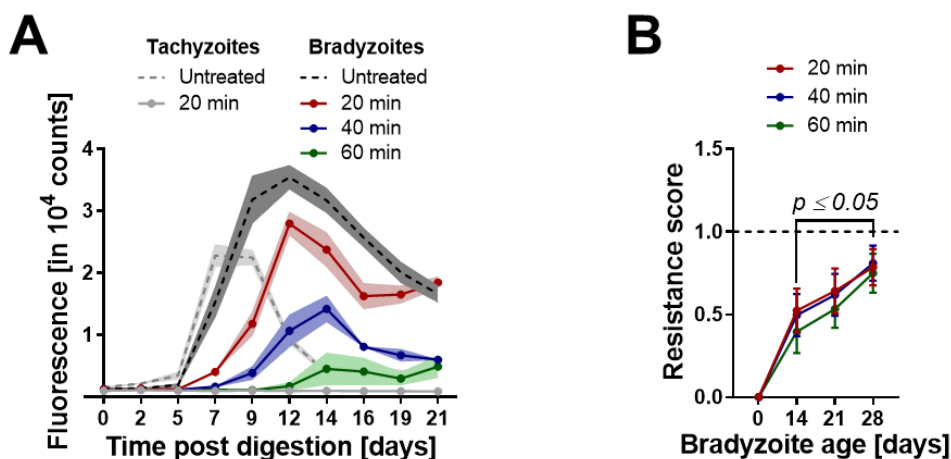
Figure 14: Gradually developing acid-pepsin resistance of *in vitro*-derived encysted bradyzoites over maturation time. Pru-tdTomato encysted bradyzoites (MOI: 0.1) and tachyzoites (MOI: 2) were cultured in myotubes for up to 28 and for two days. (A.) Raw fluorescence intensities of 21-day-old cysts digested for 20 (red), 40 (blue) and 60 min (green) and the respective tachyzoite control (grey). Dashed lines indicate corresponding untreated controls. The data represent the means and SEM of one experiment consisting of three digestion reactions (B.) Resistance scores of tachyzoite cultures (0), 14-, 21- and 28-day-old cysts after 20 (red), 40 (blue), 60 min (green) of pepsin digestion. Shown are the means and SEM of three independent experiments performed in triplicates (*p≤0.05, Mann-Whitney-U-test).

Growth of both, untreated tachyzoite and bradyzoite cultures, was observed by an increase in tdTomato fluorescence (indicative of tachyzoite replication) after two and seven days, respectively (**Figure 14**A). Interestingly, all acid-pepsin-treated bradyzoite cultures recovered after 7, 9 and 14 days, depending on the length of the acid-pepsin digest, while acid-pepsin-digested tachyzoite cultures did not recover even after a period of 21 days. We quantified acid-pepsin resistance across the time course of cyst maturation by calculating a resistance score (RS) (see section 4.3.1) based on the acid-pepsin-inflicted growth delay (**Figure 14**B). Already

after 14 days all digested cultures recovered with an RS between 0.4 to 0.5. Acid-pepsin resistance continued to increase over the course of 28 days up to an RS of 0.8.

Given the developing pepsin resistance, the *in vitro*-derived cysts were tested for their ability to survive an unmitigated human transmission scenario which includes, besides pepsin digestion, extended cold-storage and heat stress. Therefore, Pru-tdTomato cysts were matured in myotubes for 35 days. After mechanical release from the culture plates, myotubes containing the tissue cysts were subjected as pellet to: a 5 min heat shock at 55 °C or 65 °C, acid-pepsin digestion for 60 min, storage for 4 days at 4 °C followed by 60 min acid-pepsin digestion, storage for 4 days at 4 °C and a heat shock for 5 min at 55 °C followed by 60 min acid-pepsin digestion, storage for seven days at 4 °C followed by 60 min acid-pepsin digestion, storage for seven days at 4 °C and a heat shock for 5 min at 55 °C followed by acid-pepsin digestion. Storage at RT for two days served as a positive control (**Figure 15**).
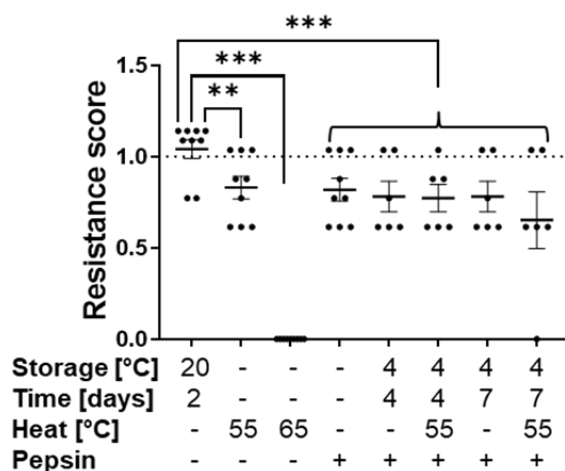
Figure 15: Resistance of matured *in vitro*-derived encysted bradyzoites to acid-pepsin, extended cold storage and heat stress. Resistance scores of 35-day-old Pru-tdTomato encysted bradyzoites cultured in myotubes (MOI: 0.1) exposed to indicated temperature stresses and acid-pepsin digestion. Values are expressed as means and SEM from three or two independent experiments in triplicates (**p<0.005, ***p<0.001, Mann-Whitney-U-test).

In comparison with untreated cysts, storage at room temperature did not decrease viability as indicated by a RS of 1. Different combinations of storage at 4 °C for four or seven days and heat shock at 55 °C combined with a 60 min acid-pepsin digestion did lower the RS to a range between 0.75 and 0.65, while heating to 65 °C effectively killed tissue cysts as expected (Dubey et al., 1990).

Summarized, these data indicate that KD3 myotubes can serve as host cells that support maturation of *T. gondii* tissue cysts for 35 days which is accompanied with gradual development of resistance to acid-pepsin and temperature stresses. Therefore, the *in vitro*-generated cysts resemble functional hallmarks of mature *in vivo* cysts and required properties for both experimental oral infection of mice and environmental transmission to humans.

5.1.6 KD3 human myotubes facilitate the development of encysted bradyzoites which are orally infectious in mice

Up to now the common "gold standard" for maturity of encysted bradyzoites is their oral infectivity to mice. To assure oral infectivity to animals, groups of five mice were infected with 50 and 500 35-day-old Pru-tdTomato *in vitro* cysts via oral gavage. Control groups included mice receiving 10,000 HFF- or myotube (MT)-derived tachyzoites (TZ) and as positive control 10 *in vivo* tissue cysts from brain tissue (mouse). To facilitate comparison of infectivity between *in vitro* and *in vivo* cysts, we measured the diameters of *in vitro* cysts (**Figure 16**A). For evaluation of infectivity, mice sera were tested via enzyme-linked immunosorbent assay (ELISA) for *T. gondii* specific immunoglobulin G and brain cyst burden of mice which showed seroconversion was analyzed for one experiment (**Figure 16**B-D).

Stage	Tz	Tz	Cyst	Cyst	Cyst
Origin	HFF	MT	MT	MT	Mouse
Inoculum	10^4	10^4	50	500	10
Seroconversion	1/10	2/10	8/10†*	9/10†*	4/5†
Brain cysts**	1/1	2/2	1/3	4/4	4/4
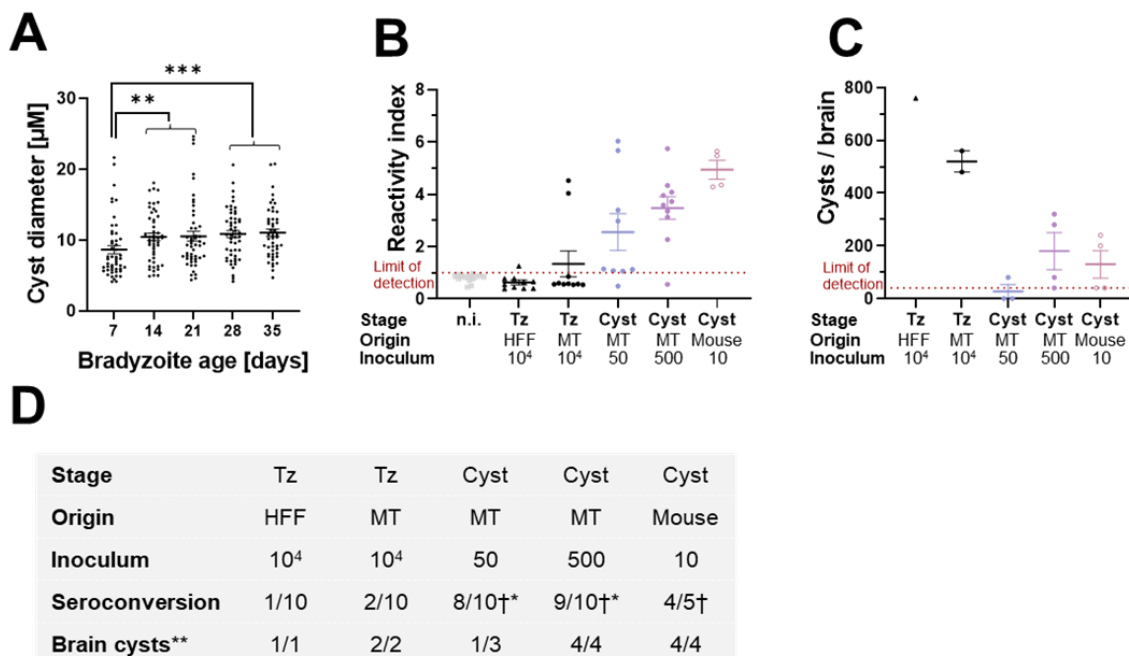
Figure 16: *In vitro* **encysted bradyzoites are orally infectious to mice and lead to manifestation of chronic infection in a size- and therefore dose-dependent manner.** Pru-tdTomato encysted bradyzoites (MOI: 0.1) and tachyzoites (MOI: 2) were cultured in myotubes for up to 35 and for two days, respectively. (A.) Quantification of cyst diameter of 7-, 14-, 21, 28 and 35-day-old Pru-tdTomato *in vitro* tissue cysts. Encysted bradyzoites were stained with *Dolichos biflorus* agglutinin (DBA) and DAPI. Images of 50 cysts were randomly taken and the diameter was measured in Zen 2.6 lite blue by defining the DBA stain as the outline of the cysts. Values are expressed as means and SEM from one experiment (**p<0.005, ***p<0.001, Mann-Whitney-U-test). (B.-D.) Reactivity index and cyst number per brain of mice that were orally infected with 10^4 human fibroblast (HFF)- or myotube (MT)-derived tachyzoites (TZ), 50 or 500 35-day-old Pru-tdTomato *in vitro* cysts or 10 Pru-tdTomato *in vivo* cysts. Brains and blood from moribund animals were collected starting from 1two days post infection. (B.) Seroconversion was checked for *T. gondii* specific immunoglobulin G via ELISA and reactivity index was calculated. Values are expressed as means and SEM from two independent experiments consisting of five mice per group. (C.) Quantification of cyst burden per brain of infected mice. Only seropositive mice were analyzed for brain cysts. Values are expressed as means and SEM from one experiment (D.) Summary of *in vivo infection* experiments. †: infected animals died during the 30-day period. *Seroconversion of moribund, but not dead animals were checked throughout the experiment. ** Brain cyst burden was only determined in seropositive animals of one experiment. Mouse infection experiments and subsequent analyses were performed by Mateo Murillo Leon.

Establishment of an *in vitro* protocol for matured *Toxoplasma gondii* cysts

Maturation over the course of 35 days increased the average diameter from 8.8 µm to 11 µm. This compares to 35-day-old *in vivo* cysts from brain tissue with a mean diameter of 56.02 µm (Watts et al., 2015). Assuming spherical cysts, this implies an approximate 150-fold difference in volume. The oral infection of mice with 50 and 500 *in vitro*-derived cysts led to seroconversion of 8 out of 10 and 9 out of 10 mice, respectively as indicated by detection of *T. gondii* specific immunoglobulin G (**Figure 16**B, D). We also observed seroconversion of one and two mice infected with HFF- and myotube-derived tachyzoites. As expected, all mice infected with 10 *in vivo*-derived tissue cysts showed seroconversion. The presence of DBA-positive *T. gondii* cysts in the brains of infected mice was quantified microscopically 30 days post infection in brain homogenates (**Figure 16**C, D). We detected cysts in all seroconverted tachyzoite infected mice and mice receiving 500 *in vitro* cysts or 10 *in vivo* cysts. Only one of three mice that seroconverted from infection with 50 cysts and survived, harbored detectable cyst burden.

During the experiment, the mice were weighted daily. The relative weight loss and the survival curves are displayed in **Figure 17**.
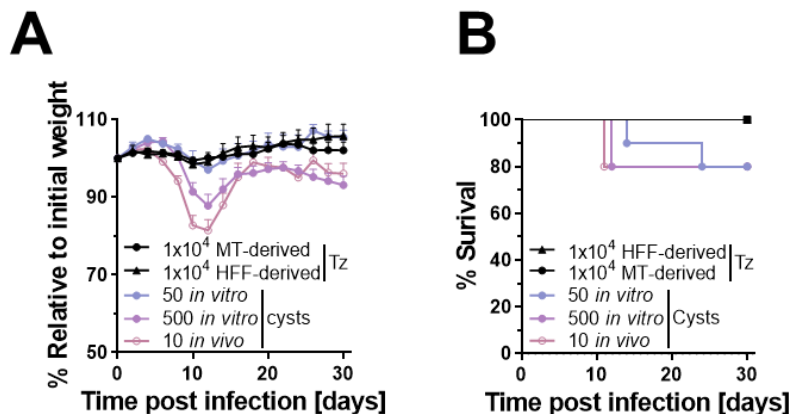
Figure 17: Weight loss and survival of mice infected with tachyzoites and tissue cysts. Pru-tdTomato encysted bradyzoites (MOI: 0.1) and tachyzoites (MOI: 2) were cultured in myotubes for up to 35 and for two days, respectively. (A.-B.) Mice were orally infected with either 1x10⁴ myotube (MT)- or human fibroblast (HFF)-derived tachyzoites (TZ), 50 or 500 *in vitro*-generated or 10 *in vivo*-generated tissue cysts for 30 days. (A.) The relative weight loss displayed in %. Each data point represents the means of two experiments consisting of five infected animals per group with ± SEM. (B.) % of surviving animals during infection period. Mouse infection experiments and subsequent analyses were performed by Mateo Murillo Leon.

Infection of mice was indicated by weight loss of mice receiving 500 *in vitro* or 10 *in vivo* cysts. In these groups, two animals succumbed to the infections while one animal that received 50 cysts needed to be culled. Animals infected with tachyzoites did not show a significant weight loss and survived the 30-day infection period (**Figure 17**A, B).

Summarized, our experiments show that *in vitro*-generated tissue cysts are significantly smaller in size than *in vivo* cysts. Considering this, the data for seroconversion, cyst load,

weight loss and survival show that KD3 myotube-derived tissue cyst are similar to *in vivo* cysts regarding their ability to orally infect mice.

5.1.7 KD3 human myotubes promote the formation of encysted bradyzoites which develop full tolerance to known antiparasitics and drug candidates

T. gondii tissue cysts pose a major health threat because they evade current toxoplasmosis treatments (Barrett et al., 2019). To test whether cysts cultured in myotubes mirror drug resistance of *in vivo* cysts, we challenged 14-, 21- and 28-day-old Pru-tdTomato cysts with antiparasitics for one week and monitored their re-differentiation into tachyzoites under CO_2-replete conditions as a measure of cyst viability (**Figure 18**).
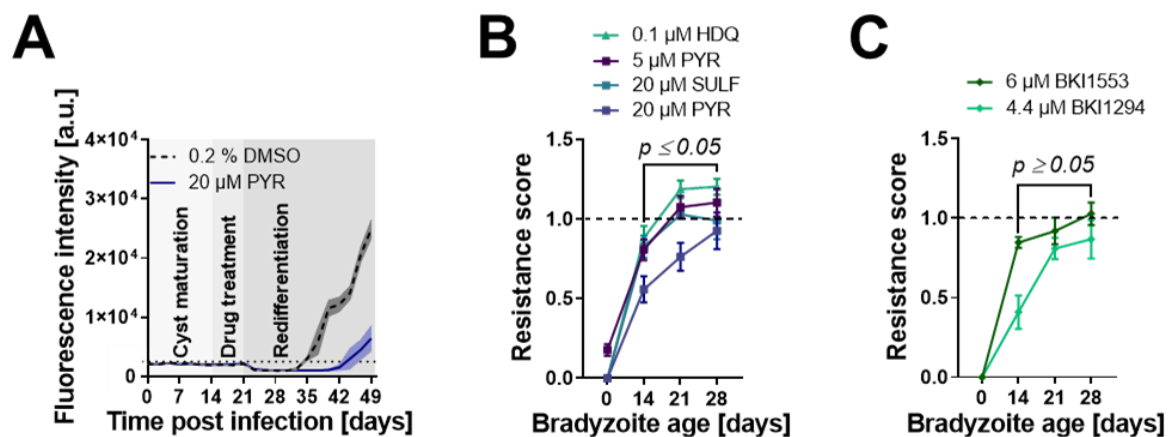
Figure 18: Tolerance of *in vitro* encysted bradyzoites against antiparasitics and drug candidates. Pru-tdTomato encysted bradyzoites (MOI: 0.1) and tachyzoites (MOI: 1) were cultured in myotubes for up to 28 days and for 4 h, followed by treatment. (A.) Raw fluorescence intensities of a representative experiment during cyst maturation for 14 days, seven days of treatment with 20 µM pyrimethamine or 0.2 % DMSO as solvent control and re-differentiation for 28 days. Black dotted line indicates the limit of detection. Data represents the means and SEM of one experiment with five replicates. (B.-C.) Resistance scores of tachyzoites (0) and 14-, 21- and 28-day-old bradyzoites treated with indicated concentrations of pyrimethamine (PYR), sulfadiazine (SULF) or 1-hydroxy-2-dodecyl-4(1*H*) quinolone (HDQ) and bumped kinase inhibitor (BKI) 1553 and 1294. Shown are means of three independent experiments with five replicates each and SEM (*p≤0.05, Mann-Whitney-U-test).

Figure 18A shows the fluorescence signal observed over 49 days, including 14 days of cyst maturation, seven days of pyrimethamine treatment and 28 days of re-differentiation in tachyzoite medium. Growth of DMSO- and pyrimethamine-treated parasites was indicated by a fluorescence intensity increase above background at 14- and 24-days post treatment, respectively. We next compared the resistance scores of tachyzoites with those of 14-, 21- and 28-days-old tissue cysts to the antifolates pyrimethamine (5 µM and 20 µM), sulfadiazine (20 µM) and the an inhibitor of dihydroorotate dehydrogenase (Hegewald et al., 2013) and alternative NADH dehydrogenase (Saleh et al., 2007) 1-hydroxy-2-hodecyl-4(1H)-quinolon (HDQ) (0.1 µM) (**Figure 18**B). All bradyzoite cultures survived all tested treatments. Interestingly, while resistance against sulfadiazine, HDQ and low doses of pyrimethamine was already fully developed after 21 days, indicated by an RS of 1, resistance against high doses

of pyrimethamine increased until 28 days of maturation (**Figure 18**B). In contrast, tachyzoite-infected myotubes, which served as a control and are shown as '0 days differentiated cultures', did not survive treatment with 20 µM pyrimethamine, 20 µM sulfadiazine and 0.1 µM HDQ. However, two out of three tachyzoite cultures survived 5 µM pyrimethamine treatment, with a low RS of 0.18. Furthermore, we tested the resistance against two different bumped kinase inhibitors (BKI), BKI1553 and BKI1294 (**Figure 18**C), that have been shown to decrease cyst burden in brains of infected mice (Scheele et al., 2018; Winzer et al., 2015). Consistent with previous results, tachyzoites did not grow after exposure to fourfold of the IC_{50} of each compound. In contrast, already 14-day-old tissue cysts were resistant to both treatments, with an RS of 0.42 and 0.83, respectively. Resistance increased further over maturation time and BKI1553 became completely ineffective against 28-day-old cysts while cysts reached an RS of 0.89 against BKI1294 (**Figure 18**C).

In summary, these data demonstrate that myotube-cultured tissue cysts gradually develop resistance against established and experimental drugs and indicate the system's suitability for phenotypic screens of drug candidates against the chronic form of *T. gondii*.

5.2 Metabolic fingerprint of tachyzoites and *in vitro* encysted bradyzoites

5.2.1 The metabolome of *Toxoplasma gondii* depends on the host cell type and parasite stage

Since the conversion of tachyzoites to encysted bradyzoites is accompanied with ubiquitous metabolic remodeling (see section 1.1.2.4), discovering the potential different metabolic phenotypes of these two stages would shed light on tolerances against antiparasitic treatments. Many antiparasitic compounds have metabolic target structures, but the metabolome of bradyzoites has only been characterized indirectly (Olson et al., 2020). Our *in vitro* system for matured *T. gondii* tissue cysts, allowed us to address this shortcoming for the first time.

We compared the metabolome of ME49 parasites in their encysted bradyzoite form with intracellular tachyzoites cultured in both HFF cells and myotubes (**Figure 19**, **Figure 20**). Parasites were differentiated into cysts for 28 days and purified using magnetic beads as described in section 4.1.5. We estimated a yield of $2x10^6$ cysts from two pooled T150 culture dishes that were used for one replicate (data not shown). To correct for background metabolites derived from contaminating host material and magnetic bead preparations, we included uninfected myotubes and bead-only controls into our analysis. These samples were treated identical to bradyzoite samples. We also estimated artefacts that are introduced by differences in quenching and preparation procedures that are applied to tachyzoites and bradyzoites. Therefore, we supplemented isolated tachyzoites with beads and processed them similar to bradyzoite samples. For data curation, the blank and host cell background was subtracted, and ion intensities were normalized to the total ion count per sample and log2-fold changes of metabolites between experimental conditions calculated (**Appendix IV**).
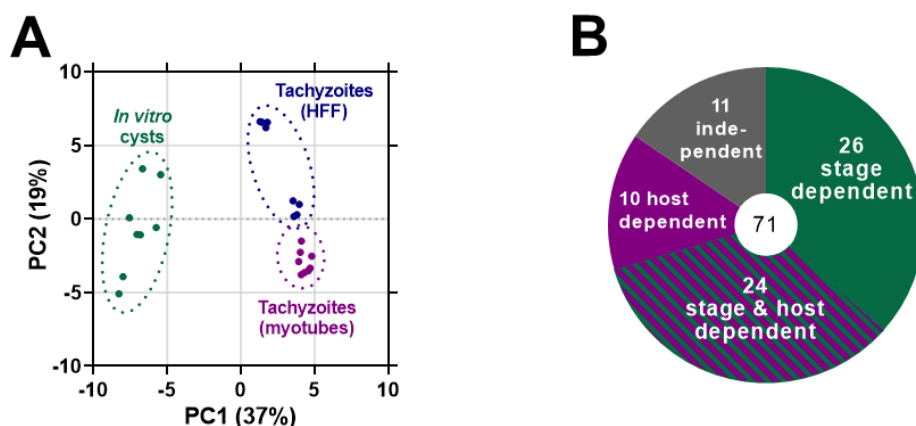
Figure 19: Stage specific and host specific regulated and independent metabolites of *T. gondii.* ME49 encysted bradyzoites (MOI: 0.1) and tachyzoites (MOI: 3) were cultured in myotubes and human fibroblasts (HFFs) for 28 days and for two days, followed by isolation and extraction. (A.) Principal component (PC) analysis of untargeted metabolomic data comparing 28-day-old ME49 *T. gondii in vitro* cysts cultivated in KD3 myotubes, tachyzoites in KD3 myotubes and tachyzoites in HFFs. Two individual

experiments with four replicates each were analyzed. (B.) Pie chart showing the number of metabolites within the dataset and how they were affected by host cell environment and parasite stage. Data analysis was mainly performed by Deborah Maus.

Bead-supplemented tachyzoite controls were indistinguishable from pure tachyzoites, and uninfected host cells were similar to bead-only samples, indicating minimal metabolite alterations and contamination due to the purification procedures (**Appendix IV**). Following data curation, principal component (PC) analysis revealed that the three groups form distinct clusters and indicated that encysted bradyzoites differed from tachyzoites along PC1, while myotube- and HFF-derived tachyzoites were separated in PC2 (**Figure 19**A). The two clusters of HFF-derived tachyzoites represent two independent experiments. We quantified the levels of 71 metabolites that excluded metabolites that occurred in uninfected controls. The levels of 26 metabolites varied between parasite stages, ten varied between types of host cells, while 24 depended on both factors, and 11 remained invariant (**Figure 19**B).
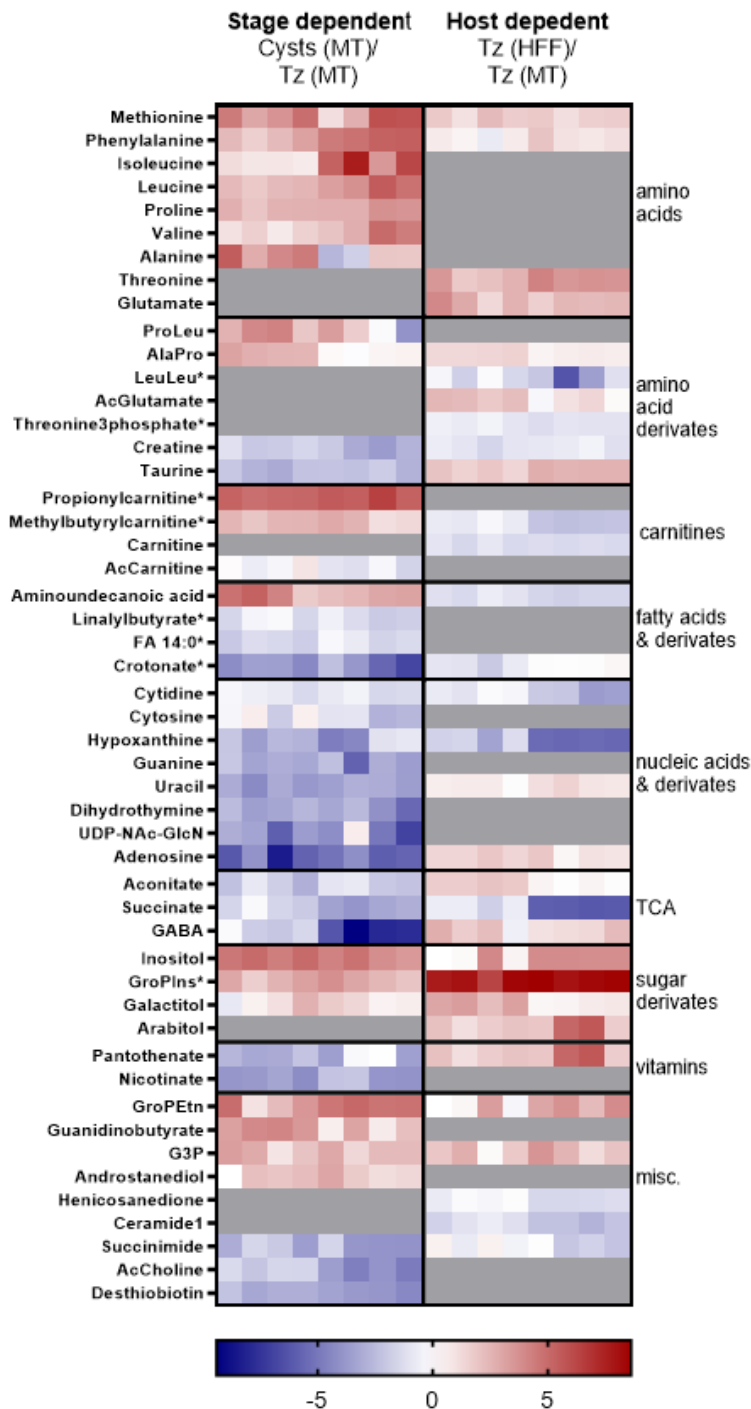
Figure 20: Stage specific and host specific regulated and independent metabolites of *T. gondii.* Heatmap showing log2-fold changes of significantly different metabolites (p<0.05, uncorrected Mann-Whitney-U test) between *in vitro* cysts and tachyzoites (Tz) in myotubes (MT) (left panel) and tachyzoites in myotubes compared to tachyzoites in human fibroblasts (HFFs) (right panel). Log2-fold changes were calculated pairwise. Grey areas indicate non-significantly changed metabolites. Asterisks denote putative metabolite identifications based on accurate mass only. Ac: acetyl, UDP-NAc-GlcN: UDP-N-acetyl-glucosamine, GABA: γ-aminobutyric acid, TCA: tricarboxylic acid; GroPIns: glycerphosphoinositol, GroPEtn: glycerophosphoethanolamine, G3P: glycero-3-phosphate, misc.: miscellaneous. Data analysis was mainly performed by Deborah Maus.

Comparing *in vitro*-derived encysted bradyzoites to tachyzoites, both cultured in myotubes, the relative abundances of sugar derivatives, dipeptides and amino acids were generally increased (**Figure 20**, left panel). Relative levels of vitamins, metabolites associated with the tricarboxylic acid (TCA) cycle and derivatives of amino acids and nucleic acids were found to be decreased. Fatty acids (FAs) and related molecules were variably affected by stage conversion. When comparing HFF-cultured tachyzoites to myotube-cultured tachyzoites, we observed that the levels of sugars and amino acids were higher in HFF-grown tachyzoites, while FAs were decreased in abundance (**Figure 20**, right panel). The parasite stage and the host cell type had mixed effects on other metabolite classes.

Summarized, our data reveal distinct metabolic features in *T. gondii* encysted bradyzoites and suggest a downregulation of the mitochondrial TCA cycle in bradyzoites.

5.2.2 The tricarboxylic acid cycle plays a diminished role in mature *Toxoplasma gondii* encysted bradyzoites

To compare the importance of the stage-specifically regulated TCA cycle between tachyzoites and bradyzoites, cultures were treated with sodium fluoroacetate (NaFAc), a specific inhibitor of the *T. gondii* aconitase (MacRae et al., 2012), to inhibit the TCA cycle flux. Freshly invaded tachyzoites and 28-day-old *in vitro*-derived Pru-tdTomato cysts cultured in myotubes were treated for one week with indicated concentrations of NaFAc and the IC_{50} value for tachyzoites (**Figure 21**A) and the RS for tachyzoites and bradyzoites (**Figure 21**B) were determined.
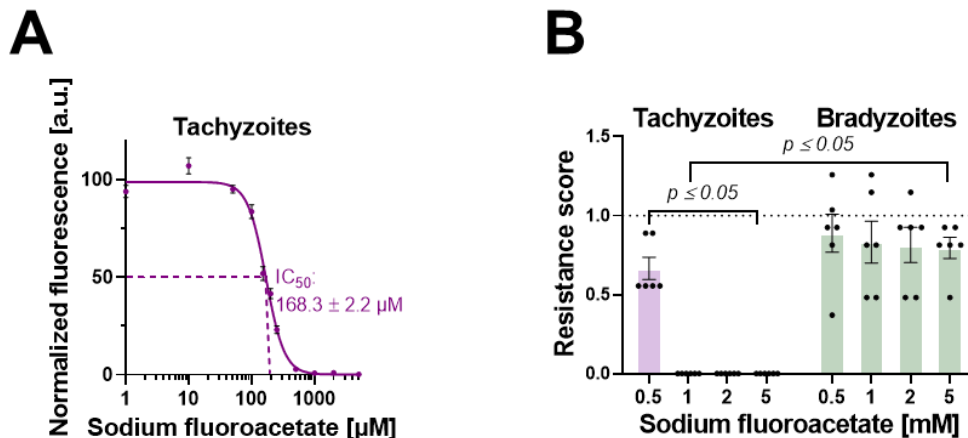
Figure 21: Impact of sodium fluoroacetate on the viability of *T. gondii* tachyzoites and mature encysted bradyzoites. Pru-tdTomato encysted bradyzoites (MOI: 0.1) and tachyzoites (MOI: 1) were cultured in myotubes for 28 days and for 4 h, followed by treatment. (A.) Calculation of half inhibitory concentration (IC_{50}) of sodium fluoroacetate (NaFAc) for Pru-tdTomato tachyzoites. Parasites were grown for seven days in presence of NaFAc and the IC_{50} value was calculated from fluorescence intensities normalized to untreated controls. Shown are means and SEM of three independent experiments with three replicates each. (B.) Resistance scores of tachyzoites and 28-day-old bradyzoites treated with NaFAc or 0.5 % water as solvent control. Shown are means and SEM of two and three independent experiments for bradyzoites and tachyzoites performed in triplicates, respectively (*p≤0.05, Mann-Whitney-U-test).

Continuous exposure to NaFAc arrests tachyzoite replication at an IC_{50} of 168 µM, and parasite replication was completely abolished at 500 µM (**Figure 21**A). While bradyzoites treated with up to 5 mM NaFAc remained viable with an RS of 0.8, tachyzoites did not recover after exposure to concentrations greater than 500 µM (**Figure 21**B).

To proof that tolerance of bradyzoites towards NaFAc does not rely on exclusion of this inhibitor from the cyst wall which acts as diffusion barrier (Acquarone, 2017; Tomita et al., 2013), we sought to measure marked direct metabolic effects of this inhibitor on tachyzoite and bradyzoite stages (MacRae 2012). We treated 28-day-old ME49 encysted bradyzoites and intracellular myotube-cultured tachyzoites with NaFAc for seven and three days, respectively and analyzed the metabolomes by HILIC-UHPLC-LC / MS (**Figure 22**).
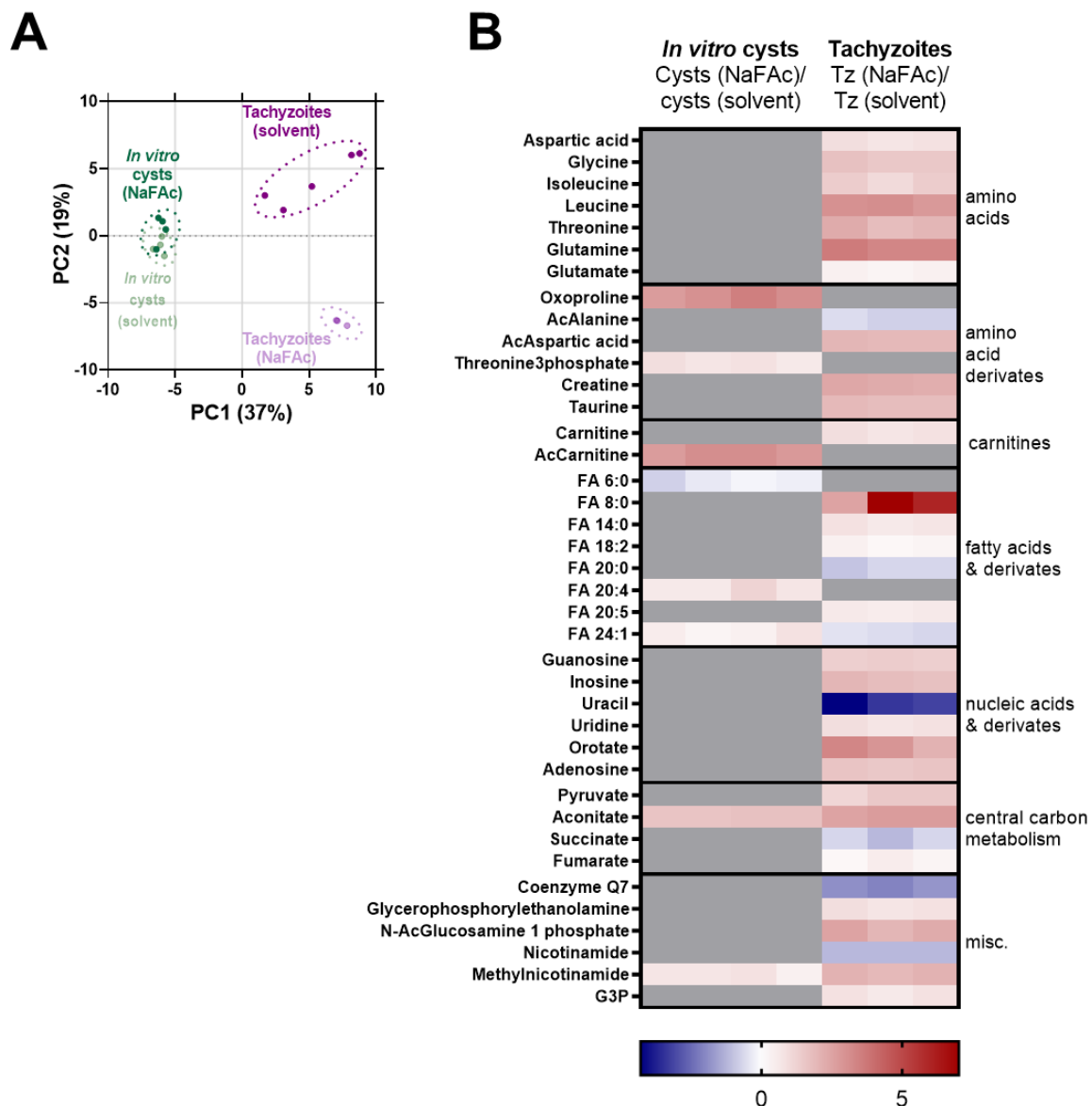
Figure 22: Sodium fluoroacetate inhibits the mitochondrial aconitase of *T. gondii* tachyzoites and bradyzoites. ME49 encysted bradyzoites (MOI: 0.1) and tachyzoites (MOI: 3) were cultured in myotubes for 28 days and for two days, followed treatment, isolation, and extraction. (A.) Principal

component (PC) analysis of untargeted metabolomic data comparing 28-day-old ME49 *T. gondii in vitro* cysts cultivated in KD3 myotubes either incubated for seven days in presence of 1 mM sodium fluoroacetate (NaFAc) or 0.5 % water as solvent control and tachyzoites cultivated in myotubes treated for three days with 500 µM NaFAc or 0.25 % water as solvent control. One experiment with four replicates for bradyzoite groups, five replicates for solvent-treated and three replicates for NaFAc-treated tachyzoites were analyzed. (B.) Heatmap showing log2-fold changes of significantly different metabolites ($p < 0.05$, uncorrected Mann-Whitney-U test) between NaFAc-treated and solvent-treated *in vitro* cysts (left panel) and between NaFAc-treated and solvent-treated tachyzoites (Tz) (right panel). Log2-fold changes were calculated pairwise. Grey areas indicate non-significantly changed metabolites. Ac: acetyl, G3P: glycero-3-phosphate, misc.: miscellaneous. Data analysis was mainly performed by Deborah Maus.

The PC analysis revealed that solvent- and NaFAc-treated tachyzoites form distinct clusters that are separated along the PC2 axis. In contrast, treatment of tissue cysts did not lead to a separation of the sample groups (**Figure 22**A). NaFAc treatment affected the relative abundance of 33 metabolites in tachyzoites but changed only eight metabolites in encysted bradyzoites. In both parasite stages aconitate levels were increased significantly upon NaFAc treatment (**Figure 22**B).

These data indicate that NaFAc crosses the cyst wall and inhibits the aconitase in bradyzoites. Finally, these measurements support our hypothesis that the viability of bradyzoites does not rely on a functional TCA cycle.

5.3 Discovery of a potential detoxification mechanism in *Toxoplasma gondii*

5.3.1 The role of carnitine in *Toxoplasma gondii*

Interestingly, within our metabolomic data sets we found that *T. gondii* encysted bradyzoites as well as both tachyzoite populations contained carnitine and several different acylcarnitines (**Figure 20**) This metabolite class was thought to be absent from the parasite, since it lacks all enzymes for carnitine biosynthesis (ToxoDB) and is functionally uncharacterized.

5.3.1.1 Host cell carnitine is taken up by *Toxoplasma gondii* tachyzoites

Since *T. gondii* does not possess gene homologues to synthesize carnitine on its own (ToxoDB), we hypothesized a host origin of the detected carnitine metabolites in the parasite. To directly test carnitine uptake of *T. gondii*, myotubes were infected with tachyzoites and medium was supplemented with partially deuterated carnitine for 6 h, 24 h, and 48 h before parasite egress (**Figure 23**).
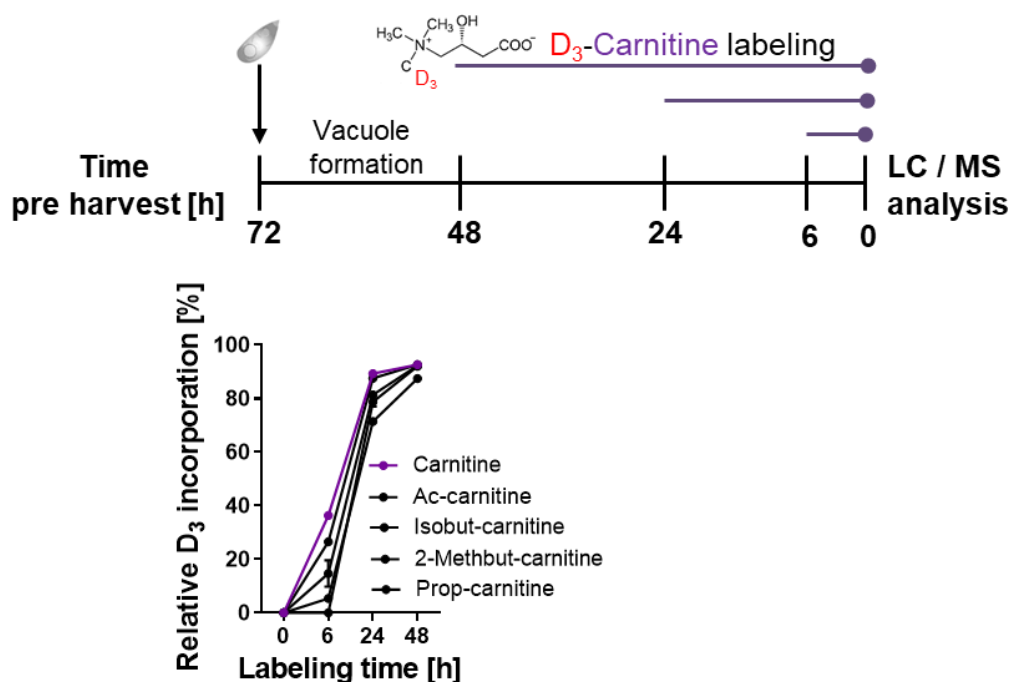
Figure 23: Import of host carnitine and acylcarnitines into *T. gondii* tachyzoites. Myotubes were infected with Pru-tdTomato tachyzoites with MOI 2, labeled for 0 h, 6 h, 24 h and 48 h with 15 µM deuterated (D_3)-L-carnitine followed by isolation and extraction. Uninfected and infected monolayers were analyzed for carnitine and acylcarnitines with LC / MS. Unlabeled cultures served as control for natural arising isotopologues and uninfected labeled and unlabeled host cells served as filter control to determine host cell contamination in the parasite samples. Relative D_3 labeling incorporation was calculated by normalizing the respective labeling time points to unlabeled control. Data represents the means of one experiment consisting of four replicates each. Shown are means ± SEM. Ac: acetyl; Do: deoxy; Isobut: isobutyryl; 2-Methbut: 2-methylbutyryl; Prop: propionyl. Data analysis was mainly performed by Deborah Maus.

LC / MS analysis revealed a time-dependent increase in deuterium incorporation into the parasite carnitine pool that reached 93 % after 48 h. Similarly, label incorporation of acylcarnitines was nearly saturated at this time.

These data indicate that *T. gondii* tachyzoites import exogenous carnitine through the host cell.

5.3.2 Medium- and long-chain fatty acids are imported by *Toxoplasma gondii* tachyzoites and bradyzoites

In eukaryotes, carnitine and acylcarnitines are known to play a central role in medium- and long-chain FA mobilization and their catabolism via β-oxidation. Although mitochondrial β-oxidation is a process which apparently does not take place in *T. gondii* tachyzoites and bradyzoites (Nolan et al., 2017; Oppenheim et al., 2014), we hypothesized, carnitine import is somehow connected to the FA household of *T. gondii*. To elucidate this, a FA import assay was established in *T. gondii* tachyzoites and in bradyzoites using a ^{U13}C FA labeling mix. For tachyzoites, myotubes were infected with type I RH, type II ME49 and type III NED. BSA-coupled ^{U13}C-FAs were added for up to 36 h until the egress of first parasites. FAs were isolated from naturally egressed parasites and analyzed as their methyl esters by GC / MS (**Figure 24**).
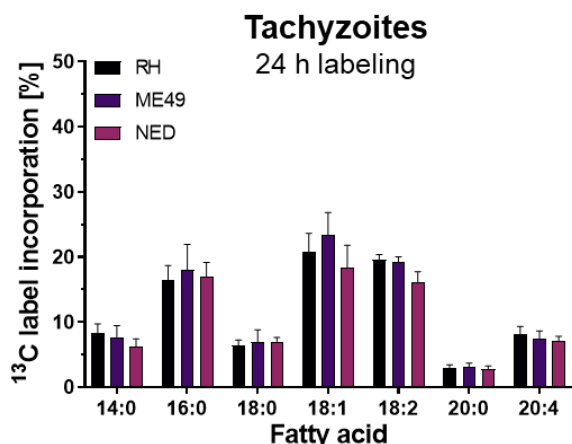
Figure 24: Fatty acid import of type I, II and III *T. gondii* tachyzoites in myotubes. Myotubes were infected with type I RH, type II ME49 and type III NED tachyzoites (MOI: 1) for 24 h, labeled for 36 h in medium supplemented with 2.5 % ^{U13}C fatty acid mix, followed by isolation and extraction. Uninfected but labeled host cells served as filter control to determine host cell contamination in the parasite samples. Shown are calculated ^{13}C label incorporation into total fatty acid pool in 24 h of type I RH, type II ME49 and type III NED cultured in myotubes. Label incorporation was calculated per 24 h to compare between experiments. Values are expressed as the mean with S.E.M. of two independent experiments with triplicate and quadruplicate cultures per condition (Mann-Whitney-U-test).

As expected from literature (Pernas et al., 2018), the data revealed that all analyzed medium- and long-chain FAs were partly scavenged from the host. Especially, unsaturated oleic (C18:1) and linoleic acid (LA, C18:2) were imported at high rates. There were no differences between strains detectable concerning the FA import.

In contrast to *T. gondii* tachyzoites, encysted bradyzoites are considered very slow growing and not dependent on continuous import of nutrients, although metabolic data are largely missing (Blume and Seeber, 2018). To monitor FA import in maturing bradyzoites, myotubes were infected with Pru-tdTomato parasites and stage formation was induced for 7, 14, 21 and 28 days in bradyzoite medium. All cultures including uninfected control cultures were exposed to BSA-coupled ^{13}C-labelled FAs for two days and isolated via DBA-coated magnetic beads (**Figure 25**).
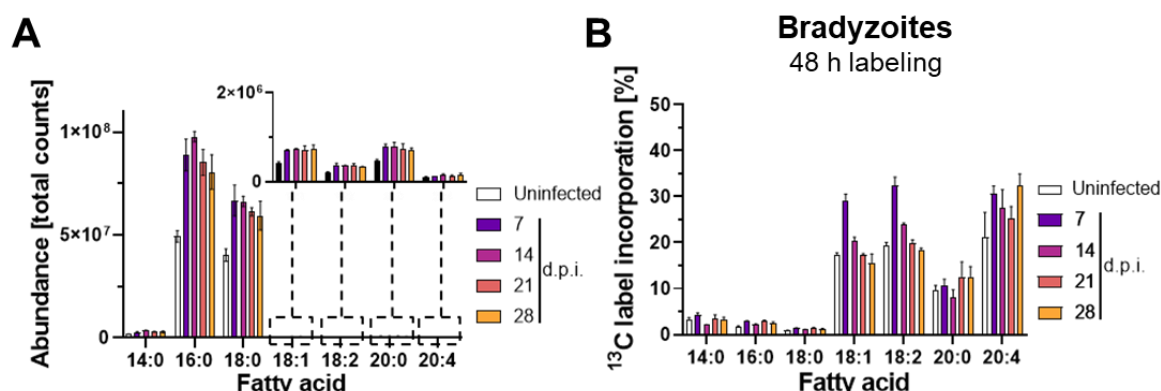
Figure 25: Fatty acid import of maturing encysted bradyzoites. Pru-tdTomato encysted bradyzoites (MOI: 0.3) were cultured in myotubes for 7, 14, 21 and 28 days, labeled for 48 h in medium supplemented with 2.5 % ^{U13}C fatty acid mix, followed by isolation and extraction. (A.) Abundances in total counts of medium- and long-chain fatty acids of 7-, 14-, 21- and 28-day-old Pru-tdTomato encysted bradyzoites and uninfected control cultures. (B.) Proportion of ^{13}C label incorporation in % of total medium- and long-chain fatty acids of 7-, 14-, 21- and 28-day-old Pru-tdTomato encysted bradyzoites and uninfected control cultures. Uninfected cultures were generated to estimate host cell contamination in parasite samples. Values are expressed as the mean with S.E.M. of one experiment with triplicate cultures per condition. d.p.i.: days post infection.

GC / MS analysis revealed molecule-specific contribution of FAs in parasite samples when compared to uninfected cultures. Abundances of FAs were equal for all bradyzoite samples independent of maturation time. Host cell FA contamination contributed 50-60 % to the overall signal, except for arachidonic acid (C20:4) that we could not significantly separate from host pools (**Figure 25**A). However, analysis of ^{13}C- incorporation revealed a trend towards attenuated FA import into maturing cysts (**Figure 25**B). In contrast to tachyzoites (**Figure 24**), encysted bradyzoites imported mainly mono- and doubly unsaturated stearic acid (C18:1, C18:2), while shorter FAs were only marginally labeled above background. This import activity declined to background levels after 14 days of maturation and cannot be distinguished from host contributions (**Figure 25**B).

We next sought to compare FA import into matured encysted bradyzoites of type I RH, type II ME49 and type III NED parasites. We matured cysts in myotubes for 28 days and prolonged the established metabolic labeling with ^{U13}C-FAs to five days (120 h) to enhance contrast from uninfected background (**Figure 26**).
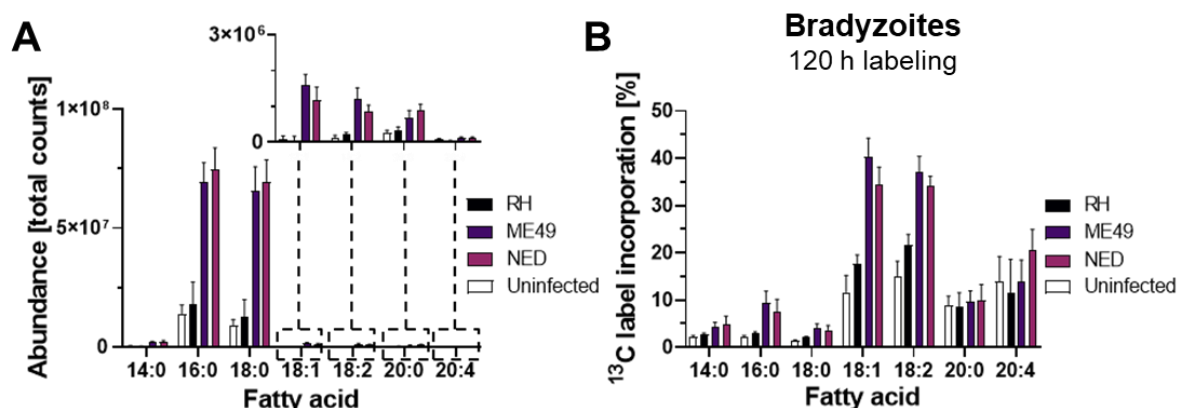
Figure 26: Fatty acid import of matured type I, II and III encysted bradyzoites. RH, ME49 and NED bradyzoites were cultured in myotubes (MOI: 0.1, 0.3, 0.3) for 28 days, labeled for 120 h in medium supplemented with 2.5 % ^{U13}C fatty acid mix, followed by isolation and extraction. (A.) Abundances of total medium- and long-chain fatty acids of 28-day-old RH, ME49 and NED encysted bradyzoites and uninfected control cultures. (B.) Proportion of ^{13}C label incorporation in % of total medium- and long-chain fatty acids encysted bradyzoites and uninfected control cultures. Uninfected cultures were generated to estimate host cell contamination in parasite samples. Values are expressed as the mean with S.E.M. of two experiments with quadruplicate cultures per condition. d.p.i.: days post infection.

We found significant label incorporation into all monitored FAs, indicating robust import into encysted bradyzoites. In this assay, host lipids contributed ~20% or less FAs to ME49 and NED samples (**Figure 26**A). Consistent with previous results, mono- and dual unsaturated stearic acid (C18:1, C18:2) showed highest incorporation of label, while shorter FAs were significantly less labeled (**Figure 26**B). Concerning label, arachidic and arachidonic acid (C20:0, C20:4) could not be distinguished from background levels. RH cysts could not be enriched from host cells, FA abundances were not distinguishable from background noise.

These results reveal for the first time that mature encysted bradyzoites actively sequester nutrients in form of a broad range of medium- and long-chain FAs from their host, although much slower compared to tachyzoites. The established isolation method is not applicable for RH encysted bradyzoites. Hence, KD3 myotubes present a cell culture model that is suitable for mass spectrometry-based methods to investigate metabolic parasite-host interactions of the bradyzoite stage of type II and type III *T. gondii*.

5.3.3 Meldonium is a potent inhibitor to deplete (acyl-) carnitine level and β-oxidation in human myotubes

To test the role of carnitine and acylcarnitine levels for *T. gondii*, we aimed to deplete host carnitine levels by blocking its biosynthesis using meldonium, a substrate analog for γ-butyrobetaine hydroxylase (Liepinsh et al., 2006). Therefore, we treated myotubes cultures with 25 μM for indicated times and investigated carnitine and acylcarnitine level via LC / MS (**Figure 27**A). Carnitines are important for mobilizing FA coenzyme A esters for transport across the mitochondrial membranes supplying the β-oxidation pathway (Liepinsh et al., 2006). The impact of depleted carnitine pools in myotubes on β-oxidation flux was analyzed.

Therefore, meldonium-treated cells were labeled with ^{U13}C FA mix and ^{13}C-acetyl-CoA incorporation into intracellular citric acid was quantified by GC / MS (**Figure 27**B).
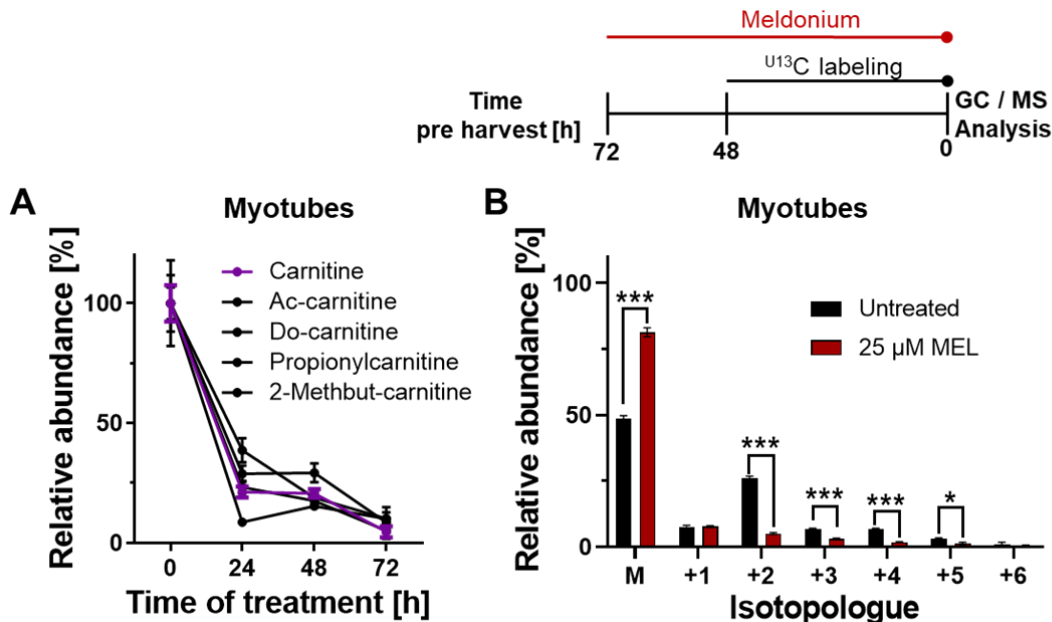
Figure 27: Impact of meldonium on (acyl) carnitine level and β-oxidation in human myotubes. (A.) Relative abundance of carnitine and acylcarnitine level of myotubes treated for 24 h, 48 h and 72 h with 25 µM meldonium. Relative abundance was calculated by normalizing respective treatment time points to untreated control. Shown are means of two independent experiments with triplicate and quadruplicate cultures, ± SEM. Ac: acetyl; Do: deoxy; 2-Methbut: 2-methylbutyryl; Prop: propionyl. Data analysis was mainly performed by Deborah Maus. (B.) Relative abundance of citrate isotopologues of myotubes labeled with ^{U13}C labeling mix for 48 h and 25 µM meldonium (MEL) treatment for 72 h. Shown are means of two independent experiments with four replicates each, ± SEM (*p<0.05; ***p<0.001, Mann-Whitney-U-test).

LC / MS analysis of myotubes treated with 25 µM meldonium showed a reduction of carnitine and all detected acylcarnitine levels by 60 % after 24 h and 90 % after 72 h (**Figure 27**A). The dually labelled M+2 isotopologue, which was taken as a measure for β-oxidation flux, decreased from 26 % to 5 % during 72 h treatment (**Figure 27**B).

These data indicate that meldonium treatment reduced carnitine levels at a functionally important extent in myotubes.

5.3.4 Meldonium treatment leads to an enhanced fatty acid uptake of several fatty acids in tachyzoites and bradyzoites

Having established the depletion of (acyl) carnitine pools and interference of the β-oxidation in myotubes via meldonium supplementation, we tested the impact of low host (acyl) carnitine levels on the growth of *T. gondii* in its tachyzoite and bradyzoite form. The IC_{50} of freshly invaded Pru-tdTomato tachyzoites and the resistance score for 28-day-old encysted bradyzoites were determined (**Figure 28**).

A

Tachyzoites

B
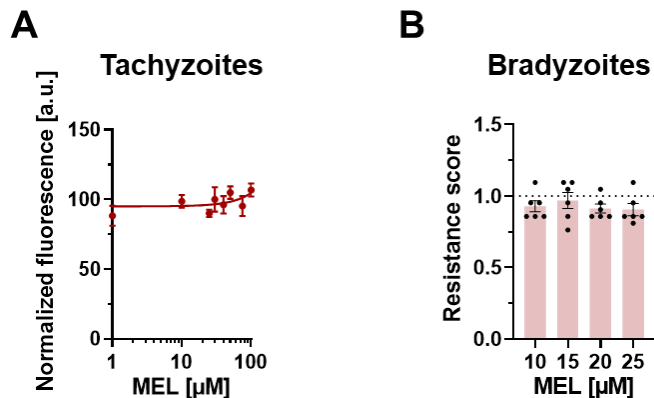
Bradyzoites

Figure 28: Impact of meldonium treatment on tachyzoite and bradyzoite viability. Pru-tdTomato encysted bradyzoites (MOI: 0.1) and tachyzoites (MOI: 1) were cultured in myotubes for 28 days and for 4 h, followed by treatment. (A.) Calculation of half inhibitory concentration (IC_{50}) of meldonium (MEL)-treated Pru-tdTomato tachyzoites. Parasites were grown for seven days in presence of meldonium or 0.05 % water as solvent control. The IC_{50} value was calculated from fluorescence intensities normalized to untreated controls. Shown are means and SEM of three independent experiments with three replicates each. (B.) Resistance scores of 28-day-old bradyzoites treated with meldonium (MEL) or 0.05 % water as solvent control. Shown are means and SEM of two independent experiments performed in triplicates.

Treatment with meldonium up to 100 µM did not lead to a significant growth defect in *T. gondii* tachyzoites and did not affect the viability of bradyzoites up to 25 µM (**Figure 28**A,B). This indicates that under cell culture conditions depleted carnitine levels were not limiting parasite fitness.

Studies indicate that mitochondria of the host cell compete with *T. gondii* for FAs (Pernas et al., 2018). Since carnitines are the key element for mitochondrial shuttle of medium- and long-chain FAs in mammalian cells, we hypothesized reduced host carnitine level would lead to a modified FA uptake of *T. gondii*. To elucidate this for both parasite stages, we treated myotubes infected with Pru-tdTomato tachyzoites and 28-day-old encysted bradyzoites with meldonium and simultaneously labeled the cells with a ^{U13}C FA mix. Total FAs of naturally egressed tachyzoites and bead-isolated tissue cysts were extracted and measured as their methyl esters using GC / MS (**Figure 29**, **Figure 30**).

A

B

Tachyzoites
24 h labeling
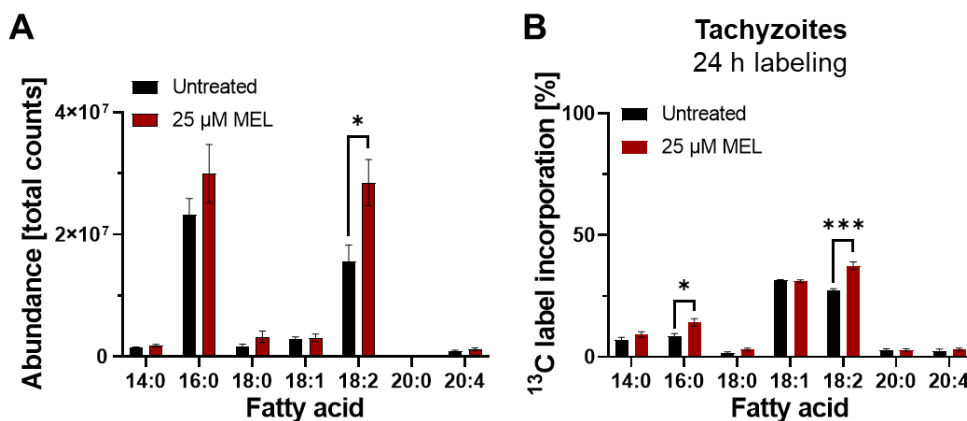
Figure 29: Impact of meldonium on fatty acid import of tachyzoites. Pru-tdTomato tachyzoites (MOI: 1) were cultured in myotubes for 4 h, labeled for up to 36 h in medium supplemented with 2.5 %

U13C fatty acid mix (Untreated) or medium supplemented with 2.5 % U13C fatty acid mix and 25 µM meldonium (MEL), followed by isolation and extraction. (A.) Abundances in total counts of total medium- and long-chain fatty acids of untreated and meldonium-treated Pru-tdTomato tachyzoites. Abundances were calculated per 1×10^6 parasites. (B.) Calculated ^{13}C label incorporation into total fatty acid pool in 24 h of untreated and meldonium (MEL)-treated Pru-tdTomato tachyzoites. Label incorporation was calculated per 24 h to compare between experiments. Values are expressed as the mean with S.E.M. of two independent experiments with triplicate and quadruplicate cultures per condition (*p<0.05; ***p<0.001, Mann-Whitney-U-test).

For tachyzoites, GC / MS analysis of total FAs showed an enhanced abundance of LA (C18:2) in meldonium-treated parasites (**Figure 29**A). Labeled FA pools of palmitic and LA (C16:0, C18:2) were increased in meldonium-treated parasites while myristic (C14:0), arachidic acid (C20:0) and oleic acid (C18:1) remained unchanged concerning abundance and labeling (**Figure 29**A-B).
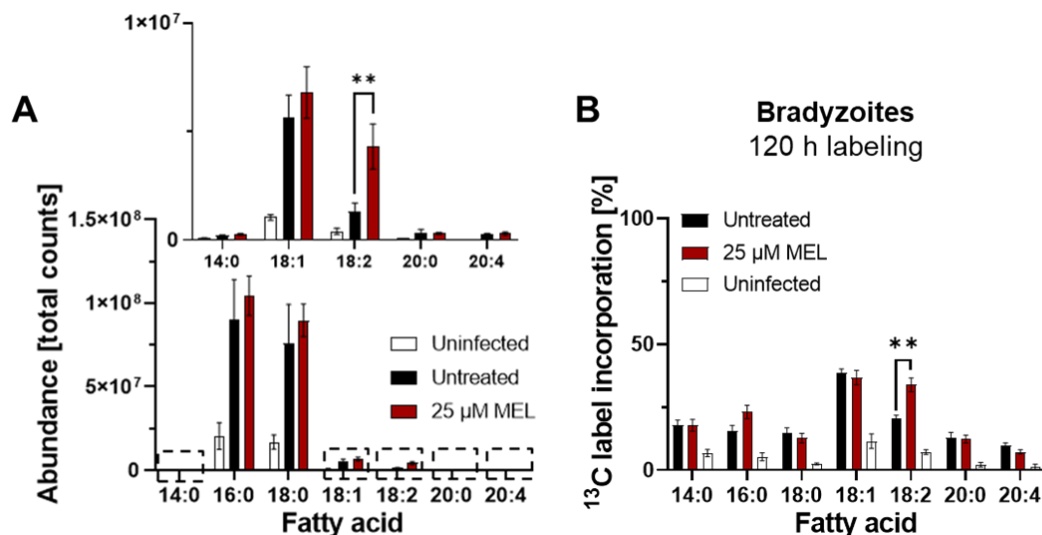
Figure 30: Impact of meldonium on fatty acid import of bradyzoites. Pru-tdTomato bradyzoites (MOI: 0.3) were cultured in myotubes for 28 days, labeled for 120 h in medium supplemented with 2.5 % U13C fatty acid mix (untreated) or medium supplemented with 2.5 % U13C fatty acid mix and 25 µM meldonium (MEL), followed by isolation and extraction. (A.) Abundances in total counts of total medium- and long-chain fatty acids of untreated and meldonium (MEL)-treated Pru-tdTomato bradyzoites. (B.) Proportion of ^{13}C label incorporation in % of medium- and long-chain fatty acids of 28-day-old untreated and meldonium-treated Pru-tdTomato encysted bradyzoites and uninfected control cultures. Uninfected cultures were generated to estimate host cell contamination in parasite samples. Values are expressed as the mean with S.E.M. of two experiments with quadruplicate cultures per condition. MEL: meldonium.

In encysted bradyzoites, FA counts of uninfected control cultures indicated a host contribution of 20 % or less to the overall signal (**Figure 30**A). Consistent with the impact of meldonium on tachyzoites, the abundance and the label incorporation into LA pools (C18:2) was increased in meldonium-treated cultures (**Figure 30**A-B).

Together, these results indicate that FA import, especially LA import, into both tachyzoites and encysted bradyzoites inversely depends on host (acyl) carnitine levels.

5.3.5 Meldonium treatment leads to an enhanced level of free antimicrobial linoleic acid in tachyzoites

FAs can act as nutrients for membrane biosynthesis, however unsaturated FAs exhibit broad antimicrobial activity in their free form (Das, 2018). In particular oleic acid (C18:1) and LA (C18:2) have previously been shown to impair *T. gondii* tachyzoite and bradyzoite viability (Nolan et al., 2018).

We hypothesized that esterification of LA to carnitine alone or its subsequent degradation through β-oxidation in the host might limit parasite exposure to free LA and lead to their detoxification. To directly determine whether carnitine-dependent β-oxidation or carnitine alone impacts free LA in the host and parasites, we infected myotubes that were pre-treated with trimetazidine, an LC 3-ketoacyl-CoA thiolase inhibitor, which specifically blocks host cell β-oxidation (Kantor et al., 2000) and additionally supplemented medium with indicated concentrations of carnitine or trimetazidine and meldonium to block β-oxidation and block carnitine synthesis simultaneously. Treatment was maintained for the time of infection and the cultures were labeled with 40 µM BSA-bound ^{U13}C-LA. We determined the levels of free LA and carnitine estered linoleoyl-carnitine using LC / MS from isolated parasites and uninfected controls (**Figure 31**). Beforehand, trimetazidine was analyzed to have no impact on *T. gondii* tachyzoite viability in the applied concentration of 40 µM (**Appendix V**).
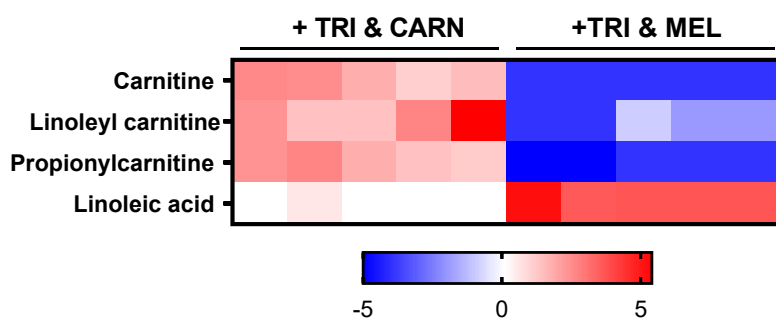
Figure 31: Impact of suppressed host cell β-oxidation and carnitine levels on free linoleic acid level in tachyzoites. Myotubes were pretreated for 24 h either with 40 µM trimetazidine (TRI & CARN) or 40 µM trimetazidine and 25 µM meldonium (TRI & MEL). Respective pretreated and untreated myotubes were infected with Pru-tdTomato tachyzoites (MOI: 1) for 4 h, labeled for 48 h in medium supplemented with 40 µM ^{13}C linoleic acid (Untreated), medium supplemented with 40 µM ^{U13}C linoleic acid, 40 µM trimetazidine and 15 µM carnitine (TRI & CARN) or medium supplemented with 40 µM ^{U13}C linoleic acid, 40 µM trimetazidine and 25 µM meldonium (TRI & MEL), followed by isolation and extraction. Heatmap showing log2-fold changes of significantly different metabolites (p<0.05, uncorrected Mann-Whitney-U test) between linoleic acid-treated and linoleic acid, trimetazidine and carnitine-treated tachyzoites (left panel) and between linoleic acid-treated and linoleic acid, trimetazidine and meldonium-treated tachyzoites (right panel). Log2-fold changes were calculated pairwise. Data analysis was mainly performed by Deborah Maus. For raw data refer to **Appendix VI**.

Tachyzoites treated with trimetazidine, and carnitine showed significantly increased carnitine and detected acylcarnitine pools. Relative abundance of the carnitine-bound version of LA, linoleoyl-carnitine, was significantly increased in this sample group. The free LA level was

unchanged compared to LA-treated control group (**Figure 31**, left panel, **Appendix VI**). In contrast, tachyzoites treated with meldonium and trimetazidine showed a significant decrease in carnitines and acylcarnitines, including linoleoyl-carnitine. In contrast free LA level was dramatically enhanced (**Figure 31**, right panel, **Appendix VI**).

In summary, these data indicated that both host cell β-oxidation and host cell carnitine pools have a significant impact on the amount of free LA arriving in the parasite and that blockage of host cell β-oxidation and depletion of carnitine pools leads to a dramatically high concentration of antimicrobial free FA in the parasite.

5.3.6 Host carnitines confer parasite tolerance towards antimicrobial fatty acids and facilitate survival of bradyzoites

Next, we tested whether the enhanced level of free LA we could detect upon supplementation with trimetazidine and meldonium also has a direct effect on *T. gondii* growth. Freshly invaded tachyzoites were exposed to LA and indicated combinations of meldonium and trimetazidine. for seven days. To test the rescue effect of carnitine, carnitine was externally added to the medium. The IC_{50} values were determined at day seven (**Figure 32**).
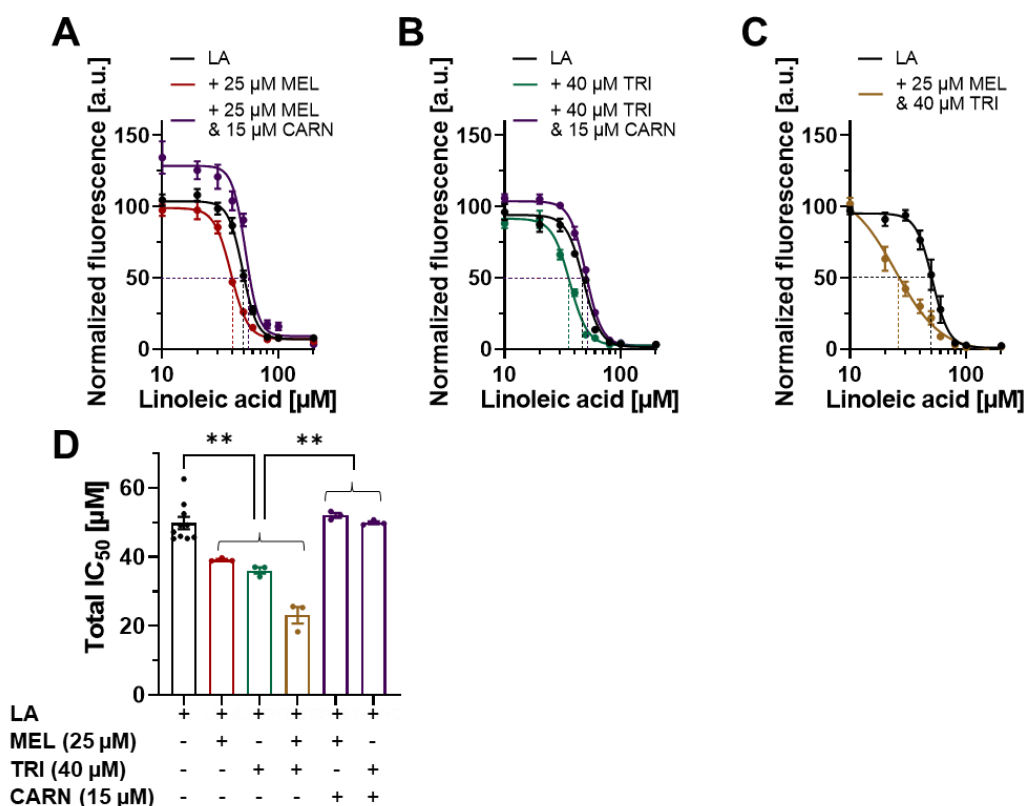
Figure 32: Impact of meldonium, trimetazidine and carnitine supplementation on linoleic acid toxicity in tachyzoites. Pru-tdTomato tachyzoites (MOI: 1) were cultured in myotubes for 4 h, followed by treatment. (A.-C.) Calculation of half inhibitory concentrations (IC_{50}) of linoleic acid (LA) and indicated combination of 40 µM trimetazidine (TRI), 25 µM meldonium (MEL) and 15 µM carnitine (CARN) for Pru-tdTomato tachyzoites. Parasites were grown for seven days in presence of indicated treatments and the

IC_{50} value was calculated from fluorescence intensities normalized to untreated controls. Shown are means and SEM of three independent experiments with three replicates each. (D.) Total IC_{50} of linoleic acid (LA) and indicated combination of trimetazidine (TRI), meldonium (MEL) and carnitine (CARN) for Pru-tdTomato tachyzoites. Shown are means and SEM of nine (LA) and three (rest) independent experiments. (**$p \leq 0.01$, Mann-Whitney-U-test).

LA abolished tachyzoite growth with an IC_{50} of 50 µM (**Figure 32**A, D). Meldonium supplementation led to a decreased IC_{50} of LA from 50 µM to 39 µM. This effect could be reversed by the supplementation of 15 µM carnitine (**Figure 32**A, D). To investigate whether this effect was dependent on carnitine-dependent decrease of LA levels by β-oxidation in the host, we treated cultures with trimetazidine. Trimetazidine alone did not impact parasite replication up to 200 µM (**Appendix V**), however 40 µM trimetazidine decreased the IC_{50} of LA from 48 µM to 36 µM (**Figure 32**B, D). Interestingly, this effect was fully reversed by carnitine supplementation (**Figure 32**B, D). Simultaneous supplementation of trimetazidine and meldonium led to a decreased IC_{50} of 23 µM (**Figure 32**C, D).

Together these data indicate that free LA level detected in the parasite directly translate into LA toxicity. Carnitine facilitates the growth of *T. gondii* tachyzoites by detoxifying LA through both host β-oxidation and by an additional mechanism that directly depends on carnitine itself.

We next tested whether host carnitines also had a pro-parasitic effect on *T. gondii* encysted bradyzoites by testing the influence of host carnitine levels on the RS of LA. 28-day-old encysted bradyzoites were treated for one week with LA in presence of indicated concentrations of meldonium, trimetazidine and carnitine (**Figure 33**).
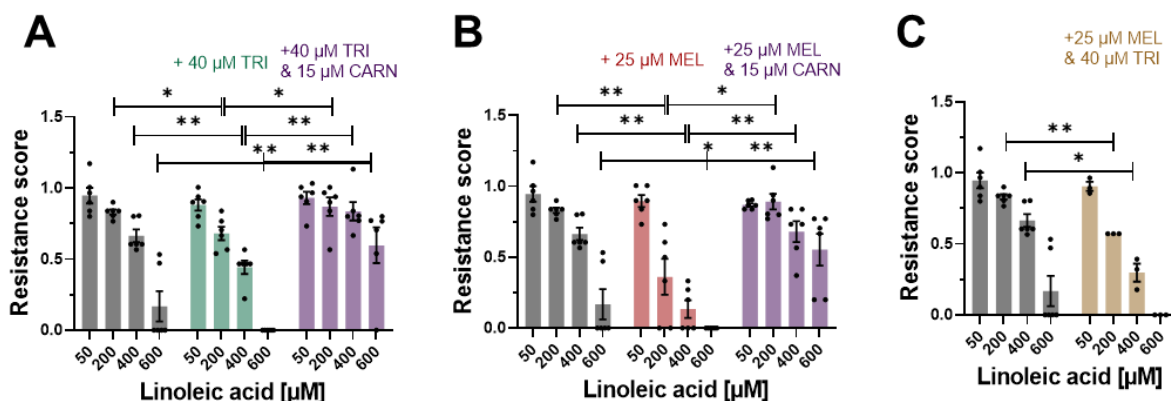
Figure 33: Impact of meldonium, trimetazidine and carnitine supplementation on linoleic acid toxicity in matured encysted bradyzoites. Pru-tdTomato encysted bradyzoites (MOI: 0.1) were cultured in myotubes for 28 days, followed by treatment. (A.-C.) Resistance scores of 28-day-old bradyzoites treated with linoleic acid only and indicated combination of trimetazidine (TRI), meldonium (MEL) and carnitine (CARN). Shown are means and SEM of two independent experiments performed in triplicates (*$p \leq 0.05$; **$p \leq 0.01$, Mann-Whitney-U-test).

RSs indicate a moderate impact of LA on bradyzoite viability up to 200 µM. At 400 µM LA decreased RS to 0.66 and at 600 µM only two of six cultures grew back with a RS of 0.16 (**Figure 33**). The presence of meldonium enhanced the toxicity of LA for the parasites and led

to a resistance score of 0.13 at 400 µM of LA, while parasites did not grow after treatment with 600 µM (**Figure 33**A). Addition of carnitine ameliorated this effect leading to robust growth after treatment with 600 µM (**Figure 33**A). We observed the same tendencies concerning a higher sensitivity of encysted bradyzoites towards LA by blocking host β-oxidation with trimetazidine, however, at lower level compared to meldonium supplementation. 40 µM trimetazidine treatment abolished cyst cultures that received 600 µM LA, while carnitine supplementation rescued the re-growth of these cultures (**Figure 33**B). Interestingly, co-supplementation with meldonium and trimetazidine showed same results as for both inhibitors alone. In contrast to tachyzoites no synergistic effect was detectable (**Figure 33**C).

Summarized, these data demonstrate that encysted bradyzoites withstand significantly higher LA concentrations than tachyzoites. Furthermore, carnitine levels are crucial for bradyzoites to detoxify free LA. In bradyzoites, carnitine-dependent detoxification processes seem to be more relevant than the detoxification of LA via host cell β-oxidation.

5.4 Establishment of a single cell division marker in tachyzoites and bradyzoites

5.4.1 Monophosphate thymidine-based nucleoside analogues are incorporated in tachyzoite DNA depending on their masking group

Bradyzoites divide asynchronously resulting in a heterogenous populations with several division states in a cyst (Watts et al., 2015). This heterogeneity is often connected to drug treatment failure (Barrett et al., 2019), thus a tool to correlate frequency of proliferation to drug susceptibility on a single cell level is of high need. For protozoan parasites like *Leishmania*, thymidine analogues are applicable to monitor single cell division and to tear apart proliferating and non-proliferating cells (Barrett et al., 2019). *T. gondii* does not possess a thymidine kinase and does not incorporate the classically used 5-Ethynyl-2'-deoxyuridine (EdU) into DNA.

To overcome these limitations, we screened already phosphorylated thymidine analogues. These compounds obtained different masking groups to facilitate diffusion of phosphorylated compounds into *T. gondii*. In a collaboration with the Griffith University 13 different thymidine-based compounds and EdU as control compound were screened. The compounds were tested between 1 and 500 µM, IC_{50} values for Pru-tdTomato tachyzoites were determined and the DNA labeling capacity was tested applying the highest non-growth inhibiting concentration for 24 h on freshly invaded RH tachyzoites in HFF cultures (**Table 15**, **Appendix VII**).

Table 15: Screening of monophosphate thymidine-based analogues. Displayed are the masking groups, impact on *T. gondii* tachyzoite viability displayed as half inhibitory concentrations (IC_{50}) within seven days pulse labeling and incorporation in host and *T. gondii* DNA detected via click chemistry within 24 h labeling at 1 µM, 10 µM and 100 µM. Shown are means and SEM of one experiment. Raw data can be accessed in **Appendix VII**. EdU: 5-Ethynyl-2'-deoxyuridine; n.d.: not defined.

Compound	Masking group	IC_{50} [µM]	Labeling Host	*T. gondii*
5	*p*-benzoyl-benzyl alcohol	2.7 ± 0.4	+	+
7	*p*-benzoyl-benzyl alcohol	7.9 ± 0.9	+	+
4	*p*-acetoxy-benzyl alcohol	33.1 ± 1.5	-	-
9	*p*-acetoxy-benzyl alcohol	45.9 ± 1.7	+	-
EdU	-	81.5 ± 1.9	+	-
1	saligenyl alcohol	121.9 ± 2.1	-	-
11	saligenyl alcohol	243.3 ± 2.4	-	-
2	3-methyl saligenyl alcohol	260.3 ± 2.4	-	-
12	3-methyl saligenyl alcohol	297.2 ± 2.5	+	-
6	*p*-nitro-benzyl alcohol	405.7 ± 2.8	-	-
3	saligenyl alcohol	635.3 ± 2.8	+	-
13	saligenyl alcohol	n.d.	-	-
8	*p*-nitro-benzyl alcohol	n.d.	+	-
10	No structure	n.d.	+	-

The IC_{50} values of 10 pyrimidine-based analogues and EdU could be determined. Compound 8, 10 and 13 showed a very low impact on *T. gondii* growth and started to be toxic at 500 µM. Interestingly, assorting the compounds by IC_{50} values, the growth inhibitory effect of compounds seems to be closely connected to the respective masking group. Performing labeling on intracellular tachyzoites, six compounds were incorporated into HFF DNA, two compounds were incorporated into HFF and *T. gondii* DNA and five compounds were not incorporated at all.

Summarized, monophosphorylated thymidine analogues containing a certain masking group, in this case *p*-benzoyl-benzyl alcohol, can be indeed further metabolized and incorporated into *T. gondii* DNA.

5.4.2 *p*-benzoyl-benzyl alcohol-bearing pyrimidine analogues possess a non-toxic therapeutic labeling window for tachyzoites

Our screen revealed that compound 5 and compound 7 are efficiently incorporated into *T. gondii* DNA. Nucleoside analogues are antimetabolites and toxicity can be significantly decreased with shorter labeling times (Ewald et al., 2008). To determine the optimal therapeutic labeling window for each compound, we reduced pulse labeling to 24 h and determined IC_{50} values of freshly invaded Pru-tdTomato tachyzoites and the cytotoxicity on HFFs for indicated concentrations of the respective compounds (**Figure 34**). Additionally, to compound 5 and compound 7 which are detectable via click chemistry, compounds 32, 33 and 20 were investigated. These compounds were structurally based on compound 7 but possess other biorthogonal groups for potential dual labeling experiments. Compound 20 is the brominated version of compound 7.
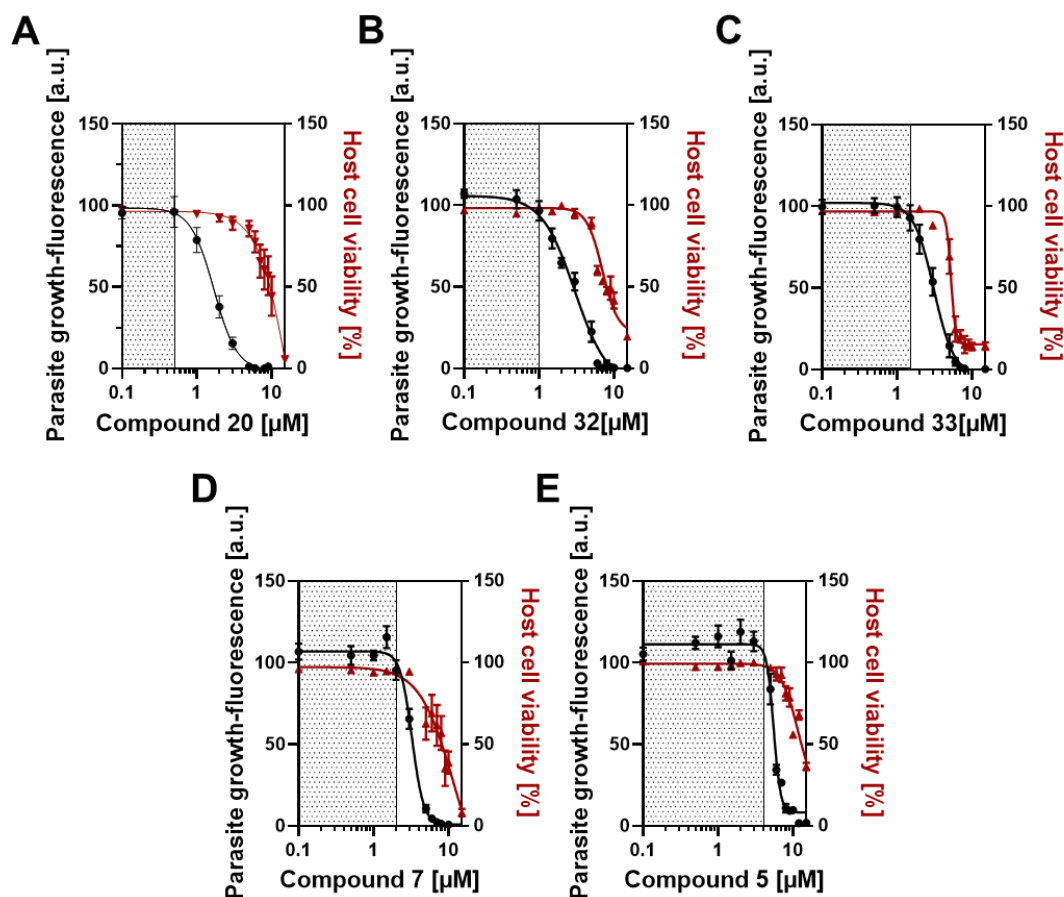
Figure 34: Impact of monophosphorylated pyrimidine-based nucleoside analogues on the viability of tachyzoites and human fibroblasts. HFFs were grown uninfected or infected with Pru-tdTomato tachyzoites (MOI: 1) for 4 h, followed by treatment. (A.-E.) Determination of half inhibitory concentrations (IC_{50}) and host cell viability in % of nucleoside analogues for Pru-tdTomato tachyzoites and HFFs. Parasites and HFFs were grown for 24 h in presence of indicated concentrations of nucleoside analogues. Growth of parasites was monitored for seven days and the IC_{50} value was calculated on day five from fluorescence intensities normalized to untreated controls. IC_{50} value for HFFs was determined after 24 h compound exposure via resazurin assay by normalizing untreated to treated controls. Shown are means and SEM of three independent experiments with three replicates each. Black dotted area represents non-toxic therapeutic labeling window.

All compound 7-based analogues showed an IC_{50} value ~3.0 µM. The brominated version compound 20 revealed a significantly higher impact on *T. gondii* growth with an IC_{50} value of 1.7 µM. The IC_{50} value, referring to the cytotoxicity on host cells, for compound 20 was at 18.0 µM, for compound 32 at 7.0 µM, for compound 33 at 5.2 µM and for compound 7 at 11.9 µM. Treatment with compound 5 led to an IC_{50} value of 5.5 µM for *T. gondii* and an IC_{50} of 11.7 µM for HFFs. Based on this data we defined a potential labeling window which did neither impair *T. gondii* growth nor the host cell viability during pulse label experiments (**Table 16**).

Table 16: Therapeutic labeling window of monophosphorylated pyrimidine-based nucleoside analogues for tachyzoites. Displayed is the impact on *T. gondii* tachyzoite and human fibroblasts (HFFs) viability displayed as half inhibitory concentrations (IC$_{50}$) within 24 h pulse labeling Shown are means and SEM of three independent experiments with three replicates each.

Compound	IC$_{50}$ [µM] (*T. gondii*)	IC$_{50}$ [µM] (HFFs)	Highest non-toxic concentration [µM]
20	1.7 ± 0.2	18.0 ± 1.3	0.5
32	3.0 ± 0.5	7.0 ± 0.9	1.0
33	3.1 ± 0.5	5.2 ± 0.7	1.5
7	3.5 ± 0.5	11.9 ± 1.1	2.0
5	5.5 ± 0.7	11.7 ± 1.1	4.0

For compound 20 labeling could be applied with up to 0.5 µM. Compound 32 could be used up to 1.0 µM and compound 33 up to 1.5 µM. Compound 7 was applicable up to 2.0 µM and compound 5 is compatible with HFFs and *T. gondii* up to 4.0 µM.

These data indicate that all investigated compounds possessed a therapeutic labeling window in which the viability of host cells and *T. gondii* is not impaired.

5.4.3   Compound 5 and compound 7 are incorporated into *Toxoplasma gondii* DNA

After successful determination of a therapeutic labeling window for each compound, we labeled intracellular type I RH parasites with click chemistry-based compound 5 and compound 7 in indicated concentrations for 24 h. The samples were co-stained with DAPI to visualize host cell and parasite DNA. EdU was titrated as click chemistry control (**Figure 35**).
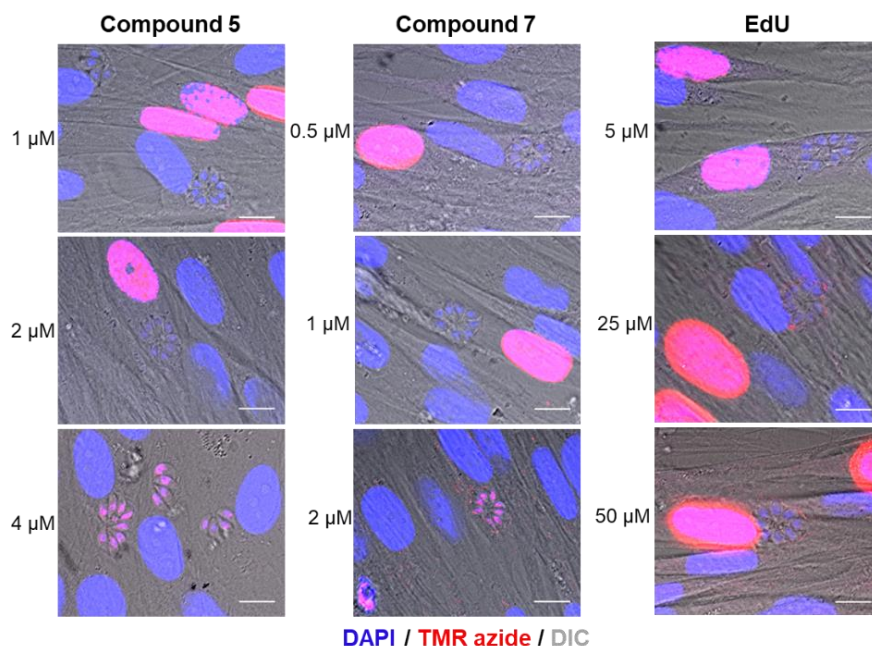
Figure 35: Labeling titration of compound 5 and compound 7 for tachyzoites. Representative immunofluorescence images of HFFs infected with RH parasites (MOI: 1.0) and 24 h pulse labeling with

compound 5 (Left panel), compound 7 (middle panel) or 5-Ethynyl-2'-deoxyuridine (EdU) (right panel) in indicated concentrations. Samples were stained for total DNA (DAPI) and for newly synthesized DNA via click chemistry with 5-carboxytetramethylrhodamine-azide (TMR azide). Scale bar indicates 10 µm.

Supplementing the medium with 4.0 µM compound 5 led to successful labeling of the whole parasite pool, whereas lower concentrations did not show labeling above background (**Figure 35**, left panel). Dividing host cells also incorporated compound 5 and observed labeling intensity increased to enhanced concentrations. The same pattern was observed for compound 7 (**Figure 35**, middle panel). Some parasites incorporated nucleoside analogue working with a concentration of 0.5-1.0 µM at a level which could not be distinguished from background-level, whereas 2.0 µM was sufficient to label the whole parasite population above background-level. Host cells incorporated nucleoside analogue as well in a concentration-dependent manner. EdU supplementation resulted in sufficient labeling of host cell nuclei in a concentration-dependent manner, whereas parasites did not incorporate EdU into newly synthesized DNA up to the highest applied concentration of 50.0 µM (**Figure 35**, right panel). Titration of compounds bearing different detection groups (compound 32, compound 33) are not shown here, since labeling protocols could not be established (data not shown).

Summarized, our data shows that pyrimidine-based nucleoside analogues are a promising tool to investigate single cell division events in *T. gondii* tachyzoites.

5.4.4 7-deaza-7-ethynyl-2′-deoxyadenosine is incorporated into tachyzoite DNA

T. gondii is a purine auxotroph and relies on the import via transporters (Chiang et al., 1999; De Koning et al., 2003). In a study investigating the adenosine kinase of *T. gondii*, 7-deaza-7-ethynyl-2′-deoxyadenosine (EdA) was shown to efficiently label the nuclei of parasites (Galazka et al., 2006). Since EdA was not further investigated for its suitability as cell division marker, we determined a therapeutic labeling window by analyzing IC_{50} values for Pru-tdTomato tachyzoites and HFFs and performed "click" chemistry-based labeling of RH parasites for 24 h applying the respective concentrations (**Figure 36**).
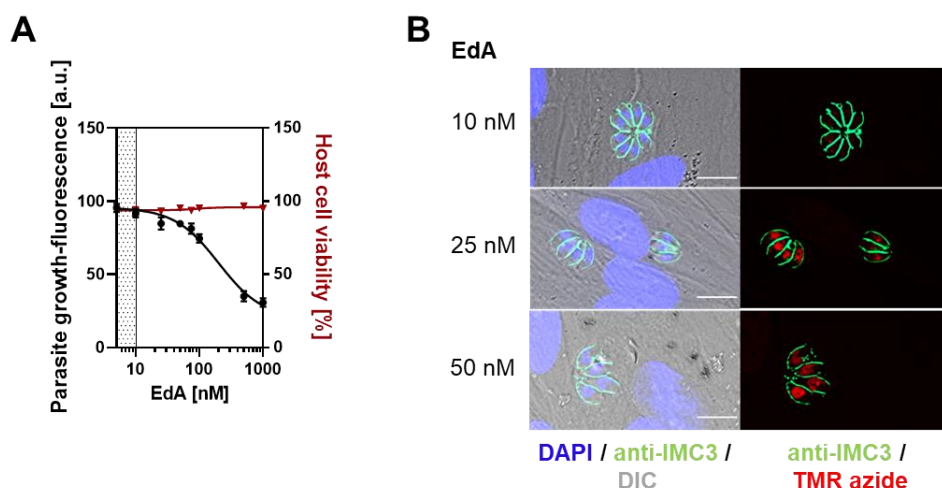
Figure 36: Impact of purine-based nucleoside analogue 7-deaza-7-ethynyl-2′-deoxyadenosine on the viability of tachyzoites and human fibroblasts and the incorporation into newly synthesized DNA. (A.) Calculation of half inhibitory concentrations (IC_{50}) of 7-deaza-7-ethynyl-2′-deoxyadenosine (EdA) for Pru-tdTomato tachyzoites and HFFs. Pru-tdTomato tachyzoites in HFFs (MOI: 1) and uninfected HFFs were grown for 24 h in presence of indicated concentrations of EdA. Growth of parasites was monitored for seven days and the IC_{50} value was calculated on day five from fluorescence intensities normalized to untreated controls. Host cell viability in % of HFFs was determined after 24 h compound exposure via resazurin assay by normalizing untreated to treated controls. Shown are means and SEM of three independent experiments with three replicates each. Black dotted area represents non-toxic therapeutic labeling window. (B.) Representative immunofluorescence images of HFFs infected with RH parasites (MOI: 1) and 24 h pulse labeling with EdA in indicated concentrations. Samples were stained for total DNA (DAPI), for newly synthesized DNA via "click" chemistry with 5-carboxytetramethylrhodamine-azide (TMR azide) and inner membrane complex 3 (IMC3) of parasites. Scale bar indicates 10 µm.

T. gondii growth was significantly impaired applying higher EdA concentrations than 10.0 nM and 201.5 nM was determined as IC_{50} value. The host cell viability was not impacted upon the tested concentrations (**Figure 36**A). Investigating the labeling profile, incorporation of EdA into parasite DNA was observed in a concentration-dependent manner (**Figure 36**B). 25.0 nM and 50.0 nM EdA led to the consistent labeling of the whole parasite pool with a distinct signal above background. Nevertheless, non-toxic concentration ≤10.0 nM did only show faint labeling of parasite nuclei and observed signal was not distinguishable from background for most parasites.

Together, EdA is incorporated into newly synthesized *T. gondii* DNA, but toxic side effects prevented the labeling of *T. gondii* in sufficient concentration without growth inhibition.

5.4.5 Forodesine dampens the toxicity of 7-deaza-7-ethynyl-2′-deoxyadenosine in tachyzoites

The toxic effect of purine analogues was reported for other purine auxotroph protozoan parasites (Wang, 1984). The suggested mechanism was the further metabolism of nucleoside analogues to the respective triphosphate which than has toxic side effects by e.g. acting on a DNA polymerase (Furth and Cohen, 1967). To suppress this potential toxic side effects of EdA, we introduced forodesine, which is a known purine (Chaudhary et al., 2006). Before studying

the impact of forodesine on EdA toxicity and incorporation efficiency, forodesine was shown to not impair tachyzoite or host cell viability (**Appendix VIII**). In applied concentrations forodesine did not show an impairment of *T. gondii* growth and host cell viability stayed equal to solvent-treated control. Subsequently, we performed same experiments as described for EdA (**Figure 36**) but co-supplemented the medium with 10.0 µM forodesine (**Figure 37**).
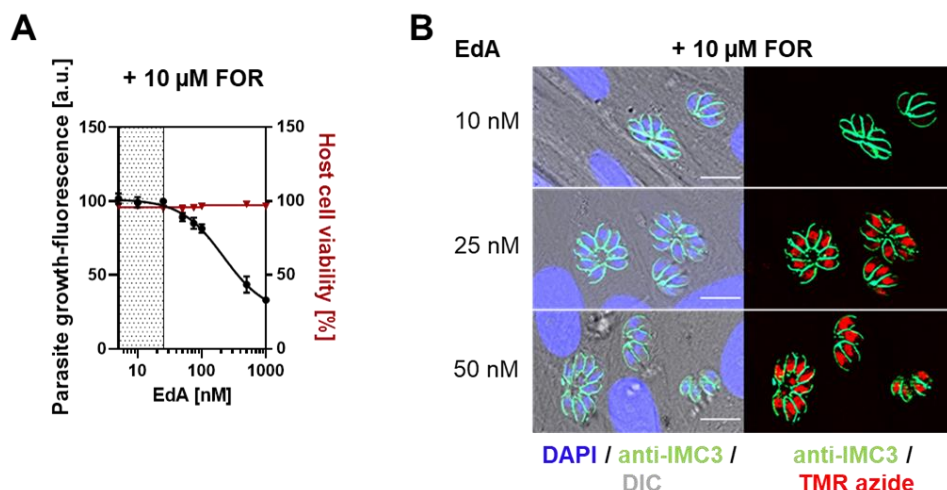
Figure 37: Impact of forodesine co-supplementation on the toxic effect and incorporation profile of 7-deaza-7-ethynyl-2′-deoxyadenosine in tachyzoites and human fibroblasts. (A.) Calculation of half inhibitory concentrations (IC$_{50}$) of 7-deaza-7-ethynyl-2′-deoxyadenosine (EdA) co-supplemented with forodesine for Pru-tdTomato tachyzoites and HFFs. Pru-tdTomato tachyzoites in HFFs (MOI: 1) and uninfected HFFs were grown for 24 h in presence of indicated concentrations of EdA and 10 µM forodesine (FOR). Growth of parasites was monitored for seven days and the IC$_{50}$ value was calculated on day five from fluorescence intensities normalized to untreated controls. Host cell viability in % of HFFs was determined after 24 h compound exposure via resazurin assay by normalizing untreated to treated controls. Shown are means and SEM of three independent experiments with three replicates each. Black dotted area represents therapeutic labeling window. (B.) Representative immunofluorescence images of HFFs infected with RH parasites (MOI: 1) and 24 h pulse labeling with EdA in indicated concentrations and 10 µM forodesine. Samples were stained for total DNA (DAPI), for newly synthesized DNA via "click" chemistry with 5-carboxytetramethylrhodamine-azide (TMR azide) and inner membrane complex 3 (IMC3) of parasites. Scale bar indicates 10 µm.

Indeed, co-supplementation with forodesine widened the therapeutic window to 25 nM (**Figure 37**A) which was also shown to be a sufficient concentration to detect *T. gondii* newly synthesized DNA distinguishable from background noise (**Figure 37**B).

Summarized, these data demonstrate that purine-based nucleoside analogue EdA reaches the parasite and is sufficiently incorporated into *T. gondii* DNA. Co-supplementation with forodesine led to lower toxicity of EdA and enables the detectable and quantifiable monitoring of cell division events using this purine-based analogue applying non-toxic concentrations.

5.4.6 Purine-and pyrimidine-based nucleoside analogues are a promising tool to monitor single cell division in matured bradyzoites

Having established pyrimidine- and purine-based nucleoside analogues as a sufficient single cell labeling tool in *T. gondii* tachyzoites, we next aimed to test them on their suitability to track

bradyzoite proliferation. First, we examined the toxicity of the nucleoside analogues in indicated concentrations on bradyzoite viability (**Figure 38**). Bradyzoites are known to proliferate at a slower rate than tachyzoites (Jerome et al., 1998) and since preliminary labeling experiments demonstrated that nucleoside analogues were not incorporated within a detectable level after 24 h (data not shown), we extended pulse labeling to 48 h for 28-day-old Pru-tdTomato bradyzoites. Supplementation of the pyrimidine nucleoside uridine was shown to inhibit the conversion of tachyzoites to bradyzoites complementing the defect in pyrimidine synthesis induced by the metabolic stress of CO_2 restriction (Weilhammer et al., 2012). To exclude that the pyrimidine-based nucleoside analogues led to re-differentiation from bradyzoite to the tachyzoite form, a control was included treating parasites with indicated concentrations of nucleoside analogues and in parallel with 20 µM pyrimethamine, which was demonstrated to sufficiently kill tachyzoites beforehand (**Figure 18**).
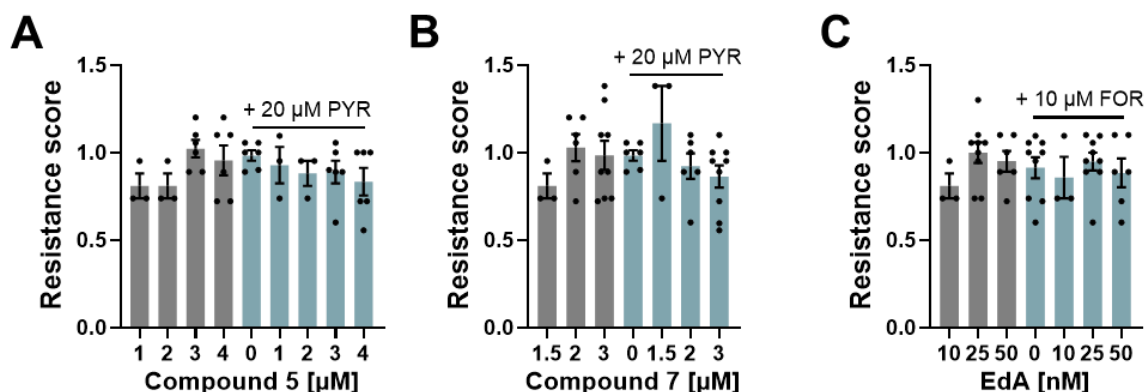
Figure 38: **Impact of pyrimidine-based and purine-based nucleoside analogues on bradyzoite viability**. Pru-tdTomato encysted bradyzoites (MOI: 0.1) were cultured in myotubes for 28 days, followed by treatment. (A.-C.) Resistance scores of 28-day-old bradyzoites treated with indicated concentrations of (A.) compound 5 (+/- 20 µM pyrimethamine (PYR)), (B.) compound 7 +/- 20 µM pyrimethamine or (C.) 7-deaza-7ethynyl-2´-adeoxyadenosine (EdA) +/- 10 µM forodesine (FOR). Shown are means and SEM of one to three independent experiments performed in triplicates, respectively.

The RSs indicated that neither incubation with pyrimidine and purine based-nucleoside analogues in indicated concentrations nor co-supplementation with pyrimethamine or forodesine showed impact on the bradyzoite re-growth and therefore viability (**Figure 38**A-C).

After it was demonstrated that pyrimidine- and purine-based analogues do not impair bradyzoite viability in the applied concentrations, we applied 48 h pulse labeling on 28-day-old ME49 encysted bradyzoites in the highest non-toxic concentration established for tachyzoites and bradyzoites (**Figure 39**).
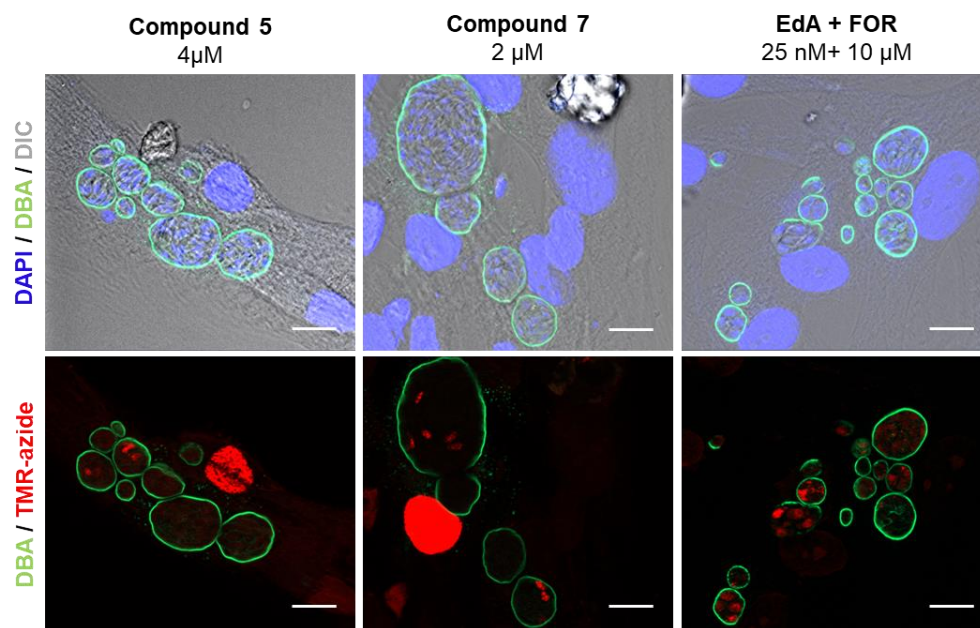
Figure 39: Incorporation profile of purine- and pyrimidine nucleoside analogues into newly synthesized DNA of *T. gondii* bradyzoites. Shown are representative immunofluorescence images of 28-day-old ME49 encysted bradyzoites cultured in myotubes (MOI: 0.1) and labeled for 48 h with 4 μM compound 5 (left panel), 2 μM compound 7 (middle panel), or 25 nM 7-deaza-7ethynyl-2´-adeoxyadenosine (EdA) and 10 μM forodesine (FOR) (right panel). Samples were stained for total DNA (DAPI), for newly synthesized DNA via click chemistry with 5-carboxytetramethylrhodamine-azide (TMR azide) and their cyst wall (*Dolichos biflorus* agglutinin (DBA)). Scale bar indicates 10 μm.

In contrast to tachyzoites, bradyzoites showed a heterogenous labeling pattern (**Figure 39**). Not all bradyzoites, although in the same cyst, showed incorporation of nucleoside analogues and the detected labeling intensity differed between individual bradyzoites. In the applied concentrations, purine-based nucleoside analogue EdA seemed to be more efficiently incorporated than pyrimidine-based analogues.

Summarized, this data indicates for the first time that pyrimidine- and purine-based analogues are incorporated into newly synthesized bradyzoite DNA. Thus, pulse labeling experiments with these compounds offer a promising tool to study heterogeneity and dynamics of cell division in bradyzoites on a single cell level.

Chapter 6: Discussion

6.1 Establishment of an *in vitro* protocol for matured *Toxoplasma gondii* tissue cysts

Early events in bradyzoite formation were widely studied and many underlying mechanisms could be elucidated with the help of current *in vitro* and *in vivo* culture systems. Nevertheless, the currently available models do not facilitate the generation and long-term *in vitro* culture of *in vivo*-like cysts. Current methods to experimentally generate mature *T. gondii* tissue cysts are confined to murine infections with cystogenic *T. gondii* strains. *In vivo* models, however, are highly restricted, e.g., concerning scalability and variability. The limited availability of adequate *in vitro* models for the long-term culture of matured encysted bradyzoites restricts the investigation of bradyzoite biology and underlying mechanism of persistence.

In this work, a cell culture model was established based on immortalized human skeletal muscle cells (Shiomi et al., 2011) that support maturation of tissue cysts of type I, II and III *T. gondii* strains. These myotube-grown encysted bradyzoites exhibit key characteristics including typical ultrastructural features, stress resistance and tolerance towards antimicrobials.

The conducted experiments established that KD3 myoblasts started displaying features of differentiated myotubes such as myosin heavy chain and cellular fusion and spontaneous contraction (Bettadapur et al., 2016; Tang et al., 2018) (**Figure 7**). This successfully indicates differentiation into matured skeletal muscle cells that act as natural host cells for *T. gondii* encysted bradyzoites. We did not investigate which molecular factors of KD3 myotubes facilitate stage conversion of *T. gondii* and this would be an opportunity for future studies. Our investigations concerning spontaneous encysted bradyzoite formation upon infection of control human fibroblasts (HFFs), myoblasts and myotubes revealed that only myotubes favored spontaneous stage conversion of *T. gondii* as evidence by the formation of a *Dolichos biflorus* agglutinin (DBA)-positive cyst wall and the upregulation of bradyzoite specific genes indicated by lactate dehydrogenase 2 (LDH2)-dependent GFP expression (**Figure 8**, **Figure 9**, **Figure 10**). Furthermore, a reduced proliferation of tachyzoites was observed in myotubes compared to control cell lines. This goes in line with observations of the Lüder´s group which performed equal experiments in a murine myotube cell line (C2C12) with control myoblasts and control HFFs (Swierzy and Lüder, 2015). Infection of skeletal muscle cells induces a number of transcriptomic changes that have been shown to induce stage conversion of *T. gondii*. Infection of C2C12 cells significantly increase interleukin-12 and interferon gamma levels that favor tissue cyst formation (Gomes et al., 2014; Takács et al., 2012). In addition, the negative

Establishment of an *in vitro* protocol for matured *Toxoplasma gondii* cysts

cell cycle regulator CDA-1/Tspyl2 and the cell cycle inhibitor p21$^{Waf1/Cip1}$ are upregulated and coincide with decreased expression of cyclin B1 and mediate an arrest in G1 phase of the cell cycle. This CDA-1/Tspyl2-mediated cell cycle withdrawal also appears to act as a physiological trigger of *T. gondii* stage conversion in mature skeletal muscle cells (Swierzy and Lüder, 2015). Furthermore, the reduced proliferation of tachyzoites in myotubes, which in turn supports stage differentiation (Weiss et al., 1998), might be facilitated by the cell cycle arrest. In cell cycle-arrested human trophoblasts and dermal fibroblasts the proliferation of *T. gondii* tachyzoites was significantly decreased (Brunet et al., 2008). Additionally, for type I strains it was demonstrated that they push host cells to enter the S phase but arrest them in G2 phase to maintain parasite proliferation (Brunet et al., 2008; Molestina et al., 2008). It must be mentioned that our findings of decreased replication of tachyzoites and enhanced formation of encysted bradyzoite do not go in line with a study performed in 2012. Albeit we did not test the metabolism of KD3 myotubes directly and myotubes are considered rich in mitochondria (Malinska et al., 2012; Remels et al., 2010) they are thought to be highly glycolytic cells (Malinska et al., 2012). The activation of host cell glycolysis and release of the glycolytic metabolite lactate was shown to fuel parasite replication and to inhibit bradyzoite formation in distinct cell types under metabolic stress conditions (Weilhammer et al., 2012). However, the influence of lactate on spontaneous stage conversion has not been tested. Interestingly, lactate was shown to be not only a waste product of glycolytic activity, but also a source which is directly used by terminally differentiated myotubes for energy generation, suggesting lactate does not accumulate in the system and is directly consumed by the myotubes themselves (Lund et al., 2018). This should be further investigated by metabolomic investigation of myotubes and lactate levels during infection. Interestingly, during the course of infection, we first detected DBA positive structures indicating a forming cyst wall and subsequently GFP-expression indicating the expression of bradyzoite-specific genes. Hence, cystogenesis and the expression of bradyzoite genes appear to represent chronologically ordered events. In agreement with this observation, both events have been found to be subject to different checkpoints. For example, treatment of a non-cystogenic type I strain with sodium arsenite led to the induction of bradyzoite genes, but not cyst formation (Soete et al., 1994). In contrast, the treatment of type I and type II parasites with the histone deacetylase inhibitor FR235222 lad to cyst formation, but not to the expression of bradyzoite-specific genes (Bougdour et al., 2009; Maubon et al., 2010). Nevertheless, to our knowledge no attention has been paid to the chronological sequence and dependency of these events during stage conversion.

We found that KD3 myotubes harbor the capacity to promote the formation of encysted bradyzoites of eight different *T. gondii* strains of the three major isotypes (Howe and Sibley, 1995) (**Figure 11**, **Figure 12**). Tissue cyst formation was facilitated by bicarbonate starvation.

This method likely works via restricted pyrimidine synthesis, in which bicarbonate acts as a co-factor and has been established to induce stage conversion in different strains (Bohne et al., 1994; Dzierszinski et al., 2004; Weilhammer et al., 2012). Bicarbonate starvation was used solely or in combination with alkaline stress (pH 8.3) which was shown itself to be a trigger for stage conversion (Soête et al., 1994; Weiss et al., 1995). As expected, the alkaline pH promotes cyst maturation at a higher rate than the physiological pH. All strains show a time-dependent loss of surface antigen 1 (SAG1)-expression over the time period of 21 days. This timing is in line with *in vivo* (Weiss and Kim, 2000) and other *in vitro* studies (Dzierszinski et al., 2004) which also show the appearance of cyst-like vacuoles still expressing SAG1 after 14 days.

Interestingly, in both pH conditions, the strains cluster in a lineage-specific and time-dependent manner concerning their maturation capacity. Type III strain show a faster and higher maturation grade than type II strains followed by type I strains. The type I GT1 strain is an exception showing a high grade of maturation under alkaline pH, corresponding to literature describing GT1 as a strain that obtained the ability to form normal cysts under stress conditions since it is has not been laboratory domesticated by extensive *in vitro* culture (Khan et al., 2009). Broadly, type I strains proliferate faster than type II and type II faster than type III (Sibley and Ajioka, 2008; Sibley et al., 2009). Since strains with a slower replication rate were more likely to develop cysts *in vitro* (Matsubayashi et al., 1963), the observation of the lineage specific clustering may reflect the genotype-specific replication rate and its influence on stage-conversion. Besides the intrinsic capacity to form cysts, it is also shown for other Apicomplexa, e. g. *Besnoitia jellisoni,* that prolonged *in vitro* passaging might lead to the loss of an ability to differentiate into other stages (Weiss and Kim, 2000). Consistently, our data shows that high-passaged laboratory strain RH-Δ*ku80*Δ*hxgprt* strain formed cysts and did not overgrow the culture over the course of 21 days, but staying mostly SAG1-positive, indicating the formation of immature cysts. Although, our data indicated faster maturation of cysts under alkaline stress, we decided to generate tissue cysts at physiological pH for further experiments as pH 8.3 leads to a significantly decreased viability of the host cells (Ferreira da Silva Mda et al., 2008) and may introduce unnecessary artefacts.

Electron microscopic analysis of the ultrastructure of myotube-derived tissue cysts revealed typical features such as a developing cyst wall, amylopectin granules and posterior positioned nuclei in the bradyzoites (**Figure 13**) (Ferguson et al., 1994a). Interestingly, we also found evidence of disintegrating bradyzoites at all time points up to 21 days post infection. This has also been described previously in mice after four and eight weeks of infection (Ferguson (Ferguson et al., 1994a; Watts et al., 2015; Yap et al., 1998). Parasite turnover likely

Establishment of an *in vitro* protocol for matured *Toxoplasma gondii* cysts

contributes to the heterogeneous appearance with respect to cyst size and bradyzoite packaging density (Ferguson and Hutchison, 1987b; Watts et al., 2015). A similar phenotypic heterogeneity has been ascribed to the ability of other intracellular pathogens to persist in the presence of stressors such as drugs and immune effectors (Bakkeren et al., 2020).

In a natural transmission scenario acid pepsin resistance is the critical parameter for horizonal transmission between intermediate hosts. During oral infections, *T. gondii* encysted bradyzoites need to withstand stomach passage. The resistance of tissue cysts and bradyzoites to digestion by acidic gastric juice is known since 1960 and established as a widely accepted criterion to discriminate bradyzoites from non-resistant tachyzoites (Jacobs et al., 1960). Previously it was shown that three to nine percent of *in vitro*-derived cysts of *T. gondii* became resistant to low levels of pepsin (0.26 mg/ml) after nine days of differentiation in HFF cells, resulting in their low ability to orally infect mice (Fux et al., 2007). However, the pepsin concentration in a human stomach is estimated between 0.5-1 mg/ml with a pH of 1.5 (Liu et al., 2015) that has been reflected in previous pepsin resistance assays on *T. gondii* (Dubey, 1998; Jacobs et al., 1960). Incubation of tachyzoites in acid-pepsin solution at RT and 37 °C suggested that the leading course of the destruction of tachyzoites due to acid-pepsin solution is not the enzyme itself, but rather the acidic environment (Pettersen, 1979). Our data indicates that resistance to high concentrations of pepsin (5 mg/ml) and acidic pH of 1.5, of *in vitro*-derived encysted bradyzoites significantly increased over the course of 28 days when cysts started to fully tolerate acid-pepsin exposure (**Figure 14**).

To establish KD3-derived *T. gondii* cysts as a model for transmission to humans via undercooked meat products, we tested tolerance of *in vitro* cysts to acid-pepsin and cold and warm temperatures (**Figure 15**). Cold storage was simulated by exposing the cysts to 4 °C for four or seven days. The cooking process was mimicked by exposure to heat (55 °C or 65 °C) for 5 min. The stomach passage was recapitulated by an acidic pepsin digestion for 60 min. Strikingly, 35-day-old *in vitro*-derived tissue cysts show resistance to all single and combined conditions except the exposure to 65 °C for 5 min. This profile mimics the temperature resistance of *ex vivo* cysts that are able to survive extended storage at 4 °C (Dubey, 1997) and survive heat stress at 52 °C for 9.5 min (Dubey et al., 1990) and >61 °C for 3.5 min. Heating to 58 °C for 9.5 min or 64 °C for 3 min is required to inactivate *ex vivo* cysts (Dubey et al., 1990).

The gold standard and benchmark for maturity of *T. gondii* tissue cysts up till now is their capacity to orally infect mice. Nevertheless, we think this common benchmark should be reconsidered. On the one hand for obvious ethical reasons, on the other hand we hold *in vitro* assays, which offer much harsher conditions to discriminate mature encysted bradyzoites than

oral infectivity to mice. Our pepsin digestion was performed at pH 1.5, recapitulating the human stomach, whereas a stomach of mice maintains milder conditions between pH 3.0 and 4.0 (McConnell et al., 2008). As mentioned above, the infectivity of encysted bradyzoites to mice has already been observed five to nine days after differentiation in HFF cells (Fux et al., 2007), whereas other maturity markers like pepsin and drug resistance develop multiple weeks longer (**Figure 14**, **Figure 18**). HFF-derived cysts were not very infectious to mice and 10,000 cysts applied through oral gavage were needed to seroconvert mice consistently (Fux et al., 2007). This would correspond to approximately five mouse brains with variable cyst burden around 2,000 cysts. Noteworthy, ≥1,000 orally applied tachyzoites have also shown to lead to seroconversion in few animals (Dubey, 1998). However, since the data serves as an important point of comparison to other publications, we tested the oral infectivity of the *in vitro*-generated tissue cysts in mice (**Figure 16**, **Figure 17**). Therefore, 50 and 500 35-day-old *in vitro*-derived cysts were fed to mice by oral gavage. As control groups 10,000 tachyzoites generated in myotubes and HFFs and 10 *in vivo*-generated cysts were used for the infection of mice. We found seroconversion and cysts in one and two of ten mice that received tachyzoites from HFF and myotubes respectively. The infection of mice by oral injection of ≥1,000 tachyzoites was already described and can happen at a low frequency (Dubey, 1998). Eight or nine of ten mice seroconverted after receiving 50 and 500 myotube-derived cysts and four of four animals converted after receiving 10 *in vivo*-generated cysts. Brain cysts, indicative for an established chronic infection, were found in only one animal which received 50 *in vitro*-derived cysts and in all animals, which were injected with 500 *in vitro* or 10 *in vivo* cysts. We noticed that animals infected with 50 *in vitro* cysts did not show a significant decrease in body weight. In comparison, 10 *in vivo* cysts led to responses that were similar to those generated by 500 *in vitro* cysts. Since it is known that *in vitro* cysts differ in size and bradyzoite number and therefore infectious units (Dubey et al., 1998), we determined the diameter of 7- to 35-day-old *in vitro* cysts to facilitate comparability to brain-derived cysts. We measured a mean diameter of around 10 µm, whereas *ex vivo* cysts from brain tissue are reported to grow to 56 µm (Watts et al., 2015). Approximating the cysts as spheres, we estimated a 100-fold smaller volume of *in vitro* cysts. In accordance with this, our data demonstrates that bradyzoites from myotube-derived cysts are similar in their infectivity to *in vivo*-derived cysts. Summarized our data indicates that myotube-derived tissue cysts meet or exceed temperature and pepsin resistance levels that were found to correlate with oral infectivity in laboratory and natural settings.

Acute toxoplasmosis is currently treated with antifolates (sulfadiazine, pyrimethamine) or bc-1 complex inhibitor atovaquone. Nevertheless, there are currently no drugs available or in development that eradicate *T. gondii* cysts. *In vivo* cysts possess resistance to inhibitors of well-established drug targets including the calcium-dependent protein kinase 1 (CDPK1)

Establishment of an *in vitro* protocol for matured *Toxoplasma gondii* cysts

(Scheele et al., 2018; Winzer et al., 2015), dihydrofolate reductase-thymidylate synthase (Roos, 1993) and the mitochondrial bc1-complex (Bajohr et al., 2010; Saleh et al., 2007; Scheele et al., 2018; Winzer et al., 2015). Atovaquone and CDPK1-targeted bumped kinase inhibitors (BKIs) can reduce the cyst count by up to 90 % in chronically infected mice (Araujo et al., 1992; Ferguson et al., 1994b; Gormley et al., 1998; Sordet et al., 1998)**.** However, even after 12 weeks of treatment with atovaquone, *T. gondii* cysts remain detectable in mice brain (Araujo et al., 1992). Consistent, with this behavior of chronic infections in mice, KD3 myotube-derived *in vitro* cyst gradually develop tolerance against inhibitors of folate metabolism (sulfadiazine, pyrimethamine), the mitochondrial dihydroorotate dehydrogenase (Hegewald et al., 2013) and alternative NADH dehydrogenase (Saleh et al., 2007) inhibitor 1-hydroxy-2-hodecyl-4(1H)-quinolon (HDQ) and bumped-kinase inhibitors (BKIs) against CDPK1 (BKI1294, BKI1553) (**Figure 18**). The mechanism of the apparent pan-drug tolerance remains unclear. The onset of tolerance has been suggested to correlate with the establishment of a cyst wall, which acts as a physical barrier preventing the interaction of drugs with bradyzoites (Acquarone, 2017). The cyst wall of *ex vivo* and early *in vitro* cysts appears permeable to a range of fluorescent tracer molecules that are smaller than 40 kDa. However, the incubation with fluorescent reporters was only for 45 min (Lemgruber et al., 2011) and slower uptake mechanisms for larger molecules cannot be excluded. It is known that encysted bradyzoite do import molecules of large size, e.g. lactate (Blume and Seeber, 2018) or long-chain fatty acids (FAs) (**Figure 25**; **Figure 26**) (Nolan et al., 2017). The cyst wall of *T. gondii* is permissive to endocytosis-like mechanism that can import bovine serum albumin (BSA)-FITC, a 66.5 kDa molecule (Acquarone, 2017). Distinguishing properties of permeable molecules might also include physicochemical properties such as polarity or hydrophobicity. The delayed onset of resistance to high a dose of pyrimethamine (5 µM vs 20 µM) would be consistent with a diffusion barrier that can be overcome by a steeper concentration gradient. Likewise, BKI1553 appears less able to diffuse than the more active BKI1294 (Van Voorhis et al., 2017) and consistently 14-day-old *in vitro* cysts are almost fully tolerant towards the former but not the later BKI. Nevertheless, at least for pyrimethamine neither the blood brain barrier nor the cyst wall represents barriers (Barrett et al., 2019; Schoondermark-van de Ven et al., 1997). Additionally, bradyzoites are suggested to be themselves resistant towards many metabolic inhibitors since the targeted structures that are essential in tachyzoites become dispensable in slow-dividing bradyzoites. The lower proliferation of bradyzoites necessitates less folate for nucleotides (Roos, 1993), a lower demand on pyrimidine synthesis and may also lead to fewer CDPK1-dependent invasion events (Lourido et al., 2012). Furthermore, the metabolic remodeling suggests the dispensability of the mitochondrial electron transport chain (mETC) (Araujo et al., 1992; Ferguson et al., 1994b). Although, drug resistance has not been connected

to the phenotypic heterogeneity of *T. gondii* bradyzoites (Watts et al., 2015), this phenomenon has been identified as a bet-hedging strategy that promotes the survival of other microbes in catastrophically environmental changes including antibiotic exposure (Grimbergen et al., 2015).

In summary, our model enables the generation of encysted bradyzoites which resemble *in vivo* cysts concerning their tolerance to drugs. This qualifies our model as a tool for *in vitro* drug screens. Noteworthy, in contrast to *in vivo* systems, our system also enables the screen of drugs which cannot pass the blood brain barrier. Since Toxoplasmosis is considered a zoonotic disease, the screening of compounds which successfully eradicate *T. gondii* cysts in tissue of farm animals, could lead to a significantly lower vertical transmission via undercooked meat products. Furthermore, our *in vitro* model will facilitate dissecting the molecular basis of the impressive drug tolerance and stress resistance of *T. gondii* tissue cyst.

6.2 Metabolic fingerprint of tachyzoites and *in vitro* encysted bradyzoites

The metabolic state of microbes has important implications for the lethality of antimicrobials (Lopatkin et al., 2019) and these metabolic phenotypes are associated with resistance mechanisms in *Escherichia coli* strains (Lin et al., 2019). We used untargeted metabolomics to characterize the metabolome of the pan-tolerant bradyzoite stage of *T. gondii* for the first time. We interpreted the lower levels of tricarboxylic acid (TCA) cycle intermediates with lower significance of this pathway in bradyzoites. Interestingly, inhibition of the aconitase kills tachyzoites (MacRae et al., 2012), but not bradyzoites. This indicates that bradyzoite may entirely rely on glycolysis for ATP generation. Congruently, genetic ablation of the hexokinase causes impaired tissue cyst formation in the brains of infected mice (Shukla et al., 2018).

The metabolome of tachyzoites was investigated extensively (King et al., 2020), whereas direct metabolomic analysis on matured encysted bradyzoites was not feasible up till now. On the one hand, metabolomic liquid chromatography coupled mass spectrometry (LC / MS)-based workflow requires a large amount of cell equivalents which cannot easily be obtained from mouse models, where brains are typically loaded with 2,000-4,000 cysts (Watts et al., 2015). In addition, *ex vivo* cysts require percoll-based isolation protocols (Watts et al., 2015) that introduce MS-incompatible chemical contaminants and artefacts by exposing the cysts to non-physiological environments for extended periods of time. In this work, a protocol was established which overcomes the problems of scalability and percoll-based isolation and therefore enabled us to perform untargeted metabolomics on *T. gondii* encysted bradyzoites for the first time (**Figure 19**; **Figure 20**). We used a magnetic affinity-based isolation protocol based on a protocol developed by the Weiss´s lab for the isolation of *T. gondii* cyst wall proteins (Zhang et al., 2010). We used magnetic streptavidin beads which were coated with DBA. DBA coated beads bind to CST-1 protein in the cyst wall and cysts can be captured via a magnetic stand. During establishment of this protocol, we visually confirmed the capturing of the cysts, but also free bradyzoites to the DBA-coated beads (data not shown). This protocol is scalable and allows isolation and purification of cysts in large quantities, making them available for MS-based metabolomics. We obtained an estimated yield of 2×10^6 cysts per two T150 culture dishes that were sufficient for one technical replicate. It must be mentioned, that DBA-based isolation of the cyst wall was criticized since it might also bind to biotinylated host cell molecules (Tu et al., 2019). To exclude these contaminations in our metabolomic data set we included uninfected host cell samples which we processed in the same way as encysted bradyzoites. Metabolites found in this control group were excluded from the data set. This is a conservative approach to data curation and might disqualify bradyzoite-associated metabolites from our

analysis. Concerning the general approach, it is also important to keep in mind that the detected metabolites differ when applying different column chemistry. For untargeted characterization of encysted bradyzoites, we compared the myotube-derived *in vitro* cysts with isolated tachyzoites cultivated in myotubes and isolated tachyzoites cultivated in HFFs. We chose these three main groups to distinguish stage-dependently regulated and host-dependently regulated metabolites. We anticipated both factors to be influencing the metabolome as the host cell type and stage conversion impact the transcriptome of *T. gondii* (Buchholz et al., 2011; Swierzy et al., 2017). Principal component (PC) analysis revealed that the three sample classes form distinct clusters demonstrating that encysted bradyzoites and tachyzoites possess a distinct different metabolic fingerprint. Stage-specific differences clustered along the PC1 axis and host cell specific differences were found along the PC2 axis (**Figure 19**). Previously, it was shown that skeletal muscle cells greatly differ in their transcriptome compared to HFFs (Swierzy et al., 2017). Especially clusters of genes implicated in cell cycle progression, pentose phosphate way, cell redox homeostasis and protein catabolism, which are suggested to be important host regulators of *T. gondii* stage differentiation. *T. gondii* tachyzoites in turn show a different transcriptomic profile due to infection in different host cell background. Genes which are indicative for active replication and a large demand for RNA are more abundant in *T. gondii* tachyzoites cultured in HFFs, whereas genes involved in metabolic processes were upregulated in *T. gondii* from skeletal muscle cells. This underpinned that *T. gondii* indeed senses the host cell background and the respective created microenvironment and responds to this by changing or adapting its transcriptional and therefore likely metabolic program. However, stage conversion had the dominant impact on the metabolome in our analysis and lead to changes that are largely homogeneous across classes of metabolites such as amino acids, nucleic acids and their derivates, TCA cycle intermediates and vitamins (**Figure 20**, left panel). This indicates the operation of distinct metabolic homeostasis mechanisms in bradyzoites.

Several detected amino acids were found to be accumulated in encysted bradyzoites (**Figure 20**, left panel). Most of these amino acids can be imported by extracellular tachyzoites, indicating the presence of respective Apicomplexan Amino Acid Transporters (ApiATs) (Parker et al., 2019). Except *Tg*ApiAT5-2, which is induced in bradyzoites, the transcript expression of these transporters appears only marginally affected by stage conversion (**Appendix IX**) (Pittman et al., 2014), suggesting that also bradyzoites have the ability to import required amino acids. Proline and alanine can be both *de novo* synthesized from glutamate and pyruvate, respectively, and they are also suggested to be imported by the parasite although underlying transporters were not identified up to now (Krishnan and Soldati-Favre, 2021). Nevertheless, upon tachyzoite infection of HFFs, glutamate import is significantly enhanced in the host cell

(Baumeister et al., 2011), which correlates with the reported upregulation of the transcripts of the epithelial high affinity glutamate transporter EAAT3 in HFFs upon infection with *T. gondii* tachyzoites (Fouts and Boothroyd, 2007). The synthesis from pyruvate to alanine is orchestrated by two enzymes, namely alanine dehydrogenase and alanine transaminase, both enzymes are shown to be upregulated in bradyzoites (Krishnan and Soldati-Favre, 2021). Interestingly, D-alanine occurs in peptidoglycans of some bacterial cell walls (Cava et al., 2011), nevertheless its role in Apicomplexa is not known. All branched chain amino acids (BCAAs) are significantly upregulated in encysted bradyzoites. Transcriptomic *in vivo* data reveals that BCAA aminotransferase (TGME49_297850) is significantly upregulated in the chronic form (ToxoDB). This enzyme catalyzes the synthesis or the degradation of the BCAAs leucin, isoleucine and valine (Hutson, 2001). The accumulated amino acids except for proline, which can also be synthesized from glutamate (Krishnan and Soldati-Favre, 2021), are less concentrated in the Roswell Park Memorial Institute 1640 (RPMI)-based bradyzoite medium compared to the Dulbecco´s Modified Eagle Medium (DMEM)-based medium used for tachyzoites, implying an intracellular origin of these differences. Hence, these changes may reflect a lowered demand for protein biosynthesis and may also be associated with an additional source. Autophagy and proteolysis through autophagy-related protein ATG9 (Smith et al., 2021) and cathepsin L (Dou et al., 2014) has been shown to be essential in bradyzoites and may constitute an endogenous source for amino acids. Together, these data support a model in which differentiation to bradyzoites presents a mechanism to cope with limited availability of exogenous amino acids. The diversification of nutrient sources would resemble the stringent metabolic response of *Leishmania mexicana* amastigotes that adopt a slow growing phenotype within the phagolysosome of macrophages (Saunders et al., 2014).

Encysted bradyzoites consistently harbored lower levels of TCA cycle-associated metabolites (**Figure 20**, left panel), which likely reflects the lower activity of this pathway. To test the relevance of this, we treated 28-day-old encysted bradyzoites and intracellular tachyzoite cultures with sodium fluoroacetate (NaFAc) which was shown to efficiently block the aconitase in tachyzoites (MacRae et al., 2012) (**Figure 21**, **Figure 22**). The tolerance of bradyzoites towards NaFAc would be consistent with the dispensability of mitochondrial aconitase along with a fully functional TCA cycle. To exclude that tolerance towards NaFAc relies on exclusion of this inhibitor from the cyst wall (Tomita et al., 2013), we measured direct metabolic effects of this inhibitor on both stages (**Figure 22**). NaFAc treatment leads to drastically increased levels of citrate and aconitate in *T. gondii* tachyzoites (MacRae et al., 2012). Through our applied column chemistry, we could not detect citrate, but LC / MS analysis of treated tachyzoites and bradyzoites confirmed an accumulation of aconitate (**Figure 22**). This demonstrates that the inhibitor is taken up into the cyst lumen and directly blocks the parasite

aconitase. This also shows that the TCA cycle maintains a flux that can be inhibited. However, without simultaneous stable isotope labeling we cannot exclude that low-level flux escapes the inhibition by NaFAc. To address this, a stage-specific genetic knock-out would be required which may be achieved by adapting the degron system (Brown and Sibley, 2018) into a type II strain or by swapping the aconitase promoter to a tachyzoite-specific SAG1 promoter as achieved for the *TgATG8* gene (Smith et al., 2021). Our data do not exclude the possibility that parts of the TCA cycle remain operational and process anaplerotic substrates, such as glutamine to generate NADH for subsequent ATP production through the mETC. However, full resistance to HDQ, the inhibitor of the alternative type 2 NADH-dehydrogenase (Fleige et al., 2008) (**Figure 18**, **Appendix X**), suggests that this source of ATP is equally dispensable. HDQ appears to decrease the mitochondrial membrane potential only partially in bradyzoites (**Appendix X**), indicating the presence of HDQ-independent sources of reduction equivalents or a very slow rate of mitochondrial ATP synthesis concomitant with negligible depolarization of the electric potential. Furthermore, our data demonstrates that the metabolome of tachyzoites is globally altered by NaFAc treatment, whereas only a minor part of detected metabolite levels differed in NaFAc-treated bradyzoites, demonstrating the central role of the TCA cycle in *T. gondii* tachyzoites (MacRae et al., 2012), but not bradyzoites. Together, these data underpinned our prior established hypothesis that a functional TCA cycle is dispensable in encysted bradyzoites and is consistent with activity of the isocitrate dehydrogenase enzyme in lysates of 28-day-old *ex vivo* bradyzoites (Denton et al., 1996). Suggesting the TCA cycle may represent an active, but dispensable source of ATP in this stage. The TCA cycle is an important pathway which contributes to manifold cellular functions. In *T. gondii* tachyzoites it was shown to be first of all important for producing reducing electron equivalents for the mETC (Sheiner et al., 2013). Through succinate dehydrogenase, the only membrane-bound protein of the TCA cycle and also complex II of the mETC, mETC and TCA cycle are directly connected. Intracellular and extracellular tachyzoites were shown to rely on their mETC for over 90 % of their ATP production via oxidative phosphorylation (Lin et al., 2011; MacRae et al., 2012). In bradyzoites however, no succinate dehydrogenase activity was detectable in lysates of *ex vivo* bradyzoites (Denton et al., 1996) and oxidative phosphorylation activity appears to be significantly down regulated (MacRae et al., 2012; Shukla et al., 2018; Vercesi et al., 1998). Other roles of the TCA cycle involve the supply of the heme biosynthesis pathway with succinyl-Coenzyme A (CoA). In tachyzoites, heme biosynthesis is highly fitness conferring. While low amounts of precursors can be salvaged from the host, the last step appears to be essential (Krishnan et al., 2020). Heme is an essential co-factor for several enzymes involved in the mETC (Kloehn et al., 2021). Considering RNA sequencing data, heme synthesis seems to be less active in bradyzoites and all enzymes appear repressed, excluding

putative oxygen-independent coproporphyrinogen III dehydrogenase (Hehl et al., 2015) that is dispensable in tachyzoites and bradyzoites (Krishnan et al., 2020). This may indicate lower demand or enhanced scavenging in bradyzoites. Our metabolome data showed a lower relative abundance of γ-aminobutyric acid (GABA) in bradyzoites. In *T. gondii* glutamate can be converted to GABA and then be fed into the TCA cycle via the GABA shunt (MacRae et al., 2012) and hence serves as an important energy source in tachyzoites. Interestingly, GABA accumulates in extracellular tachyzoites, and GABA-depleted parasites partially lose gliding motility activity (MacRae et al., 2012). The lower abundance in encysted bradyzoites might reflect a combination of lower activity of the TCA cycle and lower importance of gliding motility and invasion events during the encysted life-cycle stage. The latter is also supported by diminishing impact of CDPK1 inhibitors in maturing bradyzoites (**Figure 18**). The observations concerning the decreased relevance of the TCA cycle in bradyzoites go in line with previous reports that point towards glycolytic ATP production in bradyzoites, which does not require heme-containing enzymes (MacRae et al., 2012; Shukla et al., 2018; Vercesi et al., 1998). Intriguingly, encysted bradyzoites possess huge carbon stores in form of amylopectin, so it is likely that this form relies on the energy generated from degradation of amylopectin to lactate (Denton et al., 1996). Consistently, it was shown that the number of *T. gondii* cysts in brain tissue of latently infected mice depends on the turnover of their amylopectin pool (Sugi et al., 2017) and on the expression of several glycolytic enzymes including hexokinase (Shukla et al., 2018) and LDH (Abdelbaset et al., 2017; Xia et al., 2018). Both, bradyzoites and the activity of bradyzoite-specific isoforms of glycolytic enzymes were shown to be more resistant to low pH environments than tachyzoite-specific isoforms (Al-Anouti et al., 2004). This phenomenon is thought to be an adaptation to acid conditions in the hosts stomach but might also reflect a critical adaption of bradyzoites to a lactic acid-acidified microenvironment (Denton et al., 1996). In yeast strains the acidification of the cytoplasm was shown to trigger the transition of the cytoplasm to a solid-like state with enhanced mechanical stability resulting in a state of dormancy. This transition promotes the survival under starvation conditions (Munder et al., 2016). Consistently, transcriptomic analyses of *P. vivax* hypnozoites, a persistent stage of this malaria parasite, indicates a similar metabolic shift towards glycolysis (Bertschi et al., 2018).

Nucleobase-containing molecules were consistently found to be less abundant in *T. gondii* encysted bradyzoites (**Figure 20**, left panel). While the parasite is auxotroph for purines (Abrahamsen et al., 2004; Chaudhary et al., 2004), pyrimidines can both be imported and synthesized (Schwartzman and Pfefferkorn, 1981). It is obvious that slow growing or dormant bradyzoites likely have a lower demand for nucleobases to synthesize new DNA and RNA than proliferative tachyzoites. Consistently, the transcription of the corresponding low affinity and high-capacity adenosine transporter *Tg*AT (Chiang et al., 1999; De Koning et al., 2003)

appears to be down-regulated in four-week-old bradyzoites *in vivo* (**Appendix IX**) (Pittman et al., 2014). Two other membrane proteins, containing nucleoside transport signatures, however, remain expressed and may represent the unidentified high affinity purine transporter that is thought to be responsible for maintaining a slow influx of nucleobases into tachyzoites (**Appendix IX**) (Pittman et al., 2014). In tachyzoites pyrimidine *de novo* synthesis is essential for virulence and knock-out of the central enzyme carbamoyl phosphate synthetase II led to attenuated virulence in mice (Fox and Bzik, 2002). In four-week-old bradyzoites the enzyme is equally expressed suggesting continued pyrimidine *de novo* synthesis in the chronic stage (ToxoDB). Similar to *Plasmodium falciparum* (Painter et al., 2007), pyrimidine synthesis in *T. gondii* tachyzoites depends on the mETC to provide an electron acceptor to the dihydroorotate dehydrogenase (Hortua Triana et al., 2012). The role and relevance of the mETC in bradyzoites remains to be formally established. While we showed that *in vitro* bradyzoites develop tolerance towards the tachyzoite dihydroorotate dehydrogenase inhibitor HDQ (Hegewald et al., 2013; Lin et al., 2009) (**Figure 18**), other mETC inhibitors, including atovaquone and other quinolones appeared to have some effect and led to a decrease in cyst counts in brains of latently infected mice (Araujo et al., 1992; Araujo et al., 1991; Doggett et al., 2012; Ferguson et al., 1994b). Activity of atovaquone against *in vitro* tissue cysts was not accurately assessed since the lack of a treatment window in KD3 myotubes (data not shown). In the absence of an obligate TCA cycle, an indispensable function of the mETC in bradyzoites likely includes pyrimidine synthesis. The pyrimidine salvage pathway was shown to be not essential in both acute (Pfefferkorn 1978; Donald and Roos 1995) and chronic (Fox and Bzik, 2015) stages. During the salvage pathway pyrimidine nucleosides are converted to uracil as central molecule of the salvage pathway. This salvage capacity is funneled exclusively through uracil phosphoribosyl transferase (Pfefferkorn 1978; Iltzsch 1993). In our dataset all quantified pyrimidines are part of the salvage pathway of *T. gondii* and are significantly less abundant in encysted bradyzoites than in tachyzoites. Strikingly, transcriptomic data of *in vivo* cysts reveals the significant down regulation of the central enzyme uracil phosphoribosyl transferase and other enzymes of the salvage pathway in the chronic form (Pitmann et al., 2014). Pyrimidine starvation via both, restricting *de novo* synthesis and salvage, were shown to efficiently induce tachyzoite to bradyzoite formation *in vitro* (Dzierszinski et al., 2004; Roos, 1993). Consistently, supplementation of uridine monophosphate in turn led to reduced tachyzoite to bradyzoite conversion in CO_2-depleted environments (Weilhammer et al., 2012). However, it was also shown that blocking *de novo* synthesis and salvage of pyrimidines in parallel first resulted in enhanced bradyzoite formation, but in further course led to a severe decreased viability of *in vitro* bradyzoites (Paredes-Santos et al., 2019). Since *T. gondii* synthesizes pyrimidines *de novo* in a bicarbonate-dependent way (Schwartzman and Pfefferkorn, 1981), it must be noted

that pyrimidine levels might be affected by our applied method to induce stage conversion. Hence, in CO_2-depleted environments and in the absence of supplemented bicarbonate, pyrimidine synthesis is likely restricted and needs to be salvaged from the host. Summarized, taking in account literature and in this work generated data, bradyzoite have a demand for uridine monophosphate and pyrimidines, although less then tachyzoites for previously stated reasons. The low level of pyrimidines which bradyzoites need to maintain "healthy" are either synthesized *de novo* or salvaged depending on available sources. Summarized, studies point towards a decreased, but indispensable, pyrimidine metabolism in bradyzoites.

T. gondii is a remarkably promiscuous pathogen, and the ability to infect disparate host cell types demands metabolic flexibility. We found that the metabolome of *T. gondii* indeed depends on the host cell type, although the influence of stage conversion appears much larger (**Figure 19**, **Figure 20**). Notably, the levels of the three essential amino acids methionine, threonine and phenylalanine were increased in HFF-grown tachyzoites compared to myotube-grown tachyzoites. These lowered levels may reflect a higher abundance of these amino acids in HFFs. Essential amino acids including phenylalanine and tryptophan were reported to be decreased during myotube differentiation of primary human skeletal muscle cells (Kumar et al., 2020). Similar metabolic changes are caused by induction of the FOXO1 transcription factor (Matsuda et al., 2019) that is typically induced in skeletal muscle cells (Gross et al., 2009). Limited supply of these amino acids may facilitate stage conversion in myotubes through slowing down tachyzoite growth (Cerutti et al., 2020; Jeffers et al., 2018).

Summarized, we took advantage of our prior established *in vitro* model for mature encysted bradyzoites and recorded the metabolomic fingerprint of encysted bradyzoite for the first time. Intriguingly, untargeted metabolomic analyses revealed a distinct different metabolic fingerprint of encysted bradyzoites compared to tachyzoites with global up and down regulation of metabolite classes. Metabolomic data and subsequent targeted pharmacological modulation of the aconitase underpinned that the TCA cycle is an active, but dispensable in the chronic form.

6.3 Discovery of a potential detoxification mechanism in *Toxoplasma gondii*

Our metabolomic data identified the presence of carnitine and acylcarnitines, a prior uncharacterized metabolite class in *T. gondii* tachyzoite and bradyzoite stages. In mammalian cells, carnitines are essential for the mobilization of long-chain FAs across the inner mitochondrial membrane to make them accessible for β-oxidation (Longo et al., 2016). Furthermore, they are involved in shuttling acetyl-groups from the peroxisome to the mitochondria and import acyl-chains into the lumen of the endoplasmic reticulum (Gooding et al., 2004). During this process acyl-CoA esters transfer acyl-groups to carnitine and thereby function in balancing the pool of available free CoA (Bieber et al., 1982; Brass and Hoppel, 1980; Pearson and Tubbs, 1967). Since acylcarnitines are mobile and diffuse across biological membranes, they are important for the excretion of poorly metabolizable, toxic acyl-groups (Bremer, 1983). Thus, in humans acylcarnitines are found in a variety of biofluids such as serum and urine (Chalmers et al., 1984).

Although, the genome of *T. gondii* encodes homologues for enzymes needed for lipid oxidation, it lacks homologs of genes involved in carnitine synthesis (ToxoDB). Since *T. gondii* is known to satisfy its needs by scavenging of a broad range of molecule classes from its host (Blume and Seeber, 2018), we suggested the detected carnitine to be host cell-derived. The performed labeling experiment using deuterated carnitine revealed the time-dependent saturation of the *T. gondii* (acyl) carnitine pool, indicating an intact uptake pathway (**Figure 23**). Nevertheless, the uptake mechanism of carnitine in *T. gondii* remains unclear. The responsible transporters for carnitine uptake in mammalian cells (OCTN1, OCTN2) (Longo et al., 2016) are not encoded in the *T. gondii* genome (ToxoDB). The reliance on carnitine import is also described for bacteria and for yeast *Saccharomyces cerevisiae* since they do not possess *de novo* synthesis pathways (van Roermund et al., 1999; Verheul et al., 1998). In bacteria different transporters are involved in carnitine uptake in a species-dependent manner. One main class implied in carnitine uptake are ATP-dependent ATP-binding cassette (ABC) transport systems (Ziegler et al., 2010). The genome of *T. gondii* comprises manifold genes encoding members of the ABC transporter superfamily with till now uncharacterized functions (Sauvage et al., 2006). Acute as well as chronic *T. gondii* infection of host cells is accompanied with the reorganization of host cell organelles (Laliberté and Carruthers, 2008; Paredes-Santos et al., 2017). The best described phenomenon is the association of host cell mitochondria to the parasitophorous vacuolar membrane (PVM). The underlying process of this is not fully understood and factors both on the host cell and the parasite side seem to be involved (Blank et al., 2021; Kelly et al., 2017; Pernas et al., 2014). *T. gondii* can delocalize host cell

transporters to the PVM for its own use as shown for host cell P-glycoprotein for cholesterol import (Bottova et al., 2009). Thus, another possibility might be the recruitment of host cell carnitine transporter to the PVM to ensure carnitine import of the pathogen. Immunofluorescence assay and localization of respective candidates would be sufficient to analyze this. Interestingly, *T. gondii* expresses a protein (TGME49_300360) which shows relatively high identity (25.7 %) and high similarity (43.7 %) to the human carnitine-acylcarnitine transporter protein (ToxoDB). This protein is predicted to be a member of the mitochondrial carrier domain super family. The phenotype score reveals the dispensability in tachyzoites (ToxoDB) and transcriptomic data demonstrates the expression in both stages (Pittman et al., 2014). Although, we did not observe evidence for carnitine being implied in *T. gondii* β-oxidation, TGME49_300360 would be an interesting candidate for localization and functional knockout studies.

Since the main function of carnitines in mammalian cells is the mobilization of FAs and is inalienable for the catabolism of long-chain FAs, we aimed to characterize the FA import of both tachyzoite and bradyzoite stages. *T. gondii* tachyzoites synthesize bulk palmitic acid (C16:0) via cytosolic fatty acid synthesis (FAS) pathway I and dodecanoic (C12:0), myristic (14:0), palmitic (C16:0) and stearic acid (C18:0) *de novo* in the apicoplast resident FASII pathway (Ramakrishnan et al., 2012). This synthesis capacity is complemented by FA import from the host as has been shown using fluorescent analogues (Charron and Sibley, 2002; Nolan et al., 2018; Pernas et al., 2018). We extend these studies by showing that *T. gondii* tachyzoites import a full range of FAs including C14, C16, C18:1, C18:2, C:20 and C20:4 (**Figure 24**). Up till now, few studies were performed concerning lipid sources and lipid uptake pathways in encysted bradyzoites. Electron microscopy approaches on *ex vivo* cysts from mice brain demonstrated the cyst wall to be 240 nM thick containing 30 nM circular openings on the surface (Lemgruber et al., 2011), which enables interchanges with the host cytoplasm and the uptake of host macromolecules to the cyst matrix (Nolan et al., 2018). A previous study revealed the abundance of lipid droplets (LDs) in *T. gondii* bradyzoites and the enhanced number of LDs upon supplementation with oleic acid which indicated import of host cell oleic acid into the parasite (Nolan et al., 2018). However, our data demonstrates for the first time that not only tachyzoites, but also bradyzoites import a broad range of host cell FAs (**Figure 25**, **Figure 26**). A time series of 7- to 28-day-old bradyzoites revealed that import activity wanes with ongoing maturation and FA label incorporation of 28-day-old encysted bradyzoites disappears in the background noise (**Figure 25**B). It must be pointed out, that FA abundances stay the same over maturation time, which demonstrates that less detected labeling is not owed by less encysted bradyzoites (**Figure 25**A). Considering that FAs mainly serve for membrane synthesis, this waning import fits to the lower metabolic needs of slow dividing

bradyzoites. As a consequence of the time series, we extended the labeling window of 28-day-old encysted bradyzoites and as a result we could see a distinct increase of FA labeling and thus FA import above background level (**Figure 26**B). Labeling of the type I RH parasites was always at the level of the host cell background which was also reflected in FA abundances (**Figure 26**). This demonstrates that our established method is not sufficient to isolate type I RH cysts. Type II and type III bradyzoites mainly imported unsaturated oleic and linoleic acid (LA) (C18:1, C18:2), but also myristic (C14:0), palmitic (C16:0) and stearic acid (C18:0) (**Figure 26**). Comparing import of tachyzoites and bradyzoites, the data revealed on the one hand differences in FA uptake between acute and chronic stages, but on the other hand a distinct slower FA uptake in mature chronic stages. Interestingly, a study reported the loss of the apicoplast in a major part of matured *in vitro* and *ex vivo* bradyzoites (Dzierszinski et al., 2004). Since this organelle harbors the FASII system and is critical for FA synthesis in tachyzoites, this would suggest an enhanced reliance of *T. gondii* bradyzoites on FA import to satisfy their demands.

Meldonium treatment in various concentrations and the resulting depletion of host cell (acyl) carnitines and repressed β-oxidation (**Figure 27**), showed no impact on viability for both tachyzoites and bradyzoites, indicating that under normal cell culture conditions carnitines do not attribute to parasite fitness (**Figure 28**). Interestingly, depletion of carnitines directly impacts the import and abundance of total FAs in particular unsaturated LA (C18:2) in *T. gondii* tachyzoites and 28-day-old encysted bradyzoites (**Figure 29**, **Figure 30**). We questioned whether this increased delivery of FAs into *T. gondii* is an indirect effect through a repressed host cell β-oxidation caused by decreased carnitine levels or whether the carnitine level itself has a direct relevance for *T. gondii* FA household. Several studies point towards an impact of modulated host cell β-oxidation on *T. gondii* tachyzoite growth, whereas the described effects were contrary. *T. gondii* tachyzoites growth was impaired due to inhibition of host cell β-oxidation, suggesting that the parasite is dependent on ATP produced from host mitochondria (Nolan et al., 2017). In contrast, *T. gondii* tachyzoites showed promoted growth due to blockage of host β-oxidation, concluding that parasites and host mitochondria compete for nutrients and that a blocked β-oxidation leads to enhanced FA availability for *T. gondii* tachyzoites (Pernas et al., 2018). To selectively block host cell β-oxidation, we treated cultures with trimetazidine, a competitive inhibitor of 3-ketoacyl coenzyme A thiolase (Kantor et al., 2000), which is a key enzyme in the final step of fatty acid ß-oxidation generating acetyl-CoA (Aon et al., 2014). To tear apart the effects of host cell β-oxidation and carnitine level itself on free LA level, we labeled freshly invaded tachyzoites with ^{U13}C LA and treated them either with trimetazidine and carnitine to block host cell ß-oxidation but provide carnitine or with trimetazidine and meldonium to block host cell β-oxidation and deplete carnitine levels (**Figure**

31, **Appendix VI**). We performed targeted LC / MS analysis on carnitine classes and free LA and compared abundances of metabolites of treated and labeled to tachyzoites only labeled with ^{U13}C LA. Blockage of β-oxidation and supplementation of external carnitine led to significantly higher abundances of carnitine, linoleoyl carnitine and propionyl carnitine while free LA level stayed the same. Blockage of β-oxidation and parallel depletion of carnitine level vice versa resulted in reduced carnitine and acylcarnitine level and free LA level rose drastically.

FAs represent carbon sources (Pernas et al., 2018) and saturated FAs like palmitic acid have beneficial effects on *T. gondii* growth (Nolan et al., 2018). On the other hand, free unsaturated FAs, especially oleic acid and LA exhibit pan-antimicrobial activity (Das, 2018) and represent a basic immune effector mechanism (Calder, 2018). Unsaturated FAs, lead to parasite poisoning if they are not either metabolized by the host or if the parasite does not have the capacity to store them (Nolan et al., 2017; Nolan et al., 2018). Supplementation of the medium with oleic acid led to uncontrolled accumulation of large LDs which impair parasite growth and pharmacological modulation of diacylglycerol-O-acyltransferase 1, which is important for neutral lipid storage, rendered *T. gondii* tachyzoites and bradyzoites hypersensitive towards oleic acid (Nolan et al., 2018). Although being highly dependent on lipid salvage from the host to satisfy its needs, *T. gondii* is not able to balance lipid biosynthesis and salvage and thus is highly vulnerable towards excess lipid uptake and resulting lipotoxicity, especially concerning antimicrobial unsaturated FAs (Nolan et al., 2018). Consequently, we observed that modulated free LA levels directly translated into an impaired growth of *T. gondii* tachyzoites and bradyzoites (**Figure 32**, **Figure 33**). Meldonium and trimetazidine treatment rendered tachyzoites and bradyzoites hypersensitive towards free LA. The combined depletion led to a dramatic impairment of parasite growth and potential death of parasites. The observed effects could entirely be rescued by external carnitine supplementation. Low LA concentrations led to an enhanced growth of *T. gondii*, revealing that small amounts of also antimicrobial FAs are beneficial for *T. gondii* growth, and the poisoning is highly dose-dependent. Interestingly, Bradyzoites withstand much higher LA concentrations than tachyzoites. This might be promoted by the cyst wall shielding bradyzoites from uncontrolled LA uptake. Furthermore, LA is known to induce mitochondrial reactive oxygen species formation in several cell types (Hatanaka et al., 2013). In bradyzoites, numerous enzymes with roles in the metabolism of oxygen radicals are upregulated, suggesting that the encysted forms are equipped to deal with long-term exposure to reactive metabolites (Manger et al., 1998).

Summarized, we could show that excess LA and the following uncontrolled uptake is highly toxic for *T. gondii* tachyzoites and bradyzoites. The strength of LA poisoning is highly dose-

dependent and dependent on functional host β-oxidation and available (acyl) carnitine pools. Pathogens implemented several strategies to cope with antimicrobial FAs. *S. aureus* inducibly expresses an export pump (Alnaseri et al., 2015), *Leishmania* and other intracellular kinetoplastids express a 2,4-dienoyl CoA reductase for degrading polyunsaturated FAs (Semini et al., 2020). We propose that *T. gondii* tachyzoites and bradyzoites import host cell carnitines to detoxify free antimicrobial LA. In contrast to free FAs, high molarities of acylcarnitines are tolerated without membrane disruption (Ho et al., 2002). Since acylcarnitine are very motile molecules, it might be a possibility that *T. gondii* not only uses carnitine to dilute toxic free FA, but also to actively transport them out of the PVM. Nevertheless, this must be further investigated by e.g., analyzing acylcarnitine level of the supernatant during infection. Additionally, it is not set whether the function we propose is the only function of imported host cell carnitines. Interestingly, in bacteria carnitine is reported to serve against several stresses and promotes e.g. cold- and thermotolerance (Meadows and Wargo, 2015), which are also known key features of *T. gondii* bradyzoites.

For future perspective, the exact mode of LA acid impairing or killing *T. gondii* tachyzoites and bradyzoites should be further analyzed. In general, polyunsaturated FAs kill microbes by their direct action on microbial cell membranes, enhancing generation of free radicals, augmenting the formation of lipid peroxides that are cytotoxic and by increasing the formation of their bioactive metabolites (Chanda et al., 2018). Notably, LA was lately identified as being a specific inducer of the sexual cycle of *T. gondii* (Martorelli Di Genova et al., 2019). Nevertheless, in our study we used a type II strain for all experiments and many type II isolates (e.g. PLK) of *T. gondii* lost the ability to form oocysts (Frenkel et al., 1976). And most importantly, we used a distinct different cell culture system, which is likely very important for the mode of action of LA considering (acyl) carnitine levels and also the presence of delta-6-desaturase. Nevertheless, transcriptomic data comparison of both systems to see if there is a differential response to LA with the induction of genes needed to initiate the sexual cycle, would be highly valuable.

6.4 Establishment of a single cell division marker in tachyzoites and bradyzoites

For decades it has been accepted that bradyzoites are a dormant population with all being the same residing inside their cyst wall. The view on bradyzoites was changed by revealing that they are rather heterogenous populations which are marked by asynchronous division which leads to a range of cell division and therefore likely metabolic states inside one single tissue cyst (Watts et al., 2015). Phenotypic heterogeneity in other persisters is suggested to be closely connected to drug treatment failures (Barrett et al., 2019). Till now heterogeneity of bradyzoites and especially the cell division is hardly understudied due to limiting tools. Bradyzoites can be investigated concerning their maturation dynamics using established tachyzoite and bradyzoite specific markers, but till now there is no marker available which enables the resolute investigation of proliferation in bradyzoites or even tachyzoites. To overcome these limitations, we aimed to establish a cell division marker for *T. gondii* tachyzoites and bradyzoites which can be analyzed on a single cell level.

Since studies based on anti-inner membrane complex 3 (IMC3) antibodies revealed the dynamics and heterogeneity of mature *in vivo* bradyzoites (Watts et al., 2015), we aimed to fluorescently tag and monitor the dynamics of this protein. Neither exogenous tagging nor endogenous overexpression led to the successful generation of transgenic parasites. The exogenous tagging approach showed no fluorescently IMC3-expressing parasites and the endogenous tagged parasites showed fluorescent artefacts and were impaired in their growth (data not shown). The impaired growth of parasites which overexpressed IMC3 might be explained with the high essentiality of IMC3 (ToxoDB). Since "click" chemistry-detectable nucleoside analogues were shown to be sufficient tools to monitor cell division on a single cell level in other protozoan parasites (Barrett et al., 2019), we aimed to test this approach for *T. gondii*. For *Leishmania* parasites it was demonstrated that thymidine-based nucleoside analogue 5-Ethynyl-2'-deoxyuridine (EdU) can be applied to study and tear apart proliferating and non-proliferating persistent cells (Barrett et al., 2019). Although, *T. gondii* is capable of both pyrimidine *de novo* synthesis and salvage (Schwartzman and Pfefferkorn, 1981), the parasite does not possess a thymidine kinase which is the key enzyme for the phosphorylation of pyrimidine-based nucleosides (Radke and White, 1998). Thus, *T. gondii* is not capable to further metabolize and incorporate EdU into newly synthesized DNA, except thymidine kinase was transfected into transgenic parasites (Fox et al., 2001). Studies suggested that a missing thymidine kinase might be bypassed by applying *cyclo*sal phosphotriester pronucleotide analogues of EdU (Huynh et al., 2015). The so called ProTide approach originated by the McGuigan group applies nucleoside analogues which are already equipped with a phosphate

group at 5'-position of the nucleoside (Jewett and Bertozzi, 2010). Furthermore, the compounds carry a masking group which shields the negatively charged phosphate group and provides lipophilicity of the compound to pass through cell membranes. Depending on the desired approach, different masking groups can be applied varying in their size, polarity, and cleavage mechanisms (Beatty et al., 2010; Taylor et al., 1957). Once inside the cell the masking group is cleaved by e.g., pH-driven mechanisms to release the negatively charged nucleoside monophosphate which than can be further metabolized and incorporated into DNA. We screened 13 thymidine-based 5'-monophosphate-bearing compounds. These compounds were either based on the nucleoside analogue EdU or on its arabinosylnucleoside derivate. Arabinosylnucleosides contain β-D-arabinofuranose instead of β-D-ribofuranose. Furthermore, the compounds differed in their number of substituted fluorines (0, 1 or 2 substituted fluorines) and in their masking group and respective cleavage mechanism. Prior to determining incorporation competency of the 13 pyrimidine-based nucleoside analogues, we tested them for their inhibitory effect on *T. gondii* growth (**Table 15**). Although all compounds were EdU-based, they showed a wide range of half inhibitory concentration (IC_{50}) values and the IC_{50} value of three compounds could not be determined at all, since no inhibitory effect was detected in the tested concentration window. Interestingly, sorting the compounds depending on the determined IC_{50} value, the compounds bearing the same masking group clustered. Comparing the determined IC_{50} value of the compounds to the value for EdU, which is known to be not further metabolized and incorporated into parasite DNA, we concluded that only compounds with a lower IC_{50} are able to reach the parasite. The incorporation profiles were confirmed experimentally for the 13 nucleoside chemical probes and indeed only compound 5 and compound 7 were sufficiently incorporated into host cell as well as parasite DNA (**Table 15**). However, compound 4 and compound 7, which also confined a lower IC_{50} then EdU, were not detectable in *T. gondii* DNA. Since compound 5 and compound 7 are both equipped with a *p*-benzoyl-benzyl alcohol masking group, this seems to be the only investigated masking group which facilitates passage via the host cell into the parasite. Other investigated masking groups might be cleaved already in the host cell or are not capable of diffusing through the parasite PVM. EdU was shown to be toxic by causing DNA instability, necrosis and cell-cycle arrest with these effects being cell type-, time- and concentration-dependent (Diermeier-Daucher et al., 2009). Generally, toxicity can be ameliorated with shorter pulse incubations (Ligasová et al., 2015; Qu et al., 2011). Therefore, we chose an incubation time of 24 h which approximately includes two to three division cycles of *T. gondii* (Black and Boothroyd, 2000) and established an exact non-toxic therapeutic window for compound 5 and compound 7 (**Table 16**). Furthermore, we included compounds based on compound 7 which bear other bioorthogonal detection groups to facilitate tetrazine-detectable labeling which would enable

dual pulse labeling experiments (compound 32) and Raman spectroscopy (compound 33) (**Figure 34**, **Table 16**). For the sake of completeness, a detailed therapeutic window of the brominated version of compound 7 (compound 20) was determined (**Figure 34**, **Table 16**). Besides determined limited therapeutic window for labeling, the application of bromodeoxyuridine (BrdU) includes harsh treatments of the sample such as nuclease digestion or acid treatment, which leads to negative consequences when used in combination with other functional probes. Furthermore, most anti-BrdU antibodies show cross-reactivity with EdU which does exclude dual pulse chase experiments combining compound 7 and compound 20 (Liboska et al., 2012). For these reasons we excluded compound 20 from further experiments. EdU-based compound 7, 32 and 33 showed equal effects on host cell viability and *T. gondii* growth enabling a small, but accessible therapeutic window for all compounds (**Figure 34**, **Table 16**). Compound 5 showed a slightly broader therapeutic window. In contrast to the other compounds, compound 5 is based on the arabinosylnucleoside derivate and furthermore substituted with a fluorine in the 2′-position (F-*ara*-EdU). Fluorine substitution at the 2′- or 3′-position of a sugar was shown to increase chemical and metabolic stability of nucleoside analogues, especially in acidic environment (Lee et al., 2002; Zhou et al., 2004) and F-*ara*-EdU was reported to be less toxic than EdU by increased aglycone linkage stability resisting base excision DNA repair pathways (Neef and Luedtke, 2011). Performing labeling experiments applying compound 5 and compound 7, we observed incorporation of both compounds into host and parasite DNA in a concentration-dependent manner (**Figure 35**). Both compounds enabled labeling of the whole parasite pool in non-toxic concentrations and therefore can serve as valuable tool for single cell division monitoring in *T. gondii* tachyzoites.

The purine nucleoside-based analogue 7-deaza-7-ethynyl-2′-deoxyadenosine (EdA) is a sufficient tool to monitor division of mammalian cells *in vitro* and *in vivo* (Neef et al., 2012) and is also incorporated into *T. gondii* DNA (Galazka et al., 2006). However, to our knowledge it was not further investigated for its suitability as cell division marker in *T. gondii*. Accessing the potential therapeutic window for EdA, it led to impairment of *T. gondii* growth in nanomolar concentrations while having no effect on host cell viability (**Figure 36**). In labeling experiments, we observed the concentration-dependent incorporation of EdA into *T. gondii* DNA which reflects *T. gondii* being a purine auxotroph depending on purine salvage (Schwartzman and Pfefferkorn, 1982) (**Figure 36**). Adenosine is the preferred substrate for purine salvage of *T. gondii* tachyzoites (Krug et al., 1989). Nevertheless, labeling detectable above background noise was not accessible in non-toxic concentrations. Other purine auxotroph protozoan parasites have been shown to be susceptible to purine analogues (Wang, 1984) and the toxic effect of adenine arabinoside is well-established for *T. gondii* (Pfefferkorn and Pfefferkorn, 1976). The suggested inhibitory mechanism is the direct effect of ara-adenosine triphosphate

on a DNA-polymerase (Furth and Cohen, 1967), which might also be the case for EdA. To potentially suppress these toxic effects of EdA by being incorporated into other molecules than DNA, we established forodesine (Immucillin H) which inhibits the *T. gondii* purine nucleoside phosphorylase (Chaudhary et al., 2006). As expected (Chaudhary et al., 2006), forodesine itself had no impact on host cell viability and *T. gondii* growth (**Appendix VIII**). The administration of forodesine in combination with EdA indeed led to an enlarged therapeutic window and sufficient labeling above background noise could be achieved in a non-toxic concentration (**Figure 37**). Although not quantified, parasites seemed to show an enhanced incorporation of EdA into newly synthesized DNA, indicated by an increased fluorescence signal of nuclei, with same EdA concentrations upon co-administration of forodesine (**Figure 37**). This observation would go in line with a targeted incorporation of EdA into DNA. Interestingly, throughout all labeling experiments with EdA, no or only faint labeling of host cell nuclei was observed depending on the administered concentration. Since it is known that also mammalian cells incorporate EdA (Neef et al., 2012), it would be interesting to investigate whether this funneling of EdA directly into the parasite is a mechanism promoted by *T. gondii*.

To test whether these compounds are also applicable for cell division monitoring of bradyzoites, we tested their impact on bradyzoite viability on 28-day-old Pru-tdTomato bradyzoites (**Figure 38**). In the used concentrations none of the tested compounds showed an impaired regrowth of bradyzoites. In this work compounds were only applied in the concentrations which were also tolerated by *T. gondii* tachyzoites and for future studies this labeling window should be further titrated for bradyzoite cultures. Matured myotubes are cell cycle arrested, they are non-dividing cells and were shown to not incorporate BrdU (Swierzy and Lüder, 2015), this might lead to a higher tolerance of myotubes to nucleoside analogues than observed for HFFs. The higher tolerance of bradyzoite might be associated to the reduced proliferation rates of this forms. Furthermore, our bradyzoite inducing model relies on pyrimidine starvation, the overall pyrimidine concentration in this system might be lower than in the tachyzoite system leading to a shifted onset of toxicity. Supplementation of the pyrimidine nucleoside uridine was shown to inhibit the conversion of tachyzoites to bradyzoites complementing the defect in pyrimidine synthesis induced by the metabolic stress of CO_2 restriction (Weilhammer et al., 2012). Noteworthy 500 µM of uridine led to the observed effect and in this study, we apply pyrimidine-based analogues only up to 4 µM. Nevertheless, since 20 µM pyrimethamine was shown to kill tachyzoites (**Figure 18**), we included a control labeling bradyzoites with pyrimidine-based analogues and in parallel treating with pyrimethamine (**Figure 38**). Since there was no delayed onset of growth detectable, we can exclude re-differentiation of bradyzoites to tachyzoites upon nucleoside analogue supplementation. Applying pyrimidine-based and purine-based analogues for 48 h on 28-day-old type II ME49

encysted bradyzoites, all compounds revealed successful incorporation into *T. gondii* bradyzoite DNA indicated by overlapping with DAPI channel (**Figure 39**). The incorporation of pyrimidine-based nucleosides reveals intact pyrimidine salvage mechanisms in *T. gondii* bradyzoites which also goes in line with our metabolomic data. The incorporation of purine-based EdA confirms the expression and activity of purine transporters in bradyzoites which fits well with transcriptomic data of the chronic form (**Appendix IX**) (Pittman et al., 2014). Interestingly, not all bradyzoite nuclei showed labeling with applied analogues. This points towards the asynchronous cell division of *T. gondii* bradyzoites already described (Watts et al., 2015).

Summarized, two pyrimidine- and one purine-based nucleoside analogue were established which enable the monitoring of single cell division events in *T. gondii* tachyzoites and bradyzoites for the first time. Thus, the established markers offer a powerful tool to correlate the presence and frequency of cell division events to drug resistance in heterogenous bradyzoite populations.

Chapter 7: Conclusion and future perspectives

7.1 Technical perspectives

7.1.1 Establishment of an *in vitro* protocol for matured *Toxoplasma gondii* tissue cysts

We extensively characterized encysted bradyzoites, but not the myotube system itself. Since *T. gondii* tissue cysts show a high selectivity for several host cells and previous studies demonstrated host cell factors to be important for tachyzoite to bradyzoite conversion, more attention might be paid to underlying host cell backgrounds. It would be highly valuable to investigate the molecular and metabolic profile of KD3 myotubes in comparison to other host cell backgrounds. This would surely shed light on molecular and metabolic factors of KD3 myotubes facilitating early and long-term stage conversion of *T. gondii*. While having investigated type II encysted bradyzoites for structural and functional features, this lacks for type I and type III strains. Comparison between strains would facilitate dissecting further the molecular basis of the impressive drug tolerance and stress resistance of *T. gondii* tissue cyst. Spontaneous stage conversion revealed time-shifted onset of cystogenesis and the expression of bradyzoite genes. The myotube system offers a valuable tool to facilitate time-resolved investigation of chronological sequence and dependency of these events during stage conversion.

7.1.2 Metabolic fingerprint of tachyzoites and *in vitro* encysted bradyzoites

Our metabolomic data shed light on metabolic traits of bradyzoites for the first time and revealed the dispensability of a functional tricarboxylic acid (TCA) cycle this stage. The recorded metabolic fingerprint offers a fundamental basis to dig deeper into the mechanistic relevance of metabolic traits for persistence. It would be important to establish *in vivo* controls for metabolome studies and to record the transcriptome of *in vitro*-derived *T. gondii* tissue cysts. These two data sets would complement each other and promote further conclusions regarding transcriptomic and metabolic phenotypes and drug resistances. As well stable isotope labeling with labeled glucose and glutamine should be performed, to track present and absent fluxes in bradyzoites. This would also shed light on the relevance of the γ-aminobutyric acid (GABA)-shunt in bradyzoites. To proof dispensability of TCA cycle-associated enzymes, stage-specific genetic knockouts might be generated by swapping the respective promoters to a tachyzoite-specific surface antigen 1 (SAG1) promoter as achieved for the *TgATG8* gene (Smith et al., 2021). A remaining question is the relevance of the mitochondrial electron transport chain (mETC) in bradyzoites and whether the mETC is essential for mitochondrial ATP generation, for pyrimidine synthesis or not essential at all. This could be addressed by

conditional knockout studies or pharmacological modulation with e.g., HDQ and atovaquone followed by ATP-level measurements.

7.1.3   Discovery of a potential detoxification mechanism in *Toxoplasma gondii*

We detected carnitines and acylcarnitines, a prior undescribed metabolite class in *T. gondii*, in both, tachyzoite and bradyzoite stages. Via pharmacological modulation, we showed that blockage of host β-oxidation and the depletion of carnitine levels rendered parasites hypersensitive to free linoleic acid (LA) and that this effect can be rescued by supplying carnitine. It would be necessary to investigate the mode of action of LA impairing viability or even killing parasites. Polyunsaturated fatty acids (FAs) kill microbes by their direct action on microbial cell membranes, enhancing generation of free radicals, augmenting the formation of lipid peroxides that are cytotoxic by increasing the formation of their bioactive metabolites (Chanda et al., 2018). Several dyes to monitor lipid peroxidation and reactive oxygen species are commercially available and might be applied for further analysis. Host cell and parasite morphology and staining of potentially accumulating lipid droplets with BODIPY 493/503 would be sufficient, as observed in parasites treated with oleic acid (Nolan et al., 2018). Since we propose that *T. gondii* tachyzoites and bradyzoites import host cell carnitines to detoxify free antimicrobial LA and to potentially shuttle free LA in form of linoleoyl carnitine outside the parasitophorous vacuolar membrane, time-resolved analysis of acylcarnitine levels in supernatant during infection might be analyzed to proof this hypothesis. Carnitine is reported to serve against several stresses and promotes e.g. cold- and thermotolerance (Meadows and Wargo, 2015). Since these are key hallmarks of *T. gondii* encysted bradyzoites, it would be of high interest to analyze the impact of depleted carnitine levels on stress tolerance of matured encysted bradyzoites. Furthermore, it would be valuable to investigate whether this potential detoxification mechanism we propose, is also present in other protozoan parasites like *Plasmodium* or *Leishmania*.

7.1.4   Establishment of a single cell division marker in tachyzoites and bradyzoites

We established two pyrimidine-based and one purine-based nucleoside analogues, which are applicable to investigate tachyzoite and bradyzoite cell division on a single cell level. These nucleoside analogues are sufficient marker to analyze replicative competence in tachyzoites and bradyzoites. In contrast to cell counting labels like DAPI, these proliferative labels allow to distinguish between replicative dormancy with metabolic activity and actively replicating cells. Therefore, the established markers offer a powerful tool to correlate presence and frequency of cell division of parasite (sub) population to drug tolerance and persistence. We in deep established therapeutic labeling concentrations for tachyzoites. Although we saw efficient labeling of single bradyzoites, the therapeutic labeling window could potentially be widened.

For this, resistance scores with increased concentrations should be recorded and labeling titration with respective concentrations, like achieved for tachyzoites, should be performed. Furthermore, it would be highly valuable to establish a staining protocol for compound 32 bearing a tetrazine-detectable group. With this, dual labeling approaches would be feasible. Usually, cell division is assessed by incubating cells with a single "pulse" of a nucleoside analog. For some approaches, e.g., drug efficacy testing, it would be beneficial to introduce two different analogues at different time points (dual pulse labeling), which can further define cell division kinetics.

7.2 The big picture

Many zoonotic pathogens including bacteria, fungi and protozoans successfully evade clearance by the host immune system and chemotherapeutic treatment. This results in dormant and often life-long persisting infections in their host organism that are frequently linked to relapse of acute infections. Resistance of clonal microbial populations is often a consequence of phenotypic heterogeneity due to various factors. Contributing factors include particularly different cell age and cell cycle states (Sumner et al., 2003), a diversity of metabolite content (Balaban et al., 2004) and metabolic flux states (van Heerden et al., 2014). These phenotypic traits in protozoans underlie stress mechanism and have been linked to resistance against antibiotic (Balaban et al., 2004) and carbon source utilization (van Heerden et al., 2014), respectively. During protozoan infections phenotypic variation based on genomic and transcriptomic heterogeneity is well known to serve critical functions and generally, heterogeneity has been identified as a microbial bet-hedging strategy that allows the survival under potentially catastrophic environmental changes (Grimbergen et al., 2015).

In this work, we developed a model for the generation and long-term culture of matured *T. gondii* encysted cysts in a natural host cell background. These cysts mirror *in vivo*-derived encysted bradyzoites in their structural and functional hallmarks. The access to a scalable system for matured tissue cysts combined with methods and tools established in this work are a door opener for novel targeted and untargeted studies on the chronic form of *T. gondii* with many implications for therapeutic intervention with chronic *T. gondii* infections. Now it is feasible to explore which individual phenotypes of bradyzoites offer resistance against external stress factors and promote persistent infections. Since science and curiosity never ends, I will end this thesis with research questions which can now be addressed:

How do phenotypic traits correlate with cell division rates?

How does the virulence phenotype of parasite isolates and isotypes correlate with particular phenotypic traits?

How do individual phenotyopic traits contribute to resistance against stress factors such as drugs or the immune system?

Appendix

Appendix I: Instrument list

Table 17: Instruments.

Instrument	Manufacturer
Autosampler *7693*	Agilent Technologies, Santa Clara, USA
Analytical balance *A200S*	Sartorius AG, Göttingen, GER
CCD camera *Megaview III*	Emsis, Münster, GER
Centrifuge *Rotina 380 R*	Heraeus Holding GmbH, Hanau, GER
Centrifuge *Minispin G*	Eppendorf AG, Hamburg, GER
Diamond knife *45°*	Diatome, Nidau, CH
Fume hood *Delta 30*	Wesemann GmbH, Syke, GER
GC system *7890B*	Agilent Technologies, Santa Clara, USA
Incubator *Heracell*™*150i* CO_2	Thermo Fisher Scientific, Waltham, USA
Incubator *KBW240*	Klaus Binder Labortechnik, Hebertshausen, GER
LC system Vanquish Flex UHPLC	Thermo Fisher Scientific, Waltham, USA
Magnetic stand, *CelinesuperX1000*	Self 3D-printed, Berlin, GER
Mass spectrometer MSD *5977B*	Agilent Technologies, Santa Clara, USA
Mass spectrometer Q Exactive™ Plus Hybrid Quadrupol-Orbitrap™	Thermo Fisher Scientific, Waltham, USA
Microplate reader *Infinite*® *M200 PRO*	Tecan Group Ltd., Männedorf, CH
Microscope Axio Imager Z1 / Apotome	Carl Zeiss GmbH, Jena, GER
Microscope Axio Observer Z1	Carl Zeiss GmbH, Jena, GER
Microcentrifuge *Himac CT15RE*	Hitachi Koki, Tokyo, Japan
Multichannel *Transferpette*®, 20-200 µl	Brand GmbH, Wertheim, GER
pH Meter *PB-11*	Sartorius, Göttingen, GER
Pipettes *Pipetman Classic*™ 0.2-2 µl / 1-10µl / 2-20 µl / 50-200 µl / 200-1,000 µl	Gilson Inc., Middleton, USA
Pipette boy	Brand GmbH, Wertheim, GER

Rotator *SB2*	VWR International GmbH, Darmstadt, GER
Safety cabinet *Safe 2020 Labgard Class II*	Thermo Fisher Scientific, Waltham, USA
Shaker *Polymax 2040*	Heidolph Instruments GmbH & Co. KG, Schwabach, GER
Speed vac *BaVaCo-M "Mini-30"*	Bachhofer GmbH, Reutlingen, GER
Transmission electron microscope *Tecnai Spirit*	Thermo Fisher Scientific, Waltham, USA
Ultramicrotome *UC7*	Leica, Wetzlar, GER
Ultrasonic bath *Sonorex RK100H*	BANDELIN electronic GmbH&Co.KG, Berlin, GER
Vortex-Genie® 2	Scientific Industries, New York, USA
Water bath *GFL 1002*	GFL mbH, Burgwedel, GER

Appendix II: Metabolite mix for peak identification of polar metabolites for GC / MS analysis

Table 18: Metabolite mix for peak identification of polar metabolites for GC / MS analysis. Displayed are the respective concentrations, name of the metabolite, product name, company name, molecular formula, and the molecular weight of metabolites. Table was generated by Franziska Rahel.

concentration	name of metabolite	product name	company name	molecular formula	molecular weight [g/mol]
	Arabinose	L(+)-Arabinose (≥ 99%)	Roth®	$C_5H_{10}O_5$	150,13
	Galactose	D(+)-Galactose (≥ 98%)	Roth®	$C_6H_{12}O_6$	180,16
	Xylose	D(+)-Xylose (≥ 99%)	Roth®	$C_5H_{10}O_5$	150,13
	Mannose	D(+)-Mannose (≥ 98,5%)	Roth®	$C_6H_{12}O_6$	180,16
	Glucose	D(+)-Glucose	Roth®	$C_6H_{12}O_6$	180,16
1 nmol/10 µl	Ribose 5-phosphate	D-Ribose 5-phosphate barium salt hexahydrate (≥99.0% (TLC))	Sigma Aldrich®	$C_5H_9BaO_8P \cdot 6H_2O$	473,51
	Ribulose 5-phosphate	D-Ribulose 5-phosphate disodium salt (≥96% (TLC))	Sigma Aldrich®	$C_5H_9Na_2O_8P$	274,07
	Fructose 6-phosphate	D-Fructose 6-phosphate disodium salt hydrate (≥98%, amorphous powder)	Sigma Aldrich®	$C_6H_{11}Na_2O_9P \cdot xH_2O$	304,1
	Glucose 6-phosphate	D-Glucose-6-Phosphat (99%)	Sigma®	$C_6H_{11}Na_2O_9P \cdot xH_2O$	304,1
	Sucrose	D(+)-Saccharose (≥ 99% p.a.)	Roth®	$C_{12}H_{22}O_{11}$	342,3
	Trehalose	D(+)-Trehalose Dihydrate	Sigma®	$C_{12}H_{22}O_{11} \cdot 2\ H_2O$	378,33
	myo-Inositol	myo-Inositol	SERVA Feinbiochemica Heidelberg	$C_6H_{12}O_6$	180,2
	scyllo-Inositol	scyllo-Inositol	abcamBiochemicals®	$C_6H_{12}O_6$	180,16
4 nmol/10 µl	Phosphoenolpyruvate (PEP)	Phospho(enol)pyruvic acid monopotassium salt (99%)	Sigma Aldrich®	$KOP(O)(OH)OC(=CH_2)CO_2H$	206,13
	3-phosphoglycerate (PGA)	D-(−)-3-Phosphoglyceric acid disodium salt (≥93%, powder)	Sigma Aldrich®	$C_3H_5Na_2O_7P$	230,02
	α-glycerophosphate (glycerol 3-phosphate)	DL-α-Glycerol phosphate magnesium salt hydrate (85% (KT))	Sigma Aldrich®	$C_3H_7MgO_6P \cdot xH_2O$	194,36
	β-glycerophosphate (glycerol 2-phosphate)	β-Glycerophosphate disodium salt	AppliChem®	$C_3H_7Na_2O_6P \cdot xH_2O$	216,04
	Dihydroxyacetone phosphate (DHAP)	Dihydroxyacetone phosphate lithium salt (≥95.0% (TLC))	Sigma Aldrich®	$C_3H_5O_6P \cdot xLi^+$	170,06
5 nmol/10 µl	Lactic acid	L(+)-Lactic acid (BioXtra, ≥98% (titration))	Sigma Aldrich®	$C_3H_6O_3$	90,08
	Fumaric acid	Fumaric acid	ICN Biomedical Inc.	$HOOCCH=CHCOOH$	116,07
	Succinic acid	Succinic acid, SigmaUltra® (≥ 99%)	Sigma Aldrich®	$C_4H_6O_4$	118,09
	Citric acid	Citronensäure (≥ 99,5%)	Roth®	$C_6H_8O_7$	192,13
	Malic acid	L-(-)-Malic acid (ReagentPlus®, ≥ 99,%)	Sigma Aldrich®	$C_4H_6O_5$	134,09
	α-Ketoglutaric acid	α-Ketoglutarsäure-Natriumsalz (≥ 99%)	AppliChem®	$C_5H_5NaO_5$	168,08
	γ-Aminobutyric acid (GABA)	γ-Aminobutyric acid (≥99%)	Sigma Aldrich®	$NH_2(CH_2)_3COOH$	103,12
10 nmol/10 µl	Pyruvate	Pyruvic acid (99 + %)	Sigma®	$C_3H_3O_3Na$	110,0
	Oxalacetic acid	Oxalacetic acid	ICN Biomedical Inc.	$C_4H_4O_5$	132,07
	3-phosphoglyceraldehyde (GAP)	D-Glyceraldehyde 3-phosphate solution (8-13 mg/mL in H2O)	Sigma Aldrich®	$C_3H_7O_6P$	170,06
	Aspartic acid	L-Aspartic acid (reagent grade, ≥98% (HPLC))	Sigma Aldrich®	$HO_2CCH_2CH(NH_2)CO_2H$	133,1
	Alanine	DL-Alanine (≥ 99,0% (NT))	Fluka BioChemika	$C_3H_7NO_2$	89,1
	Asparagine	L-Asparagine anhydrous (≥ 99,0% (NT)) [(S)-2-Aminosuccinic acid 4-amide]	Fluka BioChemika	$C_4H_8N_2O_3$	132,12
	Glutamic acid	L-Glutamic acid (≥ 99,0% (NT))	Fluka BioChemika	$C_5H_9NO_4$	147,13
	Glutamine	L-Glutamine (≥ 99,0% (TLC))	Sigma®	$C_5H_{10}N_2O_3$	146,1
	Glycine	Glycin (≥ 99%)	Roth®	$C_2H_5NO_2$	75,07
	Histidine	L-Histidine [L-α-Amino-β-imidazole-propionic acid]	Sigma Aldrich®	$C_6H_9N_3O_2$	155,2
	Isoleucine	L-Isoleucin (≥ 98% UPS)	Roth®	$C_6H_{13}NO_2$	131,18
	Leucine	L-Leucine (≥ 99% CELL PURE®)	Roth®	$C_6H_{13}NO_2$	131,18
	Lysine	L-Lysine monohydrochloride (≥ 99,0% (AT))	Fluka BioChemika	$C_6H_{14}N_2O_2 \cdot HCl$	182,65
	Methionine	L-Methionin (≥ 99%)	Roth®	$C_5H_{11}NO_2S$	149,21
	Ornithine	L-Ornithine monohydrochlorid [(S)-2,5-Diaminopentanoic acid]	Sigma Aldrich®	$C_5H_{12}N_2O_2 \cdot HCl$	168,62
	Phenylalanine	L-Phenylalanine (≥ 99,0% (NT))	Fluka BioChemika	$C_9H_{11}NO_2$	165,19
	Proline	L-Proline (≥ 99,0% (NT)) [(S)-Pyrrolidine-2-Carboxylic acid]	Fluka BioChemika	$C_5H_9NO_2$	115,13
	Serine	L-Serin (99% (97% ee/GLC))	Sigma Aldrich®	$HOCH_2CH(NH_2)CO_2H$	105,09
	Threonine	L-Threonin (≥ 99% CELL PURE®)	Roth®	$C_4H_9NO_3$	119,12
	Valine	L-Valin (≥ 99% CELL PURE®)	Roth®	$C_5H_{11}NO_2$	117,15
20 nmol/10 µl	Tryptophan	L-Tryptophan (≥ 98,5%, Ph. Eur.)	Roth®	$C_{11}H_{12}N_2O_2$	204,23

Appendix III: Internal standards LC / MS analysis

Table 19: Internal standards for peak identification of metabolites for LC / MS analysis. Displayed are the name, molecular formula, molecular weight and the retention time of metabolites. Table was generated by Deborah Maus.

Name	Molecular formula	Molecular weight [kda]	Retention time [min]
Crotonic acid	C4 H6 O2	86.04	15.00
Pyruvic acid	C3 H4 O3	88.02	1.60
Oxamate	C2 H3 N O3	89.01	4.40
Alanine	C3 H7 N O2	89.05	14.00
Lactic acid	C3 H6 O3	90.03	4.20
2-Deoxycytosine	C4 H7 N3	97.06	18.60
Succinimide	C4 H5 N O2	99.03	4.10
Succinic semialdehyde	C4 H6 O3	102.03	4.20
Choline	C5 H13 N O	103.10	18.10
Serine	C3 H7 N O3	105.04	15.30
Diethanolamine	C4 H11 N O2	105.08	14.60
Cytosine	C4 H5 N3 O	111.04	7.40
Histamine	C5 H9 N3	111.08	19.40
Uracil	C4 H4 N2 O2	112.03	3.50
Creatinine	C4 H7 N3 O	113.06	5.90
Proline	C5 H9 N O2	115.06	12.60
Fumaric acid	C4 H4 O4	116.01	8.70
Valine	C5 H11 N O2	117.08	11.80
Betaine	C5 H11 N O2	117.08	11.00
Succinic acid	C4 H6 O4	118.03	6.40
Aminovaleric acid	C5 H11 N O2	117.08	11.80
Threonine	C4 H9 N O3	119.06	13.90
Nicotinamide	C6 H6 N2 O	122.05	10.00
Nicotinic acid	C6 H5 N O2	123.03	4.20
Taurine	C2 H7 N O3 S	125.01	9.20
Methylcytosine	C5 H7 N3 O	125.06	14.10
Thymine	C5 H6 N2 O2	126.04	3.50
Oxoproline	C5 H7 N O3	129.04	5.00
Acetylputrescine	C6 H14 N2 O	130.11	19.10

Appendix

Acetylalanine	C5 H9 N O3	131.06	4.20
Creatine	C4 H9 N3 O2	131.07	14.30
Leucine	C6 H13 N O2	131.09	10.30
Isoleucine	C6 H13 N O2	131.09	10.70
Adenine	C5 H5 N5	135.05	11.00
Hypoxanthine	C5 H4 N4 O	136.04	8.10
Methylnicotinamide	C7 H8 N2 O	136.06	19.00
Urocanic acid	C6 H6 N2 O2	138.04	5.30
Phosphoethanolamine	C2 H8 N O4 P	141.02	17.90
Caprylic acid	C8 H16 O2	144.12	1.60
Acetylcholine	C7 H15 N O2	145.11	14.50
Alpha ketoglutarate	C5 H6 O5	146.02	7.90
Glutamine	C5 H10 N2 O3	146.07	14.90
Lysine	C6 H14 N2 O2	146.11	23.50
Glutamic acid	C5 H9 N O4	147.05	13.20
Hydroxyglutaric acid	C5 H8 O5	148.04	10.70
Methionine	C5 H11 N O2 S	149.05	10.90
Guanine	C5 H5 N5 O	151.05	9.10
Propanoyl phosphate	C3 H7 O5 P	154.00	4.30
Histidine	C6 H9 N3 O2	155.07	24.40
Orotic acid	C5 H4 N2 O4	156.02	4.20
Nonanoic acid	C9 H18 O2	158.13	1.50
Methylglutamine	C6 H12 N2 O3	160.08	6.80
Carnitine	C7 H15 N O3	161.11	14.40
Phenylalanine	C9 H11 N O2	165.08	9.40
Glycerol 3 phosphate	C3 H9 O6 P	172.01	15.70
Decanoic acid	C10 H20 O2	172.15	1.50
Acetylleucine	C8 H15 N O3	173.11	4.40
Aconitic acid	C6 H6 O6	174.02	8.80
Arginine	C6 H14 N4 O2	174.11	23.30
Acetylaspartic acid	C6 H9 N O5	175.05	10.50
Glucosamine	C6 H13 N O5	179.08	12.10
Trimethyllysine	C9 H20 N2 O2	188.15	23.70
Acetylglutamine	C7 H12 N2 O4	188.08	5.80
Acetylglutamic acid	C7 H11 N O5	189.06	10.20

Threonine 3 phosphate	C4 H10 N O6 P	199.02	14.30
Laurate	C12 H24 O2	200.18	1.40
Dimethylarginine	C8 H18 N4 O2	202.14	22.00
Acetylcarnitine	C9 H17 N O4	203.12	12.50
Deoxyribose 1 phosphate	C5 H11 O7 P	214.02	4.10
Glycerophosphorylethanola mine	C5 H14 N O6 P	215.06	15.30
Acetylarginine	C8 H16 N4 O3	216.12	15.10
Pantothenic acid	C9 H17 N O5	219.11	4.40
Cystathionine	C7 H14 N2 O4 S	222.07	10.80
Myristic acid	C14 H28 O2	228.21	1.40
Cytidine	C9 H13 N3 O5	243.09	9.40
Uridine	C9 H12 N2 O6	244.07	5.80
Pseudouridine	C9 H12 N2 O6	244.07	9.70
Glycerophosphoglycerol	C6 H15 O8 P	246.05	8.00
Deoxyadenosine	C10 H13 N5 O3	251.10	4.90
Ribosylnicotinate	C11 H13 N O6	255.07	13.30
Palmitate	C16 H32 O2	256.24	1.40
Thiamine	C12 H16 N4 O S	264.10	19.90
Inosine	C10 H12 N4 O5	268.08	8.10
Adenosine	C10 H13 N5 O4	267.10	6.10
Margaric acid	C17 H34 O2	270.26	1.40
Linoleic acid	C18 H32 O2	280.24	1.40
Oleate	C18 H34 O2	282.26	1.40
Guanosine	C10 H13 N5 O5	283.09	10.70
Xanthosine	C10 H12 N4 O6	284.08	5.30
Stearate	C18 H36 O2	284.27	1.40
Sphingosine	C18 H37 N O2	299.28	1.90
Tretinoin	C20 H28 O2	300.21	1.50
Arachidonic acid	C20 H32 O2	304.24	1.40
Cyclic AMP	C10 H12 N5 O6 P	329.05	4.80
Riboflavin	C17 H20 N4 O6	376.14	8.10
Coenzyme Q7	C44 H66 O4	658.49	1.70

Appendix IV: LC / MS data curation
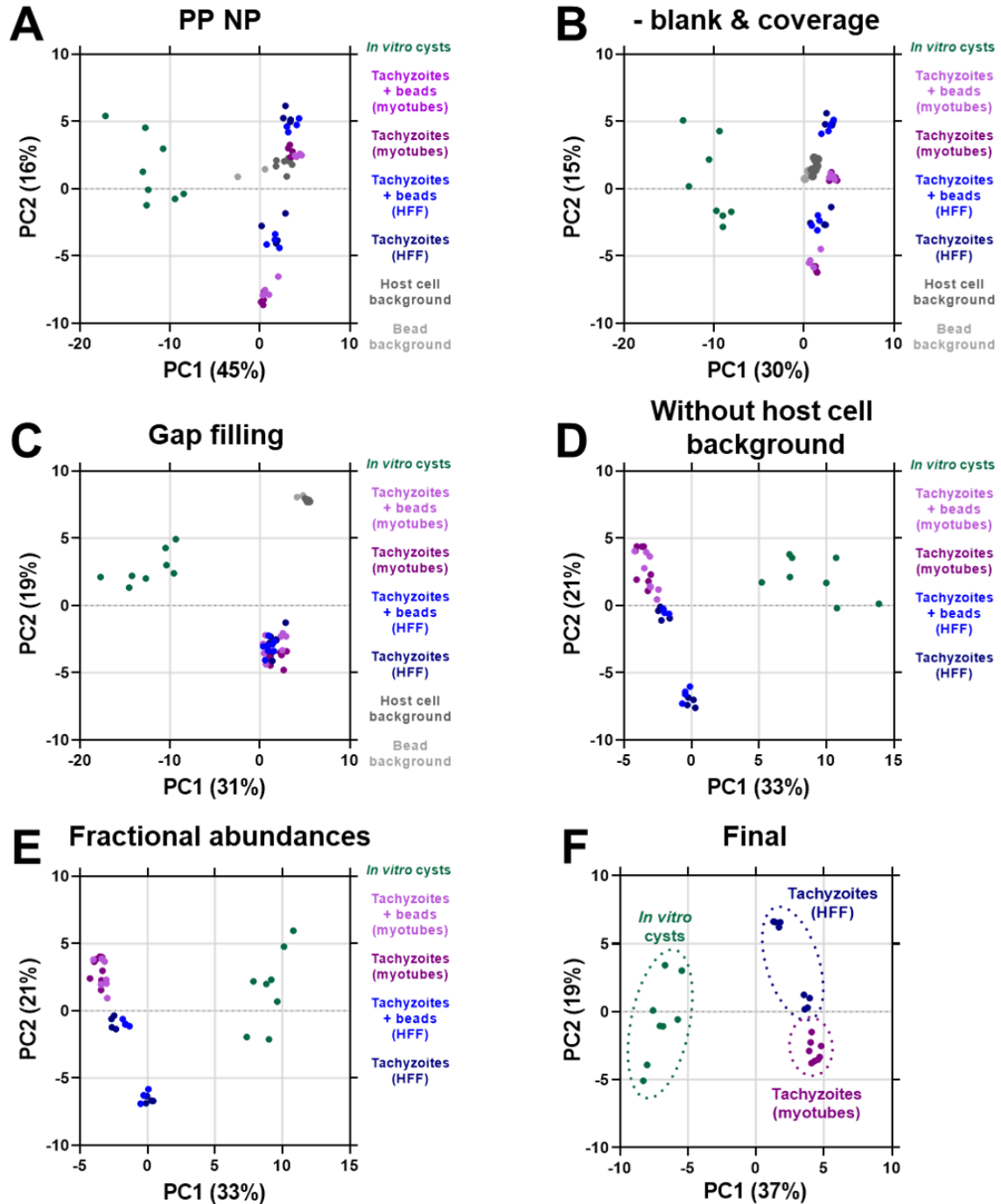
Figure 40: Data curation LC / MS. Samples were analyzed in positive and negative ionization mode separately. The principal component analyses illustrate effects of the data analysis steps. (A.) Positive and negative datasets were combined. (B.) Blanks were subtracted. Metabolites that had a coverage of less than 50 % in at least one sample set were excluded. (C.) Gaps in the dataset were filled with the mean intensity of the sample group of the respective batch. If a metabolite was not detected in sample group, the minimal intensity value was used for gap filling. (D.) Metabolites that were prominent within the magnetic bead or host cell background samples were excluded. (E.) To allow statistical comparison of the cyst samples, which were not normalized to parasite numbers, with the tachyzoites samples, the fractional abundances were calculated by dividing each metabolite intensity by the sum of all intensities per sample. (F.) Because the addition of beads to the tachyzoite samples did not play an important role, these controls were omitted from further analysis. Data analysis was mainly performed by Deborah Maus.

Appendix V: Impact of trimetazidine on tachyzoite viability
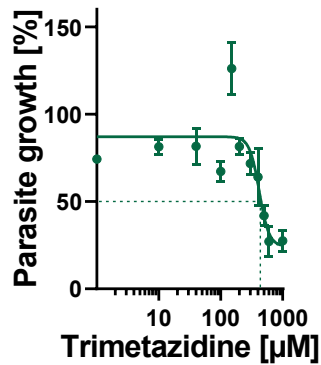
Figure 41: Impact of trimetazidine on tachyzoite viability. Pru-tdTomato tachyzoites (MOI: 1) were cultured in myotubes for 4 h, followed by treatment. (A.) Calculation of half inhibitory concentration (IC_{50}) of trimetazidine-treated Pru-tdTomato tachyzoites. Parasites were grown for seven days in presence of trimetazidine or 0.05 % water as solvent control. The IC_{50} value was calculated from fluorescence intensities normalized to untreated controls. Shown are means and SEM of three independent experiments with three replicates each.

Appendix VI: Impact of repressed host cell β-oxidation and (acyl) carnitine level on free linoleic acid level in tachyzoites
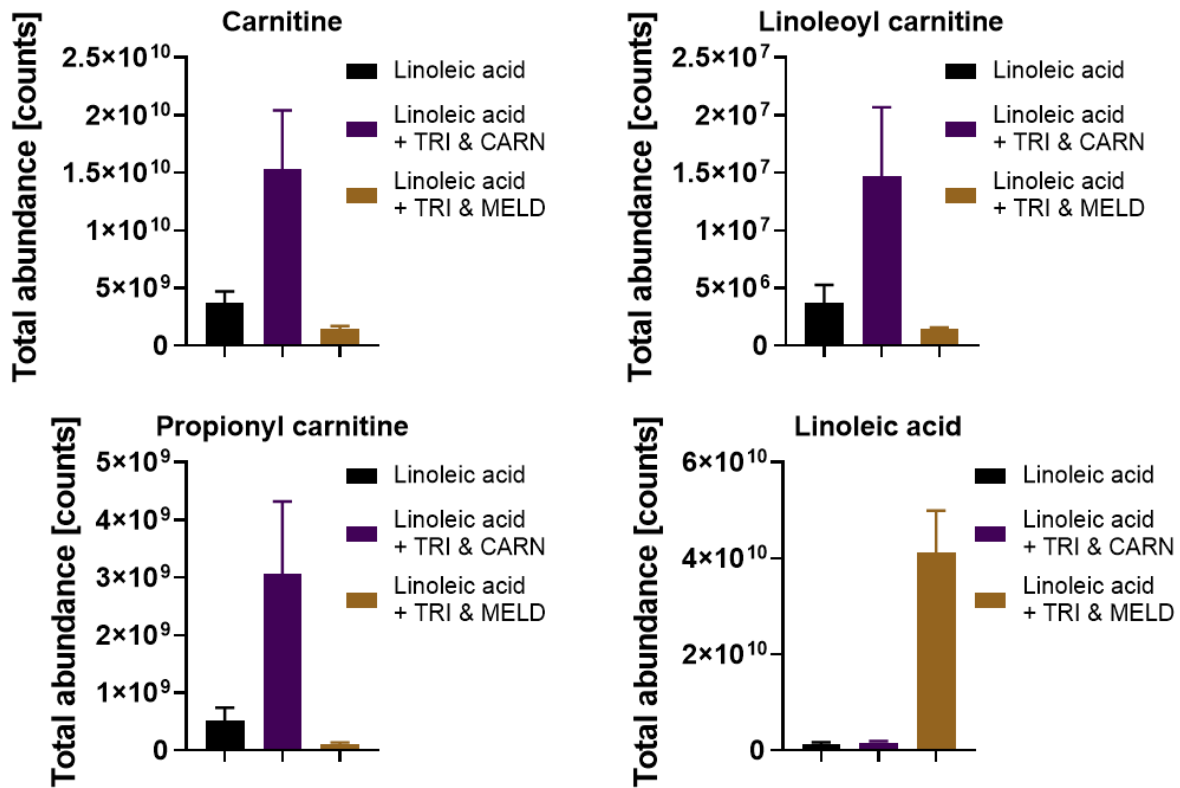
Figure 42: Impact of suppressed host cell β-oxidation and carnitine levels on free linoleic acid level in tachyzoites. Myotubes were pretreated for 24 h either with 40 µM trimetazidine (TRI & CARN) or 40 µM trimetazidine and 25 µM meldonium (TRI & MEL). Respective pretreated and untreated myotubes were infected with Pru-tdTomato tachyzoites (MOI: 1) for 4 h, labeled for 48 h in medium supplemented with 40 µM ^{13}C linoleic acid (Untreated), medium supplemented with 40 µM ^{13}C linoleic acid, 40 µM trimetazidine and 15 µM carnitine (TRI & CARN) or medium supplement with 40 µM ^{13}C linoleic acid, 40 µM trimetazidine and 25 µM meldonium (TRI & MEL), followed by isolation and extraction. Shown are means and SEM of two independent experiments with quadruplicates each Data analysis was mainly performed by Deborah Maus.

Appendix VII: Impact of monophosphorylated pyrimidine-based nucleoside analogues on *Toxoplasma gondii* tachyzoite viability
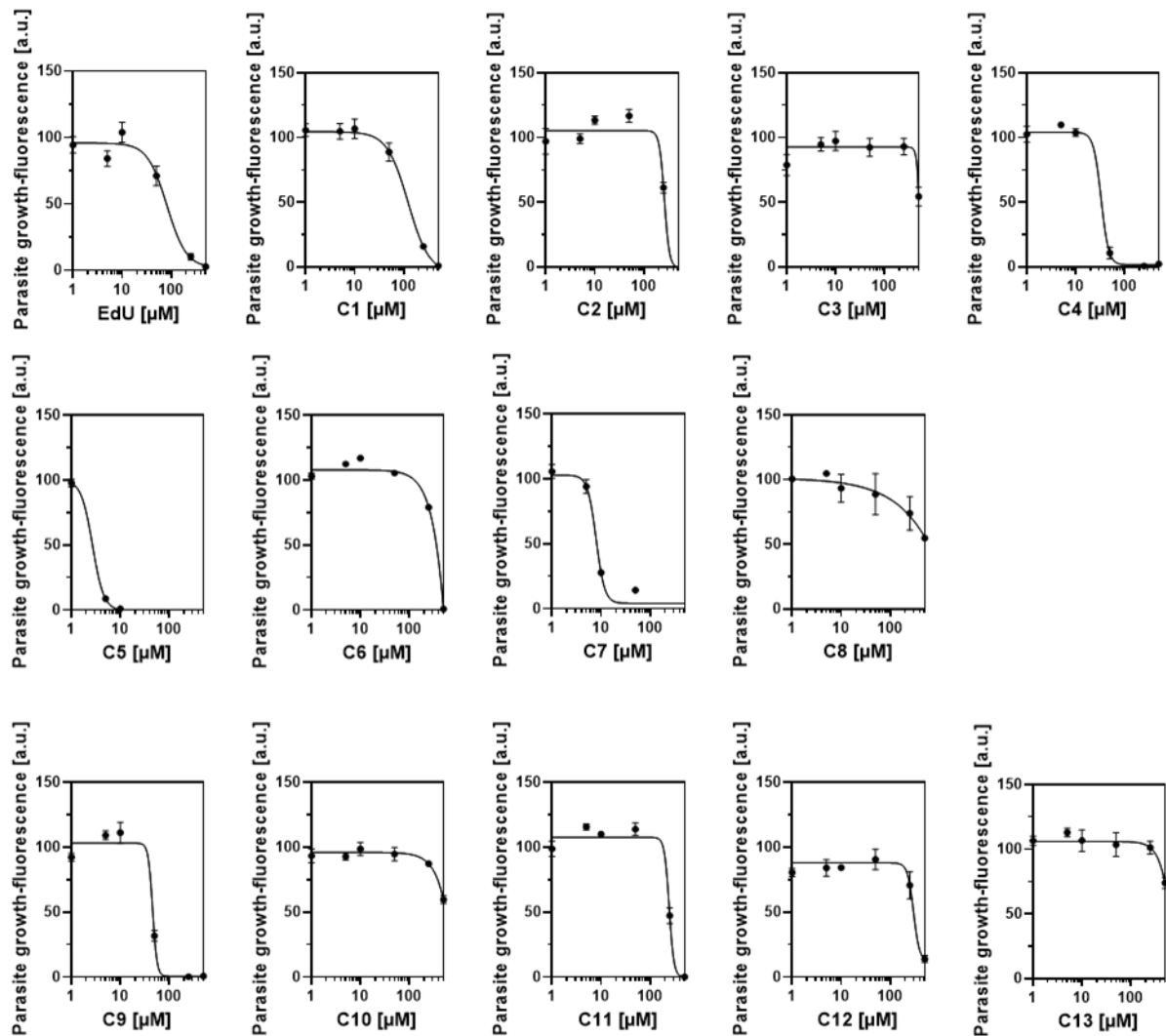
Figure 43: Impact of monophosphorylated pyrimidine-based nucleoside analogues on the viability of tachyzoites. HFFs were infected with Pru-tdTomato tachyzoites (MOI: 1) for 4 h, followed by treatment. Determination of half inhibitory concentrations (IC_{50}) of nucleoside analogues for Pru-tdTomato tachyzoites. Parasites were grown for seven days in presence of indicated concentrations of nucleoside analogues and the IC_{50} value was calculated on day seven from fluorescence intensities normalized to untreated controls. Shown are means and SEM of one experiment with three replicates each. EdU: 5-ethynyl-2-deoxyuridine.

Appendix VIII: Impact of forodesine on the viability of tachyzoites and human fibroblasts
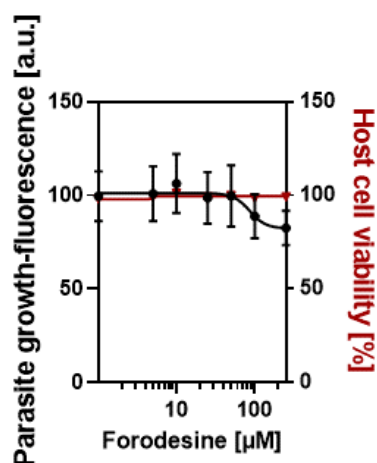
Figure 44: Impact of forodesine on the viability of tachyzoites and human fibroblasts. Calculation of half inhibitory concentrations (IC_{50}) of forodesine for Pru-tdTomato tachyzoites and HFFs. Pru-tdTomato tachyzoites in HFFs (MOI: 1) and uninfected HFFs were grown for seven days in presence of indicated concentrations of forodesine. Growth of parasites was monitored for seven days and the IC_{50} value was calculated on day seven from fluorescence intensities normalized to untreated controls. Host cell viability in % of HFFs was determined after seven day compound exposure via resazurin assay by normalizing untreated to treated controls. Shown are means and SEM of three independent experiments with three replicates each.

Appendix IX: Transcriptomic data of amino acid transporter genes of *Toxoplasma gondii*

Table 20: Transcriptomic data of amino acid transporter genes of *T gondii in vivo* acute and chronic stages. Transcripts per kilobase million were downloaded from ToxoDB (http://www.toxodb.org) and analyzed for stage specific regulation by dividing expression values for acute (10 d.p.i.) by chronic infection in mice (28 d.p.i.). d.p.i.: days post infection; *Tg*: *Toxoplasma gondii*; AT: adenosine transporter; ApiAT: Apicomplexan amino acid transporters. Data from (Pittman et al., 2014).

Name	Gene ID	Acute infection	Chronic infection]	Chronic / acute
*Tg*AT	TGME49_244440	75.64	3.5	0.05
*Tg*AT1 high affinity	TGME49_233130	27.87	76.36	2.74
*Tg*AT2 high affinity	TGME49_288540	30.4	36.33	1.20
*Tg*ApiAT5-3	TGME49_257530	1037.34	283.94	0.27
*Tg*ApiAT6-3	TGME49_249580	24.05	8.7	0.36
*Tg*ApiAT5-1	TGME49_248610	14.27	6.89	0.48
*Tg*ApiAT7-1	TGME49_263230	49.22	25.71	0.52
*Tg*ApiAT1	TGME49_215490	83.03	45.73	0.55
*Tg*ApiAT6-2	TGME49_290860	30.76	16.92	0.55
*Tg*ApiAT3-1	TGME49_318150	13.73	8.06	0.59
*Tg*ApiAT7-2	TGME49_263260	71.19	44.06	0.62
*Tg*ApiAT2	TGME49_320020	38.62	24.4	0.63
*Tg*ApiAT3-2	TGME49_248420	41.93	28.78	0.69
*Tg*ApiAT6-1	TGME49_240810	40.39	28.78	0.71
*Tg*ApiAT5-5	TGME49_293420	0.01	0.01	1.00
*Tg*ApiAT5-6	TGME49_293425	0.01	0.01	1.00
*Tg*ApiAT3-3	TGME49_220600	24.69	26.66	1.08
*Tg*ApiAT5-4	TGME49_216710	4.26	9.05	2.12
*Tg*ApiAT5-2	TGME49_205520	0.01	2.11	211.00

Appendix X:
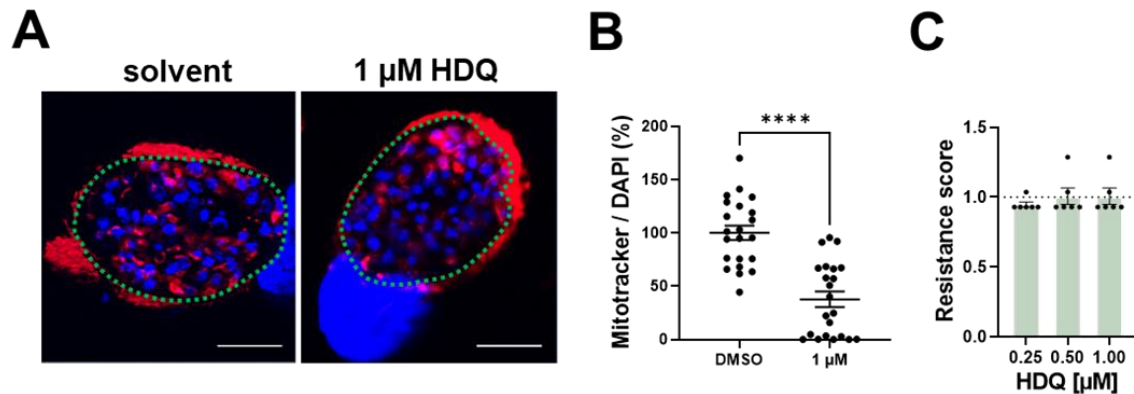
Figure 45: Impact of HDQ treatment on bradyzoite membrane potential and vitality. (A.-B.) Human KD3 myotubes were infected with ME49 tachyzoites (MOI: 0.3) under bradyzoite inducing conditions for 28 days, treated for seven days with either 0.005 % DMSO as solvent control or indicated concentration of 1-hydroxy-2-dodecyl-4(1H)-quinolone (HDQ) and stained with Mitotracker™ Deep Red, *Dolichos biflorus agglutinin* (DBA) and DAPI. Images of 22 cysts per group from two experimental replicates were randomly recorded at identical exposure times. DBA was used to determine the outline of the cysts (green dashed line). For determination of mitochondrial activity, images were converted into monochromatic images and thresholds were set for grey values. We normalized the Mitotracker™ signal (23 to 255) by that of DAPI (19 to 255) per tissue cyst. Values are expressed as means and SEM from two independent experiments. (****p≤0.0001, Mann-Whitney-U-test). Scale bar indicated 10 µm. (C.) Resistance scores of 28-day-old Pru-tdTomato bradyzoites treated with indicated concentrations of HDQ or 0.005 % DMSO as solvent control. Shown are means and SEM of two independent experiments for bradyzoites performed in triplicates.

References

Abdelbaset, A.E., Fox, B.A., Karram, M.H., Abd Ellah, M.R., Bzik, D.J., and Igarashi, M. (2017). Lactate dehydrogenase in *Toxoplasma gondii* controls virulence, bradyzoite differentiation, and chronic infection. PLOS ONE 12, e0173745.

Abrahamsen, M.S., Templeton, T.J., Enomoto, S., Abrahante, J.E., Zhu, G., Lancto, C.A., Deng, M., Liu, C., Widmer, G., Tzipori, S., et al. (2004). Complete genome sequence of the apicomplexan, Cryptosporidium parvum. Science 304, 441-445.

Acquarone, M.F.-d.-S., Marialice; Guimaraes, Eric V.; Brabosa, Helene S. (2017). *Toxoplasma gondii* Tissue Cyst: Cyst Wall Incorporation Activity and Matrix Cytoskeleton Proteins Paving the Way to Nutrient Acquisition. *Toxoplasmosis*, ISBN 978-953-51-3269.

Al-Anouti, F., Tomavo, S., Parmley, S., and Ananvoranich, S. (2004). The expression of lactate dehydrogenase is important for the cell cycle of *Toxoplasma gondii*. The Journal of Biological Chemistry 279, 52300-52311.

Alnaseri, H., Arsic, B., Schneider, J.E., Kaiser, J.C., Scinocca, Z.C., Heinrichs, D.E., and McGavin, M.J. (2015). Inducible Expression of a Resistance-Nodulation-Division-Type Efflux Pump in Staphylococcus aureus Provides Resistance to Linoleic and Arachidonic Acids. Journal of Bacteriology 197, 1893-1905.

Amiar, S., MacRae, J.I., Callahan, D.L., Dubois, D., van Dooren, G.G., Shears, M.J., Cesbron-Delauw, M.F., Maréchal, E., McConville, M.J., McFadden, G.I., et al. (2016). Apicoplast-Localized Lysophosphatidic Acid Precursor Assembly Is Required for Bulk Phospholipid Synthesis in *Toxoplasma gondii* and Relies on an Algal/Plant-Like Glycerol 3-Phosphate Acyltransferase. PLOS Pathogens 12, e1005765.

Anderson-White, B.R., Ivey, F.D., Cheng, K., Szatanek, T., Lorestani, A., Beckers, C.J., Ferguson, D.J., Sahoo, N., and Gubbels, M.J. (2011). A family of intermediate filament-like proteins is sequentially assembled into the cytoskeleton of *Toxoplasma gondii*. Cellular Microbiology 13, 18-31.

Antczak, M., Dzitko, K., and Długońska, H. (2016). Human toxoplasmosis–Searching for novel chemotherapeutics. Biomedicine & Pharmacotherapy 82, 677-684.

Aon, M.A., Bhatt, N., and Cortassa, S.C. (2014). Mitochondrial and cellular mechanisms for managing lipid excess. Frontiers in Physiology 5, 282.

Araujo, F.G., Huskinson, J., Gutteridge, W.E., and Remington, J.S. (1992). *In vitro* and *in vivo* activities of the hydroxynaphthoquinone 566C80 against the cyst form of *Toxoplasma gondii*. Antimicrobial Agents and Chemotherapy 36, 326-330.

Araujo, F.G., Huskinson, J., and Remington, J.S. (1991). Remarkable *in vitro* and *in vivo* activities of the hydroxynaphthoquinone 566C80 against tachyzoites and tissue cysts of *Toxoplasma gondii*. Antimicrobial Agents Chemotherapy 35, 293-299.

Atwal, S., Giengkam, S., VanNieuwenhze, M., and Salje, J. (2016). Live imaging of the genetically intractable obligate intracellular bacteria Orientia tsutsugamushi using a panel of fluorescent dyes. Journal of Microbiological Methods 130, 169-176.

Bajohr, L.L., Ma, L., Platte, C., Liesenfeld, O., Tietze, L.F., Gross, U., and Bohne, W. (2010). *In vitro* and *in vivo* activities of 1-hydroxy-2-alkyl-4(1H)quinolone derivatives against *Toxoplasma gondii*. Antimicrobial Agents and Chemotherapy 54, 517-521.

References

Bakkeren, E., Diard, M., and Hardt, W.D. (2020). Evolutionary causes and consequences of bacterial antibiotic persistence. Nature Reviews Microbiology 18, 479-490.

Balaban, N.Q., Merrin, J., Chait, R., Kowalik, L., and Leibler, S. (2004). Bacterial persistence as a phenotypic switch. Science 305, 1622-1625.

Barragan, A., and Sibley, L.D. (2003). Migration of *Toxoplasma gondii* across biological barriers. Trends in Microbiology 11, 426-430.

Barrett, M.P., Kyle, D.E., Sibley, L.D., Radke, J.B., and Tarleton, R.L. (2019). Protozoan persister-like cells and drug treatment failure. Nature Reviews Microbiology 17, 607-620.

Baumeister, S., Wiesner, J., Reichenberg, A., Hintz, M., Bietz, S., Harb, O.S., Roos, D.S., Kordes, M., Friesen, J., Matuschewski, K., et al. (2011). Fosmidomycin uptake into Plasmodium and Babesia-infected erythrocytes is facilitated by parasite-induced new permeability pathways. PLOS ONE 6, e19334.

Beatty, K.E., Fisk, J.D., Smart, B.P., Lu, Y.Y., Szychowski, J., Hangauer, M.J., Baskin, J.M., Bertozzi, C.R., and Tirrell, D.A. (2010). Live-cell imaging of cellular proteins by a strain-promoted azide-alkyne cycloaddition. Chembiochem 11, 2092-2095.

Bertschi, N.L., Voorberg-van der Wel, A., Zeeman, A.M., Schuierer, S., Nigsch, F., Carbone, W., Knehr, J., Gupta, D.K., Hofman, S.O., van der Werff, N., et al. (2018). Transcriptomic analysis reveals reduced transcriptional activity in the malaria parasite Plasmodium cynomolgi during progression into dormancy. eLife 7, e41081.

Bettadapur, A., Suh, G.C., Geisse, N.A., Wang, E.R., Hua, C., Huber, H.A., Viscio, A.A., Kim, J.Y., Strickland, J.B., and McCain, M.L. (2016). Prolonged Culture of Aligned Skeletal Myotubes on Micromolded Gelatin Hydrogels. Scientific Reports 6, 28855.

Bick, M.D., and Davidson, R.L. (1974). Total Substitution of Bromodeoxyuridine for Thymidine in the DNA of a Bromodeoxyuridine-Dependent Cell Line. Proceedings of the National Academy of Sciences 71, 2082-2086.

Bieber, L.L., Emaus, R., Valkner, K., and Farrell, S. (1982). Possible functions of short-chain and medium-chain carnitine acyltransferases. Federation Proceedings 41, 2858-2862.

Black, M.W., and Boothroyd, J.C. (2000). Lytic cycle of *Toxoplasma gondii*. Microbiology and Molecular Biology Reviews 64, 607-623.

Blank, M.L., Xia, J., Morcos, M.M., Sun, M., Cantrell, P.S., Liu, Y., Zeng, X., Powell, C.J., Yates, N., Boulanger, M.J., et al. (2021). *Toxoplasma gondii* association with host mitochondria requires key mitochondrial protein import machinery. Proceedings of the National Academy of Sciences 118, e2013336118.

Blume, M., and Seeber, F. (2018). Metabolic interactions between *Toxoplasma gondii* and its host. F1000Research 7.

Bohne, W., Heesemann, J., and Gross, U. (1993). Induction of bradyzoite-specific *Toxoplasma gondii* antigens in gamma interferon-treated mouse macrophages. Infection and Immunity 61, 1141-1145.

Bohne, W., Heesemann, J., and Gross, U. (1994). Reduced replication of *Toxoplasma gondii* is necessary for induction of bradyzoite-specific antigens: a possible role for nitric oxide in triggering stage conversion. Infection and Immunity 62, 1761-1767.

References

Bohne, W., and Roos, D.S. (1997). Stage-specific expression of a selectable marker in *Toxoplasma gondii* permits selective inhibition of either tachyzoites or bradyzoites. Molecular and Biochemical Parasitology 88, 115-126.

Boothroyd, J.C., Black, M., Bonnefoy, S., Hehl, A., Knoll, L.J., Manger, I.D., Ortega-Barria, E., and Tomavo, S. (1997). Genetic and biochemical analysis of development in *Toxoplasma gondii*. Philosophical transactions of the Royal Society of London. Series B, Biological sciences 352, 1347-1354.

Bottova, I., Hehl, A.B., Stefanić, S., Fabriàs, G., Casas, J., Schraner, E., Pieters, J., and Sonda, S. (2009). Host cell P-glycoprotein is essential for cholesterol uptake and replication of *Toxoplasma gondii*. The Journal of Biological Chemistry 284, 17438-17448.

Bougdour, A., Maubon, D., Baldacci, P., Ortet, P., Bastien, O., Bouillon, A., Barale, J.C., Pelloux, H., Ménard, R., and Hakimi, M.A. (2009). Drug inhibition of HDAC3 and epigenetic control of differentiation in Apicomplexa parasites. The Journal of Experimental Medicine 206, 953-966.

Brass, E.P., and Hoppel, C.L. (1980). Relationship between acid-soluble carnitine and coenzyme A pools *in vivo*. The Biochemical Journal 190, 495-504.

Bremer, J. (1983). Carnitine-metabolism and functions. Physiological Reviews 63, 1420-1480.

Bronner-Fraser, M. (1985). Alterations in neural crest migration by a monoclonal antibody that affects cell adhesion. The Journal of Cell Biology 101, 610-617.

Brown, K.M., and Sibley, L.D. (2018). Essential cGMP Signaling in *Toxoplasma* Is Initiated by a Hybrid P-Type ATPase-Guanylate Cyclase. Cell Host & Microbe 24, 804-816.

Brunet, J., Pfaff, A.W., Abidi, A., Unoki, M., Nakamura, Y., Guinard, M., Klein, J.P., Candolfi, E., and Mousli, M. (2008). *Toxoplasma gondii* exploits UHRF1 and induces host cell cycle arrest at G2 to enable its proliferation. Cellular Microbiology 10, 908-920.

Buchholz, K.R., Fritz, H.M., Chen, X., Durbin-Johnson, B., Rocke, D.M., Ferguson, D.J., Conrad, P.A., and Boothroyd, J.C. (2011). Identification of tissue cyst wall components by transcriptome analysis of *in vivo* and *in vitro Toxoplasma gondii* bradyzoites. Eukaryotic Cell 10, 1637-1647.

Bülow, R., and Boothroyd, J.C. (1991). Protection of mice from fatal *Toxoplasma gondii* infection by immunization with p30 antigen in liposomes. Journal of Immunology 147, 3496-3500.

Cabral, C.M., Tuladhar, S., Dietrich, H.K., Nguyen, E., MacDonald, W.R., Trivedi, T., Deviveni, A., and Koshy, A.A. (2016). Neurons are the Primary Target Cell for the Brain-Tropic Intracellular Parasite *Toxoplasma gondii*. PLOS Pathogens 12, e1005447.

Calder, P.C. (2018). Metabolism of Polyunsaturated Fatty Acids by Cells of the Immune System. Polyunsaturated Fatty Acid Metabolism, ISBN978-0-12-811230-4, 135-155.

Cava, F., Lam, H., de Pedro, M.A., and Waldor, M.K. (2011). Emerging knowledge of regulatory roles of D-amino acids in bacteria. Cellular and Molecular Life Sciences 68, 817-831.

Cerutti, A., Blanchard, N., and Besteiro, S. (2020). The Bradyzoite: A Key Developmental Stage for the Persistence and Pathogenesis of Toxoplasmosis. Pathogens 9, 234.

References

Chalmers, R.A., Roe, C.R., Stacey, T.E., and Hoppel, C.L. (1984). Urinary excretion of l-carnitine and acylcarnitines by patients with disorders of organic acid metabolism: evidence for secondary insufficiency of l-carnitine. Pediatric Research 18, 1325-1328.

Chanda, W., Joseph, T.P., Guo, X.F., Wang, W.D., Liu, M., Vuai, M.S., Padhiar, A.A., and Zhong, M.T. (2018). Effectiveness of omega-3 polyunsaturated fatty acids against microbial pathogens. Journal of Zhejiang University Science B 19, 253-262.

Charron, A.J., and Sibley, L.D. (2002). Host cells: mobilizable lipid resources for the intracellular parasite *Toxoplasma gondii*. Journal of Cell Science 115, 3049-3059.

Chaudhary, K., Darling, J.A., Fohl, L.M., Sullivan, W.J., Jr., Donald, R.G., Pfefferkorn, E.R., Ullman, B., and Roos, D.S. (2004). Purine salvage pathways in the apicomplexan parasite *Toxoplasma gondii*. The Journal of Biological Chemistry 279, 31221-31227.

Chaudhary, K., Ting, L.M., Kim, K., and Roos, D.S. (2006). *Toxoplasma gondii* purine nucleoside phosphorylase biochemical characterization, inhibitor profiles, and comparison with the Plasmodium falciparum ortholog. The Journal of Biological Chemistry 281, 25652-25658.

Chiang, C.W., Carter, N., Sullivan, W.J., Jr., Donald, R.G., Roos, D.S., Naguib, F.N., el Kouni, M.H., Ullman, B., and Wilson, C.M. (1999). The adenosine transporter of *Toxoplasma gondii*. Identification by insertional mutagenesis, cloning, and recombinant expression. The Journal of Biological Chemistry 274, 35255-35261.

Chtanova, T., Schaeffer, M., Han, S.J., van Dooren, G.G., Nollmann, M., Herzmark, P., Chan, S.W., Satija, H., Camfield, K., Aaron, H., et al. (2008). Dynamics of neutrophil migration in lymph nodes during infection. Immunity 29, 487-496.

Cleary, M.D., Singh, U., Blader, I.J., Brewer, J.L., and Boothroyd, J.C. (2002). *Toxoplasma gondii* asexual development: identification of developmentally regulated genes and distinct patterns of gene expression. Eukaryotic Cell 1, 329-340.

Coppens, I. (2014). Exploitation of auxotrophies and metabolic defects in *Toxoplasma* as therapeutic approaches. International Journal for Parasitology 44, 109-120.

Coppens, I., Dunn, J.D., Romano, J.D., Pypaert, M., Zhang, H., Boothroyd, J.C., and Joiner, K.A. (2006). *Toxoplasma gondii* sequesters lysosomes from mammalian hosts in the vacuolar space. Cell 125, 261-274.

Crawford, M.J., Thomsen-Zieger, N., Ray, M., Schachtner, J., Roos, D.S., and Seeber, F. (2006). *Toxoplasma gondii* scavenges host-derived lipoic acid despite its *de novo* synthesis in the apicoplast. The EMBO Journal 25, 3214-3222.

Creuzet, C., Robert, F., Roisin, M.P., Van Tan, H., Benes, C., Dupouy-Camet, J., and Fagard, R. (1997). Neurons in primary culture are less efficiently infected by *Toxoplasma gondii* than glial cells. Parasitology Research 84, 25-30.

Dagley, M.J., and McConville, M.J. (2018). DExSI: a new tool for the rapid quantitation of 13C-labelled metabolites detected by GC-MS. Bioinformatics 34, 1957-1958.

Dardé, M.L., Bouteille, B., and Pestre-Alexandre, M. (1992). Isoenzyme analysis of 35 *Toxoplasma gondii* isolates and the biological and epidemiological implications. The Journal of Parasitology 78, 786-794.

References

Das, U.N. (2018). Arachidonic acid and other unsaturated fatty acids and some of their metabolites function as endogenous antimicrobial molecules: A review. Journal of Advanced Research 11, 57-66.

De Koning, H.P., Al-Salabi, M.I., Cohen, A.M., Coombs, G.H., and Wastling, J.M. (2003). Identification and characterisation of high affinity nucleoside and nucleobase transporters in *Toxoplasma gondii*. International Journal for Parasitology 33, 821-831.

de Lima, L.P., Seabra, S.H., Carneiro, H., and Barbosa, H.S. (2015). Effect of 3-bromopyruvate and atovaquone on infection during *in vitro* interaction of *Toxoplasma gondii* and LLC-MK2 cells. Antimicrobial Agents and Chemotherapy 59, 5239-5249.

Deneris, E.S., and Hobert, O. (2014). Maintenance of postmitotic neuronal cell identity. Nature Neuroscience 17, 899-907.

Denton, H., Roberts, C.W., Alexander, J., Thong, K.W., and Coombs, G.H. (1996). Enzymes of energy metabolism in the bradyzoites and tachyzoites of *Toxoplasma gondii*. FEMS Microbiology Letters 137, 103-108.

Desmonts, G., Couvreur, J., Alison, F., Baudelot, J., Gerbeaux, J., and Lelong, M. (1965). Epidemiological study on toxoplasmosis: the influence of cooking slaughter-animal meat on the incidence of human infection. Revue Francaise d'Etudes Cliniques et Biologiques 10, 952-958.

Di Cristina, M., Dou, Z., Lunghi, M., Kannan, G., Huynh, M.H., McGovern, O.L., Schultz, T.L., Schultz, A.J., Miller, A.J., Hayes, B.M., et al. (2017). *Toxoplasma* depends on lysosomal consumption of autophagosomes for persistent infection. Nature Microbiology 2, 17096.

Diermeier-Daucher, S., Clarke, S.T., Hill, D., Vollmann-Zwerenz, A., Bradford, J.A., and Brockhoff, G. (2009). Cell type specific applicability of 5-ethynyl-2'-deoxyuridine (EdU) for dynamic proliferation assessment in flow cytometry. Cytometry Part A 75, 535-546.

Doggett, J.S., Nilsen, A., Forquer, I., Wegmann, K.W., Jones-Brando, L., Yolken, R.H., Bordón, C., Charman, S.A., Katneni, K., Schultz, T., et al. (2012). Endochin-like quinolones are highly efficacious against acute and latent experimental toxoplasmosis. Proceedings of the National Academy of Sciences 109, 15936-15941.

Dou, Z., McGovern, O.L., Di Cristina, M., and Carruthers, V.B. (2014). *Toxoplasma gondii* ingests and digests host cytosolic proteins. mBio 5, e01188-01114.

Dubey, J.P. (1980). Mouse pathogenicity of *Toxoplasma gondii* isolated from a goat. American Journal of Veterinary Research 41, 427-429.

Dubey, J.P. (1997). Survival of *Toxoplasma gondii* tissue cysts in 0.85-6% NaCl solutions at 4-20 °C. The Journal of Parasitology 83, 946-949.

Dubey, J.P. (1998). Re-examination of resistance of *Toxoplasma gondii* tachyzoites and bradyzoites to pepsin and trypsin digestion. Parasitology 116, 43-50.

Dubey, J.P., Kotula, A.W., Sharar, A., Andrews, C.D., and Lindsay, D.S. (1990). Effect of high temperature on infectivity of *Toxoplasma gondii* tissue cysts in pork. The Journal of Parasitol 76, 201-204.

Dubey, J.P., Lindsay, D.S., and Speer, C.A. (1998). Structures of *Toxoplasma gondii* tachyzoites, bradyzoites, and sporozoites and biology and development of tissue cysts. Clinical Microbiology Reviews 11, 267-299.

References

Dunay, I.R., Gajurel, K., Dhakal, R., Liesenfeld, O., and Montoya, J.G. (2018). Treatment of Toxoplasmosis: Historical Perspective, Animal Models, and Current Clinical Practice. Clinical Microbioly Reviews 31, e00057-17.

Dzierszinski, F., Nishi, M., Ouko, L., and Roos, D.S. (2004). Dynamics of *Toxoplasma gondii* differentiation. Eukaryotic Cell 3, 992-1003.

Dzierszinski, F., Popescu, O., Toursel, C., Slomianny, C., Yahiaoui, B., and Tomavo, S. (1999). The protozoan parasite *Toxoplasma gondii* expresses two functional plant-like glycolytic enzymes. Implications for evolutionary origin of apicomplexans. The Journal of Biological Chemistry 274, 24888-24895.

Eaton, M.S., Weiss, L.M., and Kim, K. (2006). Cyclic nucleotide kinases and tachyzoite-bradyzoite transition in *Toxoplasma gondii*. International Journal for Parasitology 36, 107-114.

Echeverria, P.C., Matrajt, M., Harb, O.S., Zappia, M.P., Costas, M.A., Roos, D.S., Dubremetz, J.F., and Angel, S.O. (2005). *Toxoplasma gondii* Hsp90 is a potential drug target whose expression and subcellular localization are developmentally regulated. Journal of Molecular Biology 350, 723-734.

Elowitz, M.B., Levine, A.J., Siggia, E.D., and Swain, P.S. (2002). Stochastic gene expression in a single cell. Science 297, 1183-1186.

Ewald, B., Sampath, D., and Plunkett, W. (2008). Nucleoside analogs: molecular mechanisms signaling cell death. Oncogene 27, 6522-6537.

Ferguson, D.J. (2004). Use of molecular and ultrastructural markers to evaluate stage conversion of *Toxoplasma gondii* in both the intermediate and definitive host. International Journal of Parasitoly 34, 347-360.

Ferguson, D.J., Graham, D.I., and Hutchison, W.M. (1991). Pathological changes in the brains of mice infected with *Toxoplasma gondii*: a histological, immunocytochemical and ultrastructural study. International Journal of Experimental Pathology 72, 463-474.

Ferguson, D.J., Huskinson-Mark, J., Araujo, F.G., and Remington, J.S. (1994a). A morphological study of chronic cerebral toxoplasmosis in mice: comparison of four different strains of *Toxoplasma gondii*. Parasitology Research 80, 493-501.

Ferguson, D.J., Huskinson-Mark, J., Araujo, F.G., and Remington, J.S. (1994b). An ultrastructural study of the effect of treatment with atovaquone in brains of mice chronically infected with the ME49 strain of *Toxoplasma gondii*. International Journal of Experimental Pathology 75, 111-116.

Ferguson, D.J., and Hutchison, W.M. (1987a). The host-parasite relationship of *Toxoplasma gondii* in the brains of chronically infected mice. Virchows Archiv. A, Pathological Anatomy and Histopathology 411, 39-43.

Ferguson, D.J., and Hutchison, W.M. (1987b). An ultrastructural study of the early development and tissue cyst formation of *Toxoplasma gondii* in the brains of mice. Parasitology Research 73, 483-491.

Ferguson, D.J.and Dubremetz, J.F. (2014). The Ultrastructure of *Toxoplasma gondii*. *Toxoplasma gondii*, ISBN 978-0-12-396481-6, 19-59.

References

Fernando, M.R., Reyes, J.L., Iannuzzi, J., Leung, G., and McKay, D.M. (2014). The pro-inflammatory cytokine, interleukin-6, enhances the polarization of alternatively activated macrophages. PLOS ONE 9, e94188.

Ferreira-da-Silva Mda, F., Rodrigues, R.M., Andrade, E.F., Carvalho, L., Gross, U., Lüder, C.G., and Barbosa, H.S. (2009a). Spontaneous stage differentiation of mouse-virulent *Toxoplasma gondii* RH parasites in skeletal muscle cells: an ultrastructural evaluation. Memorias do Instituto Oswaldo Cruz 104, 196-200.

Ferreira-da-Silva Mda, F., Takács, A.C., Barbosa, H.S., Gross, U., and Lüder, C.G. (2009b). Primary skeletal muscle cells trigger spontaneous *Toxoplasma gondii* tachyzoite-to-bradyzoite conversion at higher rates than fibroblasts. International Journal of Medical Microbiology 299, 381-388.

Ferreira da Silva Mda, F., Barbosa, H.S., Gross, U., and Lüder, C.G. (2008). Stress-related and spontaneous stage differentiation of *Toxoplasma gondii*. Molecular Biosystems 4, 824-834.

Fleige, T., Pfaff, N., Gross, U., and Bohne, W. (2008). Localisation of gluconeogenesis and tricarboxylic acid (TCA)-cycle enzymes and first functional analysis of the TCA cycle in *Toxoplasma gondii*. International Journal for Parasitology 38, 1121-1132.

Fouts, A.E., and Boothroyd, J.C. (2007). Infection with *Toxoplasma gondii* bradyzoites has a diminished impact on host transcript levels relative to tachyzoite infection. Infection and Immunity 75, 634-642.

Fox, B.A., Belperron, A.A., and Bzik, D.J. (2001). Negative selection of herpes simplex virus thymidine kinase in *Toxoplasma gondii*. Molecular and Biochemical Parasitology 116, 85-88.

Fox, B.A., and Bzik, D.J. (2002). *De novo* pyrimidine biosynthesis is required for virulence of *Toxoplasma gondii*. Nature 415, 926-929.

Fox, B.A., Gigley, J.P., and Bzik, D.J. (2004). *Toxoplasma gondii* lacks the enzymes required for *de novo* arginine biosynthesis and arginine starvation triggers cyst formation. International Journal for Parasitology 34, 323-331.

Frade, J.M., and Ovejero-Benito, M.C. (2015). Neuronal cell cycle: the neuron itself and its circumstances. Cell Cycle 14, 712-720.

Frenkel, J.K., Dubey, J.P., and Hoff, R.L. (1976). Loss of stages after continuous passage of *Toxoplasma gondii* and Besnoitia jellisoni. The Journal of Protozoology 23, 421-424.

Furth, J.J., and Cohen, S.S. (1967). Inhibition of mammalian DNA polymerase by the 5'-triphosphate of 9-beta-D-arabinofuranosyladenine. Cancer Research 27, 1528-1533.

Fux, B., Nawas, J., Khan, A., Gill, D., Su, C., and Sibley, L.D. (2007). *Toxoplasma gondii* Strains Defective in Oral Transmission Are Also Defective in Developmental Stage Differentiation. Infection and Immunity 75, 2580-2590.

Gajria, B., Bahl, A., Brestelli, J., Dommer, J., Fischer, S., Gao, X., Heiges, M., Iodice, J., Kissinger, J.C., Mackey, A.J., et al. (2008). ToxoDB: an integrated *Toxoplasma gondii* database resource. Nucleic Acids Research 36, 553-556.

Galazka, J., Striepen, B., and Ullman, B. (2006). Adenosine kinase from Cryptosporidium parvum. Molecular and Biochemical Parasitology 149, 223-230.

References

Galizi, R., Spano, F., Giubilei, M.A., Capuccini, B., Magini, A., Urbanelli, L., Ogawa, T., Dubey, J.P., Spaccapelo, R., Emiliani, C., et al. (2013). Evidence of tRNA cleavage in apicomplexan parasites: Half-tRNAs as new potential regulatory molecules of *Toxoplasma gondii* and Plasmodium berghei. Molecular and Biochemical Parasitology 188, 99-108.

Gehrmann, W., Würdemann, W., Plötz, T., Jörns, A., Lenzen, S., and Elsner, M. (2015). Antagonism Between Saturated and Unsaturated Fatty Acids in ROS Mediated Lipotoxicity in Rat Insulin-Producing Cells. Cellular Physiology and Biochemistry 36, 852-865.

Gollan, B., Grabe, G., Michaux, C., and Helaine, S. (2019). Bacterial Persisters and Infection: Past, Present, and Progressing. Annual Review of Microbiology 73, 359-385.

Gomes, A.F., Magalhães, K.G., Rodrigues, R.M., de Carvalho, L., Molinaro, R., Bozza, P.T., and Barbosa, H.S. (2014). *Toxoplasma gondii*- skeletal muscle cells interaction increases lipid droplet biogenesis and positively modulates the production of IL-12, IFN-g and PGE2. Parasites & Vectors 7, 47.

Gooding, J.M., Shayeghi, M., and Saggerson, E.D. (2004). Membrane transport of fatty acylcarnitine and free L-carnitine by rat liver microsomes. European Journal of Biochemistry 271, 954-961.

Gormley, P.D., Pavesio, C.E., Minnasian, D., and Lightman, S. (1998). Effects of drug therapy on *Toxoplasma* cysts in an animal model of acute and chronic disease. Investigative Ophthalmology & Visual Science 39, 1171-1175.

Gratzner, H. (1982). Monoclonal antibody to 5-bromo- and 5-iododeoxyuridine: A new reagent for detection of DNA replication. Science 218, 474-475.

Grimbergen, A.J., Siebring, J., Solopova, A., and Kuipers, O.P. (2015). Microbial bet-hedging: the power of being different. Current Opinion in Microbiology 25, 67-72.

Gross, D.N., Wan, M., and Birnbaum, M.J. (2009). The role of FOXO in the regulation of metabolism. Current Diabetes Reports 9, 208-214.

Gross, U., Bormuth, H., Gaissmaier, C., Dittrich, C., Krenn, V., Bohne, W., and Ferguson, D.J. (1995). Monoclonal rat antibodies directed against *Toxoplasma gondii* suitable for studying tachyzoite-bradyzoite interconversion *in vivo*. Clinical and Diagnostic Laboratory Immunoly 2, 542-548.

Gross, U., Müller, W.A., Knapp, S., and Heesemann, J. (1991). Identification of a virulence-associated antigen of *Toxoplasma gondii* by use of a mouse monoclonal antibody. Infection and Immunity 59, 4511-4516.

Guizetti, J., and Scherf, A. (2013). Silence, activate, poise and switch! Mechanisms of antigenic variation in Plasmodium falciparum. Cellular Microbiology 15, 718-726.

Halonen, S.K., Taylor, G.A., and Weiss, L.M. (2001). Gamma interferon-induced inhibition of *Toxoplasma gondii* in astrocytes is mediated by IGTP. Infection and Immunity 69, 5573-5576.

Harwood, J.L. (1996). Recent advances in the biosynthesis of plant fatty acids. Biochimica et Biophysica Acta 1301, 7-56.

Hatanaka, E., Dermargos, A., Hirata, A.E., Vinolo, M.A., Carpinelli, A.R., Newsholme, P., Armelin, H.A., and Curi, R. (2013). Oleic, linoleic and linolenic acids increase ros production by fibroblasts via NADPH oxidase activation. PLOS ONE 8, e58626.

References

Hegewald, J., Gross, U., and Bohne, W. (2013). Identification of dihydroorotate dehydrogenase as a relevant drug target for 1-hydroxyquinolones in *Toxoplasma gondii*. Molecular and Biochemical Parasitology 190, 6-15.

Hehl, A.B., Basso, W.U., Lippuner, C., Ramakrishnan, C., Okoniewski, M., Walker, R.A., Grigg, M.E., Smith, N.C., and Deplazes, P. (2015). Asexual expansion of *Toxoplasma gondii* merozoites is distinct from tachyzoites and entails expression of non-overlapping gene families to attach, invade, and replicate within feline enterocytes. BioMed Central Genomics 16, 66.

Ho, J.K., Duclos, R.I., Jr., and Hamilton, J.A. (2002). Interactions of acylcarnitines with model membranes: a (13)C-NMR study. Journal of Lipid Research 43, 1429-1439.

Hortua Triana, M.A., Huynh, M.H., Garavito, M.F., Fox, B.A., Bzik, D.J., Carruthers, V.B., Löffler, M., and Zimmermann, B.H. (2012). Biochemical and molecular characterization of the pyrimidine biosynthetic enzyme dihydroorotate dehydrogenase from *Toxoplasma gondii*. Molecular and Biochemical Parasitology 184, 71-81.

Howe, D.K., and Sibley, L.D. (1995). *Toxoplasma gondii* comprises three clonal lineages: correlation of parasite genotype with human disease. The Journal of Infectious Diseases 172, 1561-1566.

Hu, X., Binns, D., and Reese, M.L. (2017). The coccidian parasites *Toxoplasma* and Neospora dysregulate mammalian lipid droplet biogenesis. The Journal of Biological Chemistry 292, 11009-11020.

Hutson, S. (2001). Structure and function of branched chain aminotransferases. Progress in Nucleic Acid Research and Molecular Biology 70, 175-206.

Huynh, M.H., and Carruthers, V.B. (2009). Tagging of endogenous genes in a *Toxoplasma gondii* strain lacking Ku80. Eukaryotic Cell 8, 530-539.

Huynh, N., Dickson, C., Zencak, D., Hilko, D.H., Mackay-Sim, A., and Poulsen, S.-A. (2015). Labeling of Cellular DNA with a Cyclosal Phosphotriester Pronucleotide Analog of 5-ethynyl-2′-deoxyuridine. Chemical Biology & Drug Design 86, 400-409.

Ihara, F., and Nishikawa, Y. (2014). Starvation of low-density lipoprotein-derived cholesterol induces bradyzoite conversion in *Toxoplasma gondii*. Parasites & Vectors 7, 248.

Jacobs, L., Remington, J.S., and Melton, M.L. (1960). The resistance of the encysted form of *Toxoplasma gondii*. The Journal of Parasitology 46, 11-21.

Jara, M., Maes, I., Imamura, H., Domagalska, M.A., Dujardin, J.C., and Arevalo, J. (2019). Tracking of quiescence in *Leishmania* by quantifying the expression of GFP in the ribosomal DNA locus. Scientific Reports 9, 18951.

Jeffers, V., Tampaki, Z., Kim, K., and Sullivan, W.J., Jr. (2018). A latent ability to persist: differentiation in *Toxoplasma gondii*. Cellular and Molecular Life Sciences 75, 2355-2373.

Jerome, M.E., Radke, J.R., Bohne, W., Roos, D.S., and White, M.W. (1998). *Toxoplasma gondii* bradyzoites form spontaneously during sporozoite-initiated development. Infection and Immunity 66, 4838-4844.

Jewett, J.C., and Bertozzi, C.R. (2010). Cu-free click cycloaddition reactions in chemical biology. Chemical Society Reviews 39, 1272-1279.

References

Kantor, P.F., Lucien, A., Kozak, R., and Lopaschuk, G.D. (2000). The antianginal drug trimetazidine shifts cardiac energy metabolism from fatty acid oxidation to glucose oxidation by inhibiting mitochondrial long-chain 3-ketoacyl coenzyme A thiolase. Circulation Research 86, 580-588.

Kelly, F.D., Wei, B.M., Cygan, A.M., Parker, M.L., Boulanger, M.J., and Boothroyd, J.C. (2017). MAF1b Binds the Host Cell MIB Complex To Mediate Mitochondrial Association. mSphere 2, e00183-00117.

Khan, A., Behnke, M.S., Dunay, I.R., White, M.W., and Sibley, L.D. (2009). Phenotypic and gene expression changes among clonal type I strains of *Toxoplasma gondii*. Eukaryotic Cell 8, 1828-1836.

King, E.F.B., Cobbold, S.A., Uboldi, A.D., Tonkin, C.J., and McConville, M.J. (2020). Metabolomic Analysis of *Toxoplasma gondii* Tachyzoites. *Toxoplasma gondii*: Methods and Protocols, ISBN 978-1-4939-9856-2, 435-452.

Kirkman, L.A., Weiss, L.M., and Kim, K. (2001). Cyclic nucleotide signaling in *Toxoplasma gondii* bradyzoite differentiation. Infection and Immunity 69, 148-153.

Kloehn, J., Harding, C.R., and Soldati-Favre, D. (2021). Supply and demand-heme synthesis, salvage and utilization by Apicomplexa. The FEBS Journal 288, 382-404.

Köhler, S., Delwiche, C.F., Denny, P.W., Tilney, L.G., Webster, P., Wilson, R.J., Palmer, J.D., and Roos, D.S. (1997). A plastid of probable green algal origin in Apicomplexan parasites. Science 275, 1485-1489.

Krishnan, A., Kloehn, J., Lunghi, M., Chiappino-Pepe, A., Waldman, B.S., Nicolas, D., Varesio, E., Hehl, A., Lourido, S., Hatzimanikatis, V., et al. (2020). Functional and Computational Genomics Reveal Unprecedented Flexibility in Stage-Specific *Toxoplasma* Metabolism. Cell Host & Microbe 27, 290-306.

Krishnan, A., and Soldati-Favre, D. (2021). Amino Acid Metabolism in Apicomplexan Parasites. Metabolites 11, 253-267.

Krug, E.C., Marr, J.J., and Berens, R.L. (1989). Purine metabolism in *Toxoplasma gondii*. The Journal of Biological Chemistry 264, 10601-10607.

Kumar, A., Kumar, Y., Sevak, J.K., Kumar, S., Kumar, N., and Gopinath, S.D. (2020). Metabolomic analysis of primary human skeletal muscle cells during myogenic progression. Scientific Reports 10, 11824.

Laliberté, J., and Carruthers, V.B. (2008). Host cell manipulation by the human pathogen *Toxoplasma gondii*. Cellular and molecular life sciences 65, 1900-1915.

Lee, K., Choi, Y., Gumina, G., Zhou, W., Schinazi, R.F., and Chu, C.K. (2002). Structure-activity relationships of 2'-fluoro-2',3'-unsaturated D-nucleosides as anti-HIV-1 agents. Journal of Medical Chemistry 45, 1313-1320.

Lei, Y., Davey, M., and Ellis, J. (2005). Autofluorescence of *Toxoplasma gondii* and *Neospora caninum* cysts *in vitro*. The Journal of Parasitology 91, 17-23.

Lemgruber, L., Lupetti, P., Martins-Duarte, E.S., De Souza, W., and Vommaro, R.C. (2011). The organization of the wall filaments and characterization of the matrix structures of *Toxoplasma gondii* cyst form. Cellular Microbiology 13, 1920-1932.

References

Lescault, P.J., Thompson, A.B., Patil, V., Lirussi, D., Burton, A., Margarit, J., Bond, J., and Matrajt, M. (2010). Genomic data reveal *Toxoplasma gondii* differentiation mutants are also impaired with respect to switching into a novel extracellular tachyzoite state. PLOS ONE 5, e14463.

Liboska, R., Ligasová, A., Strunin, D., Rosenberg, I., and Koberna, K. (2012). Most anti-BrdU antibodies react with 2'-deoxy-5-ethynyluridine -- the method for the effective suppression of this cross-reactivity. PLOS ONE 7, e51679.

Ligasová, A., Strunin, D., Friedecký, D., Adam, T., and Koberna, K. (2015). A fatal combination: a thymidylate synthase inhibitor with DNA damaging activity. PLOS ONE 10, e0117459.

Lige, B., Sampels, V., and Coppens, I. (2013). Characterization of a second sterol-esterifying enzyme in *Toxoplasma* highlights the importance of cholesterol storage pathways for the parasite. Molecular Microbiology 87, 951-967.

Lin, S.S., Blume, M., von Ahsen, N., Gross, U., and Bohne, W. (2011). Extracellular *Toxoplasma gondii* tachyzoites do not require carbon source uptake for ATP maintenance, gliding motility and invasion in the first hour of their extracellular life. International Journal for Parasitology 41, 835-841.

Lin, S.S., Gross, U., and Bohne, W. (2009). Type II NADH dehydrogenase inhibitor 1-hydroxy-2-dodecyl-4(1H)quinolone leads to collapse of mitochondrial inner-membrane potential and ATP depletion in *Toxoplasma gondii*. Eukaryotic Cell 8, 877-887.

Lin, Y., Li, W., Sun, L., Lin, Z., Jiang, Y., Ling, Y., and Lin, X. (2019). Comparative metabolomics shows the metabolic profiles fluctuate in multi-drug resistant Escherichia coli strains. Journal of Proteomics 207, 103468.

Liu, Y., Zhang, Y., Dong, P., An, R., Xue, C., Ge, Y., Wei, L., and Liang, X. (2015). Digestion of Nucleic Acids Starts in the Stomach. Scientific Reports 5, 11936.

Longo, N., Frigeni, M., and Pasquali, M. (2016). Carnitine transport and fatty acid oxidation. Biochimica et Biophysica Acta 1863, 2422-2435.

Lopatkin, A.J., Stokes, J.M., Zheng, E.J., Yang, J.H., Takahashi, M.K., You, L., and Collins, J.J. (2019). Bacterial metabolic state more accurately predicts antibiotic lethality than growth rate. Nature Microbiology 4, 2109-2117.

Lorestani, A., Ivey, F.D., Thirugnanam, S., Busby, M.A., Marth, G.T., Cheeseman, I.M., and Gubbels, M.J. (2012). Targeted proteomic dissection of *Toxoplasma* cytoskeleton sub-compartments using MORN1. Cytoskeleton 69, 1069-1085.

Lourido, S., Tang, K., and Sibley, L.D. (2012). Distinct signalling pathways control *Toxoplasma* egress and host-cell invasion. The EMBO Journal 31, 4524-4534.

Lüder, C.G., Giraldo-Velásquez, M., Sendtner, M., and Gross, U. (1999). *Toxoplasma gondii* in primary rat CNS cells: differential contribution of neurons, astrocytes, and microglial cells for the intracerebral development and stage differentiation. Experimental Parasitology 93, 23-32.

Lüder, C.G.K., and Rahman, T. (2017). Impact of the host on *Toxoplasma* stage differentiation. Microbial Cell 4, 203-211.

Luft, B.J., Naot, Y., Araujo, F.G., Stinson, E.B., and Remington, J.S. (1983). Primary and reactivated *Toxoplasma* infection in patients with cardiac transplants. Clinical spectrum and problems in diagnosis in a defined population. Annals of Internal Medicine 99, 27-31.

References

Lund, J., Aas, V., Tingstad, R.H., Van Hees, A., and Nikolić, N. (2018). Utilization of lactic acid in human myotubes and interplay with glucose and fatty acid metabolism. Scientific Reports 8, 9814.

Lunde, M.N., and Jacobs, L. (1983). Antigenic differences between endozoites and cystozoites of *Toxoplasma gondii*. The Journal of Parasitology 69, 806-808.

MacRae, J.I., Sheiner, L., Nahid, A., Tonkin, C., Striepen, B., and McConville, M.J. (2012). Mitochondrial metabolism of glucose and glutamine is required for intracellular growth of *Toxoplasma gondii*. Cell Host & Microbe 12, 682-692.

Mahamed, D.A., Mills, J.H., Egan, C.E., Denkers, E.Y., and Bynoe, M.S. (2012). CD73-generated adenosine facilitates *Toxoplasma gondii* differentiation to long-lived tissue cysts in the central nervous system. Proceedings of the National Academy of Sciences 109, 16312-16317.

Malinska, D., Kudin, A.P., Bejtka, M., and Kunz, W.S. (2012). Changes in mitochondrial reactive oxygen species synthesis during differentiation of skeletal muscle cells. Mitochondrion 12, 144-148.

Manger, I.D., Hehl, A., Parmley, S., Sibley, L.D., Marra, M., Hillier, L., Waterston, R., and Boothroyd, J.C. (1998). Expressed sequence tag analysis of the bradyzoite stage of *Toxoplasma gondii*: identification of developmentally regulated genes. Infection and Immunity 66, 1632-1637.

Martins-Duarte É, S., Carias, M., Vommaro, R., Surolia, N., and de Souza, W. (2016). Apicoplast fatty acid synthesis is essential for pellicle formation at the end of cytokinesis in *Toxoplasma gondii*. Journal of Cell Science 129, 3320-3331.

Martorelli Di Genova, B., Wilson, S.K., Dubey, J.P., and Knoll, L.J. (2019). Intestinal delta-6-desaturase activity determines host range for *Toxoplasma* sexual reproduction. PLOS Biology 17, e3000364.

Matsuda, R., Uchitomi, R., Oyabu, M., Hatazawa, Y., and Kamei, Y. (2019). Metabolomic analysis of C2C12 myoblasts induced by the transcription factor FOXO1. FEBS Letters 593, 1303-1312.

Matta, S.K., Olias, P., Huang, Z., Wang, Q., Park, E., Yokoyama, W.M., and Sibley, L.D. (2019). *Toxoplasma gondii* effector TgIST blocks type I interferon signaling to promote infection. Proceedings of the National Academy of Sciences 116, 17480-17491.

Maubon, D., Bougdour, A., Wong, Y.S., Brenier-Pinchart, M.P., Curt, A., Hakimi, M.A., and Pelloux, H. (2010). Activity of the histone deacetylase inhibitor FR235222 on *Toxoplasma gondii*: inhibition of stage conversion of the parasite cyst form and study of new derivative compounds. Antimicrobial Agents and Chemotherapy 54, 4843-4850.

Mazumdar, J, E, H.W., Masek, K., C, A.H., and Striepen, B. (2006). Apicoplast fatty acid synthesis is essential for organelle biogenesis and parasite survival in *Toxoplasma gondii*. Proceedings of the National Academy of Sciences 103, 13192-13197.

McConnell, E.L., Basit, A.W., and Murdan, S. (2008). Measurements of rat and mouse gastrointestinal pH, fluid and lymphoid tissue, and implications for in-vivo experiments. The Journal of Pharmacy and Pharmacology 60, 63-70.

Meadows, J.A., and Wargo, M.J. (2015). Carnitine in bacterial physiology and metabolism. Microbiology 161, 1161-1174.

References

Merrick, C.J. (2015). Transfection with thymidine kinase permits bromodeoxyuridine labelling of DNA replication in the human malaria parasite Plasmodium falciparum. Malaria Journal 14, 490.

Molan, A., Nosaka, K., Hunter, M., and Wang, W. (2019). Global status of *Toxoplasma gondii* infection: systematic review and prevalence snapshots. Tropical Biomedicine 36, 898-925.

Molestina, R.E., El-Guendy, N., and Sinai, A.P. (2008). Infection with *Toxoplasma gondii* results in dysregulation of the host cell cycle. Cellular Microbiology 10, 1153-1165.

Morrison, L.J., Marcello, L., and McCulloch, R. (2009). Antigenic variation in the African trypanosome: molecular mechanisms and phenotypic complexity. Cellular Microbiology 11, 1724-1734.

Munder, M.C., Midtvedt, D., Franzmann, T., Nüske, E., Otto, O., Herbig, M., Ulbricht, E., Müller, P., Taubenberger, A., Maharana, S., et al. (2016). A pH-driven transition of the cytoplasm from a fluid- to a solid-like state promotes entry into dormancy. eLife 5, 638-655.

Murata, Y., Sugi, T., Weiss, L.M., and Kato, K. (2017). Identification of compounds that suppress *Toxoplasma gondii* tachyzoites and bradyzoites. PLOS ONE 12, e0178203.

Nanchen, A., Fuhrer, T., and Sauer, U. (2007). Determination of metabolic flux ratios from 13C-experiments and gas chromatography-mass spectrometry data: protocol and principles. Methods in Molecular Biology 358, 177-197.

Narasimhan, J., Joyce, B.R., Naguleswaran, A., Smith, A.T., Livingston, M.R., Dixon, S.E., Coppens, I., Wek, R.C., and Sullivan, W.J., Jr. (2008). Translation regulation by eukaryotic initiation factor-2 kinases in the development of latent cysts in *Toxoplasma gondii*. The Journal of Biological Chemistry 283, 16591-16601.

Nare, B., Allocco, J.J., Liberator, P.A., and Donald, R.G. (2002). Evaluation of a cyclic GMP-dependent protein kinase inhibitor in treatment of murine toxoplasmosis: gamma interferon is required for efficacy. Antimicrobial Agents and Chemotherapy 46, 300-307.

Nathan, C.F., Murray, H.W., Wiebe, M.E., and Rubin, B.Y. (1983). Identification of interferon-gamma as the lymphokine that activates human macrophage oxidative metabolism and antimicrobial activity. The Journal of Experimental Medicine 158, 670-689.

Neef, A.B., and Luedtke, N.W. (2011). Dynamic metabolic labeling of DNA *in vivo* with arabinosyl nucleosides. Proceedings of the National Academy of Sciences 108, 20404-20409.

Neef, A.B., Samain, F., and Luedtke, N.W. (2012). Metabolic Labeling of DNA by Purine Analogues *in vivo*. ChemBioChem 13, 1750-1753.

Neumann, A. (2014). The cell count estimator aided by area calculation. github https://github.com/neumann-alexander./ccean. doi 10..5281/zenodo.5528307

Nishikawa, Y., Quittnat, F., Stedman, T.T., Voelker, D.R., Choi, J.Y., Zahn, M., Yang, M., Pypaert, M., Joiner, K.A., and Coppens, I. (2005). Host cell lipids control cholesteryl ester synthesis and storage in intracellular *Toxoplasma*. Cellular Microbiology 7, 849-867.

Nolan, S.J., Romano, J.D., and Coppens, I. (2017). Host lipid droplets: An important source of lipids salvaged by the intracellular parasite *Toxoplasma gondii*. PLOS Pathogens 13, e1006362.

References

Nolan, S.J., Romano, J.D., Kline, J.T., and Coppens, I. (2018). Novel Approaches To Kill *Toxoplasma gondii* by Exploiting the Uncontrolled Uptake of Unsaturated Fatty Acids and Vulnerability to Lipid Storage Inhibition of the Parasite. Antimicrobial Agents and Chemotherapy 62.

Nose, A., and Takeichi, M. (1986). A novel cadherin cell adhesion molecule: its expression patterns associated with implantation and organogenesis of mouse embryos. The Journal of Cell Biology 103, 2649-2658.

Olson, W.J., Martorelli Di Genova, B., Gallego-Lopez, G., Dawson, A.R., Stevenson, D., Amador-Noguez, D., and Knoll, L.J. (2020). Dual metabolomic profiling uncovers *Toxoplasma* manipulation of the host metabolome and the discovery of a novel parasite metabolic capability. PLOS Pathogens 16, e1008432.

Oppenheim, R.D., Creek, D.J., Macrae, J.I., Modrzynska, K.K., Pino, P., Limenitakis, J., Polonais, V., Seeber, F., Barrett, M.P., Billker, O., et al. (2014). BCKDH: the missing link in apicomplexan mitochondrial metabolism is required for full virulence of *Toxoplasma gondii* and Plasmodium berghei. PLOS Pathogens 10, e1004263.

Painter, H.J., Morrisey, J.M., Mather, M.W., and Vaidya, A.B. (2007). Specific role of mitochondrial electron transport in blood-stage Plasmodium falciparum. Nature 446, 88-91.

Paredes-Santos, T., Wang, Y., Waldman, B., Lourido, S., and Saeij, J.P. (2019). The GRA17 Parasitophorous Vacuole Membrane Permeability Pore Contributes to Bradyzoite Viability. Frontiers in Cellular and Infection Microbiology 9, 321.

Paredes-Santos, T.C., Martins-Duarte, E.S., de Souza, W., Attias, M., and Vommaro, R.C. (2017). *Toxoplasma gondii* reorganizes the host cell architecture during spontaneous cyst formation *in vitro*. Parasitology 145, 1027-1038.

Parker, K.E.R., Fairweather, S.J., Rajendran, E., Blume, M., McConville, M.J., Bröer, S., Kirk, K., and van Dooren, G.G. (2019). The tyrosine transporter of *Toxoplasma gondii* is a member of the newly defined apicomplexan amino acid transporter (ApiAT) family. PLOS Pathogens 15, e1007577.

Pearson, D.J., and Tubbs, P.K. (1967). Carnitine and derivatives in rat tissues. The Biochemical Journal 105, 953-963.

Pedersen, P.L. (2012). 3-Bromopyruvate (3BP) a fast acting, promising, powerful, specific, and effective "small molecule" anti-cancer agent taken from labside to bedside: introduction to a special issue. Journal of Bioenergetics and Biomembranes 44, 1-6.

Pernas, L., Adomako-Ankomah, Y., Shastri, A.J., Ewald, S.E., Treeck, M., Boyle, J.P., and Boothroyd, J.C. (2014). *Toxoplasma* effector MAF1 mediates recruitment of host mitochondria and impacts the host response. PLOS Biology 12, e1001845.

Pernas, L., Bean, C., Boothroyd, J.C., and Scorrano, L. (2018). Mitochondria Restrict Growth of the Intracellular Parasite *Toxoplasma gondii* by Limiting Its Uptake of Fatty Acids. Cell Metabolism 27, 886-897.e884.

Peterson, P.K., Gekker, G., Hu, S., and Chao, C.C. (1995). Human Astrocytes Inhibit Intracellular Multiplication of *Toxoplasma gondii* by a Nitric Oxide-Mediated Mechanism. The Journal of Infectious Diseases 171, 516-518.

Pettersen, E.K. (1979). Destruction of *Toxoplasma gondii* by HC1 solution. Acta Pathologica et Microbiologica Scandinavica. Section B, Microbiology 87, 217-220.

References

Pfefferkorn, E.R., and Pfefferkorn, L.C. (1976). Arabinosyl nucleosides inhibit *Toxoplasma gondii* and allow the selection of resistant mutants. The Journal of Parasitology 62, 993-999.

Pittman, K.J., Aliota, M.T., and Knoll, L.J. (2014). Dual transcriptional profiling of mice and *Toxoplasma gondii* during acute and chronic infection. BioMed Central genomics 15, 806.

Plötz, T., Hartmann, M., Lenzen, S., and Elsner, M. (2016). The role of lipid droplet formation in the protection of unsaturated fatty acids against palmitic acid induced lipotoxicity to rat insulin-producing cells. Nutrition & Metabolism 13, 16.

Qu, D., Wang, G., Wang, Z., Zhou, L., Chi, W., Cong, S., Ren, X., Liang, P., and Zhang, B. (2011). 5-Ethynyl-2'-deoxycytidine as a new agent for DNA labeling: detection of proliferating cells. Analytical Biochemistry 417, 112-121.

Quittnat, F., Nishikawa, Y., Stedman, T.T., Voelker, D.R., Choi, J.Y., Zahn, M.M., Murphy, R.C., Barkley, R.M., Pypaert, M., Joiner, K.A., et al. (2004). On the biogenesis of lipid bodies in ancient eukaryotes: synthesis of triacylglycerols by a *Toxoplasma* DGAT1-related enzyme. Molecular and Biochemical Parasitology 138, 107-122.

Radke, J.R., Behnke, M.S., Mackey, A.J., Radke, J.B., Roos, D.S., and White, M.W. (2005). The transcriptome of *Toxoplasma gondii*. BioMED Central Biology 3, 26.

Radke, J.R., Donald, R.G., Eibs, A., Jerome, M.E., Behnke, M.S., Liberator, P., and White, M.W. (2006). Changes in the expression of human cell division autoantigen-1 influence *Toxoplasma gondii* growth and development. PLOS Pathogens 2, e105.

Radke, J.R., Guerini, M.N., Jerome, M., and White, M.W. (2003). A change in the premitotic period of the cell cycle is associated with bradyzoite differentiation in *Toxoplasma gondii*. Molecular and Biochemical Parasitology 131, 119-127.

Radke, J.R., and White, M.W. (1998). A cell cycle model for the tachyzoite of *Toxoplasma gondii* using the Herpes simplex virus thymidine kinase. Molecular and Biochemical Parasitology 94, 237-247.

Ramakrishnan, S., Docampo, M.D., Macrae, J.I., Pujol, F.M., Brooks, C.F., van Dooren, G.G., Hiltunen, J.K., Kastaniotis, A.J., McConville, M.J., and Striepen, B. (2012). Apicoplast and endoplasmic reticulum cooperate in fatty acid biosynthesis in apicomplexan parasite *Toxoplasma gondii*. The Journal of Biological Chemistry 287, 4957-4971.

Ramakrishnan, S., Serricchio, M., Striepen, B., and Bütikofer, P. (2013). Lipid synthesis in protozoan parasites: a comparison between kinetoplastids and apicomplexans. Progress in Lipid Research 52, 488-512.

Read, L.K., and Mikkelsen, R.B. (1991). Comparison of adenylate cyclase and cAMP-dependent protein kinase in gametocytogenic and nongametocytogenic clones of Plasmodium falciparum. The Journal of Parasitology 77, 346-352.

Remels, A.H., Langen, R.C., Schrauwen, P., Schaart, G., Schols, A.M., and Gosker, H.R. (2010). Regulation of mitochondrial biogenesis during myogenesis. Molecular and Cellular Endocrinology 315, 113-120.

Remington, J.S., and Cavanaugh, E.N. (1965). Isolation of the encysted form of *Toxoplasma gondii* from human skeletal muscle and brain. The New England Journal of Medicine 273, 1308-1310.

References

Roos, D.S. (1993). Primary structure of the dihydrofolate reductase-thymidylate synthase gene from *Toxoplasma gondii*. The Journal of Biological Chemistry 268, 6269-6280.

Rostovtsev, V.V., Green, L.G., Fokin, V.V., and Sharpless, K.B. (2002). A stepwise huisgen cycloaddition process: copper(I)-catalyzed regioselective "ligation" of azides and terminal alkynes. Angewandte Chemie 41, 2596-2599.

Sabin, A.B. (1938). Isolation of a filtrable, transmissible agent with "Neurolyti". Properties from *Toxoplasma*-infected tissues. Science 88, 189-191.

Saleh, A., Friesen, J., Baumeister, S., Gross, U., and Bohne, W. (2007). Growth inhibition of *Toxoplasma gondii* and Plasmodium falciparum by nanomolar concentrations of 1-hydroxy-2-dodecyl-4(1H)quinolone, a high-affinity inhibitor of alternative (type II) NADH dehydrogenases. Antimicrobial Agents and Chemotherapy 51, 1217-1222.

Saunders, E.C., Ng, W.W., Kloehn, J., Chambers, J.M., Ng, M., and McConville, M.J. (2014). Induction of a stringent metabolic response in intracellular stages of *Leishmania* mexicana leads to increased dependence on mitochondrial metabolism. PLOS Pathogens 10, e1003888.

Sauvage, V., Millot, J.M., Aubert, D., Visneux, V., Marle-Plistat, M., Pinon, J.M., and Villena, I. (2006). Identification and expression analysis of ABC protein-encoding genes in *Toxoplasma gondii*. *Toxoplasma gondii* ATP-binding cassette superfamily. Molecular and Biochemical Parasitology 147, 177-192.

Schaffer, J.E. (2002). Fatty acid transport: the roads taken. American Journal of Physiology. Endocrinology and Metabolism 282, e239-246.

Scheele, S., Geiger, J.A., DeRocher, A.E., Choi, R., Smith, T.R., Hulverson, M.A., Vidadala, R.S.R., Barrett, L.K., Maly, D.J., Merritt, E.A., et al. (2018). *Toxoplasma* Calcium-Dependent Protein Kinase 1 Inhibitors: Probing Activity and Resistance Using Cellular Thermal Shift Assays. Antimicrobial Agents and Chemotherapy 62, 458-473.

Schlüter, D., Deckert, M., Hof, H., and Frei, K. (2001). *Toxoplasma gondii* infection of neurons induces neuronal cytokine and chemokine production, but gamma interferon- and tumor necrosis factor-stimulated neurons fail to inhibit the invasion and growth of *T. gondii*. Infection and Immunity 69, 7889-7893.

Schneider, C.A., Rasband, W.S., and Eliceiri, K.W. (2012). NIH Image to ImageJ: 25 years of image analysis. Nature Methods 9, 671-675.

Schoondermark-van de Ven, E.M., Melchers, W.J., Galama, J.M., Meuwissen, J.H., and Eskes, T.K. (1997). Prenatal diagnosis and treatment of congenital *Toxoplasma gondii* infections: an experimental study in rhesus monkeys. European Journal of Obstetrics, Gynecology, and Reproductive Biology 74, 183-188.

Schwartzman, J.D., and Pfefferkorn, E.R. (1981). Pyrimidine synthesis by intracellular *Toxoplasma gondii*. The Journal of Parasitology 67, 150-158.

Seeber, F., Limenitakis, J., and Soldati-Favre, D. (2008). Apicomplexan mitochondrial metabolism: a story of gains, losses and retentions. Trends in Parasitology 24, 468-478.

Semini, G., Paape, D., Blume, M., Sernee, M.F., Peres-Alonso, D., Calvignac-Spencer, S., Döllinger, J., Jehle, S., Saunders, E., McConville, M.J., et al. (2020). *Leishmania* Encodes a Bacterium-like 2,4-Dienoyl-Coenzyme A Reductase That Is Required for Fatty Acid β-Oxidation and Intracellular Parasite Survival. mBio 11, e01057-20.

References

Sethi, K.K., Rahman, A., Pelster, B., and Brandis, H. (1977). Search for the presence of lectin-binding sites on *Toxoplasma gondii*. The Journal of Parasitology 63, 1076-1080.

Sheiner, L., Vaidya, A.B., and McFadden, G.I. (2013). The metabolic roles of the endosymbiotic organelles of *Toxoplasma* and Plasmodium spp. Current Opinion in Microbiology 16, 452-458.

Shiomi, K., Kiyono, T., Okamura, K., Uezumi, M., Goto, Y., Yasumoto, S., Shimizu, S., and Hashimoto, N. (2011). CDK4 and cyclin D1 allow human myogenic cells to recapture growth property without compromising differentiation potential. Gene Therapy 18, 857-866.

Shonhai, A., Maier, A.G., Przyborski, J.M., and Blatch, G.L. (2011). Intracellular protozoan parasites of humans: the role of molecular chaperones in development and pathogenesis. Protein and Peptide Letters 18, 143-157.

Shukla, A., Olszewski, K.L., Llinás, M., Rommereim, L.M., Fox, B.A., Bzik, D.J., Xia, D., Wastling, J., Beiting, D., Roos, D.S., et al. (2018). Glycolysis is important for optimal asexual growth and formation of mature tissue cysts by *Toxoplasma gondii*. International Journal for Parasitology 48, 955-968.

Sibley, L.D., and Ajioka, J.W. (2008). Population structure of *Toxoplasma gondii*: clonal expansion driven by infrequent recombination and selective sweeps. Annual Review of Microbiology 62, 329-351.

Sibley, L.D., Khan, A., Ajioka, J.W., and Rosenthal, B.M. (2009). Genetic diversity of *Toxoplasma gondii* in animals and humans. Philosophical transactions of the Royal Society of London. Series B, Biological Sciences 364, 2749-2761.

Sibley, L.D., Mordue, D.G., Su, C., Robben, P.M., and Howe, D.K. (2002). Genetic approaches to studying virulence and pathogenesis in *Toxoplasma gondii*. Philosophical Transactions of the Royal Society of London. Series B, Biological Sciences 357, 81-88.

Sidik, S.M., Huet, D., Ganesan, S.M., Huynh, M.H., Wang, T., Nasamu, A.S., Thiru, P., Saeij, J.P.J., Carruthers, V.B., Niles, J.C., et al. (2016). A Genome-wide CRISPR Screen in *Toxoplasma* Identifies Essential Apicomplexan Genes. Cell 166, 1423-1435.

Singh, U., Brewer, J.L., and Boothroyd, J.C. (2002). Genetic analysis of tachyzoite to bradyzoite differentiation mutants in *Toxoplasma gondii* reveals a hierarchy of gene induction. Molecular Microbiology 44, 721-733.

Smith, D., Kannan, G., Coppens, I., Wang, F., Nguyen, H.M., Cerutti, A., Olafsson, E.B., Rimple, P.A., Schultz, T.L., Mercado Soto, N.M., et al. (2021). *Toxoplasma* TgATG9 is critical for autophagy and long-term persistence in tissue cysts. eLife 10, e59384.

Soête, M., Camus, D., and Dubremetz, J.F. (1994). Experimental induction of bradyzoite-specific antigen expression and cyst formation by the RH strain of *Toxoplasma gondii in vitro*. Experimental Parasitology 78, 361-370.

Soête, M., and Dubremetz, J.F. (1996). *Toxoplasma gondii*: kinetics of stage-specific protein expression during tachyzoite-bradyzoite conversion *in vitro*. Current topics in Microbiology and Immunology 219, 76-80.

Sonda, S., Ting, L.M., Novak, S., Kim, K., Maher, J.J., Farese, R.V., Jr., and Ernst, J.D. (2001). Cholesterol esterification by host and parasite is essential for optimal proliferation of *Toxoplasma gondii*. The Journal of Biological Chemistry 276, 34434-34440.

References

Sordet, F., Aumjaud, Y., Fessi, H., and Derouin, F. (1998). Assessment of the activity of atovaquone-loaded nanocapsules in the treatment of acute and chronic murine toxoplasmosis. Parasite 5, 223-229.

Streilein, J.W. (1995). Unraveling immune privilege. Science 270, 1158-1159.

Su, C., Evans, D., Cole, R.H., Kissinger, J.C., Ajioka, J.W., and Sibley, L.D. (2003). Recent expansion of *Toxoplasma* through enhanced oral transmission. Science 299, 414-416.

Sugi, T., Ma, Y.F., Tomita, T., Murakoshi, F., Eaton, M.S., Yakubu, R., Han, B., Tu, V., Kato, K., Kawazu, S., et al. (2016). *Toxoplasma gondii* Cyclic AMP-Dependent Protein Kinase Subunit 3 Is Involved in the Switch from Tachyzoite to Bradyzoite Development. mBio 7, e00755-16

Sugi, T., Tu, V., Ma, Y., Tomita, T., and Weiss, L.M. (2017). *Toxoplasma gondii* Requires Glycogen Phosphorylase for Balancing Amylopectin Storage and for Efficient Production of Brain Cysts. mBio 8, e01289-17.

Sullivan, W.J., Jr, and Jeffers, V. (2012). Mechanisms of *Toxoplasma gondii* persistence and latency. FEMS Microbiology Reviews 36, 717-733.

Sullivan, W.J., Jr., Smith, A.T., and Joyce, B.R. (2009). Understanding mechanisms and the role of differentiation in pathogenesis of *Toxoplasma gondii*: a review. Memoria do Instituto Oswaldo Cruz 104, 155-161.

Sumner, E.R., Avery, A.M., Houghton, J.E., Robins, R.A., and Avery, S.V. (2003). Cell cycle- and age-dependent activation of Sod1p drives the formation of stress resistant cell subpopulations within clonal yeast cultures. Molecular Microbiology 50, 857-870.

Suzuki, Y., Orellana, M., Schreiber, R., and Remington, J. (1988). Interferon-gamma: the major mediator of resistance against *Toxoplasma gondii*. Science 240, 516-518.

Swierzy, I.J., Händel, U., Kaever, A., Jarek, M., Scharfe, M., Schlüter, D., and Lüder, C.G.K. (2017). Divergent co-transcriptomes of different host cells infected with *Toxoplasma gondii* reveal cell type-specific host-parasite interactions. Scientific Reports 7, 7229.

Swierzy, I.J., and Lüder, C.G. (2015). Withdrawal of skeletal muscle cells from cell cycle progression triggers differentiation of *Toxoplasma gondii* towards the bradyzoite stage. Cellular Microbiology 17, 2-17.

Takács, A.C., Swierzy, I.J., and Lüder, C.G. (2012). Interferon-γ restricts *Toxoplasma gondii* development in murine skeletal muscle cells via nitric oxide production and immunity-related GTPases. PLOS ONE 7, e45440.

Tang, J., He, A., Yan, H., Jia, G., Liu, G., Chen, X., Cai, J., Tian, G., Shang, H., and Zhao, H. (2018). Damage to the myogenic differentiation of C2C12 cells by heat stress is associated with up-regulation of several selenoproteins. Scientific Reports 8, 10601.

Taylor, J.H., Woods, P.S., and Hughes, W.L. (1957). The Organization and Duplication of Chromosomes as Revealed by Autoradiographic Studies using Tritium-Labeled Thymidine. Proceedings of the National Academy of Sciences 43, 122-128.

Tomavo, S., and Boothroyd, J.C. (1995). Interconnection between organellar functions, development and drug resistance in the protozoan parasite, *Toxoplasma gondii*. International Journal for Parasitology 25, 1293-1299.

References

Tomavo, S., Fortier, B., Soete, M., Ansel, C., Camus, D., and Dubremetz, J.F. (1991). Characterization of bradyzoite-specific antigens of *Toxoplasma gondii*. Infection and Immunity 59, 3750-3753.

Tomavo, S., Schwarz, R.T., and Dubremetz, J.F. (1989). Evidence for glycosyl-phosphatidylinositol anchoring of *Toxoplasma gondii* major surface antigens. Molecular and Cellular Biology 9, 4576-4580.

Tomita, T., Bzik, D.J., Ma, Y.F., Fox, B.A., Markillie, L.M., Taylor, R.C., Kim, K., and Weiss, L.M. (2013). The *Toxoplasma gondii* cyst wall protein CST1 is critical for cyst wall integrity and promotes bradyzoite persistence. PLOS Pathogens 9, e1003823.

Tornøe, C.W., Christensen, C., and Meldal, M. (2002). Peptidotriazoles on solid phase: [1,2,3]-triazoles by regiospecific copper(i)-catalyzed 1,3-dipolar cycloadditions of terminal alkynes to azides. The Journal of Organic Chemistry 67, 3057-3064.

Tu, V., Mayoral, J., Sugi, T., Tomita, T., Han, B., Ma, Y.F., and Weiss, L.M. (2019). Enrichment and Proteomic Characterization of the Cyst Wall. mBio 10, e00469-00419.

van Heerden, J.H., Wortel, M.T., Bruggeman, F.J., Heijnen, J.J., Bollen, Y.J., Planqué, R., Hulshof, J., O'Toole, T.G., Wahl, S.A., and Teusink, B. (2014). Lost in transition: start-up of glycolysis yields subpopulations of nongrowing cells. Science 343, 1245114.

van Roermund, C.W., Hettema, E.H., van den Berg, M., Tabak, H.F., and Wanders, R.J. (1999). Molecular characterization of carnitine-dependent transport of acetyl-CoA from peroxisomes to mitochondria in Saccharomyces cerevisiae and identification of a plasma membrane carnitine transporter, Agp2p. The EMBO Journal 18, 5843-5852.

Van Voorhis, W.C., Doggett, J.S., Parsons, M., Hulverson, M.A., Choi, R., Arnold, S.L.M., Riggs, M.W., Hemphill, A., Howe, D.K., Mealey, R.H., et al. (2017). Extended-spectrum antiprotozoal bumped kinase inhibitors: A review. Experimental Parasitology 180, 71-83.

van Winden, W.A., Wittmann, C., Heinzle, E., and Heijnen, J.J. (2002). Correcting mass isotopomer distributions for naturally occurring isotopes. Biotechnology and Bioengineering 80, 477-479.

Vercesi, A.E., Rodrigues, C.O., Uyemura, S.A., Zhong, L., and Moreno, S.N. (1998). Respiration and oxidative phosphorylation in the apicomplexan parasite *Toxoplasma gondii*. The Journal of Biological Chemistry 273, 31040-31047.

Verheul, A., Wouters, J.A., Rombouts, F.M., and Abee, T. (1998). A possible role of ProP, ProU and CaiT in osmoprotection of Escherichia coli by carnitine. Journal of Applied Microbiology 85, 1036-1046.

Waldman, B.S., Schwarz, D., Wadsworth, M.H., Saeij, J.P., Shalek, A.K., and Lourido, S. (2020). Identification of a Master Regulator of Differentiation in *Toxoplasma*. Cell 180, 359-372.

Waldman, F.M., Chew, K., Ljung, B.M., Goodson, W., Hom, J., Duarte, L.A., Smith, H.S., and Mayall, B. (1991). A comparison between bromodeoxyuridine and 3H thymidine labeling in human breast tumors. Modern Pathology 4, 718-722.

Waller, R.F., Keeling, P.J., Donald, R.G., Striepen, B., Handman, E., Lang-Unnasch, N., Cowman, A.F., Besra, G.S., Roos, D.S., and McFadden, G.I. (1998). Nuclear-encoded proteins target to the plastid in *Toxoplasma gondii* and Plasmodium falciparum. Proceedings of the National Academy of Sciences 95, 12352-12357.

References

Walsh, K., and Perlman, H. (1997). Cell cycle exit upon myogenic differentiation. Current Opinion in Genetics & Development 7, 597-602.

Wang, C.C. (1984). Parasite enzymes as potential targets for antiparasitic chemotherapy. Journal of Medicinal Chemistry 27, 1-9.

Watts, E., Zhao, Y., Dhara, A., Eller, B., Patwardhan, A., and Sinai, A.P. (2015). Novel Approaches Reveal that *Toxoplasma gondii* Bradyzoites within Tissue Cysts Are Dynamic and Replicating Entities *In vivo*. mBio 6, e01155-01115.

Weilhammer, D.R., Iavarone, A.T., Villegas, E.N., Brooks, G.A., Sinai, A.P., and Sha, W.C. (2012). Host metabolism regulates growth and differentiation of *Toxoplasma gondii*. International Journal for Parasitology 42, 947-959.

Weiss, L.M., and Kim, K. (2000). The development and biology of bradyzoites of *Toxoplasma gondii*. Frontiers in Bioscience 5, 391-405.

Weiss, L.M., Laplace, D., Takvorian, P.M., Tanowitz, H.B., Cali, A., and Wittner, M. (1995). A cell culture system for study of the development of *Toxoplasma gondii* bradyzoites. The Journal of Eukaryotic Microbiology 42, 150-157.

Weiss, L.M., Ma, Y.F., Takvorian, P.M., Tanowitz, H.B., and Wittner, M. (1998). Bradyzoite development in *Toxoplasma gondii* and the hsp70 stress response. Infection and Immunity 66, 3295-3302.

Wiendl, H., Hohlfeld, R., and Kieseier, B.C. (2005). Immunobiology of muscle: advances in understanding an immunological microenvironment. Trends in Immunology 26, 373-380.

Wilking, H., Thamm, M., Stark, K., Aebischer, T., and Seeber, F. (2016). Prevalence, incidence estimations, and risk factors of *Toxoplasma gondii* infection in Germany: a representative, cross-sectional, serological study. Scientific Reports 6, 22551.

Winzer, P., Muller, J., Aguado-Martinez, A., Rahman, M., Balmer, V., Manser, V., Ortega-Mora, L.M., Ojo, K.K., Fan, E., Maly, D.J., et al. (2015). *In vitro* and *In vivo* Effects of the Bumped Kinase Inhibitor 1294 in the Related Cyst-Forming Apicomplexans *Toxoplasma gondii* and Neospora caninum. Antimicrobial Agents and Chemotherapy 59, 6361-6374.

Wong, F.H.-S., Cai, Y., Leck, H., Lim, T.-P., Teo, J.Q.-M., Lee, W., Koh, T.H., Tan, T.T., Tan, K.W., and Kwa, A.L.-H. (2020). Determining the Development of Persisters in Extensively Drug-Resistant upon Exposure to Polymyxin B-Based Antibiotic Combinations Using Flow Cytometry. Antimicrobial Agents and Chemotherapy 64, e01712-01719.

Xia, N., Yang, J., Ye, S., Zhang, L., Zhou, Y., Zhao, J., David Sibley, L., and Shen, B. (2018). Functional analysis of *Toxoplasma* lactate dehydrogenases suggests critical roles of lactate fermentation for parasite growth *in vivo*. Cellular Microbiology 20, e04873-04880.

Xue, Y., Theisen, T.C., Rastogi, S., Ferrel, A., Quake, S.R., and Boothroyd, J.C. (2020). A single-parasite transcriptional atlas of *Toxoplasma gondii* reveals novel control of antigen expression. eLife 9, e54129.

Yahiaoui, B., Dzierszinski, F., Bernigaud, A., Slomianny, C., Camus, D., and Tomavo, S. (1999). Isolation and characterization of a subtractive library enriched for developmentally regulated transcripts expressed during encystation of *Toxoplasma gondii*. Molecular and Biochemical Parasitology 99, 223-235.

References

Yap, G.S., Scharton-Kersten, T., Charest, H., and Sher, A. (1998). Decreased resistance of TNF receptor p55- and p75-deficient mice to chronic toxoplasmosis despite normal activation of inducible nitric oxide synthase *in vivo*. Journal of Immunology 160, 1340-1345.

Zhang, Y.W., Halonen, S.K., Ma, Y.F., Tanowtiz, H.B., and Weiss, L.M. (2010). A Purification Method for Enrichment of the *Toxoplasma gondii* Cyst Wall. Journal of Neuroparasitology 1, 348-361.

Zhang, Y.W., Halonen, S.K., Ma, Y.F., Wittner, M., and Weiss, L.M. (2001). Initial characterization of CST1, a *Toxoplasma gondii* cyst wall glycoprotein. Infection and Immunity 69, 501-507.

Zhou, W., Gumina, G., Chong, Y., Wang, J., Schinazi, R.F., and Chu, C.K. (2004). Synthesis, structure-activity relationships, and drug resistance of beta-d-3'-fluoro-2',3'-unsaturated nucleosides as anti-HIV Agents. Journal of Medical Chemistry 47, 3399-3408.

Zhu, G., Li, Y., Cai, X., Millership, J.J., Marchewka, M.J., and Keithly, J.S. (2004). Expression and functional characterization of a giant Type I fatty acid synthase (CpFAS1) gene from Cryptosporidium parvum. Molecular and Biochemical Parasitology 134, 127-135.

Zhu, G., Shi, X., and Cai, X. (2010). The reductase domain in a Type I fatty acid synthase from the apicomplexan Cryptosporidium parvum: restricted substrate preference towards very long chain fatty acyl thioesters. BioMed Central Biochemistry 11, 46.

Ziegler, C., Bremer, E., and Krämer, R. (2010). The BCCT family of carriers: from physiology to crystal structure. Molecular Microbiology 78, 13-34.

Selbstständigkeitserklärung

Hiermit bestätige ich, dass ich die vorliegende Arbeit

„A novel *in vitro* model for mature *Toxoplasma gondii* tissue cysts allows functional characterization of bradyzoite physiology"

selbständig angefertigt habe. Ich versichere, dass ich ausschließlich die angegebenen Quellen und Hilfen in Anspruch genommen habe. Ich versichere, dass die folgende Publikation

„ A Novel *in vitro* Model for Mature *Toxoplasma gondii* Bradyzoites Reveals their Metabolome and a Diminished Role of the Mitochondrial Tricarboxylic Acid Cycle" (*bioRxiv*)

beziehungsweise

„*In vitro* maturation of *Toxoplasma gondii* bradyzoites in human myotubes and their metabolomic characterization" (*Nature Communications*)

maßgeblich von mir mitverfasst wurde. Mögliche Übereinstimmungen mit Textpassagen aus meiner Dissertation stellen somit keinen Plagiatsfall dar.

Dies wird bei Bedarf durch die aufgeführten Co-Autoren bestätigt: Deborah Maus, Ellen Hoppenz, Mateo Murillo Leon, Tobias Hoffmann, Jana Scholz, Florian Melerowicz, Tobias Steinfeldt, Frank Seeber, Martin Blume.

Berlin, 21th of january 2022

_____

Céline Christiansen